5-2021

Biofabricated Constructs of Carbon-based Nanoparticles with Mesenchymal Stem Cells for Orthopedic Repair

Steven D. Newby
University of Tennessee, Knoxville, snewby@vols.utk.edu

To the Graduate Council:

I am submitting herewith a dissertation written by Steven D. Newby entitled "Biofabricated Constructs of Carbon-based Nanoparticles with Mesenchymal Stem Cells for Orthopedic Repair." I have examined the final electronic copy of this dissertation for form and content and recommend that it be accepted in partial fulfillment of the requirements for the degree of Doctor of Philosophy, with a major in Comparative and Experimental Medicine.

Madhu S. Dhar, Major Professor

We have read this dissertation and recommend its acceptance:

Madhu S. Dhar, David E. Anderson, Gina M. PIghetti, Shawn E. Bourdo

Accepted for the Council:

Dixie L. Thompson

Vice Provost and Dean of the Graduate School

(Original signatures are on file with official student records.)

Biofabricated Constructs of Carbon-based Nanoparticles with Mesenchymal Stem Cells for Orthopedic Repair

A Dissertation Presented for the
Doctor of Philosophy
Degree
The University of Tennessee, Knoxville

Steven D. Newby
May 2021

DEDICATION

I dedicate this work to my wife Michelle and daughter Skylar, family, friends, and educators; both here and in memory; that were there for support throughout my long journey. From you came the unwavering strength to find sure footing regardless of terrain.

ACKNOWLEDGEMENTS

An exceptional gratitude for my advisor and mentor Dr. Madhu Dhar, for the opportunity in taking me into her stem cell laboratory and whose guidance this work would not have been possible. I appreciate her contribution of time and resources into my project and me. My knowledge of 3D bioprinting and stem cell culture has been greatly expanded due to her being a true mentor. I would also like to acknowledge my lab mates/colleagues for such strong support and advice, in particular Dr. Austin Bow, Lisa Amelse, and Dr. David Anderson and other team players of the department of Large Animal Clinical Sciences, with emphasis on valuable input and support for the development and execution of this research.

I would like to thank my additional committee members Drs.' Gina Pighetti and Shawn Bourdo. Their input over the years have made my research better and I am grateful for their time and support. Furthermore, help and program advise and leadership from both Kim Rutherford and Dr. Stephen Kania in navigating the requirements of the Comparative and Experimental Medicine (CEM) program and the University of Tennessee, Knoxville Graduate School was invaluable and deserves appreciation. I would also like to extend my gratitude to the members of the College of Veterinary Medicine for their time and help in molding my research to focus its scope and streamline methodologies.

Lastly, I would like to recognize the collaborative research teams with which I have had the pleasure of working. The material design and development team based in the Center for Integrative Nanotechnology Sciences at the University of Arkansas at Little Rock (UALR) characterized and provided all materials utilized in this research. For those portions of this work that have been published I would like to thank the editors, reviewers, and publishers for their time and patience.

ABSTRACT

Breakthroughs in tissue engineering are moving at a rapid rate, especially in regenerative bone biofabrication. Technology growth in the field of additive manufacturing (AM) such as 3D bioprinting which provides the ability to create a biocompatible 3D construct on which a cell source could be seeded is an encouraging substitute to autologous grafts.

This present research aims to biofabricate a construct for bone tissue engineering using AM technology. The biocompatible material was chosen corresponding to the skeletons extracellular matrix (ECM) composition, which demonstrates an inorganic and organic development phase: Poly (lactic-glycolic acid) was chosen as the polymeric matrix of the compound, due to its bioactivity, biocompatibility, and ability to regulate biodegradability to support cell and bone function; graphene-nanoparticle were chosen for mechanical and organic reinforcement to support the mineral phase of the ECM.

A commercial 3D bioprinter called the Aether 1 was used. The printer is a pneumatic based printer, which allows printing from hydrogels to thermo polymers. The bioprinter is located in the Regenerative Medicine Lab in the Large Animal Clinical Sciences.

The first part of our study was to show the relationship of mesenchymal stem cells and graphene-nanoparticles. This was to evaluate the ECM layout on the graphene for biocompatibility and establish markers for supporting osteogenesis. Second part of the research dealt with finding a safe solvent to melt the different molar ratios of PLGA and the blending in of graphene-nanoparticles for low thermodynamic and low-pressure printing. This work dealt with the characterization, constating in the evaluation of different extrusion speeds, pressure values and nozzle diameters to construct a 3D print for testing the biocompatibility and cellular behavior. The final study was to utilize the 3D constructs in a long bone segmental defect model to characterize its *in vivo* capabilities.

This work proved that the biofabrication of the PLGA+graphene nanoparticle blend could be achieved and repeatable with 3D bioprinting, supports cellular behavior for regeneration and provided results in the long bone defect study.

TABLE OF CONTENTS

LIST OF FIGURES

LIST OF ABBREVIATIONS

2D……. Two-Dimensional

3D …… Three-Dimensional

3DP……..….Three-Dimensional printing

AM…… Additive Manufacturing

ASC……..…… Adipose-derived stem cells

BMSC ……. Bone Marrow Stem Cell

BTE ……. Bone Tissue Engineering

BV …… Bone Volume

CAD……. Computer Aided Design

CATE…….. Computer-Aided Tissue Engineering

CEM……. Comparative and Experimental Medicine

CSD ……Critical Size Defect

ECM ……..….. Extracellular Matrix

FBS……...Fetal Bovine Serum

FDA …… Food and Drug Administration

FDM …… Fused Deposition Modelling

GA ……Glycolic Acid

GBR …… Guided Bone Regeneration

GFP …… Green Fluorescent Protein

GO ……Graphene Oxide

LA …… Lactic Acid

LOG……. Low Oxygen Graphene

MSC …… Mesenchymal Stem Cell

PBS ……. Phosphate Buffered Saline

PCL ……. Poly Caprolactone

PGA …… Poly Glycolic Acid

PLA ……. Poly Lactic Acid

PLGA……Poly (lactic-glycolic acid)
rGO …… Reduced Graphene Oxide
RFP …….. Red Fluorescent Protein
RM……Regenerative Medicine
SEM …… Scanning Electron Microscopy
SFF…….. Solid Free Form Fabrication
SLA…….. Stereolithography
SVF …….. Stromal Vascular Fraction
TBV …….. Total Bone Volume
TE ……Tissue Engineering
UALR …….. University of Arkansas at Little Rock
XPS ……X-ray Photoelectron Spectroscopy

CHAPTER I:
3D PRINTING: INSIGHT INTO THE MATRIX ARCHITECTURE AND CONTACT GUIDANCE OF CELL BEHAVIOR

This Agreement between Dr. Madhu Dhar (“You”) and Springer Nature (“Springer Nature’) consist of your license details and the terms and conditions provided by Springer Nature and Copyright Clearance Center.

License Number:	5013910902153
License Date:	Feb 21, 2021
Licensed Content Publication	Springer eBook
Title:	Tissue Engineering Modalities and Nanotechnology
Licensed Content Author:	Hoda Elkhenany, Mohamed Abd Elkodous, Steven D. Newby et al
Type of Use:	Thesis/Dissertation
Format:	Text extract

The versions of this chapter were originally published by Springer Nature:

Permission was obtained from the Publishers, Springer Nature. Permission was obtained by Dr. Madhu Dhar, mentoring author of the chapter.

Abstract

Nearly thirty years ago a technology was brought to light that had no understanding how it would change science, medicine and manufacturing. The production of 3D models used in many avenues has grown greatly over the years. The reviewed literature works has gone back many years, but this review will cover a period of the last 10-15 years when printing manufactures entered, and 3D printing grew at a pace from only structure formations to new construct biocompatible materials with stem cells and supporting components. This chapter outlines the application of 3D printing in tissue and organ regeneration, productions of new materials for fabrication and biofabrication and its effects on economics for this technology. Stereolithography is what Hull, 3D printing inventor, called his first 3D printing automation. He secured a patent for his invention and established a 3D System to make and commercialize 3D printers (Prince, 2014).

Introduction

To heal or replace, which treatment for tissue damage or organ failure? This is where regenerative medicine comes into play with a goal to engineer tissues for transplantation and replacement. This is primarily due to organ shortage and the tool to aid in this task of bio-manufacturing is three-dimensional printing or bioprinting. The goal of 3D printing is to meet the need and match patient specific resolution. The approach of 3D bioprinting is a growing application for multiple tissue engineering challenges with tissue regeneration being the end goal. The body of any animal is profoundly complex with a multiplex of tissue types. Organs of these complex systems are formed by extremely specialized cells with complex functions. Three-dimensional framework of multicellular tissues defines different roles, providing organ structural integrity but also indicate functional organ perimeters and depict the microenvironment niche (Mecham, 2012). With an avenue of cells, bioactive/growth molecules or factors and a scaffold, it is imperative to consolidate the foundation of cellular and molecular biology with material science to form the cocktail to engineer this needed 3D environment. Controlling and understanding the cellular surroundings is a vital step for engineering a material for cellular function (Jiang, 2003). No matter the application or the need, the approach is to achieve cell survival with an objective for the restoration and function of a tissue. Regardless of the strategic approach the ultimate host response to the implanted construct will direct the accomplishment or collapse of 3D bioprinting.

Many primary cell lineages are complex to isolate and culture *in vitro* with a narrow lifespan (Dimri, 1995). Mesenchymal stem cells (MSCs) which can be isolated from any adult somatic tissue have the potential to self-renew and differentiate leading to an unlimited cell source for tissue regeneration when they are combined with a well-developed 3D bioprinted/-biofabricated construct. The stem cell niche is a convoluted 3D environment which impacts cell fate. Within the stem cell system, the exchange of oxygen and growth factors, cell-cell association as well as cell-matrix adherence are required for regulation (Discher, 2009). Therefore, the accurate biofabrication of this niche-like environment is a crucial matter in stem cell biology and regenerative

medicine. The construction of stem cell niches and tissue constructs is very challenging from a technical point of view because of their complexity.

By this measure there is a demand to cultivate a genuine matrix substitute to replace traditional 3D scaffolds. Bioprinting is an additive manufacturing (AM), where the scaffold design for fabrication layout starts with computer-aid design (CAD) software, then data is transferred into a code that directs the 3D printer to print in a layer-by-layer composition (**Figure 1.1**). This chapter is subdivided to include the details of the most common 3D printing and bioprinting technologies. Attention has been placed in extrusion-based printing/bioprinting automation. In the last section, it details the importance of the biofabrication in mimicking of extracellular matrix to improve cell survival for implantation.

3D Bioprinting Building Blocks

According to the National Institute of Health, tissue engineering is a strategy that uses a combination of cells, specifically designed and engineered materials, and suitable biochemical and physicochemical factors to restore, maintain, improve, or replace different types of biological tissues. Regenerative medicine is a broad filed of tissue engineering. Tissue engineering using stem cells requires the appropriate niche for proper proliferation and differentiation. Technically, engineering the stem cell niche is considered as the most challenging aspect of tissue engineering. 3D printing provides the three-dimensional environment for the cells and helps them to maintain their cell-cell contact and thus, their function. In conventional 2D cultures, primary cells rapidly lose their function, in large part due to distressed cell-cell contacts, further emphasizing the importance of 3D printing. As a result, 3D printing of materials provides a structure for the function of endogenous and exogenous cells. The 3D scaffold alone i.e., an acellular scaffold has the potential to provide a structure for endogenous cells to function appropriately. It can also be combined with exogenous cell populations to design highly sophisticated constructs that mimic the natural tissue and hence, can be adapted for use of living material. The approach of 3D bioprinting of either material alone or of constructs consisting of materials and living cells has the potential to

reconstruct tissue from various regions of the body. This technology can also potentially be applied to bone, skin, cartilage and muscle tissue.

In 3D printing, several technical issues have to be considered before any cellular component can be included. These include the choice of printing technology, choice of the biomatrix, printing parameters, and subsequently, considerations of the interaction between the materials and cells. The scaffold is designed in a CAD program, then coded to the 3D printer for a structure formation in a layer-by-layer format. The 3D bioprinter is a multi-tool printer allowing for multiple fabrication methods and printing cells and biological materials in programed patterns and gradients. Microextrusion is the common choice of printing and is essentially the same as that used in thermal inkjet printing, which can attain a spatial resolution of hundreds of micrometers. Microjet extruder bioprinting is the process in which designed droplets are deposited onto the scaffolds in a layer-by layer preprogrammed design. The choice of the materials that can be printed is endless, and in biomedicine, the choice of the material is highly dependent on the applications and the cells that will be either printed or manually added onto the printed scaffold, or the nature of the cells that the implanted scaffold will be exposed to in the body (Tappa, 2018).

Additive Manufacturing – Making Three Dimensional Scaffolds

The additive process is the formation of a 3D printed scaffold or object. It is developed by the blending of materials. The material is placed through a technology which creates successive layers of blended materials and a physical object is assembled. The common desktop printer, the inkjet, which was brought to use in the seventies was attached to a computer to receive commands. This constituted the whole building platform for the 3D printer. The inkjet required a data file and a computer connection controller to have complete operation. A modern 3D printer also requires a data file based on the physical objects' 3D model, and post-modeling code after the model is printed. Metal alloy, synthetic polymers and now biological tissues must be considered because the choice of the material alters the processing method and hence is needed to achieve the needed design. The American Society for Testing and Materials produced a white paper in 2017 by Picariello that categorized the process of

additive manufacturing into seven groups based on the manufacturing process. These groups include material extrusion, energy direct deposition, sheet lamination, powder bed fusion, binder jetting, material jetting and vat photo polymerization (Picariello, 2017).

Computer-aided Design, G-code and Computer – aided Tissue Engineering

CAD software is where 3D printing begins for the manufacturing process. The operator designs a digital model of the desired architecture in the levels of macro, micro and nano scales for the overall shape of the needed scaffold. In the fabrication or biofabrication the microarchitecture of the overall design allows for the complex structures of anatomical features; the micro design mirrors the tissue layout including pore size and interconnectivity and spatial distribution; and the nano design looks at the constructs' surface properties for cell adhesion, proliferation, differentiation and biomolecular attachment. CAD has allowed for complex biofabrication of 3D scaffolds to meet specific patient needs. CAD software has the coding for integration of imaging techniques such as computer tomography and magnetic resonance imaging, thereby, translating the CT and the MRI images directly into the printer. The ability of utilizing this technology has allowed for more advanced prototype scaffold designing, manipulation and biofabrication of macro to nanoarchitecture. Once the scaffold is developed in the CAD software, the CAD file is converted to a standard industry format as a stereolithography file. The stereolithography file is known as the STL file, developed by Hull, is based on a geometrical format using triangular shapes (Kwok et al., 2017). The STL file is then split into layers in the layer-by-layer design by a process known as slicing. The slicing software effectively translates the 3D scaffold into a control language known as a G-code. A G-code is a language written in a numerical control program that sends a code or instructions to the printer. A G-code is specific to the printer or the bioprinter and the additive manufacturing method which is being utilized (Kwok et al., 2017). The G-code provides the language that the 3D printer can translate and use to print.

The architecture of computer-aided tissue engineering (CATE) allows for advancement of biomaterials and biomedical device to be designed and biofabricated

into a complex 3D construct and be patient tissue specific. The careful layout must review all levels of the macro, micro and nano components. The complexity of the overall macroarchitecture shape being the anatomical structure must be mimicked, the microarchitecture must relate closely to the tissue matrix being porosity, spatial distribution and interconnectivity. The nanoarchitecture will build the strong attraction for cell adhesion, proliferation, and differentiation for a mature development. Using CATE with micro-CT and MRI data allows for the layout for a rapid prototyping of the construct's macro and micro biofabrication quality (Winder, 2005). The support of CATE leads the way to a rapid prototyping, called solid free form fabrication (SFF), allowing the design of the construct's complex macro and microarchitecture for detailed engineering.

Solid Freeform (SFF) Biofabrication

The process of forming a 3D device is done in a layer-by-layer method with SFF biofabrication. A computer model using data from a medical image such as micro-CT and radiology views is developed for the proper geometry. Next, the 2D computer model images are software generated forming a 3D rendering. A layer-by-layer model for biofabrication has the ability to input nanoarchitecture modification on any surface in post process if needed. The use of SFF has advantages to print complex designs, allowing for highly convoluted structure overhangs or volume infills. The ability of processing multiples of parameters and layouts before processing, specifically with control of pore morphology and varying porosities at different levels of biofabrication is a very important manufacturing process. This becomes significant when dealing with the complexity of mammal anatomy. A modified method of 3D printing, stereolithography (SLA), fused deposition modeling (FDM), and bioplotting are a few SFF technologies briefly described below.

Structural Parameter - Limitations and Accuracy

How closely does the 3D fabricated scaffold compare to the CAD file to give a sound call for accuracy? Many software features and the location of the XY resolution are some of the factors involved in maintaining the dimensional accuracy.

Structural resolution dictates a printing system's ability to accurately build the detailed features of the scaffold. In the fabrication process, repeatability of measurement is processed by the printer and not the CAD design. An important variable in 3D printing is spatial resolution. Tissue extracellular matrix and construction varies in the hundreds of microns making this variable one of the most challenging to control in biofabrication. Within most body tissues, cells need to maintain homeostasis staying generally no more than 100 – 200 μm away from capillaries (Lovett et al.,2009). Therefore, bioengineered devices and scaffolds are diffusion limited in size due to lack of vasculature. As a result, culturing cells at physiological densities without ample vascularization can lead to necrosis (Miller et al., 2012).

3D Printing

Massachusetts Institute of Technology has taken the technology to develop a modified version of three-dimensional printing (3DP) (Wu, 1996). The process design for this method was to first build a 3D object with particles of a layer of thin loose powder, next the printhead deposits a liquid binder creating a pattern from the bound powder particles. This was a layer-by-layer design system. When complete, the designed components are removed from the print bed of powder and loose powder is detached. This method of printing utilized the loose powder to support overhand structural features and channels within the structure. As a result, the 3DP was composed of the powder and the binder. Organic solvent such as Diethylene Glycol can be utilized as binders while most powders were composed of synthetic polymers such as poly (ε-caprolactone), polylactide–coglycolide or poly (L- lactic acid) (Wu, 1996). Other inkjet systems used natural polymer powders such as starch, gelatin mix and dextran with water as the binding agent (Seitz et al., 2005). Indirect method of 3DP utilizes a printed mold design which is later cast with a porogen material and polymer mix. Calcium sulfate hemihydrate plaster powder with a water-based binder, is typically cast as the mold later mixed to form a biodegradable polymer slurry which is dissolved in polylactide–coglycolide in chloroform mixed with NaCl as the solvent (Lee, 2008).

The abundant range of natural and synthetic material powder forms and the ability to print at room temperature is a key to 3DP. Controlling all levels of overhang

extensions, design with microstructure manipulation and set full adjustments to internal architecture gives many advantages. The 3DP disadvantages include the limited organic solvents that can be used as binders due to the damage caused to the printhead and, secondly the powders clog small pores and curved channels within the construct.

Stereolithography - Photopolymerization

The design of this printer is to utilize a controlled irradiated laser or light to solidify the geometrically created 2D pattern through photopolymerization in the resin reservoir. This method was used by Hull when 3D printing came to light (Hull, 1986). Overall, the primary improvement of stereolithography-based bioprinting is the ability to simply fabricate multiplex scaffold designs with high resolution and rapidly print constructs without needed support material (Murphey, S.V. and Atala, A., 2014; Park et al., 2017). SLA materials used are limited because they should be photocrosslinkable. Hence, poly (propylene fumarate) (Lee, et al., 2007) and PEG dimethacrylate formulations are commonly used. SLA is moving towards using biodegradable materials by synthesizing different polymers like macromers. SLA has a higher resolution but a longer print time than Fused Filament. The future of cell work with SLA includes encapsulation of cells during polymerization in processed hydrogels. The method still has many limitations such as cytotoxicity of the initiator and exposure to UV light, but teams are reviewing the needed changes including the use of hydrogels, which can prove very helpful in regenerative medicine.

Fused Deposition or Fused Filament Printing

This fabrication method works by building consecutive layers of a polymer at high temperatures, allowing the adjacent layers to cool and form a bond before the next deposited layer is extracted. This fabrication method has limited resolution and accuracy due to the motors and print time. Fused fabrication has the ability to be easily customized for scaffold designs and can be hollow or infill to save material cost. Depending on the scaffold and the CAD design, the structures may need support anchors which could inhibit the fused deposition process.

Inkjet Bioprinting

Inkjet bioprinting is based on the usage of cell-laden bioink droplets which are generated and deposited to established pre-defined scaffold regions (**Figure 1.2**). An advantage to droplet bioprinting is the ability to allow for concentration gradients of cells, materials or growth factors throughout the 3D scaffold by altering droplet densities or proportions (Nakamura, 2005). Current research is utilizing droplet bioprinting for "scaffold-free" print design which consists of depositing layers of concentrations of cells in a sacrificial scaffold mold.

3D Plotting and Bioplotting

This technology is an all-purpose rapid prototyping printer that is capable of transforming an assortment of biomaterials using biofabrication from CATE. Being very similar to FDM, a nozzle is used to extrude the melted material into the form of filament which solidifies on the cooled print bed. A well-built bioplotter system can fabricate or Biofabricate scaffolds using an extensive spectrum of materials, ranging from hydrogels, polymers and hard ceramics and metals. In the biofabrication process, 3D bioplotting has the capability for the design to incorporate multiple cell types into the structure during the printing phase of the complete process.

Bioink Selection for Tissue Scaffold

The extracellular matrix is the backbone to tissue regeneration for cell proliferation, adhesion and differentiation. The ECM is generated either by the cells that are implanted exogenously or by the endogenous cells when they are exposed to 3D printed scaffolds (Newby et al., 2020). Hence, the choice of the "bioinks" for a specific printer is an important factor in tissue engineering. Bioinks constitutes the biomaterial (s) that is extruded by a printing nozzle or needle that generates a biofabricated matrix for cells while they produce the needed extracellular matrix for tissue regeneration. Alternatively, the ECM can be generated by blending natural or synthetic materials *in vitro* and used as a bioink. Bioinks are characterized as structural, functional or supportive (Chia, 2015). The mechanical means of the developed bioink must target

the needed cell forces allowing for signaling pathways leading to cell survival and tissue development (Dussoyer et al., 2000). The development of these materials needs to be studied in a step-by-step process for purification, material modification and the most challenging sterilization to be utilized in regenerative medicine applications.

Acellular and Cellular Biofabrication

Acellular scaffolds are those that typically mimic the biochemical and mechanical properties of the tissue ECM Scaffolds provide the environment for cellular attachment to stimulate tissue regenerative response. Acellular bioprinting allows for a greater extent for material selection for biofabrication. Acellular scaffolds must be bioresorbable and biocompatible and should demonstrate the potential to generate signals for biochemical, biomechanical and biophysical cues for cell migration and differentiation (Hutmacher, 2000). Additionally, cellular scaffolds without any cellular component can be merely implanted into patients for structural and functional support in the regenerative process.

The biofabrication of a 3D cellular construct implements living cells in the design procedure. Assorted emulsions have been developed to generate a 3D matrix of living tissue with each iteration having different strengths and limitations. Bioinks incorporating cells have additional requirements, and thus, pose significant challenges. The printing process must preserve cell integrity and viability during resuspension and passage through the bioprinter nozzle and preparation of an environmental niche for cell growth and function within the printed biofabricated scaffold [Wust et al., 2011]. The deposition of the bioink depends on the printing mechanism. The representative techniques of cellular bioprinting can be categorized into three methods: extrusion-based (pneumatic-, mechanical-, and solenoid-based), stereolithography and droplet-based (Skardal, 2015).

Tissue Engineering

Different designs of scaffolds and printing as mentioned earlier greatly depend on the method of additive manufacturing process. The ability to control degradation and resorption rates to resemble normal tissue with favorable mechanical properties and

exceptional biocompatibility both *in vitro* and *in vivo* are required in engineering experimental steps (Cancedda, 2007). The biofabrication design of the scaffold should provide a three-dimensional support for tissue regeneration. This process should support cell proliferation leading to differentiation while promoting growth with surrounding vessels, resulting in an iteration with an end goal to replace the sustaining loads and functions of the flawed tissue. The biofabricated construct should acquire a repository of biochemical and biophysical cues to promote precise response at the cellular level for tissue development.

Cells for Biofabrication

The most abounding cell source in the body to support bioengineering is the MSCs. MSCs may be isolated from adipose tissue and bone marrow and have capability for self-renewal and to differentiate into multiple cell linages in proper conditions *in vitro* and *in vivo* (Lee et.al., 2001). Our focus in the use of cells in biofabrication centers on the use of adipose - and bone marrow - derived MSCs. MSCs can also be classified as autologous and allogenic. Autologous cells are transplanted from yourself, while allogenic cells are transplanted from a donor. In human medicine, autologous stem cells have been used in medical treatment of injury and disease (Tobiat, 2011), while a number of clinical trials are ongoing to promote the use of allogenic cells (www.clinicaltrial.gov) Combination of the cell's ability for self-renewal and capacity to differentiate into chondrogenic, adipogenic, osteogenic and angiogenic lineages and a well-designed architecture construct plays an important role in the various stages for regeneration of tissue (Cherubino et al., 2011).

Various cell types have been printed using a 3D bioprinter. One of the impediments of engineering any scaffold is the ineffectiveness to biomimic the extracellular matrix of healthy tissue in the body when multiple cell types are integrated (Xu et al., 2013). With the ability to design a structured pattern providing an optimal environment for cells can prove to be very advantageous in regenerative medicine. Printers are adjustable, multitask, easily reprogrammed with a new CAD template and are provided with interchangeable stainless-steel blunt tip needles for injection to accommodate different biomaterials and/or multiple cell types. Recent momentum has

been placed on printing scaffolds which can serve as biomimetic components that can orchestrate tissue regeneration, provide tissue support, direct tissue regeneration and integration within a host tissue. As a result, some of the basic material elements that are considered during the printing process include percent porosity with ranging dimensions, internal geometric and projection modeling, biodegradation dynamics, mechanical properties, and cell biocompatibility. As a result, a lot of research and design is required to find an optimal material for a particular application (Guvendiren, 2016).

With the recent advances in cell-based therapies, 3D printing is becoming an increasingly common technique to generate scaffolds and medical devices for tissue engineering applications. In the last decade, extensive research has been carried out towards developing biomaterials that are capable of mimicking the physiological and biological microenvironment of mesenchymal stem cells along with physicochemical properties that will control the cell behavior and fate. Controlling cell behavior is one of the most important topics in regenerative medicine and is of particular interest to researchers by which the lessons can be transferred to the clinic with improved outcomes. Some of the factors that need special consideration in 3D printing of materials conducive for controlled cell behavior are highlighted below.

Extracellular Matrix

Remembering that the role the ECM plays is a critical position in providing structural support through ligands such as type I collagen and fibronectin which interact with MSCs in promoting remodeling (Salmasi et al., 2015). During the tissue repair process the interaction between MSCs, native tissue cells, biofabricated construct and the ECM trigger cell signaling, release a variety of growth factors, and stimulate the healing process (Chen, 2016).

A multitude of variables must be evaluated when designing constructs for stem cell responses to the simulated extracellular matrix compatibility. Stimulus variables such as oxygen values, nutrient concentrations and mechanical cues stimulate cells to modify the secreted ECM to regulate the biological process including differentiation of stem cells and angiogenesis for the regenerative process (Gattazzo, 2014). In the

natural construct, the ECM serves as an adhesive support not only for cells but the detachment of morphogens and growth factors that contribute to the maintenance of tissue function. The engineered ECM construct must incorporate the rigor and control of synthetic material manufacturing and favoring bioactivity to promote tissue remodeling at various levels. The use of biomimetic regulated biodegradable materials can be engineered using a variety of biofabricated procedures such as 3D printing in an endeavor to mimic the biological cues of the natural ECM to incorporate the best mechanical and degradation profile.

Extracellular Matrix-Material Interactions

The physiochemical properties of base materials, whether synthetic or natural, must support cell viability during biofabrication, culture and degradation. The 3D parameters of the constructs should not evoke cellular death, induce cell stress biomarkers or alter DNA makeup to cause a negative cellular change. Many three-dimensional fabricated porous constructs using single or mixed biomaterial types for *in vitro* and *in vivo* studies for cell-construct communications and tissue integrations have been used broadly to induce a tight cell matrix bond for tissue development. These constructs are trying to clone the extracellular matrix and form a physical reinforcement to allow cellular migration, adhesion, proliferation which are required for tissue differentiation. As the progression of material science and tissue physiology continues, the advancement of material biofabrication production to biomimic the ECM construct is required. A precise value of porosity, cell to material surface area, safe chemical composition and a controlled degradation rate for a stronger end result (Yannas, 1989) are needed. For the design of an effective ECM construct platform four properties have been laid out in the biofabrication process. First is the biodegradation rate as period of time, second is a biocompatible chemical cocktail to reduce cytotoxicity, third is the calculation of the microstructure taking in consideration the pore size, locations and geometrical orientation, and fourth the overall construct size for cell migration and angiogenesis support (Yannas,2001).

Cell-Scaffold Interactions

The primary objective for regenerative engineering is to optimize the biocompatibility of the 3D constructs supporting strong cell-tissue interactions. Cell-to-cell biochemical communication is indispensable to instigate initial attachment, while provoking ques for cell proliferation by the constructs surface texture and topography. These interactions give a clear interrelationship between the surface roughness of the biocompatible material and the tight relationship to adhesion, proliferation, and morphology of the cells (Linez-Bataillon, 2002). Surface roughness of the biomaterial's mixture plays a very important role in the expression of the ECM and cell adhesion proteins depending on the type of tissue that is being replaced by the 3D print (Grellier, 2009, Linez-Batailion, 2002). 3D biofabrication progression to finite shapes and sizes for the ideal cell niche to promote adherence and growth has changed biomedical device engineering. Printing constructs with high porosity and varying micrometer pore diameters with interconnective channels to increase cell to matrix surface area for cell attachment and tissue ingrowth are being generated. Properties of the construct being physical, and chemical are also crucial in relation to the cell-matrix surface area interaction. Any variation in the 3D bioprinted structure factors can have a significant effect on cell adhesion, proliferation and differentiation in the tissue development *in vitro* and *in vivo*.

Biofabrication Material Combinations

Ceramics, metals and polymers both natural and synthetic have been recommended in bone tissue biofabrication (Salgado, 2004). Each material or mix of material has many pros and cons to being the perfect implantable medical device leading to desired shapes to mimic or having osteoinductive and osteoconductive properties or the perfect biodegradation rate for cell and tissue survival (Peppas, 1994). The process of biodegradability plays the greatest role in tissue regeneration if not controlled properly tissue may reproduce but may also struggle or die due to growth replacement rates. The period of time a biomaterial remains insoluble in the body is crucial in characterizing the material bioactivity. Under normal physiological conditions

the tissue must incorporate with the biofabricated construct to reinforce cell migration, adhesion, proliferation and fully support differentiation but the biofabricated material must biodegrade in a safe manner that will not interfere with the native tissue remodeling development. Increasing density of the construct increases resistance to degradation but may also be achieved with increasing the crosslink density between the fibers (Yannas, 1989). Crosslinking has an effect on cells and used in controlling natural and synthetic constructs. Constructs of the natural blend are derived from sources such as fibrinogen, polysaccharides (chitosan, alginate, starch), proteins or collagen base. Each of these biomaterials promotes and expedite cell attachment, migration through the design, differentiation and vascularization of tissue (Salago, 2004). Over the years natural constructs have been replaced with the use of synthetic biomaterials for bone tissue engineering (Nair,2006; Li et al., 2014).

Various types of biodegradable synthetic polymers have widely been used to replace tissue damage at many organ levels. Poly (glycolic acid) (PGA) causes inflammatory reactions to the surrounding tissue but has high tensile mechanical strength and stiffness with low solubility (Yamane, 2014). Modification of poly (ε-caprolactone) (PCL) allows it to be highly compatible and has been examined as a material for controlled applications of various drug delivery models due to its low degradation rate of 2-3 years by microorganisms. 3D printing of a composite scaffold of PCL/hydroxyapatite (HA) with HA exposed onto the surface of scaffold for enhanced cellular response and osteochondral engineering. (Dwivedi et al.,2020; Idris et al., 2010). Designing for excellent compatibility and bioabsorbability for the body is Poly (lactic acid) (PLA) as well as the PLA based copolymer poly (lactic-glycolic acid) (PLGA) which has been approved by the FDA for clinical use. The use of a nanocomposite with PLA has acceptable properties processing and mechanical support and as a result of its low degradation rate. It is extensively used as a fixative device in dental applications for bone fracture support, in medical devices for drug delivery, as well as possessing an outstanding biocompatibility, osteoinductive and osteoconductive properties for guiding biofabrication tissue regeneration (Zhang, 2015). PLA has four different variation's that are available but only poly (l-lactic acid) and poly (dl-lactic acid) have been widely

explored as an alternative to ceramic biomaterials (Chen,2003; Zhang 2015). Poly (LLA) has been used as resorbable suture under the product name Vicryl® and Fixsorb® an orthopedic fixator device (Ulery, 2011). It has been suggested that copolymers such as Poly (L-Lactide-co-caprolactone) {poly (LLA-co-CL)} copolymers are appropriate materials for enhancing cell differentiation for bone tissue repair (Idris,2010) These copolymers acquire acceptable mechanical properties, favorable biocompatibility and degradability that can be used to assemble constructs and increase behavior for cellular adhesion and proliferation (Nair, 2011).

The synthetic constructs in material science biofabrication has allowed for designing in a variety of methods. With pore architecture being so important the method of chemical/gas foaming came about. This technique using high pressure carbon dioxide gas developed the method of continuous extrusion process for a high porous structure. The saturation of the thermoplastic polymer mixes allowed designers to have precise pore distribution and size to achieve infiltration of cells in the construct with a suitable mechanical support (Mathieu, 2005). Leaching of particles/salts, is solvent casting, which is a method that depends on totally on removal and complete evaporation of the solvent utilized. This technique is a low-cost method with the fabrication not requiring a great deal of equipment. Fabricating a multi-channel with high interconnectivity and porosity rate is completed by the method of freeze drying. The polymers are dissolved into a slurry and frozen then placed under very high vacuum, so the solvent is removed yielding a fabricated construct for tissue repair (Whang, 1995). However, each of the techniques for fabrication has some disadvantages, such as the breakdown of the polymers using highly toxic solvents, limitations on structure design and mechanical properties, maintain added nanoparticles within the construct's matrix, increased inconsistencies with pore sizes and shapes and yielding long processing times in the lab (Bose, 2013).

To overcome these material design challenges the development of the various 3D printing methods are being used to support a higher biocompatibility and less cytotoxicity material methodology. 3D printing allows for detailed construct design to

support formation of blood vessels within the matrix and use geometric shapes to form stronger mechanical supports to develop a functional replacement for bone or soft organ tissue engineering. As the growth in regenerative medicine climbs the demand for 3D biofabrication is expected to increase exponentially. The use of computer-aided tissue engineering technology to customize medical devices and to procedure constructs in a high reproducible manner with high quality control will improve the function of tissues with high mechanical properties, increased cell adhesion for proliferation and distribution in every surgeon's operating room (Bose, 2013).

Biofabrication – Summarizing Trends and Strategies

With the significant progress made in all facets of biomedicine described in the above sections, there are many different options to approach a biofabrication project which can be successfully translated into the clinic (Gloria, 2010). Based on the literature described above, this section summarizes the tools and the considerations that should be taken into account by researchers and clinicians for safe and efficacious cell-based therapies.

1) Cell based therapy by taking tissue samples from the donor after breaking down to a cell platform and then seeding it directly to a tissue structure, supporting proliferation and differentiation, and promoting angiogenesis.

2) A cell focus approach by using growth factor stimuli to develop a correlative regenerated tissue

3) Design of a bioreactor as an internal or external device containing tissue. These are linked to the body to support or replace physiological functions, and

4) Biofabricate a scaffold onto which tissue or mesenchymal stem cells are loaded and implanted to regenerate tissue.

In order to achieve any of the above – mentioned method, the choice of the scaffold design is of prime importance. The scaffold design should be carefully chosen so as to allow a specific cell type to show in-growth and out- growth with the material so to restimulate the endogenous progenitor cells and regrow the damaged area of tissue by a cooperative action with the exogenous cells. The scaffold can be designed from natural or synthetic material, which gives varying degradation response and temporarily

supporting cells via cell matrix-material interactions and biochemical release. As described in the above sections, scaffolds can be acellular or cellular. An acellular design aids regeneration by angiogenesis, as vessels from the encompassing tissues attach or penetrate the scaffold layout. This process allows the tissue to fill and modify the biofabricated scaffold, which over a period of time biodegrades and allows the tissue to sustain further growth supplied by the blood vessels. Second, is a cellular design, where the patients stem cells, or an allogenic cell approach can be taken to seed the biofabricated design. This method of scaffold design becomes intergraded and allows for expansion of the engineered tissue. In order to be used in some form of tissue engineering the biofabricated scaffolds must meet the prerequisites summarized below (Causa, 2007; Gloria et al., 2013; Hutmacher, 2004). All the desired properties are interdependent and hence, in many instances, it is difficult to describe them as mutually exclusive, and hence, might result in some redundancy.

Scaffold structure and design: Regeneration of the human body is a very complex cascade of pathways, which have a very complex coordinated event of spatial and temporal modalities. Signal transduction is highly governed by biochemical cues which trigger the ECM microenvironment for development (Causa, 2007). The biofabricated structure must provide a dimensional/porous balance so as to allow for cellular adhesion and proliferation controlling the expression of the extracellular matrix. The extracellular matrix provides a structural and dynamic communication between cells playing a very complex role in cellular fate, direct cell-ECM interactions, such as migration, adhesion and remodeling influence tissue development (Alford et al, 2015). Optimal porosity is one of the main features in the biofabricated design. Its primary responsibility as an interconnected labyrinth is for cell-to-cell communication, adhesion, diffusion and supportive network for vascularization as well as nutrients to cells and tissue and removal of cellular metabolic waste (Causa, 2007). Degradation of the biomaterial can also affect pore dimensions and could potentially change the development of the tissue.

As a result, the design layout should provide a three-dimensional space, so to bolster the developing tissue; support cell to cell or cell to matrix interaction while

stimulating tissue production, whilst gaining support from vasculature. The scaffold design should temporarily sustain tissue operations such as a load bearing support until the new bone is formed as expected in bone regeneration.

Biocompatibility: The biomaterial choice of the biomaterial is a key feature. Natural or synthetic material selected for biofabrication must integrate and be compatible to the host and must have minimal to no host tissue inflammatory response. If a response triggers an immunological cascade, the biomaterial must be non-cytotoxic, so that the biomaterial can modulate the tissue response (Hutmacher, 2000). As a result, various concentrations of material mixes and solvents should be tested. The testing for cell viability or apoptotic activity represents a crucial marker in gene regulators for overall cellular apoptosis and can be performed *in vitro* prior to *in vivo* application. In summary, material design must support cell survival, with regulated biodegradation and resorption rates to mimic the structural tissue extracellular matrix, and proper mechanical properties to optimize the rate of tissue regeneration *in vitro* and *in vivo* (Butscher, 2011; Hutmacher, 2000).

Surface topography: A 3D biofabricated construct is a template for cell adhesion, proliferation and differentiation to promote regeneration of a damaged or replaced tissue (Salgado, 2004; Müller, 2009). Surface area for cell-matrix contact must be appropriate to support cellular nutrients and metabolic waste. adhesion, migration and differentiation are key factors in a cellular process and one factor that can change the whole outcome is the substrate topography. The integration between the biofabricated materials' topographic patterns and cellular response can greatly improve the functionality and long-term stability of the scaffold implant. Topography of the scaffold can be used in a very effective manner to regulate cell adhesion migration and differentiation (Ventre, 2012).

Degradation and restorability: Biomaterial degradation are a very complex but important feature to consider when determining the biomaterial of choice and to be sure it completely degrades as a tissue is reformed. Degradation rate can be tailored by the

addition or subtraction of working groups on the material composition. It is important to understand the discordance between degradation and regeneration times which could lead to a problem during development. If a degradation rate is too fast this can lead to a non-complete tissue development, while a slower degradation might result in incomplete regeneration. Ultimately, when the biomaterial degrades it should be easily processed and expelled without an inflammatory response within the host physiological system.

Mechanical tradeoff: Responsibility of the scaffold is to be a temporary replacement to support the damaged tissue and all functions, especially mechanical if dealing with osteo regeneration, while the new tissue is being regenerated. Hence, understanding the connection between degradation of the scaffold and its mechanical properties is imperative. Understanding that there will be a transition where the regenerative tissues embrace a greater mechanical role as the scaffold degrades is of prime importance.

Sterilization: Another very challenging priority to scaffold properties is the requirement of having a sterile environment guaranteed for *in vivo* implantation and *in vitro* cell work. A crucial prerequisite to the design process is providing a sterile environment for cell growth plate ration and avoiding contamination. To that point the biomaterial of choice, which can be sterilized without losing its material properties, is a crucial consideration in scaffold biofabrication.

Challenges

One of the impediments of engineering any scaffold is the ineffectiveness to biomimic the extracellular matrix of healthy tissue in the body when multiple cell types are integrated (Xu et al., 2013). With the ability to design a structured pattern of cells in 3D bioprinting, an optimal structure can be produced. 3D printing allows for several advantages in regenerative medicine. Printers are adjustable and can multitask; they can be easily reprogrammed with a new CAD template and interchangeable stainless-steel blunt tip needles for injection to accommodate different biomaterials or cell types. 3D bioprinting is an efficient process that can reduce the waiting time of the needed transplant organs for human or animal patients (Sachs, 2013; Xu et al., 2013) and

hence, has a huge potential in biomedicine. 3D bioprinting could facilitate fabrication of patient-specific tissues, and possibly formulation of complete system organs in the future.

Conclusion

3D printing and bioprinting is versatile for tissue applications and has emerged as a new tool for biofabrication of constructs to create well-defined intricate and reproducible matrix architectures to replace human anatomy from disease. The use of a 3D printed applications also allows for detailed reproducible iterations for a solid platform for in vitro models for studying geometrical architecture on various cellular feedback pathways, leading to enhanced mechanical production of bioengineered constructs. With the use of CAD technology and integrations with medical software the allows for building of custom-made iterations based on each patient-specific tissue needs. The needed understanding of chemistry and biology for material properties, CAD and slicers for software and the dynamics of the printer for hardware yields the interactions for the involvement of the printing process. Therefore, choosing the correct processing conditions and the precise material properties facilitates in the reproduction of a high-quality 3D biofabrication. Several biodegradable polymers such as PCL, PLGA, PLA, and PGA, and their copolymers have been used to Biofabricate 3D printed iterations (Chen, 2013). The preference of using a synthetic polymer and their copolymer materials is ease in processing into tissue biofabricated constructs and extreme versatility, which allow characteristic tailoring of biocompatibility, and the ability to vary biodegradation time, vary softness with solvents, wettability, mechanical strength (Li, 2014). Utilization of 3D bioprinted bioinks and hydrogels for soft tissues including skin, liver, and vasculature have been demonstrated to create in-vitro models for bioreactor studies and drug testing applications, which is closer to reality than 3D bioprinted tissues for organ transplantation. Over the past years, many new exciting developments in the bioprinting field has been enabled by the development of bioinks and hydrogels us be used in combination with polymers. Multiple new breakthroughs in

bioink development will remain the key highlights of the future models in 3D bioprinting for tissue engineering.

3D bioprinted constructs and bioinks/hydrogels utilized should empower three main objectives; First, being define a space that sculpts the regenerating tissue, Second, maintain a temporary matrix to allow for tissue functions and Third, permit a model for tissue ingrowth support (Billiet et al., 2012). The ideal biomaterial should mimic ECM properties and support cellular activity with interconnectivity for waste and nutrient flow without leading to cell functional damage and to maintain mechanical stability as biodegradation progresses to allow ECM from the cells inside the construct to gradually replace the lost biomaterial, this highlights the development of 3D printing/bioprinting/biofabrication for tissue engineering.

In view of the challenges and the multifactorial nature of tissue engineering and regenerative medicine described in this chapter, it is very difficult to identify a strategy that can go from bench to bedside. As described in the next four chapters, I have used the information from our laboratory and the published reports to implement a bone tissue engineering strategy which could be used in a large animal preclinical model with a long-term goal of translating it into human medicine. This strategy consisted of generating *in vitro* models of human MSCs (Chapters 2, 3), identifications of the type and the form of the polymers and nanoparticles, and 3D biofabrication of the scaffold (Chapter 4), and ultimately evaluation of the polymer/nanoparticle/cell constructs in a rat femoral weight – bearing bone model (Chapter 5).

References

Alford, Andrea I., et al. "Extracellular Matrix Networks in Bone Remodeling." *The International Journal of Biochemistry & Cell Biology,* vol. 65, 2015, pp. 20-31.
Ventre M, Causa F, Netti PA. 2012 Determinants of cell – material crosstalk at the interface: towards engineering of cell instructive materials. J. R. Soc. Interface 9, 2017 – 2032. (doi:10.1098/rsif.2012.0308

Balletti, C., Ballarin, M., & Guerra, F. (2017). 3D printing: State of the art and future perspectives. Journal of Cultural Heritage 26(July-August) 172-182.

Bose S, Vahabzadeh S, Bandyopadhyay A. Bone tissue engineering using 3D printing. Mater Today. 2013;16.

Billiet, T., Vandenhaute, M., Schelfhout, J., Van Vlierberghe, S. & Subruel, P. (2012) A review of trend and limitations in hydrogel-rapid prototyping for tissue engineering. *Biomaterials*, 33(26), pp. 6020-6041.

Butscher A, Bohner M, Hofmann S, Gauckler L, Müller R. Structural and material approaches to bone tissue engineering in powder-based three-dimensional printing. Acta biomaterialia. 2011;7(3):907-20.

Chen D, Hao H, Fu X, Han W. Insight into reepithelialization: how do mesenchymal stem cells perform? *Stem Cells Int*. 2016; 2016:6120173.

Mecham, R. P. Overview of extracellular matrix. *Curr. Protoc. Cell Biol. Chapter* **57**, 10.1.1–10.1.16 (2012).

Chen G, Sato T, Ushida T, Hirochika R, Shirasaki Y, Ochiai N, et al. The use of a novel PLGA fiber/collagen composite web as a scaffold for engineering of articular cartilage tissue with adjustable thickness. J Biomed Mater Res A. 2003;67(4):1170-80

Cherubino M, et al. Adipose-derived stem cells for wound healing applications. Ann Plast Surg 2011;66(2):210e5.

Chia, H. N. & Wu, B. M. Recent advances in 3D printing of biomaterials. *J. Biol. Eng*. **9**, https://doi.org/10.1186/s13036-015-0001-4 (2015).

Dimri GP, Lee X, Basile G, et al. A biomarker that identifies senescent human cells in culture and in aging skin in vivo. Proceedings of the National Academy of Sciences 1995; 92:9363–7.

Discher DE, Mooney DJ, Zandstra PW. Growth factors, matrices, and forces combine and control stem cells. Science 2009; 324:1673-7. 10.1126/science.1171643

Dussoyer M, Courtial E, Albouy M, Thepot A, Dos M, Marquette C. Mechanical properties of 3D bioprinted dermis: characterization and improvement. Int J Regen Med. 2019;2(1):2-5.

Dwivedi Ruby, Kumar Sumit, Pandey Rahul, Mahajan Aman, Nandana Deepti, Katti Dhirendra S., Mehrotra Divya, Polycaprolactone as biomaterial for bone scaffolds: Review of literature, Journal of Oral Biology and Craniofacial Research, Volume 10, Issue 1,2020, Pages 381-388, ISSN 221 4268 https://doi.org/10.1016/j.jobcr.2019.10.003.

Gattazzo F, Urciuolo A, Bonaldo P. Extracellular matrix: A dynamic microenvironment for stem cell niche. Biochim Biophys Acta. 2014; 1840:2506–19. DOI: 10.1016/j.bbagen.2014.01.010 [PubMed: 24418517]

Grellier M, Bordenave L, Amédée J. Cell-to-cell communication between osteogenic and endothelial lineages: implications for tissue engineering. Trends in Biotechnology. 2009;27(10):562-71.

Guvendiren M, Molde J, Soares RMD, Kohn J. ACS Biomater. Sci. Eng. 2016; 2:1679. [PubMed: 28025653] b) Hofmann M. ACS Macro Lett. 2014; 3:382.

Hull, C. W. (1986). *Patent: Apparatus for Production of Three-Dimensional Objects by Stereolithography*. U.S. Patent No. 4,575,330. Washington, DC: U.S. Patent and Trademark Office

Hutmacher DW. Scaffolds in tissue engineering bone and cartilage. Biomaterials. 2000;21(24):2529-43.

Idris SB, Dånmark S, Finne-Wistrand A, Arvidson K, Albertsson A-C, Bolstad AI, et al. Biocompatibility of Polyester Scaffolds with Fibroblasts and Osteoblast-like Cells for Bone Tissue Engineering. Journal of Bioactive and Compatible Polymers. 2010;25(6):567-83.

Kwok, T., Ye, H., Chen, Y., Zhou, C., & Xu, W. (2017). Mass customization: Reuse of digital slicing for additive manufacturing. *Journal of Computing and Information Science in Engineering*, *17*(2). doi:10.1115/1.4034010

Lee K, Majumdar MK, Buyaner D, Hendricks JK, Pittenger MF, Mosca JD. Human Mesenchymal Stem Cells Maintain Transgene Expression during Expansion and Differentiation. Mol Ther. 2001;3(6):857-66.
Lee K-W, Wang S, Fox BC, Ritman EL, Yaszemski MJ, Lu L. Poly (propylene fumarate) bone tissue engineering scaffold fabrication using stereolithography: effects of resin formulations and laser parameters. Biomacromolecules. 2007; 8:1077-84.

Lee M, Dunn JCY, Wu BM. Scaffold fabrication by indirect three-dimensional printing. Biomaterials. 2005; 26:4281-9.

Lee M, Wu BM, Dunn JCY. Effect of scaffold architecture and pore size on smooth muscle cell growth. Journal of Biomedical Materials Research Part A. 2008; 87:1010-6.

Li X, Cui R, Sun L, Aifantis KE, Fan Y, Feng Q, et al. 3D-Printed Biopolymers for Tissue Engineering Application. International Journal of Polymer Science. 2014; 2014:13.

Linez-Bataillon P, Monchau F, Bigerelle M, Hildebrand HF. In vitro MC3T3 osteoblast adhesion with respect to surface roughness of Ti6Al4V substrates. Biomol Eng. 2002;19(2-6):133-41.

Lovett, M., Lee, K., Edwards, A., & Kaplan, D. L. (2009). Vascularization strategies for tissue engineering. *Tissue engineering. Part B, Reviews*, *15*(3), 353–370. doi: 10.1089/ten.TEB.2009.0085

Mathieu LM, Montjovent MO, Bourban PE, Pioletti DP, Manson JA. Bioresorbable composites prepared by supercritical fluid foaming. J Biomed Mater Res A. 2005;75(1):89- 97.

Miller J, Stevens K, Yang M, Baker B, Nguyen DH, Cohen D, Toro E, Chen A, Galie P, Yu X, Chaturvedi R, Bhatia S, Chen C. Rapid casting of patterned vascular networks for perfusable engineered three-dimensional tissues. Nature Materials, 2012, 11: 768 – 774.

Müller B, Deyhle H, Fierz FC, Irsen SH, Yoon JY, Mushkolaj S, et al., editors. Bio-mimetic hollow scaffolds for long bone replacement2009.

Murphy, S.V. and A. Atala, Nat Biotechnol, 2014. **32**(8) 10.1038/nbt.2958

Nair L, Laurencin C. Polymers as Biomaterials for Tissue Engineering and Controlled Drug Delivery. In: Lee K, Kaplan D, editors. Tissue Engineering I. Advances in Biochemical Engineering/Biotechnology. 102: Springer Berlin Heidelberg; 2006. p. 47-90.

Nakamura M, Kobayashi A, Takagi F, Watanabe A, Hiruma Y, Ohuchi K, et al. Biocompatible inkjet printing technique for designed seeding of individual living cells. Tissue Eng. 2005;11(11-12):1658-66.

Newby SD, Masi T, Griffin CD, King WJ, Chipman A, Stephenson S, Anderson DE, Biris AS, Bourdo SE, Dhar M. Functionalized Graphene Nanoparticles Induce Human Mesenchymal Stem Cells to Express Distinct Extracellular Matrix Proteins Mediating Osteogenesis. Int J Nanomedicine. 2020 Apr 15; 15:2501-2513. doi: 10.2147/IJN.S245801. PMID: 32368037; PMCID: PMC7171876.

Park, J.H., et al., Ann Biomed Eng, 2017. **45**(1) 10.1007/s10439-016-1611-9

Peppas NA, Langer R. New challenges in biomaterials. Science. 1994;263(5154):1715-20.

Picariello, P., (2017). Committee F42 on additive manufacturing technologies. *ASTM International*. Retrieved from https://www.astm.org/COMMITTEE/F42.htm

Prince, J. D. (2014). 3D printing: An industrial revolution. *Journal of Electronic Resources in Medical Libraries*, *11*(1), 39-45. doi:10.1080/15424065.2014.877247

R Cancedda, P Giannoni, and M Mastrogiacomo. A tissue engineering approach to bone repair in large animal models and in clinical practice. Biomaterials, 28(29):4240–4250, 2007

Tobita M, Orbay H, Mizuno H. Adipose-derived stem cells: current findings and future perspectives. Discov Med 2011;11(57):160e70.
Winder J, Bibb R. Medical rapid prototyping technologies: state of the art and current limitations for application in oral and maxillofacial surgery. Journal of Oral and Maxillofacial Surgery. 2005; 63:1006-15.

Salgado AJ, Coutinho OP, Reis RL. Bone tissue engineering: state of the art and future trends. Macromol Biosci. 2004;4(8):743-65.

Salmasi S, Kalaskar DM, Yoon WW, Blunn GW, Seifalian AM. Role of nanotopography in the development of tissue engineered 3D organs and tissues using mesenchymal stem cells. *World J Stem Cells*. 2015;7(2):266–280.

Seitz H, Rieder W, Irsen S, Leukers B, Tille C. Three-dimensional printing of porous ceramic scaffolds for bone tissue engineering. Journal of Biomedical Materials Research Part B: Applied Biomaterials. 2005; 74:782-8.

Skardal, A. and A. Atala, Ann Biomed Eng, 2015. **43**(3) 10.1007/s10439-014-1207-1

Tappa K, Jammalamadaka U. Novel Biomaterials used in medicaln3D printing techniques. J Funct Biomater. 2018;9(1):17.

Ulery BD, Nair LS, Laurencin CT. Biomedical Applications of Biodegradable Polymers. Journal of polymer science Part B, Polymer physics. 2011;49(12):832-64.

Whang K, Thomas CH, Healy KE, Nuber G. A novel method to fabricate bioabsorbable scaffolds. Polymer. 1995;36(4):837-42

Winder J, Bibb R. Medical rapid prototyping technologies: state of the art and current limitations for application in oral and maxillofacial surgery. Journal of Oral and Maxillofacial Surgery. 2005; 63:1006-15.

Wu BM, Borland SW, Giordano RA, Cima LG, Sachs EM, Cima MJ. Solid free-form fabrication of drug delivery devices. Journal of Controlled Release. 1996; 40:77-87

Wust, S., R. Muller, and S. Hofmann, J Funct Biomater, 2011. **2**(3) 10.3390/jfb2030119.

Xu T, Zhao W, Zhu JM, Albanna MZ, Yoo JJ, Atala A. Complex heterogeneous tissue constructs containing multiple cell types prepared by inkjet printing technology. Biomaterials. 2013;34(1):130-9.

Yamane, K., Sato, H., Ichikawa, Y. *et al.* Development of an industrial production technology for high-molecular-weight polyglycolic acid. *Polym J* **46,** 769–775 (2014). https://doi.org/10.1038/pj.2014.69

Yannas IV, Lee E, Orgill DP, Skrabut EM, Murphy GF. Synthesis and characterization of a model extracellular matrix that induces partial regeneration of adult mammalian skin. Proc Natl Acad Sci USA 1989;86(3):933e7

Yannas IV. Tissue and Organ Regeneration in Adults. New York: Springer; 2001.

Zagris, N. Extracellular matrix in development of the early embryo. *Micron* **32**, 427–438 (2001).

Y. Zhang, J. Wang, J. Wang et al., “Preparation of porous PLA/DBM composite biomaterials and experimental research of repair rabbit radius segmental bone defect,” *Cell and Tissue Banking*, vol. 16, no. 4, pp. 615–622, 2015.

Appendix

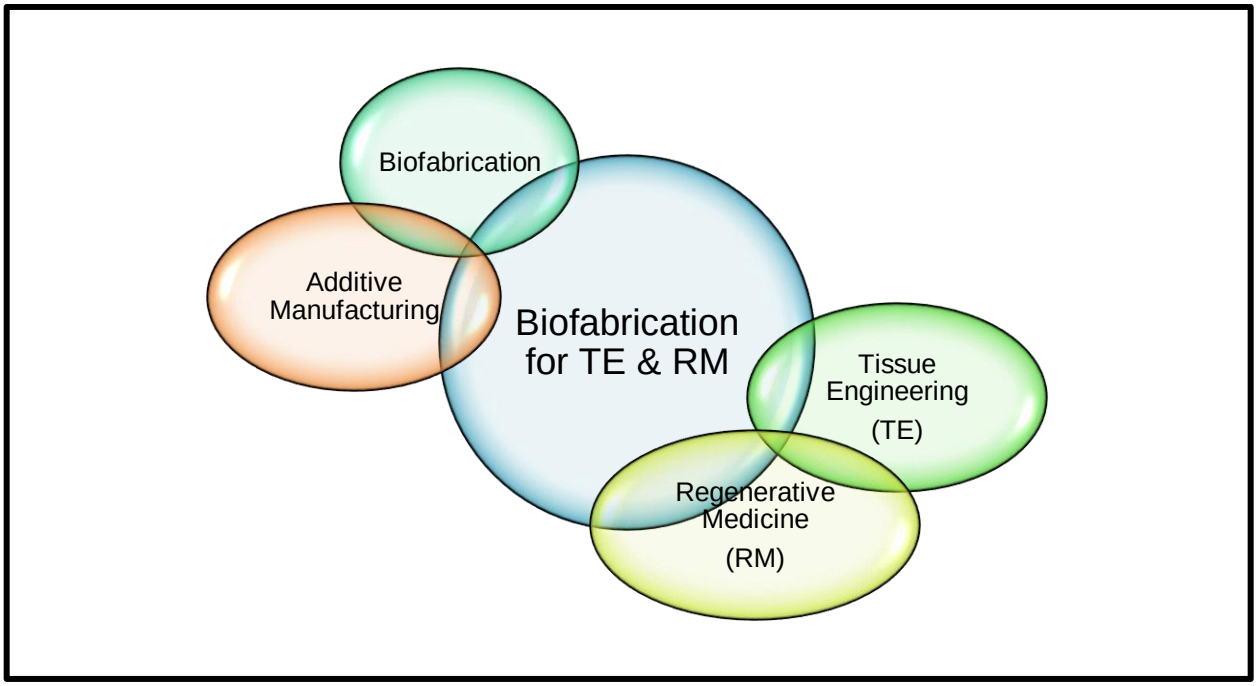

Figure 1.1. Interrelation between Biofabrication, Additive Manufacturing and the Tissue Engineering and Regenerative Medicine fields.

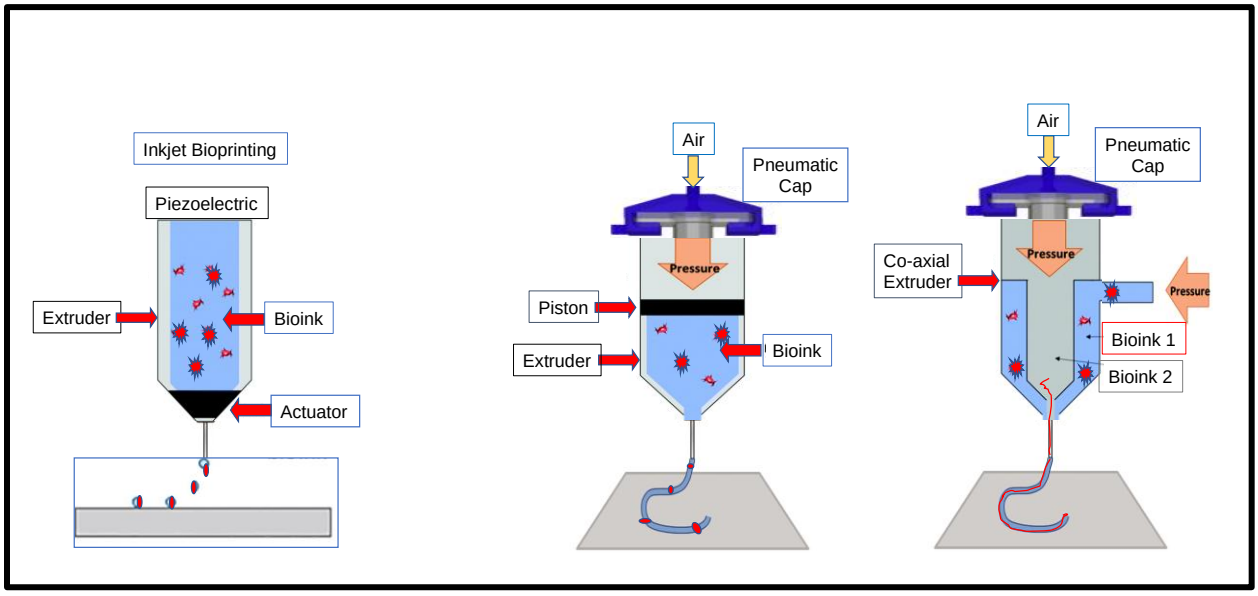

Figure 1.2 Schematic Illustration of Inkjet printing on the left and pneumatic extrusion printing on the right.

CHAPTER II:
FUNCTIONALIZED GRAPHENE NANOPARTICLES INDUCE HUMAN MESENCHYMAL STEM CELLS TO EXPRESS DISTINCT EXTRACELLULAR MATRIX PROTEINS MEDIATING OSTOGENESIS

The versions of this chapter was originally published by Steven Newby:

Steven Newby[a,b], Tom Masi[c], Christopher D. Griffin[d], William J. King[d], Anna Chipman[a], Stacy Stephenson[c], David E. Anderson[a], Alexandru S. Biris[d], Shawn E. Bourdo[d, *], Madhu Dhar[a, *]

This article was published by International Journal of Nanomedicine 2020:15 2501–2513 2501 http://doi.org/10.2147/IJN.S245801 DovePress Material fabrication and characterization of physical and chemical properties were carried out by listed authors from the Center for Integrative Nanotechnology Sciences at the University of Arkansas at Little Rock (UALR). The biologic assessment of the material through *in vitro* experimentation was conducted at the University of Tennessee in Knoxville.

Affiliations:
[a] College of Veterinary Medicine, University of Tennessee, Knoxville, TN 37996, USA
[b] Comparative and Experimental Medicine, University of Tennessee, Knoxville, TN 37996, USA
[c] University of Tennessee Graduate School of Medicine, Knoxville, TN, 37996, USA
[d] Center for Integrative Nanotechnology Sciences, University of Arkansas at Little Rock, Little Rock, AR, 72204, USA

Co - Corresponding authors:
Madhu Dhar, Ph.D., College of Veterinary Medicine, University of Tennessee, 2407 River Dr. Knoxville, Tennessee 37996, USA; email: mdhar@utk.edu; phone: 865-974-5703; Fax: 865-974-5773

Shawn Bourdo, PhD., Center for Integrative Nanotechnology Sciences, University of Arkansas at Little Rock, Little Rock, AR, 72204, USA; email: sxbourdo.ualr.edu; phone: 501-683-7222; Fax: 501-683-7601

Abstract

Purpose: The extracellular matrix (ECM) labyrinthine network secreted by mesenchymal stem cells, provides a microenvironment to enhance cell adherence, proliferation, viability, and differentiation. The potential of graphene-based nanomaterials to mimic tissue –specific ECM has been recognized in designing bone tissue engineering scaffolds. In this study, we investigated the expression of specific ECM proteins when human fat derived adult MSCs adhered and underwent osteogenic differentiation in presence of functionalized graphene nanoparticles.

Methods: Graphene nanoparticles with 6-10% oxygen content were prepared and characterized by XPS, FTIR, AFM and Raman spectroscopy. Calcein-am and crystal violet staining were performed to evaluate viability and proliferation of human fat –derived MSCs on graphene nanoparticles. Alizarin red staining and quantitation was used to determine the effect of graphene nanoparticles on osteogenic differentiation. Finally, immunofluorescence assays were used to investigate the expression of ECM proteins during cell adhesion and osteogenic differentiation.

Results: Our data shows that in presence of graphene, MSCs express specific integrin heterodimers, and exhibit a distinct pattern of the corresponding bone - ECM proteins, primarily fibronectin, collagen I and vitronectin. Furthermore, MSCs undergo osteogenic differentiation spontaneously without any chemical induction, suggesting that the physicochemical properties of graphene nanoparticles might trigger the expression of bone-specific ECM.

Conclusion: Understanding the cell-graphene interactions resulting in an osteogenic niche for MSCs will significantly improve the application of graphene nanoparticles in bone repair and regeneration.

Keywords: Graphene nanoparticles; functionalized graphene, human mesenchymal stem cells, extracellular matrix, fibronectin, collagen I, osteogenic niche

Introduction

Bone tissue engineering scaffolds designed to utilize cell therapies function as delivery vehicles for osteoprogenitor cells and display their ability to attenuate the biological function of cells capable of osteogenic differentiation. Biomimetic scaffolds are dynamic, and their function is dependent on the interactions between the biomaterial and the cells (Sanz-Herrera and Reina-Romo 2011). These cells can be endogenous and be recruited from the tissues in which the scaffold is implanted, or exogenous cells delivered to the site of injury. Cell adhesion to the scaffolds triggers signals that can ultimately affect bone cell formation, referred to as osteogenic differentiation.

Adult mesenchymal stem cells have emerged as a therapeutic modality in various realms of regenerative medicine and are the preferred cells for bone-tissue engineering. Compared to embryonic or induced pluripotent stem cells, the use of adult MSCs avoids ethical concerns and the cells can be obtained relatively easily from a variety of adult tissues. MSCs are typically isolated from bone marrow but can also be isolated from whole blood, umbilical cord blood, dental pulp, skin and adipose tissue. MSCs are spindle shaped, adherent, fibroblast-like cells that can be expanded in tissue culture to generate primary cultures (Caplan 2007, Bieback, Kern et al. 2008). Tissue culture expanded MSCs are a heterogenous population of cells, a subset of which have the potential to differentiate into osteoblasts (bone forming cells), *in vitro* and *in vivo*, when placed in an osteogenic environment. Hence, MSCs are a reliable and preferred source of osteoprogenitors (Pittenger, Mackay et al. 1999, Dominici, Le Blanc et al. 2006).

The progression of cells into an osteogenic lineage is regulated by the differential expression of osteoblast-associated transcription factors (Runt-related transcription factor 2; Runx2), adhesion molecules (integrins β1/ITGB1), and extracellular matrix (ECM) proteins (fibronectin, collagen I) (Daley, Peters et al. 2008, Frantz, Stewart et al. 2010, He, Jiang et al. 2013, Wan, Lu et al. 2013). During osteogenic differentiation, cells initiate the synthesis of ECM, and express osteocyte-specific markers such as alkaline phosphatase, osteopontin and osteocalcin, thus enabling the cell to progress through

bone cell development. ECM is the non-cellular component present within all tissues and organs, providing structural support, promoting cell migration and adhesion, and triggering cell differentiation. ECM is tissue-specific in its composition and topology and determines the “tissue – specific” niche. For instance, bone ECM consists of a specific and unique organization of collagen I fibers and hydroxyapatite (Alford, Kozloff et al. 2015). Collagen I makes up more than 90% of the organic phase of bone, and the remaining 10% consists of proteins including fibronectin, laminin and vitronectin. Fibronectin, the major non-collagenous ECM protein, is ubiquitously expressed and contributes to the construction and organization of the ECM, having a significant role in cell adhesion and differentiation. Vitronectin works with fibronectin to promote cell adhesion and proliferation at early stages of the cell–material interaction processes (Felgueiras, Evans et al. 2015). Vinculin is a component of focal adhesions has a major role in both the cell-to-cell and cell-to-matrix adhesion physiology. Vinculin also plays an important role in the control of binding of actin filaments in cell adhesion to the matrix (Bays and DeMali 2017).

Since ECM is tissue – specific, in bone tissue engineering particular attention has recently been given to the study of bone-specific ECM (structure, topography and biological composition). Hence, interest has shifted from inert biomaterials to constructs that are biomimetic with the native bone ECM (Curry, Pensa et al. 2016). These constructs can be generated either by adding MSCs (osteoprogenitors), specific growth factors (VEGF, PDGF etc.), coating bone - specific ECM proteins such as fibronectin and vitronectin (Mistry and Mikos 2005, Khademhosseini, Vacanti et al. 2009, Kundu, Khatiwala et al. 2009)onto the surface of scaffolds, or by using inherently bioactive scaffolds alone with physicochemical properties to match the native ECM. The use of specific growth factors can be expensive and using protein coatings alone does not result in a composition, function, microstructure, and architecture that is sufficiently similar to native ECM. Therefore, the long-term goal of bone tissue engineering is to develop scaffolds that can create an “osteogenic” or “bone –specific niche” for cells by inducing the expression of bone - specific ECM proteins.

Despite the lack of knowledge on the *in vivo* function of MSCs, it is widely believed that they are crucial for tissue homeostasis and regeneration in mammals

(Nombela-Arrieta, Ritz et al. 2011). As such, MSCs are the preferred choice for use in bone tissue engineering. When MSCs are implanted *in vivo*, their survival, proliferation, differentiation and fate are dependent on the microenvironment or "niche" in which they are placed. Cell fate is dictated not only by the ECM of the environment, but also by the response of the MSCs to the environment. When exogenous MSCs interact with biomimetic scaffolds, they can trigger the endogenous cells to produce ECM, or the MSCs themselves can express ECM proteins to form the matrix (Daley, Peters et al. 2008, Frantz, Stewart et al. 2010, Assis-Ribas, Forni et al. 2018, Carvalho, Silva et al. 2019) . Thus, understanding the niche signals that are triggered, e.g., evaluating the ECM that is generated when MSCs are implanted in a bone defect will help the consistency and efficacy of bone tissue engineering and regenerative medicine approaches (Gattazzo, Urciuolo et al. 2014).

Biomaterials for bone tissue engineering should be biocompatible, biodegradable, and bioactive as determined by their ability to be osteoinductive, osteoconductive, and be osseointegrated *in vivo*. Biomaterials fabricated into nanoscale (1-100 nm) structures (nanomaterials) have been shown to mimic the native ECM and thus, promote cell adhesion and osteogenic differentiation. Nanomaterials have been shown to have increased bioactivity for bone regeneration compared to their micron-sized counterparts and hence, warrant study as new types of biomaterials potentially useful for bone repair (Zhang, Li et al. 2011, Grattoni, Tasciotti et al. 2012, Nosouhian, Razavi et al. 2015). The use of nanomaterials as scaffolds has the potential to enhance the mechanical stability, biocompatibility, and cellular survival of implanted constructs. Graphene-based nanomaterials have recently been recognized as useful components of bone tissue engineering scaffolds. Graphene derivatives are preferred over the pristine form and can be produced relatively easily by functionalization of pristine graphene, with the ultimate goal of reducing pristine graphene's toxicity and increasing its usability in biomedical applications (Dubey, Bentini et al. 2015, Majeed, Bourdo et al. 2017). Graphene derivatives, including nano-sheets, ribbons, and low/high/partially oxidized graphene, graphene oxide and reduced graphene oxide have varying physical and chemical properties and minimal to no toxicity. (Mao, Laurent et al. 2013) These iterations can be used as components of biocompatible and biomimetic scaffolds

specifically for bone tissue engineering (Zhang, Wang et al. 2016, Zhang, Wei et al. 2016). Therefore, despite the concerns due to toxicity, graphene-based nanomaterials and scaffolds have been used successfully in bone tissue engineering (Dervishi, Li et al. 2009, Mahmood, Casciano et al. 2010, Nayak, Jian et al. 2010, Nayak, Andersen et al. 2011, Wang, Ruan et al. 2011, Mahmood M. 2013, Elkhenany, Amelse et al. 2015, Jeong, Choi et al. 2016, Majeed, Bourdo et al. 2016, Bourdo, Al Faouri et al. 2017, Elkhenany, Bourdo et al. 2017).

Our laboratory has demonstrated that a low oxygen (6-10%) functionalized form of graphene nanocomposite (LOG – low oxygen graphene) is cytocompatible and exhibits osteoinductive effects *in vitro* and osteoconductive effects *in vivo* when used with fat-derived goat MSCs (Elkhenany, Amelse et al. 2015, Elkhenany, Bourdo et al. 2017). The aim of the current study was to evaluate the effect of low oxygen graphene nanoparticles on cellular adhesion and osteogenic differentiation of human adipose tissue derived MSCs (hMSCs), with a focus on the spatiotemporal expression profiles of ECM proteins during these processes. Our long-term goal is to evaluate the signaling mechanism(s) that are initiated when hMSCs are seeded on graphene nanoparticles, and the current study is the first step in that direction. We hypothesized that the structure and topographical features of functionalized graphene nanoparticles will create an “osteogenic niche” for human MSCs, which will be demonstrated by an attenuation of osteogenic differentiation and the expression and unique distribution pattern of ECM proteins.

Methods

Isolation, ex vivo Expansion, and Characterization of Human MSCs

Stromal vascular fraction cells were obtained from human adipose tissue from patients undergoing panniculectomies in accordance with a protocol approved by the IRB at the University of Tennessee Medical Center, Knoxville. The hMSCs were isolated, *ex vivo* expanded and characterized as described previously (Alghazali, Newby et al. 2017). All experiments were performed using cells, from passages 2

through 6 only, and were incubated in complete growth media (DMEM/F12, 1% penicillin-streptomycin/amphotericin B, 10% FBS).

MSCs obtained were confirmed by their morphology, potential to undergo tri-lineage differentiation, and expression of specific protein markers, using methods reported previously (Dominici, Le Blanc et al. 2006, Alghazali, Newby et al. 2017). *In vitro* experiments were carried out simultaneously on control (polystyrene or plastic) and graphitic surfaces. The control substrates were chosen as appropriate for the assays under experimentation.

In addition to the basic characterization of hMSCs, the expression of specific integrin heterodimers on their cell surface was evaluated in expanded cells. 1×10^6 of hMSCs were stained with anti-human α2β1, α5β1and αVβ6 (Millipore Sigma), α9β1 and αVβ3 (BioLegend), and αVβ5 (Developmental Studies Hybridoma Bank – University of Iowa), and their corresponding isotype matched controls. The manufacturer's recommended concentrations of antibodies were used. For immunophenotyping, cells were harvested and counted, blocked in 1% goat serum in PBS for 20 minutes at room temperature, then stained with each primary antibody for 20 minutes at room temperature in the dark. Subsequently, cells were washed with PBS, collected by centrifugation and then incubated with either IgG1/APC or IgG2b/PE (Biolegend) secondary antibodies for 20 minutes at room temperature in the dark. Finally, cells were fixed with 4% paraformaldehyde/PBS for 10 minutes at room temperature in the dark. Roughly 20,000 events from each staining were analyzed using a BD FACS Calibur. The raw data was analyzed by FlowJo software.

Preparation and Characterization of Functionalized Graphene Films

Pristine graphene was modified to produce a low-oxygen functionalized form of graphene (LOG) with 6 to 10% oxygen content as reported previously (Elkhenany, Bourdo et al. 2017, Majeed, Bourdo et al. 2017). Briefly, graphene nanoplatelets (Product # N002-PDR, 1-1.2nm thick, ≤10μm lateral dimensions) were purchased from Angstron Materials (Dayton, OH) and subjected to an aqueous acidic environment (conc H_2SO_4: conc HNO_3: DI-water (volume ratio of 6:2:3) for oxidation.

For coating a surface, a 15 mg mass sample of LOG was mixed with 30 mL of 90% ethanol (200 proof, ACS reagent grade, Acros) /10%ultrapure water (18.2Mohm, 0.055uS/cm). The mixture was bath sonicated for 60 min followed by probe sonication (Sonics Vibra-cell VCX-130 equipped with 6 mm probe tip, 100% power for 60 min in pulses of 5sec ON, 5sec OFF). The dispersed material was then dropped using a micropipette onto individual 15 mm plastic coverslips or in each well of a 12 well plate, to give a coating of 0.21mg/cm^2.

The physico-chemical nature of the LOG nanoparticles was confirmed by X-ray photoelectron spectroscopy (XPS), structural analysis by Raman spectroscopy, functional group analysis by infrared (FTIR) spectroscopy, and the surface roughness after coating of substrates was evaluated using atomic force microscopy (AFM). XPS, Raman, and FTIR analyses were carried out as described previously (Bourdo, Al Faouri et al. 2017, Majeed, Bourdo et al. 2017). Briefly, XPS was performed on powder samples placed on double-sided tape on a glass substrate, and their elemental composition was studied using a Thermo K-alpha (Waltham, MA) XPS. IR was performed on pressed pellets made from LOG powder sample and KBr using a Thermo Scientific FTIR Nicolet Model 6700 Spectrometer (Waltham, MA). Raman measurements were performed on samples of graphene powders placed on a silicon substrate using a 514 nm laser with Horiba Jobin Yvon LabRam 800 Micro-Raman (Edison, NJ). For AFM, the scans were obtained using tapping mode (3.90 V) at 0.5 Hz and 256 lines, with integral gains between 0.5 and 2.5 and amplitude setpoint averaging around 19 nm. Three different 50µm x 50µm randomly selected regions (edge, middle, and the center) were selected. The scans were then analyzed for surface roughness using NanoScope Analysis 1.5 (Bruker) software. Each surface scan was analyzed with the selection command across at least two dimensions to determine average roughness, Ra and root mean square, Rq.

In vitro Cell Viability and Proliferation on LOG Nanoparticles

Cell viability and proliferation of hMSCs on LOG was evaluated using two independent assays over a study period of 8 days. Calcein-am fluorescence imaging,

and crystal violet staining and quantitation were used, as described previously (Feoktistova, Geserick et al. 2016, Austin Bow 2019).

Cell viability on LOG was assessed using calcein-am staining as per the manufacturer's recommendations. Briefly, $25X10^3$ / cm^2 hMSCs were seeded on LOG and control substrates and were incubated with a 2µg/mL calcein-am/dimethyl sulfoxide mix in HBSS at 37^0 for 5 minutes at 2, 4, 6 and 8 days post seeding. Green, fluorescent staining was visualized and imaged using All-in-one Microscope BZ-X700 (Keyence).

Crystal violet staining and quantitation was used to determine changes in cell mass reflecting cell viability (Feoktistova, Geserick et al. 2016). For staining, at 2-, 4-, 6- and 8-days post-seeding, cells were fixed for 10 min with 4% paraformaldehyde/PBS. The fixed cells were stained with a 0.1% crystal violet solution in deionized water for 30 min at room temperature then washed three times with deionized water. Crystal violet-stained cells were visualized and imaged using All-in-one Microscope BZ-X700 (Keyence). For quantitation, the stain was dissolved in 10% acetic acid and quantified by measuring the absorbance at 595 nm (Synergy HT). Data was plotted and statistics performed in Prism (Graphpad).

Osteogenic Differentiation and Mineralization

For osteogenic differentiation, hMSCs at a seeding density of $25X10^3$ cells/cm^2 were induced to undergo differentiation by exposing to complete growth media supplemented with 100nM dexamethasone, 10nM β-glycerophosphate and 155µM ascorbic acid. At 21 days, cells were fixed in 4% paraformaldehyde/PBS for 10 minutes at room temperature and stained with alizarin red to detect calcium in the osteoblasts. The accumulation of calcium in hMSCs was quantitated by the elution of alizarin red dye with 10% cetylpyridium chloride and the color was read at 570 nm (Elkhenany, Amelse et al. 2016). Background readings due to the substrates alone without any cells were subtracted from the sample readings to eliminate nonspecific values. Data was plotted and statistics performed in Prism (Graphpad).

Cytoskeletal Organization and ECM Proteins

Cytoskeletal organization and MSC morphology were assessed by evaluating the expression patterns of F-actin and vimentin using previously reported methods (Alghazali, Newby et al. 2017). The expression of ECM proteins during cell attachment (i.e., within 24hrs of seeding) and osteogenic differentiation (21 days after seeding) was assessed qualitatively by immunofluorescence detection assays. A panel of ECM proteins including, two distinct fibronectin antibodies, 181 and 182, vitronectin, collagen I and II, laminin and vinculin were used. Briefly, hMSCs at specified time points were fixed with 4% paraformaldehyde at room temperature for 10 minutes, permeabilized with 0.1% Triton X-100 in HBSS at room temperature for 10 minutes, and subsequently blocked with the Universal Blocking Reagent (BioGenex) for 30 minutes at room temperature. Cells were incubated with 1-2ug of all primary antibodies and samples were incubated at 4°C for 24 hours. Alexa Fluor 594 phalloidin (A12381; Invitrogen), Vimentin (#550513; BD Pharmingen), Collagen I (#ab3470; Abcam), Collagen II (#ab34712; Abcam), Fibronectin 181 (MAB19172; R&D Systems), Fibronectin 182 (#MAB19182; R&D Systems), Vinculin (#ab129002; Abcam), Vitronectin (#ab113700; Abcam), and Laminin (#MAB2144; R&D Systems). The cells were washed and incubated with appropriate Alexa Fluor – labelled secondary anti-mouse or anti-rabbit antibodies at room temperature for 30 minutes in dark. Alexa Fluor 594 Phalloidin was preconjugated and hence, did not require any secondary antibody treatment step. The cells were washed twice and mounted on microscope slides with a drop of Prolong Gold antifade reagent with 4′, 6-diamidino-2-phenylindole (DAPI; Molecular Probes by Life Technologies). The cells were analyzed under a fluorescence microscope (Leica DMi8).

Results

Pristine Graphene was Functionalized to Produce LOG Nanoparticles

Pristine graphene was functionalized to improve dispersibility, and a form containing 6 to 10% oxygen was synthesized. This is referred to as low-oxygen graphene (LOG). The LOG nanoparticles used in these experiments are distinct from commercially available graphene oxide and reduced graphene oxide forms and have been extensively characterized and distinguished from the other forms, as described previously (Bourdo, Al Faouri et al. 2017, Majeed, Bourdo et al. 2017, Nima, Vang et al. 2019). The functionalized form of graphene was characterized by a variety of physicochemical techniques. The XPS spectrum shows distinct photoemission peaks corresponding to C1s at 284.8eV, O1s at 533eV, N1s at 405eV, S2p at 164eV, with an average elemental composition of 88.73% carbon, 10.57% oxygen, and <0.5% of nitrogen and sulfur (remaining from reagents used during the oxidation procedure); thus, confirming that the synthesized form of graphene nanoparticles are indeed LOG. Further details from the XPS spectrum demonstrate the types of functional groups present in the samples. Both carbon (C1s) and oxygen (O1s) narrow scan spectra were collected and analyzed. After fitting analysis, the C1s narrow scan exhibited peaks at 248.78eV (aliphatic/aromatic C), 286.14eV (C-O), 287.26eV (C=O), 288.83eV (carboxyl, O-C=O), and 290.70 eV for $\pi-\pi^*$ shakeup satellite peak. For the oxygen scan (O1s), 2 main underlying peaks are present at 532.06eV for O-C and 533.69eV for O=C (Datsyuk V 2008, Yang D 2009). This data suggests a predominantly carbon – rich sample with hydroxyl, carbonyl, and carboxyl functional groups on the surface.

In addition to XPS, Raman and infrared spectroscopy were used to characterize the graphene material. Raman spectroscopy provides information on the lattice structure of the materials and is displayed in Figure1D. The main spectral features are observed at approximately 1350 cm^{-1}, 1600 cm^{-1}, and 2700 cm^{-1} corresponding to the D-, G-, and 2D-bands, respectively (Malard, Pimenta et al. 2009). By analyzing the intensity of the D- and G-bands, the defect nature of the material was determined. The nanoparticles generated in this study displayed an I_D/I_G ratio of 1.34, which is consistent with other published reports from our group on this form of graphene. The FTIR spectra

shown in Figure 1E provided evidence of oxygen functional groups, such as hydroxyl groups by stretching mode at ~3400cm^{-1} and bending mode at ~1400cm^{-1}. Carbon-hydrogen and C-OH stretches are seen in the 2950–2850 cm^{-1} region and in the 1200–1050 cm^{-1}region, respectively. Carbonyl stretching mode was present at ~1720cm^{-1}, with sp^2 stretching from the extensive hexagonal carbon framework observed at 1630 cm^{-1}(Wojtoniszak, Chen et al. 2012). These vibrational modes observed in FTIR, coupled with results from Raman and XPS confirm that the synthesized form of graphene nanoparticles are indeed LOG as described previously (Bourdo, Al Faouri et al. 2017, Majeed, Bourdo et al. 2017, Nima, Vang et al. 2019).

LOG Nanoparticles Exhibit Rough Surface

Surface roughness was evaluated using atomic force microscopy. AFM images show that the LOG surface had mean roughness values of ~630nm Rq (or RMS, root mean square) and ~460 nm Ra (average roughness), suggesting potential sites for cell attachment.

Progenitor Cells are MSCs and Express Specific Integrin Heterodimers

Fibroblast morphology and tri-lineage differentiation patterns of primary cultures generated from the human stromal vascular fraction confirm the MSC nature of cells as described previously (Alghazali, Newby et al. 2017). Of relevance to this study, the integrin heterodimer profile of MSCs was compared between tissue culture polystyrene substrate and LOG surfaces. Data shows that the expression pattern is conserved on both substrates. Specifically, there was a >90% expression of α2β1, αVβ5, α5β1 and α5β3 heterodimers on both surfaces, suggesting that the adhesion of hMSCs on the LOG surface is similar to that of the polystyrene surface and could be mediated via any one or a combination of these heterodimeric integrin subunits.

LOG Surface is Cytocompatible

Calcein – am staining and fluorescence imaging was used to confirm cell viability as well as distribution of hMSCs on LOG surface at specific time points (**Figure 2.1a**). Calcein – am is a fluorogenic, cell-permeant probe that indicates cellular health. Native Calcein-am is non-fluorescent and shows a green fluorescence only when it reacts with the esterase's that are present within live, healthy cells. As a result, the green, fluorescent signal indicates cell viability. Additionally, data shows that hMSCs were healthy, viable and subjectively grew in population over a period of 8 days. Cells showed a distinct pattern of adhesion and clustering on LOG surfaces relative to the random distribution observed on tissue culture polystyrene substrate. This pattern could be due to the clustering of cells to specific areas of LOG surfaces or that the graphene coating in those areas is too dark to image cells. In any case, the cells that are imaged appear healthy and hence, the LOG surface was deemed cytocompatible.

Crystal violet staining (**Figure 2.1b**) and quantitation (**Figure 2.1c**) were used to evaluate cell proliferation. Data showed that cells adhered to LOG surface and proliferated with time and the cell numbers were comparable with tissue culture polystyrene substrate, further supporting the Calcein-am staining and confirming the cytocompatibility of LOG surfaces.

LOG Nanoparticles Inherently Induce Osteogenic Differentiation

In view of the data from our previously published study (Elkhenany, Amelse et al. 2015, Elkhenany, Bourdo et al. 2017), osteogenic differentiation and mineralization of hMSCs on LOG surfaces was assessed using Alizarin red staining and quantitation (**Figure 2.2**). Data shows that hMSCs seeded on LOG nanoparticles, demonstrated significantly greater calcium content relative to the cells on the control surface ($p=0.0018$). Interestingly, this upregulation was observed in the absence of any osteogenic inducing reagents (dexamethasone, beta-glycerophosphate or ascorbic acid), suggesting that the LOG surface induces accumulation of calcium in MSCs spontaneously, i.e., induces osteogenic differentiation *in vitro*. Calcium content was further enhanced ($p=0.0088$) in hMSCs on LOG when osteogenic inducers were added to the media. This increase was similar and as expected to that observed in hMSCs

seeded on the control surface in the presence of the osteogenic inducers (p=0.05), suggesting a potential synergistic effect of LOG nanoparticles and the osteogenic inducing reagents.

In order to study the osteoinductive effect of LOG nanoparticles without any interference from the osteogenic inducers, *in vitro* assays described below were carried out in the absence of osteogenic inducers and in growth media only. Correspondingly, to maintain the uniformity of the osteogenic status of the cells, hMSCs on the control substrates were differentiated in the growth media supplemented with the osteogenic inducers.

Human MSCs Display Cytoskeletal Integrity on LOG Surfaces

Cytoskeletal health and integrity of hMSCs was further confirmed on LOG surfaces by visualizing F actin filaments using a fluorescent derivative of Phalloidin. Fetal bovine serum in the cell media (growth and osteogenic media) is the main source of proteins that can adsorb onto a biomaterial and stimulate production of ECM. As a result, cytoskeletal integrity and morphology of hMSCs was evaluated in varying concentrations of FBS, ranging from 0% - 10%. Cells were fixed 24hrs post seeding and morphological evaluation of F-actin fluorescence showed that hMSCs on LOG in media containing 2, 5 and 10% FBS were relatively healthy and displayed robust cytoskeletal morphology. Cells in absence of FBS (0%) appeared rounded and unhealthy. Although cells survived the 2, 5 and 10% FBS media on LOG surface, corresponding cells on the control surface appeared unhealthy, were not viable and did not proliferate in media with <10% FBS (data not shown). In order to maintain identical cell culture conditions, hMSCs were seeded on both the control and LOG surfaces in media containing 10% FBS in all subsequent experiments. The cytoskeletal integrity of cells was first confirmed at 24hrs during cell adhesion e, and subsequently, during osteogenic differentiation at day 21.

Simultaneous to the above experiments, we ensured that the stem cell nature of hMSCs was maintained throughout the study period by evaluating the expression of vimentin, a mesenchymal stem cell marker (Secunda, Vennila et al. 2015). Data confirmed that hMSCs adhered to the LOG surface and expressed vimentin confirming

that hMSCs did not lose their “stem cell” characteristics during the cell culture process on LOG surfaces.

ECM Proteins are Expressed on LOG Surfaces

In order to evaluate the expression of ECM proteins that might be contributed by the serum in the media, IF assays were carried out on LOG surface in the absence of cells and only in presence of 10% FBS-containing media at 24 hours and at day 21. The expression patterns of collagen I, collagen II, fibronectin, laminin, vinculin, and vitronectin were evaluated. IF analyses on the LOG surface did not show the expression of any ECM proteins in the absence of hMSCs in any of the samples tested, clearly demonstrating that the serum proteins do not contribute to the ECM on LOG surface and hence, do not have a role in cell adhesion or differentiation.

Next, we evaluated the expression of ECM proteins when hMSCs were seeded on the LOG surface (**Figure 2.3**). The expression patterns were evaluated at 24hrs to assess the ECM proteins involved in cell adhesion and at day 21, to evaluate proteins involved in osteogenic differentiation. There was expression and a discrete pattern of distribution for collagen I, fibronectin 182, vinculin and vitronectin was evident within 24hrs post-seeding. Collagen II was weakly expressed and there was no expression of laminin, suggesting that either these proteins are not involved in adhesion and osteogenic differentiation of hMSCs on the LOG surface, or that the specific antibodies did not cross react. Qualitatively, the distribution patterns appeared striking and discrete.

Discussion

In this study, we present *in vitro* data to show that in presence of functionalized graphene nanoparticles with 6-10% oxygen content, human fat-derived MSCs express and secrete a discrete and organized pattern of bone–specific ECM proteins within 24hrs post seeding. This pattern persists throughout the osteogenic differentiation process through day 21. Noteworthy is the fact that these ECM proteins were found only in the presence of hMSCs without any contribution from the FBS present in the media. The cells also expressed specific integrin heterodimers, and, as judged by the

calcium content accumulated in the cells, undergo osteogenic differentiation, suggesting that the interaction between integrin and the corresponding ECM proteins might mediate cell adhesion and subsequent osteogenic differentiation. Most importantly, in the presence of LOG substrates, hMSCs undergo osteogenesis spontaneously without any osteogenic inducers. These results prove our hypothesis that the surface chemistry and topography of LOG nanoparticles create an osteogenic niche for hMSCs, at least in part by inducing the expression of specific ECM proteins and thus, eliminating the need for osteogenic inducing agents.

Graphene nanocomposites that are being developed for bone tissue engineering are intended to serve as ECM analogs, but little is known about the mechanisms by which they regulate cell function. It is possible that similar to gold nanoparticles, graphene nanoparticles may interact with the ECM to up-regulate β1-integrin, generate mechanical stress on the MSCs resulting in activation of the p38 MAPK pathway, and, in turn, may induce spontaneous osteogenic differentiation (Yi, Liu et al. 2010, Nayak, Andersen et al. 2011, Zhang, Lee et al. 2015). Furthermore, osteogenic inducers included in the growth media may create an osteogenic environment for MSCs to commit towards osteoblast lineage. The expression of specific ECM proteins by hMSCs on LOG surfaces potentially provides cues for cells to undergo osteogenic differentiation, the exact signaling mechanism(s) of which needs to be elucidated.

One major challenge in bone tissue engineering is to develop novel scaffolds capable of controlling cell fate. This is the essence of biomimicry. Besides biochemical stimuli, physical properties of scaffolds including, surface patterns, elasticity and nanotopography have been shown to affect osteogenic differentiation of MSCs (Qian, Gong et al. 2017, Goriainov, Hulsart-Billstrom et al. 2018, Metavarayuth, Maturavongsadit et al. 2019). It is possible that the areas of cell clustering observed on LOG nanoparticles overlap with areas of increased surface roughness, and hence, provide an ideal niche for anchoring, proliferation, and potentially osteogenic differentiation and mineralization. Published research supports that rough surfaces allow cells to attach more easily due to the multiple sites for cell–surface interaction and increasing cytoskeletal stresses result in recruitment of more adhesive molecules (Gentile, Tirinato et al. 2010, Tang, Lee et al. 2012). The results of the studies reported

herein demonstrate that attenuation of osteogenesis may be partially due to the rough topography of LOG nanoparticles, further supported by published studies (Deng, Liu et al. 2015, Xu, Liu et al. 2015, Wang, Deng et al. 2016, Damiati, Eales et al. 2018, Zhang, Lin et al. 2018, Zhang, Chen et al. 2018).

Detailed evaluation of F actin staining, and ECM protein expression profiles showed that hMSCs adhered, spread and covered the LOG surface within 24 hours. Distinct areas with filipodia extensions were observed, suggesting tight cell-material interactions. Furthermore, cells arrange in multilayers, and form clusters with time, suggesting that the LOG surface offers some cell guidance, i.e., attachment is not random, but organized. Clustering of hMSCs, a hallmark of osteogenic differentiation (Jackson, Bow et al. 2018) further supports the commitment towards osteoblast lineage, which was confirmed via alizarin red staining and quantitation.

Conclusion

Our data supports our hypothesis and confirms that the LOG nanoparticles used in these studies are cytocompatible, inductive of osteogenic differentiation and, that hMSCs recognize graphene nanoparticles as biomimetic *in vitro* substrates for the purpose of osteogenic cell culture experiments. These results are similar to that previously reported for goat MSCs (Elkhenany, Amelse et al. 2015, Elkhenany, Bourdo et al. 2017). We demonstrate the expression of specific ECM proteins by hMSCs in response to a specific form of LOG graphene nanoparticles. The graphene nanoparticles + MSC constructs provide us with a system that can be used to understand the signaling mechanisms, or cues, that are triggered when MSCs are committed towards the osteogenic lineage. Future experiments using this system will potentially aid in exploring the mechanisms underlying osteogenesis mediated by the specific ECM proteins on LOG nanoparticles, which will further improve the applicability and the use of graphene nanoparticles in bone tissue engineering.

References

Alford, A. I., K. M. Kozloff and K. D. Hankenson (2015). "Extracellular matrix networks in bone remodeling." Int J Biochem Cell Biol 65: 20-31.

Alghazali, K. M., S. D. Newby, Z. A. Nima, R. N. Hamzah, F. Watanabe, S. E. Bourdo, T. J. Masi, S. M. Stephenson, D. E. Anderson, M. S. Dhar and A. S. Biris (2017). "Functionalized gold nanorod nanocomposite system to modulate differentiation of human mesenchymal stem cells into neural-like progenitors." Sci Rep 7(1): 16654.

Assis-Ribas, T., M. F. Forni, S. M. B. Winnischofer, M. C. Sogayar and M. Trombetta-Lima (2018). "Extracellular matrix dynamics during mesenchymal stem cells differentiation." Dev Biol 437(2): 63-74.

Austin Bow, S. N., Rebecca Rifkin, Bailey K. Jackson, Alicia Matavosian, Christopher Griffin, William King, Karrer Alghazali, Anwer Mhannawee, Stuart B. Berryhill, Roy Morello, Silke Hecht, Alexandru S. Biris, David E. Anderson, Shawn E. Bourdo, Madhu Dhar (2019). "Evaluation of a Polyurethane Platform for Delivery of Nanohydroxyapatite and Decellularized Bone Particles in a Porous Three-Dimensional Scaffold." ACS Appl. Bio Mater. 2(5): 1815-1829.

Bays, J. L. and K. A. DeMali (2017). "Vinculin in cell-cell and cell-matrix adhesions." Cell Mol Life Sci 74(16): 2999-3009.

Bieback, K., S. Kern, A. Kocaomer, K. Ferlik and P. Bugert (2008). "Comparing mesenchymal stromal cells from different human tissues: bone marrow, adipose tissue and umbilical cord blood." Biomed Mater Eng 18(1 Suppl): S71-76.

Bourdo, S. E., R. Al Faouri, R. Sleezer, Z. A. Nima, A. Lafont, B. P. Chhetri, M. Benamara, B. Martin, G. J. Salamo and A. S. Biris (2017). "Physicochemical characteristics of pristine and functionalized graphene." J Appl Toxicol 37(11): 1288-1296.

Caplan, A. I. (2007). "Adult mesenchymal stem cells for tissue engineering versus regenerative medicine." Journal of Cellular Physiology 213(2): 341-347.

Carvalho, M. S., J. C. Silva, J. M. S. Cabral, C. L. da Silva and D. Vashishth (2019). "Cultured cell-derived extracellular matrices to enhance the osteogenic differentiation and angiogenic properties of human mesenchymal stem/stromal cells." J Tissue Eng Regen Med 13(9): 1544-1558.

Curry, A. S., N. W. Pensa, A. M. Barlow and S. L. Bellis (2016). "Taking cues from the extracellular matrix to design bone-mimetic regenerative scaffolds." Matrix Biol 52-54: 397-412.

Daley, W. P., S. B. Peters and M. Larsen (2008). "Extracellular matrix dynamics in development and regenerative medicine." J Cell Sci 121(Pt 3): 255-264.

Damiati, L., M. G. Eales, A. H. Nobbs, B. Su, P. M. Tsimbouri, M. Salmeron-Sanchez and M. J. Dalby (2018). "Impact of surface topography and coating on osteogenesis and bacterial attachment on titanium implants." J Tissue Eng 9: 2041731418790694.

Datsyuk V, K. M., Papagelis K, Parthenios J, Tasis D, Siokou A, Kallitsis I, Galiotis C. (2008). "Chemical oxidation of multiwalled carbon nanotubes." Carbon 46: 833-840.

Deng, Y., X. Liu, A. Xu, L. Wang, Z. Luo, Y. Zheng, F. Deng, J. Wei, Z. Tang and S. Wei (2015). "Effect of surface roughness on osteogenesis in vitro and osseointegration in vivo of carbon fiber-reinforced polyetheretherketone-nanohydroxyapatite composite." Int J Nanomedicine 10: 1425-1447.

Dervishi, E., Z. R. Li, F. Watanabe, A. Biswas, Y. Xu, A. R. Biris, V. Saini and A. S. Biris (2009). "Large-scale graphene production by RF-cCVD method." Chemical Communications(27): 4061-4063.

Dominici, M., K. Le Blanc, I. Mueller, I. Slaper-Cortenbach, F. C. Marini, D. S. Krause, R. J. Deans, A. Keating, D. J. Prockop and E. M. Horwitz (2006). "Minimal criteria for defining multipotent mesenchymal stromal cells. The International Society for Cellular Therapy position statement." Cytotherapy 8(4): 315-317.

Dubey, N., R. Bentini, I. Islam, T. Cao, A. H. Castro Neto and V. Rosa (2015). "Graphene: A Versatile Carbon-Based Material for Bone Tissue Engineering." Stem Cells Int 2015: 804213.

Elkhenany, H., L. Amelse, M. Caldwell, R. Abdelwahed and M. Dhar (2016). "Impact of the source and serial passaging of goat mesenchymal stem cells on osteogenic differentiation potential: implications for bone tissue engineering." J Anim Sci Biotechnol 7: 16.

Elkhenany, H., L. Amelse, A. Lafont, S. Bourdo, M. Caldwell, N. Neilsen, E. Dervishi, O. Derek, A. S. Biris, D. Anderson and M. Dhar (2015). "Graphene supports in vitro proliferation and osteogenic differentiation of goat adult mesenchymal stem cells: potential for bone tissue engineering." J Appl Toxicol 35(4): 367-374.

Elkhenany, H., S. Bourdo, S. Hecht, R. Donnell, D. Gerard, R. Abdelwahed, A. Lafont, K. Alghazali, F. Watanabe, A. S. Biris, D. Anderson and M. Dhar (2017). "Graphene nanoparticles as osteoinductive and osteoconductive platform for stem cell and bone regeneration." Nanomedicine 13(7): 2117-2126.

Felgueiras, H. P., M. D. M. Evans and V. Migonney (2015). "Contribution of fibronectin and vitronectin to the adhesion and morphology of MC3T3-E1 osteoblastic cells to poly(NaSS) grafted Ti6Al4V." Acta Biomater 28: 225-233.

Feoktistova, M., P. Geserick and M. Leverkus (2016). "Crystal Violet Assay for Determining Viability of Cultured Cells." Cold Spring Harb Protoc 2016(4): pdb prot087379.

Frantz, C., K. M. Stewart and V. M. Weaver (2010). "The extracellular matrix at a glance." J Cell Sci 123(Pt 24): 4195-4200.

Gattazzo, F., A. Urciuolo and P. Bonaldo (2014). "Extracellular matrix: a dynamic microenvironment for stem cell niche." Biochim Biophys Acta 1840(8): 2506-2519.

Gentile, F., L. Tirinato, E. Battista, F. Causa, C. Liberale, E. M. di Fabrizio and P. Decuzzi (2010). "Cells preferentially grow on rough substrates." Biomaterials 31(28): 7205-7212.

Goriainov, V., G. Hulsart-Billstrom, T. Sjostrom, D. G. Dunlop, B. Su and R. O. C. Oreffo (2018). "Harnessing Nanotopography to Enhance Osseointegration of Clinical Orthopedic Titanium Implants-An in Vitro and in Vivo Analysis." Front Bioeng Biotechnol 6: 44.

Grattoni, A., E. Tasciotti, D. Fine, J. S. Fernandez-Moure, J. Sakamoto, Y. Hu, B. Weiner, M. Ferrari and S. Parazynski (2012). "Nanotechnologies and regenerative medical approaches for space and terrestrial medicine." Aviat Space Environ Med 83(11): 1025-1036.

He, J., B. Jiang, Y. Dai, J. Hao, Z. Zhou, Z. Tian, F. Wu and Z. Gu (2013). "Regulation of the osteoblastic and chondrocytic differentiation of stem cells by the extracellular matrix and subsequent bone formation modes." Biomaterials 34(28): 6580-6588.

Jackson, B. K., A. J. Bow, G. Kannarpady, A. S. Biris, D. E. Anderson, M. Dhar and S. E. Bourdo (2018). "Polyurethane/nano-hydroxyapatite composite films as osteogenic platforms." J Biomater Sci Polym Ed 29(12): 1426-1443.

Jeong, J. T., M. K. Choi, Y. Sim, J. T. Lim, G. S. Kim, M. J. Seong, J. H. Hyung, K. S. Kim, A. Umar and S. K. Lee (2016). "Effect of graphene oxide ratio on the cell adhesion and growth behavior on a graphene oxide-coated silicon substrate." Sci Rep 6: 33835.

Khademhosseini, A., J. P. Vacanti and R. Langer (2009). "Progress in tissue engineering." Sci Am 300(5): 64-71.

Kundu, A. K., C. B. Khatiwala and A. J. Putnam (2009). "Extracellular matrix remodeling, integrin expression, and downstream signaling pathways influence the osteogenic differentiation of mesenchymal stem cells on poly(lactide-co-glycolide) substrates." Tissue Eng Part A 15(2): 273-283.

Mahmood, M., D. A. Casciano, T. Mocan, C. Iancu, Y. Xu, L. Mocan, D. T. Iancu, E. Dervishi, Z. R. Li, M. Abdalmuhsen, A. R. Biris, N. Ali, P. Howard and A. S. Biris (2010).

"Cytotoxicity and biological effects of functional nanomaterials delivered to various cell lines." Journal of Applied Toxicology 30(1): 74-83.

Mahmood M., V., H., Dervishi, E. et al. (2013). "Role of the carbonaceous nanomaterials in stimulation of osteogenesis in mammalian bone cells." Journal of Materials Chemistry B: 3220-3230.

Majeed, W., S. Bourdo, D. M. Petibone, V. Saini, K. B. Vang, Z. A. Nima, K. M. Alghazali, E. Darrigues, A. Ghosh, F. Watanabe, D. Casciano, S. F. Ali and A. S. Biris (2016). "The role of surface chemistry in the cytotoxicity profile of graphene." J Appl Toxicol.

Majeed, W., S. Bourdo, D. M. Petibone, V. Saini, K. B. Vang, Z. A. Nima, K. M. Alghazali, E. Darrigues, A. Ghosh, F. Watanabe, D. Casciano, S. F. Ali and A. S. Biris (2017). "The role of surface chemistry in the cytotoxicity profile of graphene." J Appl Toxicol 37(4): 462-470.

Malard, L. M., M. A. Pimenta, G. Dresselhaus and M. S. Dresselhaus (2009). "Raman spectroscopy in graphene." Physics Reports-Review Section of Physics Letters 473(5-6): 51-87.

Mao, H. Y., S. Laurent, W. Chen, O. Akhavan, M. Imani, A. A. Ashkarran and M. Mahmoudi (2013). "Graphene: promises, facts, opportunities, and challenges in nanomedicine." Chem Rev 113(5): 3407-3424.

Metavarayuth, K., P. Maturavongsadit, X. Chen, P. Sitasuwan, L. Lu, J. Su and Q. Wang (2019). "Nanotopographical Cues Mediate Osteogenesis of Stem Cells on Virus Substrates through BMP-2 Intermediate." Nano Lett 19(12): 8372-8380.

Mistry, A. S. and A. G. Mikos (2005). "Tissue engineering strategies for bone regeneration." Adv Biochem Eng Biotechnol 94: 1-22.

Nayak, T. R., H. Andersen, V. S. Makam, C. Khaw, S. Bae, X. Xu, P. L. Ee, J. H. Ahn, B. H. Hong, G. Pastorin and B. Ozyilmaz (2011). "Graphene for controlled and accelerated osteogenic differentiation of human mesenchymal stem cells." ACS Nano 5(6): 4670-4678.

Nayak, T. R., L. Jian, L. C. Phua, H. K. Ho, Y. P. Ren and G. Pastorin (2010). "Thin Films of Functionalized Multiwalled Carbon Nanotubes as Suitable Scaffold Materials for Stem Cells Proliferation and Bone Formation." Acs Nano 4(12): 7717-7725.

Nima, Z. A., K. B. Vang, D. Nedosekin, G. Kannarpady, V. Saini, S. E. Bourdo, W. Majeed, F. Watanabe, E. Darrigues, K. M. Alghazali, R. A. Alawajji, D. Petibone, S. Ali, A. R. Biris, D. Casciano, A. Ghosh, G. Salamo, V. Zharov and A. S. Biris (2019). "Quantification of cellular associated graphene and induced surface receptor responses." Nanoscale 11(3): 932-944.

Nombela-Arrieta, C., J. Ritz and L. E. Silberstein (2011). "The elusive nature and function of mesenchymal stem cells." Nat Rev Mol Cell Biol 12(2): 126-131.

Nosouhian, S., M. Razavi, N. Jafari-Pozve and M. Rismanchian (2015). "Comparative evaluation of hydroxyapatite and nano-bioglass in two forms of conventional micro- and nano-particles in repairing bone defects (an animal study)." Indian J Dent Res 26(4): 366-371.

Pittenger, M. F., A. M. Mackay, S. C. Beck, R. K. Jaiswal, R. Douglas, J. D. Mosca, M. A. Moorman, D. W. Simonetti, S. Craig and D. R. Marshak (1999). "Multilineage potential of adult human mesenchymal stem cells." Science 284(5411): 143-147.

Qian, W., L. Gong, X. Cui, Z. Zhang, A. Bajpai, C. Liu, A. B. Castillo, J. C. M. Teo and W. Chen (2017). "Nanotopographic Regulation of Human Mesenchymal Stem Cell Osteogenesis." ACS Appl Mater Interfaces 9(48): 41794-41806.

Sanz-Herrera, J. A. and E. Reina-Romo (2011). "Cell-biomaterial mechanical interaction in the framework of tissue engineering: insights, computational modeling and perspectives." Int J Mol Sci 12(11): 8217-8244.

Secunda, R., R. Vennila, A. M. Mohanashankar, M. Rajasundari, S. Jeswanth and R. Surendran (2015). "Isolation, expansion and characterisation of mesenchymal stem cells from human bone marrow, adipose tissue, umbilical cord blood and matrix: a comparative study." Cytotechnology 67(5): 793-807.

Tang, L. A., W. C. Lee, H. Shi, E. Y. Wong, A. Sadovoy, S. Gorelik, J. Hobley, C. T. Lim and K. P. Loh (2012). "Highly wrinkled cross-linked graphene oxide membranes for biological and charge-storage applications." Small 8(3): 423-431.

Wan, Y., C. Lu, J. Cao, R. Zhou, Y. Yao, J. Yu, L. Zhang, H. Zhao, H. Li, J. Zhao, X. Zhu, L. He, Y. Liu, Z. Yao, X. Yang and X. Guo (2013). "Osteoblastic Wnts differentially regulate bone remodeling and the maintenance of bone marrow mesenchymal stem cells." Bone 55(1): 258-267.

Wang, K., J. Ruan, H. Song, J. L. Zhang, Y. Wo, S. W. Guo and D. X. Cui (2011). "Biocompatibility of Graphene Oxide." Nanoscale Research Letters 6.

Wang, S., Z. Deng, X. Ye, X. Geng and C. Zhang (2016). "Enterococcus faecalis attenuates osteogenesis through activation of p38 and ERK1/2 pathways in MC3T3-E1 cells." Int Endod J 49(12): 1152-1164.

Wojtoniszak, M., X. C. Chen, R. J. Kalenczuk, A. Wajda, J. Lapczuk, M. Kurzawski, M. Drozdzik, P. K. Chu and E. Borowiak-Palen (2012). "Synthesis, dispersion, and cytocompatibility of graphene oxide and reduced graphene oxide." Colloids and Surfaces B-Biointerfaces 89: 79-85.

Xu, A., X. Liu, X. Gao, F. Deng, Y. Deng and S. Wei (2015). "Enhancement of osteogenesis on micro/nano-topographical carbon fiber-reinforced polyetheretherketone-nanohydroxyapatite biocomposite." Mater Sci Eng C Mater Biol Appl 48: 592-598.

Yang D, V. A., Bozoklu G, Park S, StollerM, Piner RD, Stankovich S, Jung I, Field DA, Ventrice CA, Ruoff RS (2009). "Chemical analysis of graphene oxide films after heat and chemical treatments by X-ray photoelectron and Micro-Raman spectroscopy." Carbon 47: 145-152.

Yi, C., D. Liu, C. C. Fong, J. Zhang and M. Yang (2010). "Gold nanoparticles promote osteogenic differentiation of mesenchymal stem cells through p38 MAPK pathway." ACS Nano 4(11): 6439-6448.

Zhang, B., Y. Wang and G. Zhai (2016). "Biomedical applications of the graphene-based materials." Mater Sci Eng C Mater Biol Appl 61: 953-964.

Zhang, B., P. Wei, Z. Zhou and T. Wei (2016). "Interactions of graphene with mammalian cells: Molecular mechanisms and biomedical insights." Adv Drug Deliv Rev 105(Pt B): 145-162.

Zhang, R., P. Lee, V. C. Lui, Y. Chen, X. Liu, C. N. Lok, M. To, K. W. Yeung and K. K. Wong (2015). "Silver nanoparticles promote osteogenesis of mesenchymal stem cells and improve bone fracture healing in osteogenesis mechanism mouse model." Nanomedicine 11(8): 1949-1959.

Zhang, T., S. Lin, X. Shao, S. Shi, Q. Zhang, C. Xue, Y. Lin, B. Zhu and X. Cai (2018). "Regulating osteogenesis and adipogenesis in adipose-derived stem cells by controlling underlying substrate stiffness." J Cell Physiol 233(4): 3418-3428.

Zhang, Y., S. E. Chen, J. Shao and J. van den Beucken (2018). "Combinatorial Surface Roughness Effects on Osteoclastogenesis and Osteogenesis." ACS Appl Mater Interfaces 10(43): 36652-36663.

Zhang, Z. G., Z. H. Li, X. Z. Mao and W. C. Wang (2011). "Advances in bone repair with nanobiomaterials: mini-review." Cytotechnology 63(5): 437-443.

Appendix

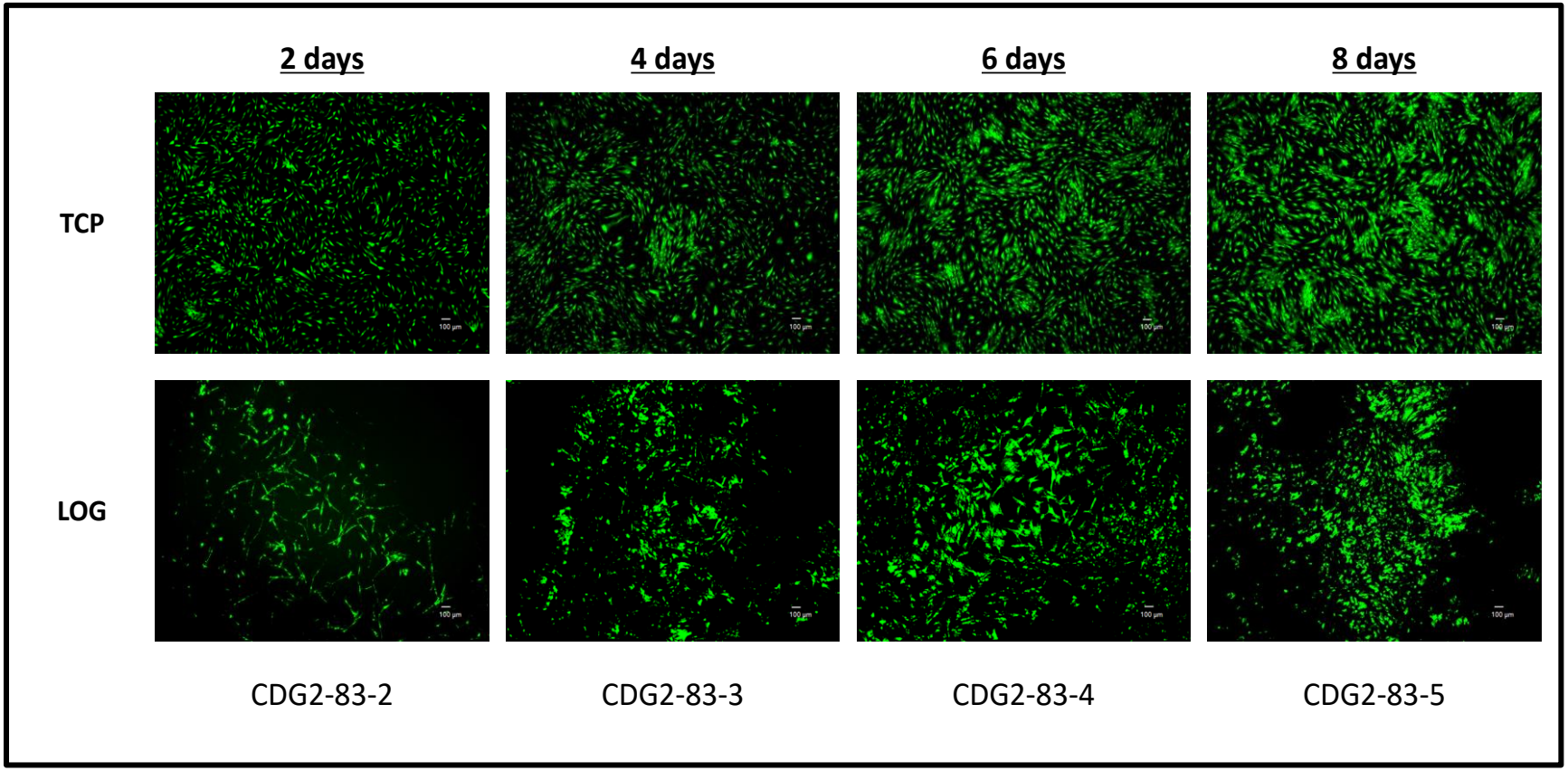

Figure 2.1 (a) Cell viability staining. Cell viability was evaluated on tissue culture polystyrene (I) and low-oxygen graphene (LOG) (II) by calcein-am staining. Calcein-am exhibits green fluorescence and demonstrates live cells. Fluorescent images show that human mesenchymal stem cells (hMSCs) adhered to and were viable on LOG surfaces similar to tissue culture polystyrene at all -time points. A distinct clustering of cells was, however, observed on LOG surface as early as 2 days post seeding and continued throughout the experiment on day 8.
Scale bar =100um.

(b)

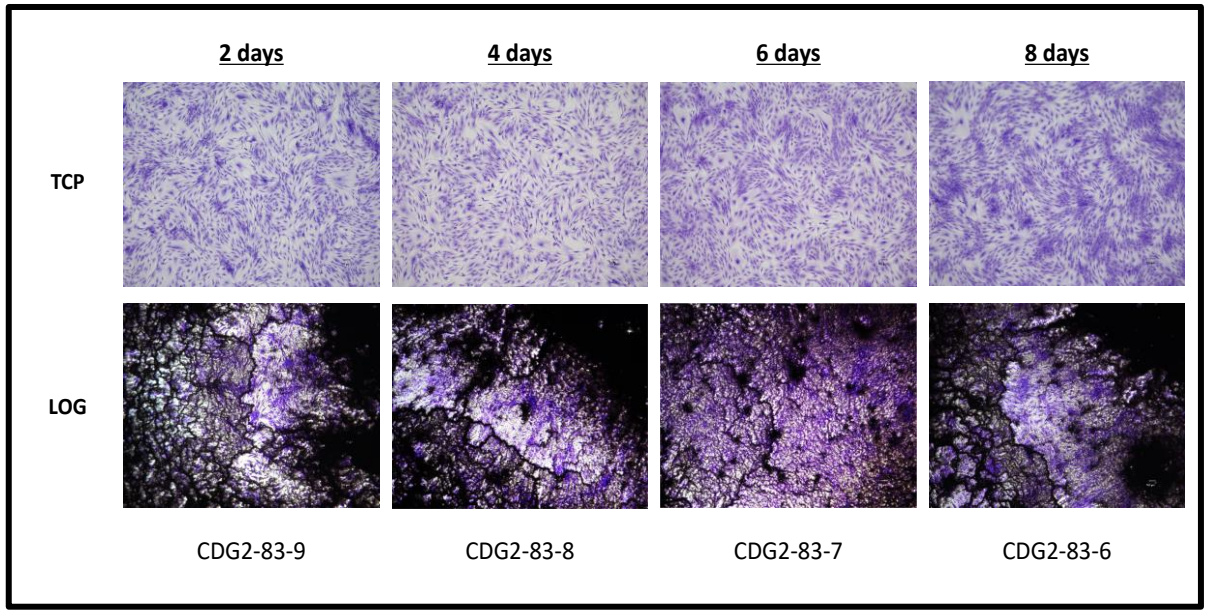

(c)

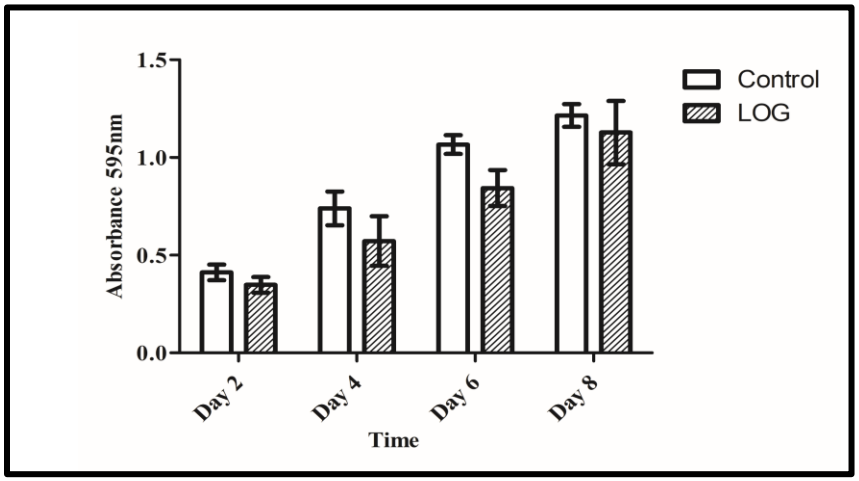

Figure 2.1 (b) Indirect staining **(c)** Crystal violet quantification. Further confirmed cell viability and proliferation when hMSCs adhered to tissue culture polystyrene (I) and LOG(II) surfaces using crystal violet staining between days 2–8.

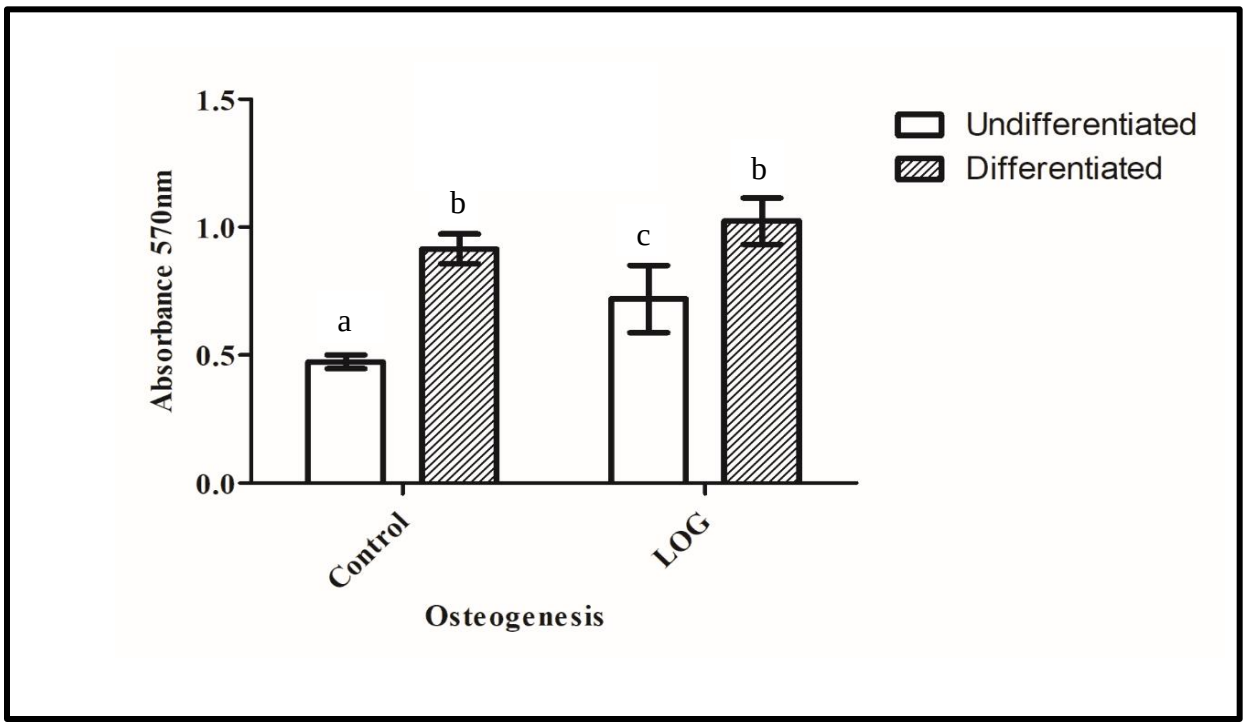

Figure 2.2. Osteogenic differentiation assay. Calcium content of cells that were seeded on tissue culture polystyrene (Control) and low-oxygen graphene (LOG) surfaces were visualized by Alizarin red staining and subsequently quantitated. The calcium content of cells seeded in growth media without any osteogenic inducers (undifferentiated) was compared to cells that were exposed to differentiation media (differentiated) for 21 days. Media blank, i.e., the tissue culture polystyrene and LOG surfaces without any cells were used as blanks and the corresponding absorbance readings were subtracted. Significantly different values ($p<0.05$) are indicated by letters. Identical letters indicate no significance.

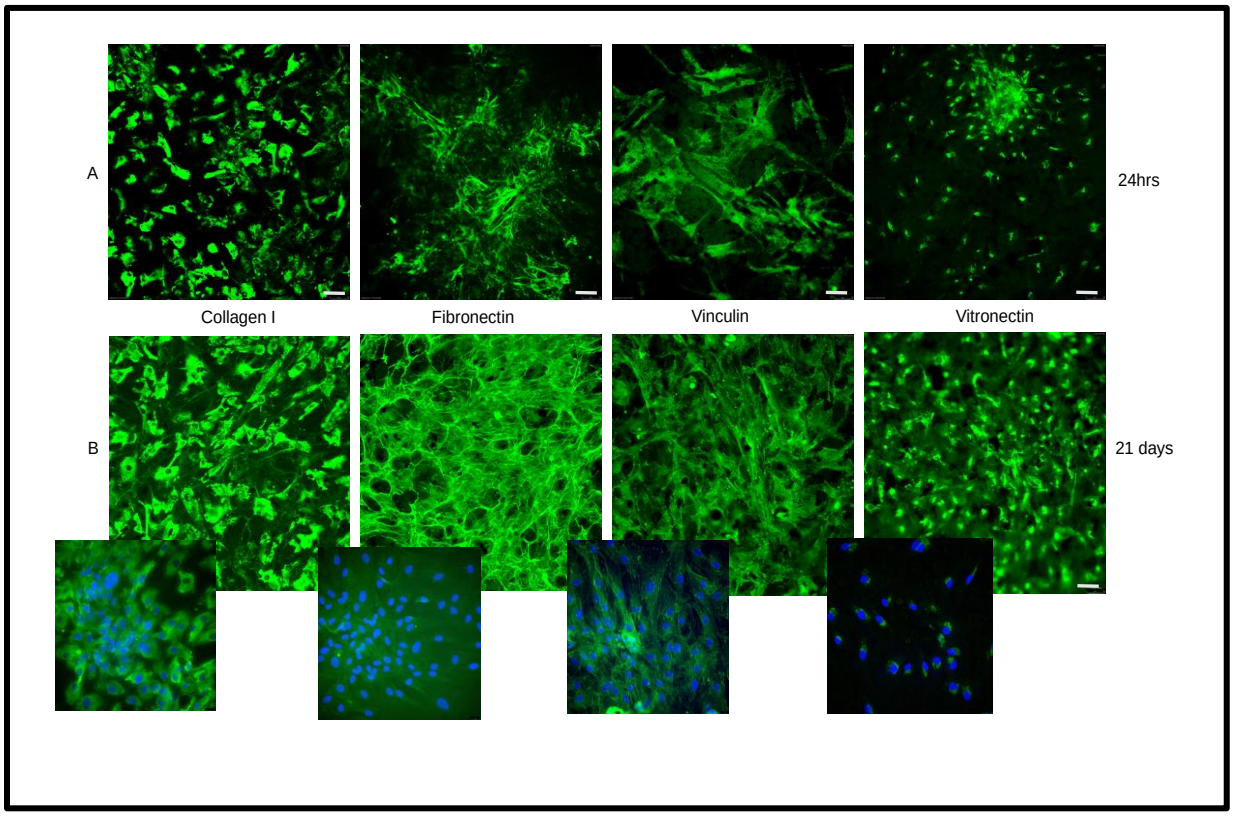

Figure 2.3. Expression of ECM proteins. Proteins expressed during cell adhesion i.e., within 24hrs (A) and differentiation i.e., at day 21 (B) were assessed using IF assays. The insets show the expression of the same proteins on tissue culture substrate at 24hrs. Note the lack of discrete organization on the tissue culture

Chapter III:
VERSATILITY OF CELL RESPONSE TO GRAPHENE NANOPARTICLES

Portions of this chapter have been accepted for a poster presentation at the Experimental Biology 2021 conference.

Lentiviral Transduced Adipose Derived Stem Cells (ADSCs) Undergo Spontaneous Osteogenesis on Low-Oxygen Content Graphene (LOG) Surfaces

Thomas J. Masi [1], Ruby D. Trotter [2], Steven D. Newby[3], Austin J. Bow[3], Nicholas S Millis[3], Shawn E. Bourdo[2], Madhu S. Dhar[3], Stacy J. Stephenson[1]

[1] University of Tennessee Graduate School of Medicine, Knoxville, TN, 37996, USA
[2] Center for Integrative Nanotechnology Sciences, University of Arkansas at Little Rock, Little Rock, AR, 72204, USA
[3] College of Veterinary Medicine, University of Tennessee, Knoxville, TN, 37996, USA

Portions of this data is being combined with MacDonald et al. manuscript that has been submitted

Genetic profiling of human bone marrow and adipose tissue – derived mesenchymal stem cells reveals differences in osteogenic signaling mediated by graphene

Amber F. MacDonald[a], Ruby D. Trotter [b], Christopher D. Griffin [b], Austin J. Bow[a], Steven D. Newby[a], William J. King [b], Lisa L. Amelse[a], Thomas J. Masi [c], Shawn E. Bourdo [b], Madhu S. Dhar[a, *]

[a] College of Veterinary Medicine, University of Tennessee, Knoxville, TN, 37996, USA
[b] Center for Integrative Nanotechnology Sciences, University of Arkansas at Little Rock, Little Rock, AR, 72204, USA
[c] University of Tennessee Graduate School of Medicine, Knoxville, TN, 37996, USA
[*] Corresponding author: mdhar@utk.edu

Portions of the Methods section on immunofluorescence are used from Chapter 2

Abstract

Mesenchymal stem cells (MSCs) can be isolated from any adult somatic tissue. Bone marrow and adipose tissue are the two common sources. Furthermore, the biological quality of the MSCs from both sources can vary with the donor. A functionalized form of graphene containing 6-10% oxygen (referred to as low oxygen graphene, LOG, by our group) is distinct from graphene oxide but shares similar properties with the commercially available reduced graphene oxide (rGO). The effects of LOG and rGO can be utilized as a cell-adhesion construct and/or a possible transporter for growth factors to support osteogenic differentiation of MSCs. Understanding the graphene-cellular interaction is essential for considering graphene nanoparticles as a potential candidate for biofabricated applications. The biocompatibility of LOG and rGO surfaces were assessed subjectively by cell adhesion. Cell morphology was assessed with green fluorescent protein (GFP) transduced MSCs. Expression of ECM proteins by human adipose stem cells and human bone marrow mesenchymal stem cells (BMSCs) were evaluated by immunofluorescence. A panel of specific antibodies, including vimentin, fibronectin, F-Actin, collagen I, vinculin and vitronectin at multiple time points after seeding were used. Cell adhesion plays a crucial part in facilitating cell fate and it is influenced by the cellular environment. This study suggests that a surface coated with LOG or rGO or incorporated into a scaffold will be beneficial for cell attachment, proliferation, and osteoblast differentiation/osteogenesis.

Introduction

The extracellular matrix of tissue forms a physical microenvironment construct where cells reside and are cued to secret factors to support the surrounding environment. This microenvironment niche allows for a dynamic biochemical and biophysical signaling to influence cells to complete many tasks for development, with these cells being stem cells (Gattazzo, 2014). Stem cells express ECM molecules at the very earliest embryonic stages of development (Zagris, 2001). The ability to identify and isolate cells, from a variety of tissue sources from human or animal is of extraordinary significance. Cells can be expanded boundlessly in tissue culture, and under controlled conditions directed to differentiate into the appropriate cell type of importance. Tissue-derived adult stem cells, such as adipose, epithelial and bone marrow have limited potential for multi patient use due to histo-incompatibility driving a need for a compatible therapeutic cell source.

Even though, bone marrow and adipose tissue derived MSCs exhibit similar cell properties, their efficacy however, i.e., their biological function *in vivo* can vary. This is primarily due to donor-to-donor variations. Furthermore, the cell-scaffolds' interaction may vary as well. In summary, the performance and efficacy of MSCs is dependent on a multitude of factors (**Figure 3.1**). Mesenchymal stem cells have the ability to differentiate into myocytes, osteocytes, chondrocytes and neurons in vitro and in vivo (Seong, 2010). Biocompatibility of the construct is directly related in the adhesion, proliferation rate and viability of cells (Naujoks et al., 2011). Specific physiochemical properties of graphene-based constructs and the biocompatible is capable of aiding stem cells proliferation and osteogenic differentiation without supplementary inducers (Dubey, 2015).

Methods

Adipose Tissue MSCs – Patient 3

Human adipose tissue was isolated from patients undergoing panniculectomies in accordance with a protocol approved by the Institution Review Board at the University of Tennessee Medical Center. After resection, the adipose tissue was transported to the lab and immediately processed as previously described (Alghazali et al., 2017). Briefly, the lipoaspirate was rinsed with phosphate buffered saline (PBS) and then minced into smaller pieces for efficient digestion. Tissue was enzymatically digested in 0.1% collagenase, 1% bovine serum albumin (BSA) and 2mM calcium chloride in PBS at 37ºC for 30-45 mins, with intermittent shaking until a homogenous solution was obtained. After digestion, the samples were centrifuged at 300xg for 5 minutes at room temperature then shaken to disrupt the pellet and centrifuged a second time (**Figure 3.2**). The oil/fat and supernatant were removed, and the pellet of the stromal vascular fraction (SVF) was washed with PBS. The pellet was suspended in stromal medium (DMEM/F12, 1% penicillin-streptomycin/amphotericin B, 20% fetal bovine serum (FBS) and passed through a 100μm cell strainer to remove undigested tissue. The single cell suspension was seeded in tissue culture flasks and incubated for 48 hours in a humidified 5% CO_2 incubator at 37ºC. The flasks were washed with PBS to remove loosely attached cells and fresh stromal media was added. The cells were grown to 80-90% confluence and then harvested with 0.05% trypsin EDTA, for cryopreservation in 80% FBS, 10% DMEM/F12, 10% DMSO or, split and seeded into new flasks for expansion. All experiments were performed using cells from passage 2-6 in complete growth media (DMEM/F12, 1% penicillin-streptomycin/amphotericin B, 10% FBS).

Adipose tissue derived MSCs were characterized by flow-cytometric analysis for expression of MSC markers and their potential to undergo tri-lineage differentiation by in vitro adipogenesis, osteogenesis and chondrogenesis as described earlier (Dominici et al., 2006). Differentiation was confirmed by Oil Red O staining of the lipid droplets, Alcian blue staining of collagen, and Alizarin red staining of calcium, respectively.

Bone Marrow MSCs

Human bone marrow mesenchymal stem cells were purchased from ATCC (Manassas, VA USA) at passage 1. They were cultured in flasks using ATCC recommended protocol in an incubator with humidified atmosphere, 5% CO_2, and 37^{o}C. Cell culture was maintained until the flask reached 85-90% confluency. Cells were then trypsinized (trypsin 0.05%, USA) and cultured for further passages following same protocol until passage 5. For this study passage 4 was used on all experiments. The commercially obtained BMSCs have been demonstrated by the vendor to express the stem cell markers and have been demonstrated to undergo *in vitro* trilineage differentiation.

Alizarin Red Staining Calcium Content During Osteogenesis

Patient 3 -ADMSCs and BMSCs were cultured to 80-85% confluency in growth media. For experimental conditions, cells were harvested and seeded at $25x10^3$ on LOG thin films as described in chapter 2. Cells were cultured on LOG for 21 days and maintained in growth media without support from osteo-differentiation media. At 21-day time points films were stained with Alizarin red.

Alizarin Red allows for visualization of calcium production which is evaluated by staining the samples with alizarin red solution, which is a dye that binds to extracellular calcium salts. The evaluation for calcium production was carried out comparing Patient 2 from previous study in chapter 2 to Patient 3 and bone marrow cells on graphene for osteogenesis. The accumulation of calcium in hMSCs was quantitated by the elution of alizarin red dye with 10% cetylpyridium chloride and the color was read at 570 nm (Newby et al., 2020). Background readings due to the substrates alone without any cells were subtracted from the sample readings to eliminate nonspecific values. Data was plotted and statistics performed in Prism (Graphpad).

Green Fluorescent Protein /Red Fluorescent Protein Transduction of MSCs
Production of Lentivirus

Modification of human adipose mesenchymal stem cells were cultured in the lab of Dr. Tom Masi. Construction and production of transduced MSCs using a functional

population of lentiviral (LV) victors expressing enhanced red fluorescent protein (RFP) and green fluorescent protein (GFP) were processed (Masi, unpublished). Infected MSCs were cultured and passaged for future cell studies on biomaterials or constructs.

Cytoskeletal Organization and ECM of Patient 3 and BMSCs Proteins on LOG and rGO

Cytoskeletal organization and MSC morphology were assessed by evaluating the expression patterns of F-actin and vimentin using previously reported methods (Alghazali et al., 2017). The expression of ECM proteins during cell attachment (i.e., within 24hrs of seeding) and osteogenic differentiation (21 days after seeding) was assessed qualitatively by immunofluorescence detection assays. A panel of ECM proteins including, two distinct fibronectin antibodies 182, vitronectin, collagen I and II and vinculin were used. Briefly, hMSCs at specified time points were fixed with 4% paraformaldehyde at room temperature for 10 minutes, permeabilized with 0.1% Triton X-100 in HBSS at room temperature for 10 minutes, and subsequently blocked with the Universal Blocking Reagent (BioGenex) for 30 minutes at room temperature. Cells were incubated with 1-2ug of all primary antibodies and samples were incubated at 4°C for 24 hours. Alexa Fluor 594 phalloidin (A12381; Invitrogen), Vimentin (#550513; BD Pharmingen), Collagen I (#ab3470; Abcam), Collagen II (#ab34712; Abcam), Fibronectin 181 (MAB19172; R&D Systems), Fibronectin 182 (#MAB19182; R&D Systems), Vinculin (#ab129002; Abcam) and Vitronectin (#ab113700; Abcam). The cells were washed and incubated with appropriate Alexa Fluor – labelled secondary anti-mouse or anti-rabbit antibodies at room temperature for 30 minutes in dark. Alexa Fluor 594 Phalloidin was preconjugated and hence, did not require any secondary antibody treatment step. The cells were washed twice and mounted on microscope slides with a drop of Prolong Gold antifade reagent with 4′, 6-diamidino-2-phenylindole (DAPI; Molecular Probes by Life Technologies). The cells were analyzed under a fluorescence microscope (Leica DMi8).

Preparation of Reduced Graphene Oxide Nanoparticle Thin Surfaces

Reduced graphene oxide was obtained commercially from Cheap Tubes Inc (Grafton, VT, USA). Graphite powder yields graphite oxide when synthesized by the Hummer's method (Wu, 2010). The reduction by thermal methods to synthesize GO yields rGO in achievement to minimize the number of oxygen groups attached (Pei, 2012) (**Figure 3.3**).

Reduced graphene oxide with a thickness of 0.7-1.2nm, Y&Y dimension at 300-800nm, Purity of 99 wt.%, method by modified Hummer's was used to generate 2D films for this study. 4mg of rGO was mixed with 2 mL of 95% EtOH and sonicated with an Ultrasonic unit for 1 hour keeping the water at 20-25^{o}C. The resulting dispersion is 2mg/mL and 0.2mg/cm^2 (i.e., 100μl/cm^2) was the desired surface amount for a 15mm coverslip receiving 150μl. Coverslips were then transferred to a vacuum oven with at 50^{o}C and -25 psi for 1 to 1.5 hours. Coverslips were then taken for gas sterilization and stored in the dark until needed for experiments.

Following methods were used to characterize rGO dispersions. These characterizations were carried out at the Center for Integrative Nanotechnology Sciences, University of Arkansas at Little Rock by Dr. Shawn Bourdo.

X-ray Photoelectron Spectroscopy (XPS) and Raman Spectroscopy on rGO

The physico-chemical nature of the rGO nanoparticles was confirmed by X-ray photoelectron spectroscopy (XPS), structural analysis by Raman spectroscopy. XPS is a qualitative and quantitative technique used to characterize surface chemical states for elemental composition and binding states of the synthesized materials. An X-ray beam excites the atoms on the surface of the sample causing a release of photoelectrons. Synthesized rGO was prepared as films by aqueous dispersion on glass slides and dried prior to characterization.

The synthesized constructs were analyzed via Raman spectrum. The chemical analysis is expressed by a number of peaks, displaying the intensity and wavelength position of the scattered light. Each of the peaks correlate to a specific molecular bond vibration.

Results

Patient 3 Characterization

Patient 3 MSCs were successfully isolated form adipose tissue. Flow-cytometric analysis was used to characterize specific cell surface markers. Analysis showed that ADSCs expressed MSC markers CD29, CD44, CD73, CD90, and CD105 in all cells and were negative for hematopoietic markers CD34, CD45, HLA-DR and endothelial marker CD106 expression (**Figure 3.4.**). Tri-lineage differentiation potential was performed for each lineage by being supplemented by the proper induction media. Adipogenic lineage confirmed oil droplets by staining Oil Red O, chondrogenic differentiation was confirmed by staining with Alcian blue and osteogenic differentiation was confirmed by Alizarin red. (**Figure 3.5**)

Alizarin Red in vitro Differentiation

Cells were cultured for 21 days on a graphene film coated 12 well plate. When cultured for 21 days in presence of growth media a thin layer of mineralized tissue is represented on the graphene film. Quantification of the alizarin red stain confirmed that patient 3 cells performed as well as patient 2 did in pervious graphene experiments. (**Figure 3**.**6**). Upregulation was observed in the absence of any osteogenic inducing reagents (dexamethasone, beta-glycerophosphate or ascorbic acid), suggesting that the LOG surface induces accumulation of calcium in MSCs spontaneously, i.e., induces osteogenic differentiation *in vitro*. hBMSCs seed on LOG for 21 days expressed significantly greater calcium content relative to the cells on the control suggesting that the LOG surface induces accumulation of calcium in hBMSCs spontaneously without osteogenic inducers *in vitro* (**Figure 3.7**).

Green Fluorescent Protein Transduction of MSCs

The adipose cells that were transduced were tested to see if they would be usable in future studies. The test showed cells performed well over multiple time points with no problems in proliferation morphology and reduction in fluorescence. Images were taken at 24 hours and 7 days (**Figure 3.8**). This methodology is repeatable for

cells and can definitely be utilized in future studies for tracking proliferation and possible differentiation in biofabricated constructs.

XPS and Raman Spectroscopy of rGO

XPS spectrum at 3 sample spots of rGO were investigated and the average values showed elemental composition of 83.45%C, 12.48%O, and 4.07%N (**Figures 3.9 – 3.10**).

Raman of the 3 sample spots showed the ratio of intensity of D/G bands that is a measure of the defects present on graphene the structure and particularly for distinguishing the disorder in the crystal structures of carbon (**Figure 3.11**). The G band arises from the stretching of the C–C sp2 bond in graphitic materials a result of in-plane vibrations of carbon atoms whereas the D band is due to out of plane vibrations attributed to the presence of structural defects and dangling sp2 carbon bonds that break the symmetry.

Adipose tissue MSCs – Patient 3 Response to Graphene

LOG

The analysis of ECM proteins by immunofluorescence we performed in chapter 2 were repeated here using ADMSCs from patient 3 on LOG. The expression of ECM proteins evaluated at 24 hours and 21 days by using media only on LOG as a control. The expression patterns of collagen I, collagen II, fibronectin, vinculin, and vitronectin were evaluated. IF analyses on the LOG surface did not show the expression of any ECM proteins in the absence of hMSCs in any of the samples tested, clearly demonstrating that the serum proteins do not contribute to the ECM on LOG surface and hence, do not have a role in cell adhesion or differentiation. The evaluated expression of ECM proteins when patient 3 MSCs were seed on LOG showed at 24 hours to assess the ECM proteins involved in cell adhesion (**Figure 3.12**), and, at day 21, to express proteins involved in osteogenic differentiation (**Figure 3.13**).

rGO

Patient 3 ECM protein evaluated images on control and rGO. No ECM protein expression of any ECM proteins in the absence of hMSCs in any of the samples tested, clearly demonstrating that the serum proteins do not contribute to the ECM on rGO surface and hence, do not have a role in cell adhesion or differentiation. Evaluation at 24 hours of ECM proteins involved in cell adhesion (**Figure 3.14**) were expressed and at 21 days all ECM proteins were expressed (**Figure 3.15**) involved in osteogenic differentiation, showing that rGO could be utilized as a possible construct in future studies.

Bone Marrow Cellular Response to Graphene

LOG

Bone marrow stem cells were seeded to LOG under the same conditions and time points 24 hours and 21 days were tested on the same ECM proteins. At the 24-hour time point proteins were evaluated vimentin was positive and showed signs of stress morphology, Fibronectin expression was evaluated but limited compared to adipose cells, F-Actin showed microtubule formation with vinculin confirming cell adhesion, Collagen I and vitronectin was expressed but defused. 21-day time point showed signs of proliferation and adhesion. Vimentin showed a more defined morphology, fibronectin was expressed but again limited as to adipose cells, F-Actin and vinculin were expressed showing morphology and adhesion to the rGO film, Collagen I expression was increased and vitronectin showing cell adhesion and migration also increased (**Figure 3.16**).

rGO

Bone marrow cell expression showed remarkably different results on rGO. At the 24-hour time point vimentin showed bipolar morphology, fibronectin had increased showing tight communication or aggregation of the cells. Evaluation of F-Actin showed high cell communication and microtubule response and was confirmed by vinculin, Collagen I expression was abundant and vitronectin confirmed adhesion. Evaluation at 21-day time point, expression of cellular behavior and morphology showed with a

pattern described as a brush stroke in a circular formation. The patterns by each protein expressed formed a tighter cell-cell and cell-matrix showing cell communication and adhesion (**Figure 3.17**) on the rGO film.

Conclusion

We reported the comparative osteogenic capabilities of ADMSCs and BMSCs on LOG and rGO films. The properties of graphene nanoparticles such as sizable surface area, ability to aid in mechanical properties and utility to blend with other synthetic or natural substrates allows for multiple material constructs to be used in cell research. This study showed that two derivatives of graphene nanoparticles are biocompatible, allowing for cell viability, adhesion, proliferation and support to stem cells into osteogenic lineage identified by ECM proteins. Adipose stem cell ECM proteins expressed immunofluorescence on both derivatives. Observation of these cells showed increased ECM protein synthesis indicating cell-matrix adhesion to the film surface. Observation of bone marrow stem cells on LOG showing cell morphology at both time points became smaller and more stressed at 24 hours than 21 day which may be a result of oxidative stress that must be further evaluated. Observations of cultured bone marrow cells of rGO exhibited distinctly stronger capability of ECM protein expression at 24 hour and 21-day time points. Comparability of graphene nanoparticle in modified forms blended with natural or synthetic biomaterials for biofabricated implants must be performed to achieve the regenerative support of graphene. A *in vivo* animal study will allow for the study of biodistribution of the nanoparticles and gain knowledge of a cellular metabolic pathways that can be used to engineer future tissue biofabricated constructs.

References

Alghazali KM, Newby SD, Nima ZA, et al. Functionalized gold nanorod nanocomposite system to modulate differentiation of human mesenchymal stem cells into neural-like progenitors. Sci Rep. 2017;7(1):16654. doi:10.1038/s41598-017-16800-9

Aubin JE. Bone stem cells. Journal of cellular biochemistry Supplement. 1998;30-31:73-82.

C. Naujoks, F. Langenbach, K. Berr et al., “Biocompatibility of osteogenic predifferentiated human cord blood stem cells with biomaterials and the influence of the biomaterial on the process of differentiation,” *Journal of Biomaterials Applications*, vol. 25, no. 5, pp. 497–512, 2011.

Chen D, Hao H, Fu X, Han W. Insight into epithelialization: how do mesenchymal stem cells perform? *Stem Cells Int*. 2016; 2016:6120173.

Dominici M, Le Blanc K, Mueller I, et al. Minimal criteria for defining multipotent mesenchymal stromal cells. The International Society for Cellular Therapy position statement. *Cytotherapy.* 2006;8(4):315-317.

Dubey N., Bentini R., Islam I., Cao T., Castro Neto A.H., Rosa V., Graphene: a versatile carbon-based material for bone tissue engineering, Stem Cells Int. 2015 (2015) 12.

Gattazzo F, Urciuolo A, Bonaldo P. Extracellular matrix: A dynamic microenvironment for stem cell niche. Biochim Biophys Acta. 2014; 1840:2506–19. DOI: 10.1016/j.bbagen.2014.01.010 [PubMed: 24418517]

Jiang X, Whitesides GM. Engineering microtools in polymers to study cell biology. Eng Life Sci 2003; 3:475e80.

Mecham, R. P. Overview of extracellular matrix. *Curr. Protoc. Cell Biol. Chapter* **57**, 10.1.1–10.1.16 (2012).

S. Pei, H.M. Cheng The Reduction of Graphene Oxide (2012), pp. 3210-3228

Salmasi S, Kalaskar DM, Yoon WW, Blunn GW, Seifalian AM. Role of nanotopography in the development of tissue engineered 3D organs and tissues using mesenchymal stem cells. *World J Stem Cells*. 2015;7(2):266–280.

Seong JM, Kim BC, Park JH, Kwon IK, Mantalaris A, Hwang YS. Stem cells in bone tissue engineering. Biomed Mater. 2010;5(6):062001

J. Wu, X. Shen, L. Jiang, K. Wang, and K. Chen, “Solvothermal synthesis and characterization of sandwich-like graphene/ZnO nanocomposites,” *Applied Surface Science*, vol. 256, no. 9, pp. 2826–2830, 2010.

Yacoub, N.a., Romanowska, M., Haritonova, N. and Foerster, J. (2007), Optimized production and concentration of lentiviral vectors containing large inserts. J. Gene Med., 9: 579-584. https://doi.org/10.1002/jgm.1052

Yannas IV, Lee E, Orgill DP, Skrabut EM, Murphy GF. Synthesis and characterization of a model extracellular matrix that induces partial regeneration of adult mammalian skin. Proc Natl Acad Sci USA 1989;86(3):933e7

Yannas IV. Tissue and Organ Regeneration in Adults. New York: Springer; 2001.

Zagris, N. Extracellular matrix in development of the early embryo. *Micron* **32**, 427–438 (2001).

Appendix

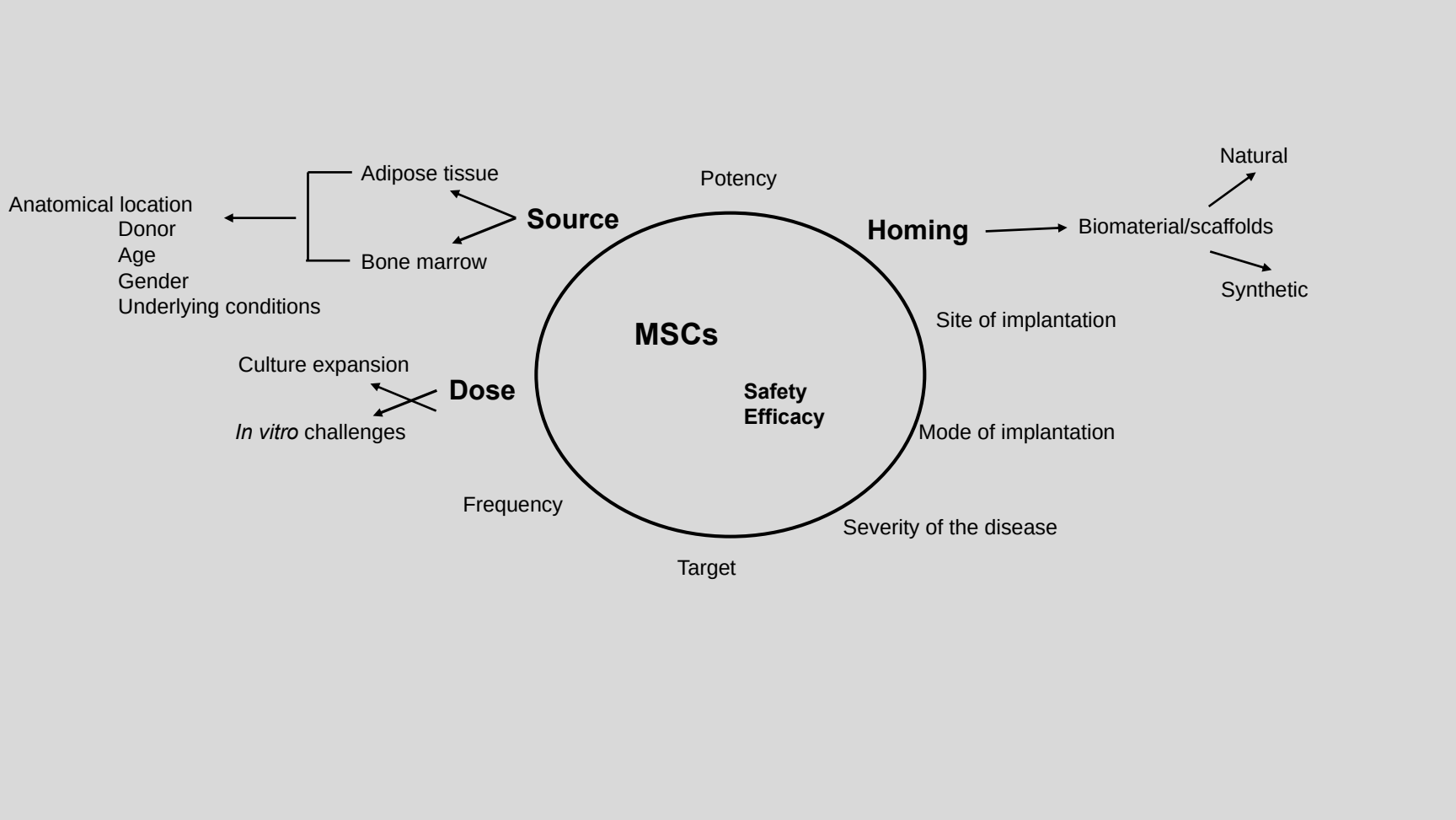

Figure 3.1. A figure to show the multitude of factors that affect the safety and efficacy of MSCs.

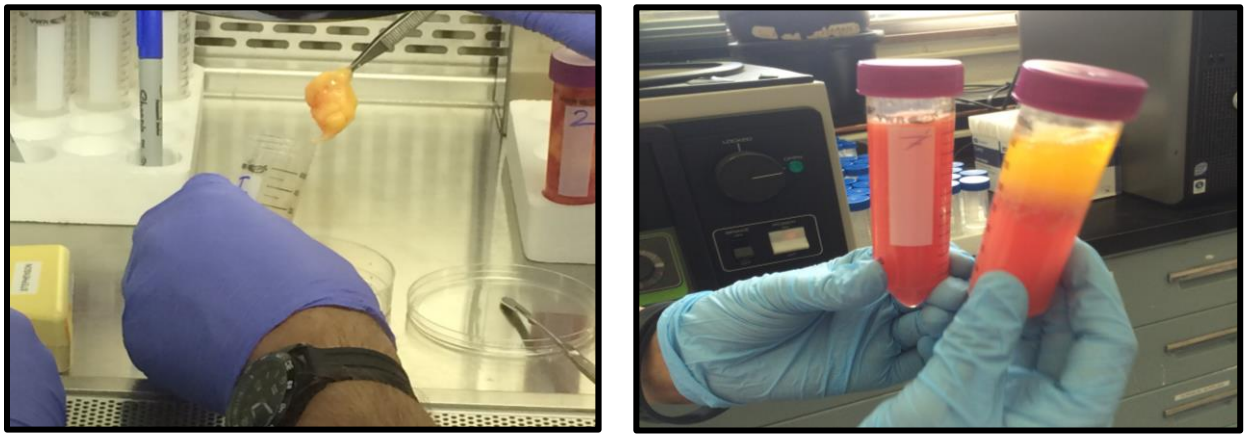

Figure 3.2. Patient 3. Isolation of collected adipose-derived mesenchymal stem cells from panniculectomies. Approved IRB protocols.

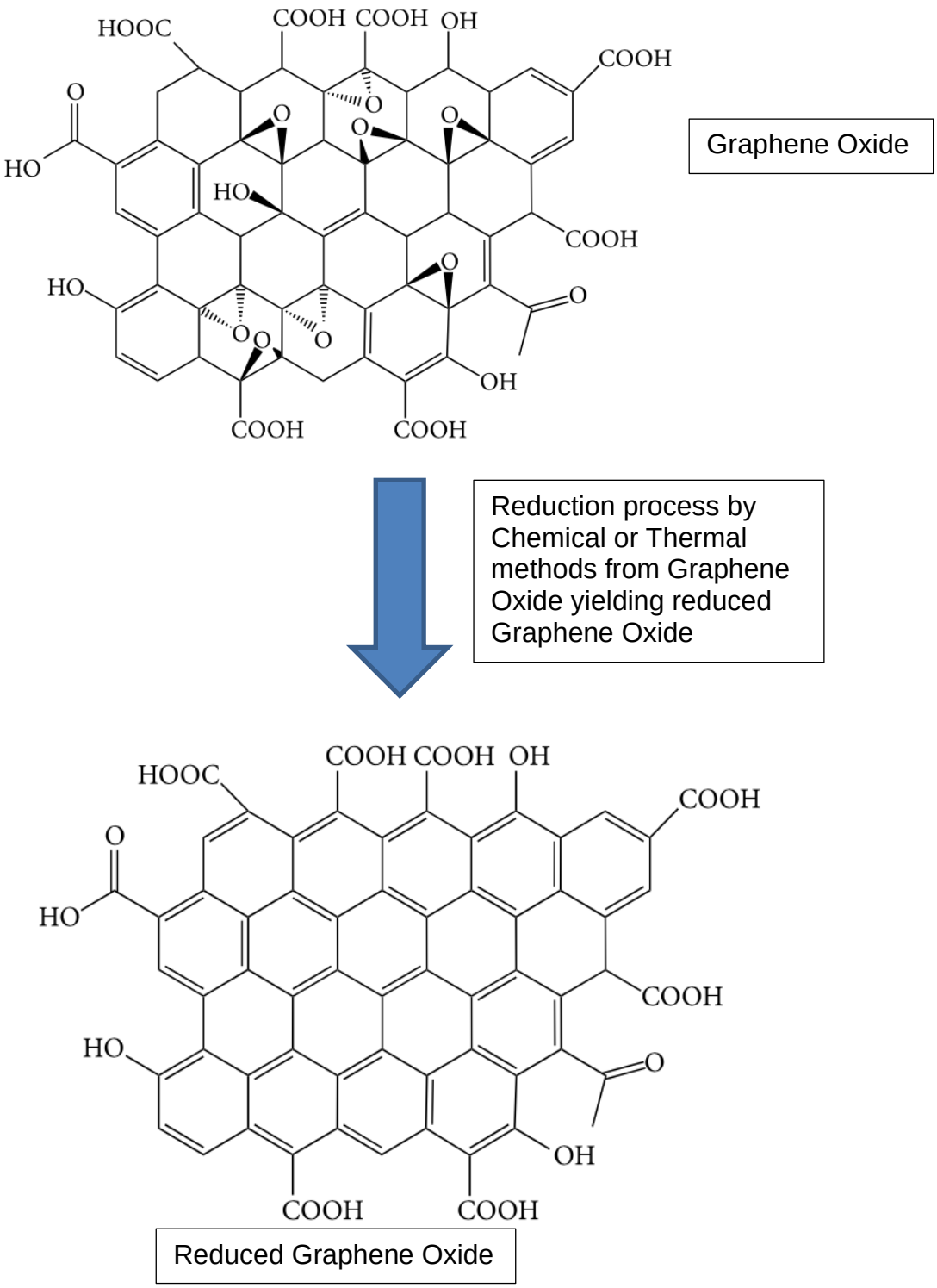

Figure 3.3. Methods for obtaining reduced Graphene Oxide. Image source from Graphene-info.com

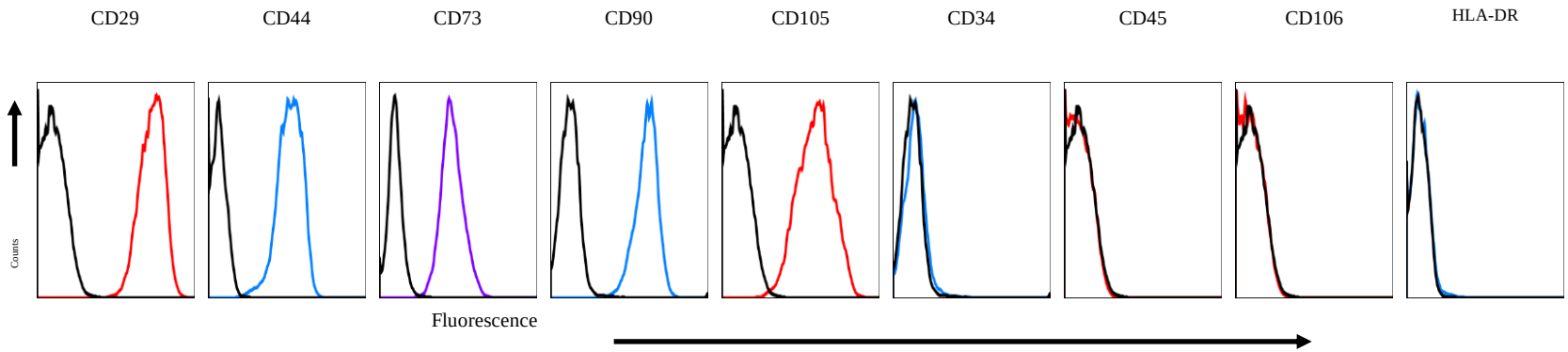

Figure 3.4. Immunophenotyping of hMSCs by flow cytometry. Human MSCs were stained with the indicated antibodies and then analyzed for expression by flow cytometry. MSCs all strongly express markers associated with the mesenchymal stem cells (CD29, CD44, CD73, CD90, CD105), while expression of hematopoietic (CD34, CD45, HLA-DR) and endothelial (CD106) markers are negative. Colored open histograms represent reactivity with the indicated antibodies; black open histograms indicate isotype matched controls for each antibody.

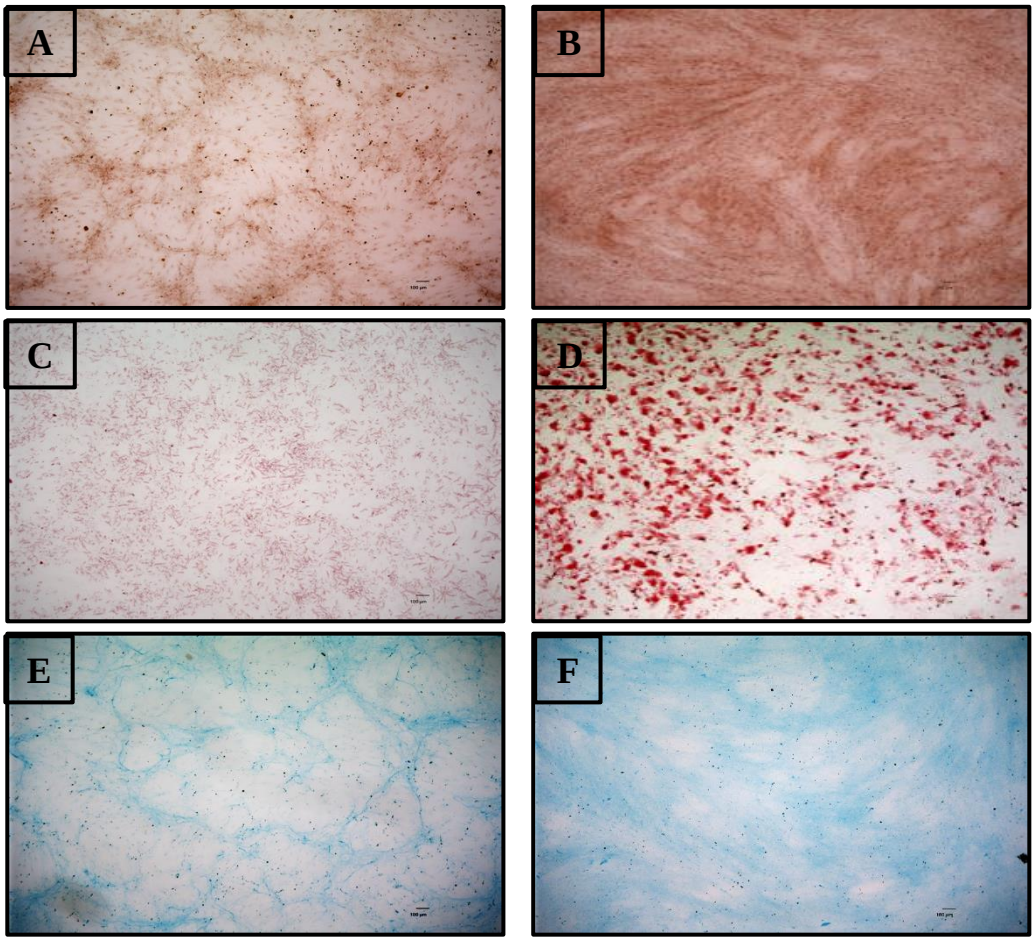

Figure 3.5. Tri-lineage differentiation assays of hMSCs. Representative images of Alizarin Red, oil-red-o, and alcian blue stained cells demonstrating (B) osteogenesis, (D) adipogenesis, and (F) chondrogenesis respectively, after in vitro differentiation. A, C and F are stained, undifferentiated control cells of B, D and F, respectively.

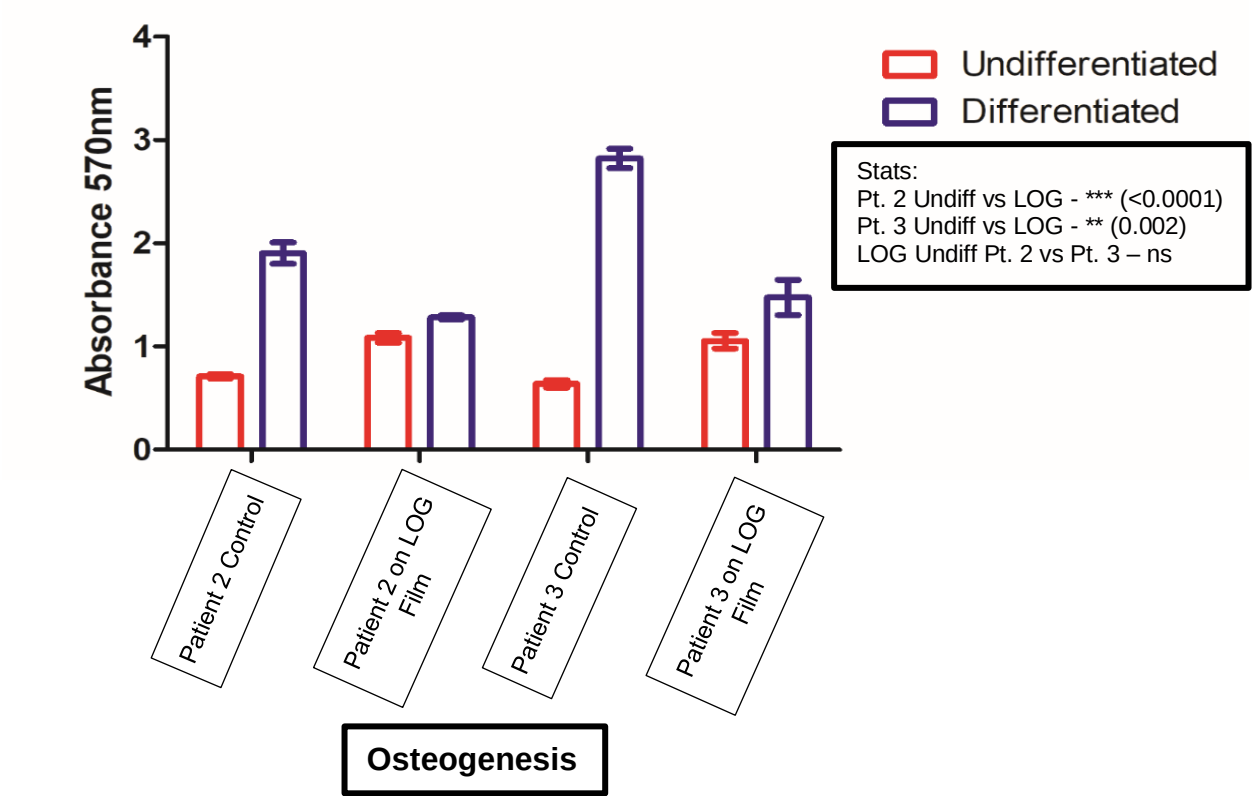

Figure 3.6. Comparison of Patient 2 cells to Patient 3 cells on Graphene for Osteogenesis**.** Data shows that patient 3 cells perform on graphene films the same as patient 2. This allows for patient 3 cells to be used in future studies.

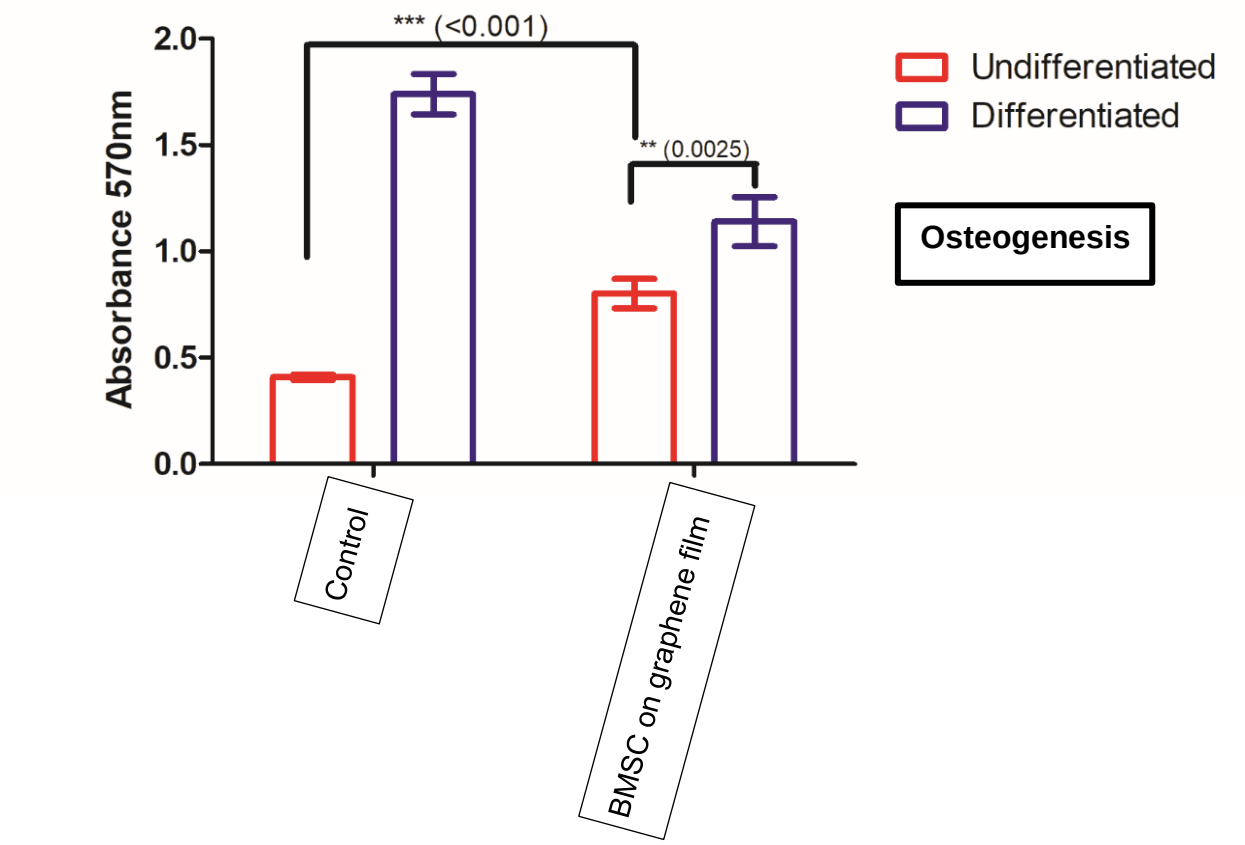

Figure 3.7. hBMSC on Graphene. Osteogenesis by bone marrow stem cells on a LOG surface.

(a) 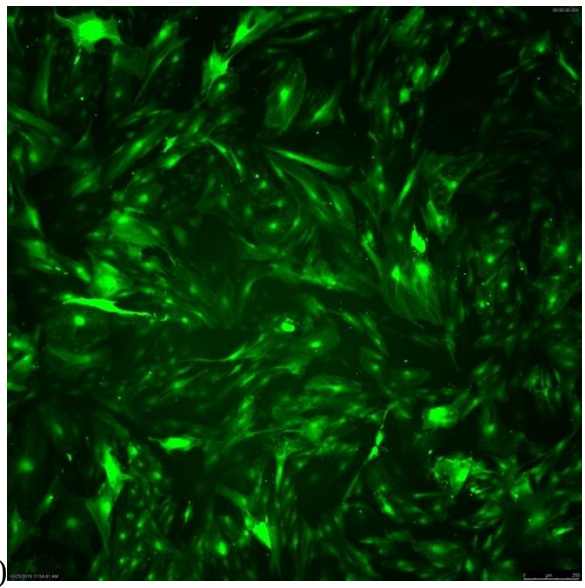 (b) 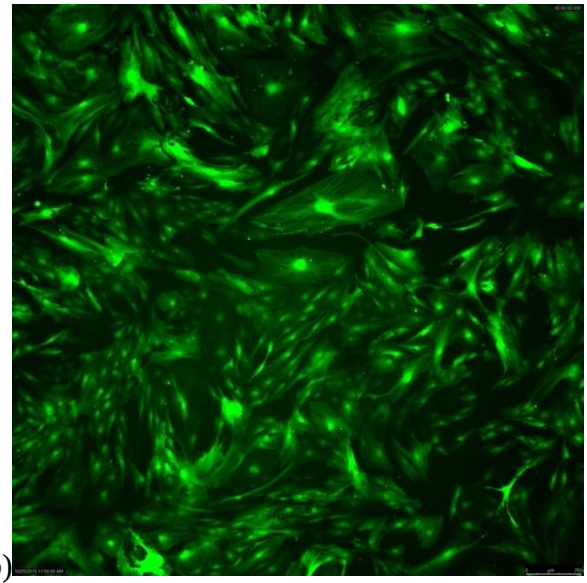

Figure 3.8. Transduction of Adipose Stem Cells. (a) 24-hour image (b) Day 7 of tracking cells to show proliferation and retention of fluorescence.

	spot1	spot2	spot3		
Name	Atomic %	Atomic %	Atomic %	**average**	**std dev**
C1s	82.54	83.61	84.2	***83.45***	***0.69***
O1s	13.16	12.48	11.79	***12.48***	***0.56***
N1s	4.29	3.91	4.01	***4.07***	***0.16***

Figure 3.9. XPS showed an approximate elemental composition of 83.45%C, 12.48%O, and 4.07%N. Summary of XPS results on rGO sample3 spots were investigated and the averages reported for the elements of interest: C, O, and N.

Common Acquisition Parameters Table-spot1

Parameter	
Total acquisition time	11 mins 20.5 secs
Number of Scans	10
Source Gun Type	Al K Alpha
Spot Size	400 µm
Lens Mode	Standard
Analyzer Mode	CAE : Pass Energy 200.0 eV
Energy Step Size	1.000 eV
Number of Energy Steps	1361

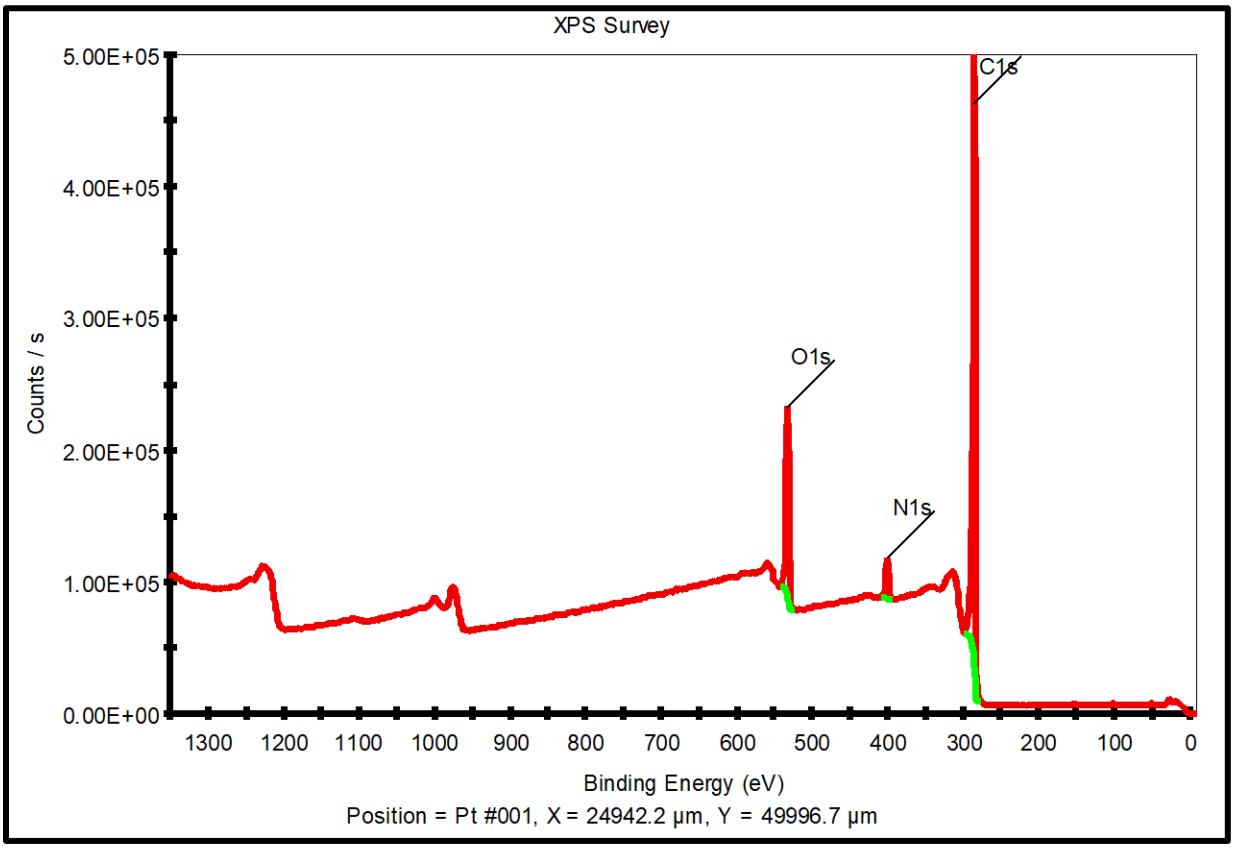

Elemental ID and Quantification

Name	***Peak BE***	***FWHM eV***	***Area (P) CPS.eV***	***Atomic %***	***Q***
C1s	285.09	3.05	1712876.45	82.54	1
O1s	532.36	4.02	660156.20	13.16	1
N1s	399.92	3.70	138222.48	4.29	1

Figure 3.10. Representative data of 3 spots of rGO that were analyzed.

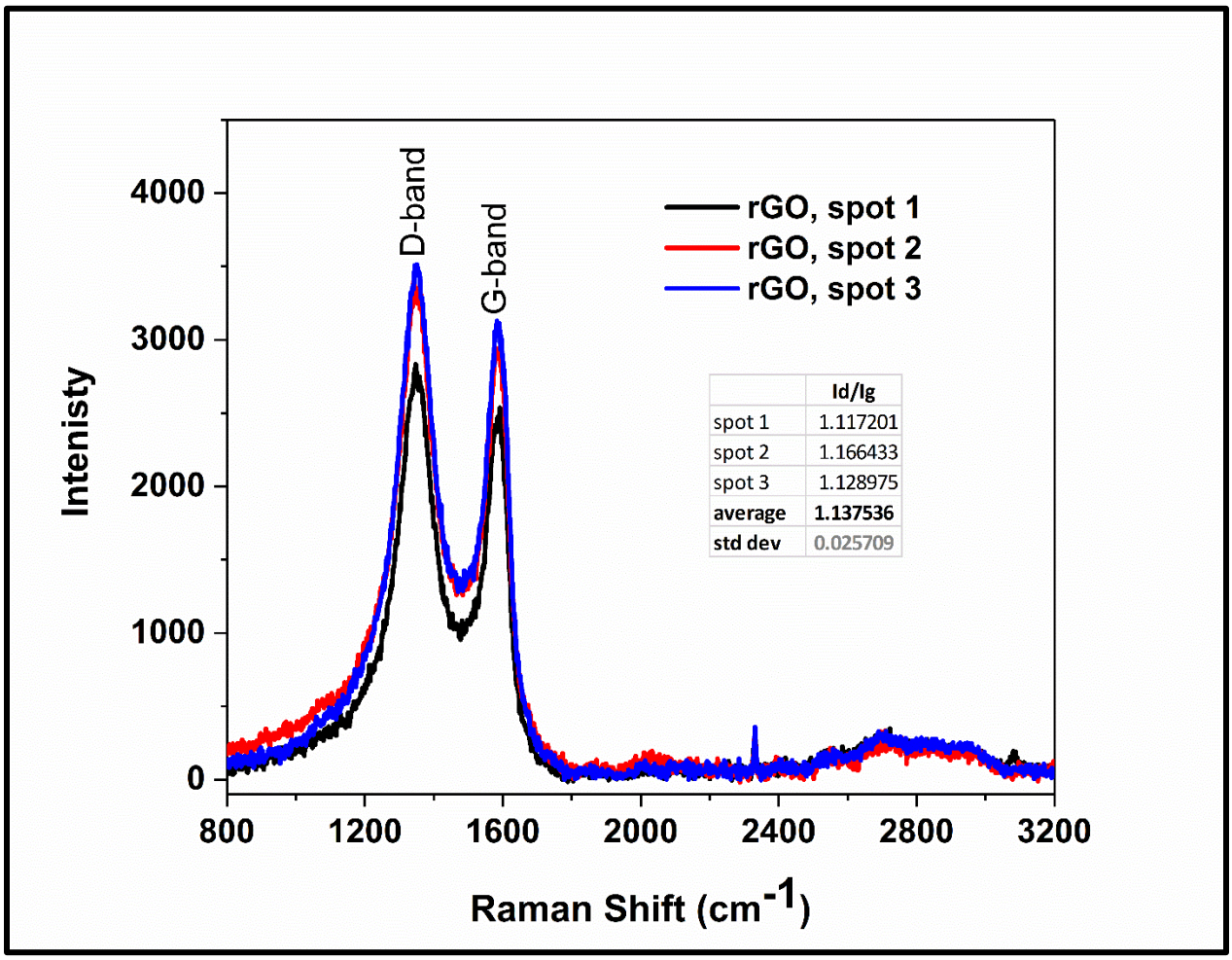

Figure 3.11. Raman showed a D-band and G-band situated at approximately 1347cm^{-1} and 1588cm^{-1}. When comparing the intensity of these 2 peaks it was determined they exhibited an I_D/I_G ration of ~1.14.

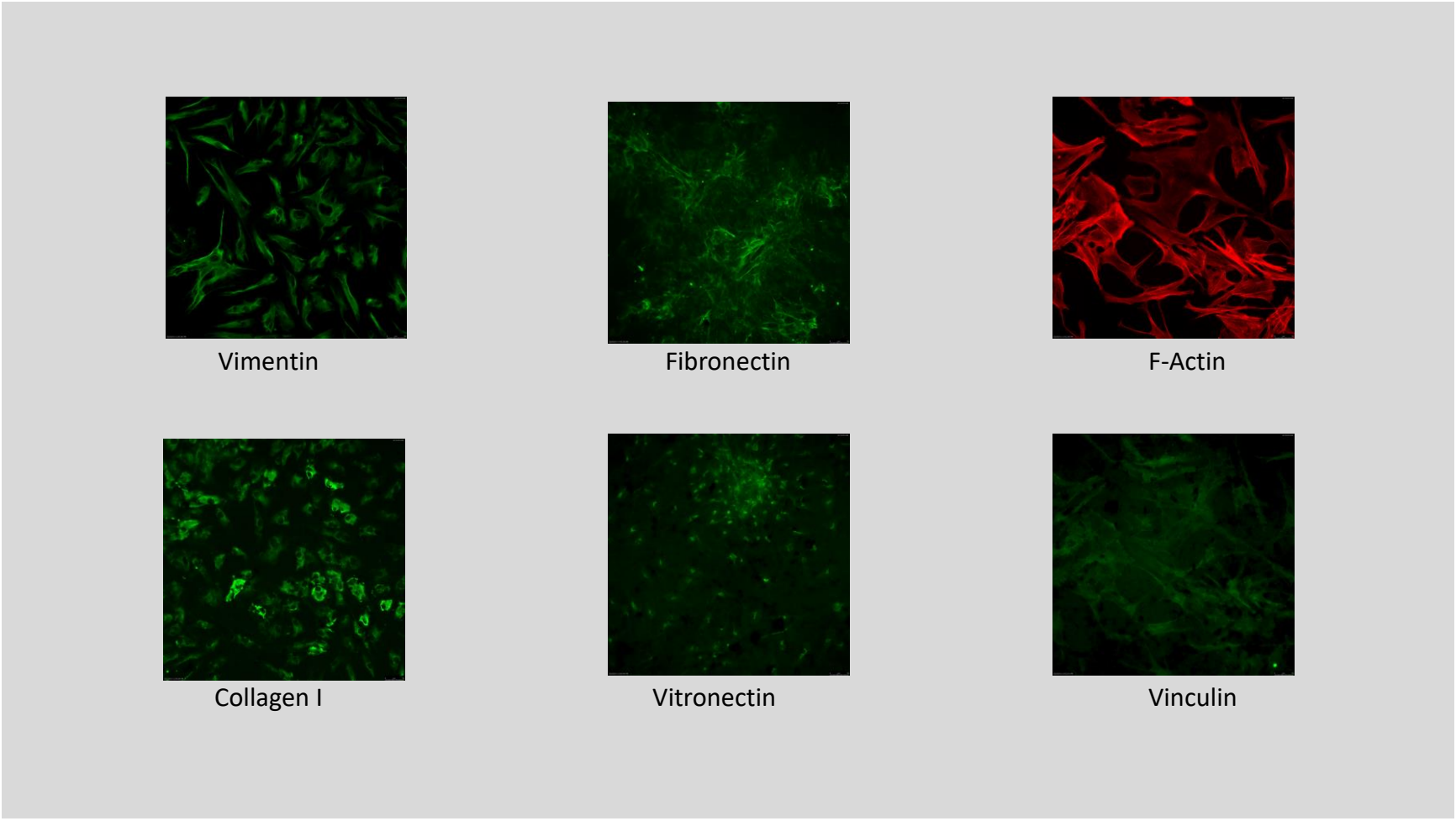

Figure 3.12. Representative image of expression of extracellular matrix proteins. Proteins of Patient 3 adipose stem cells expressed during cell adhesion at 24 hours on Low Oxygen Graphene using immunofluorescence.

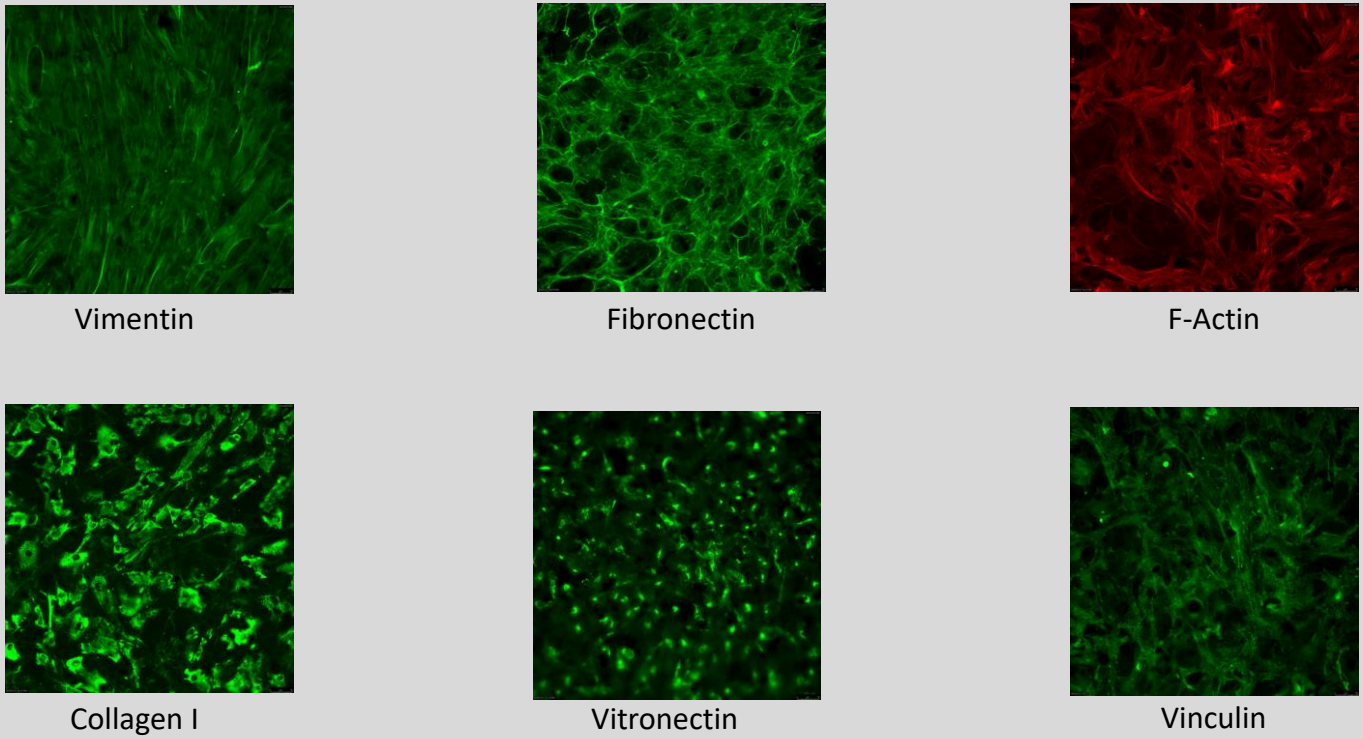

Figure 3.13. Representative image of expression of extracellular matrix proteins. Proteins of Patient 3 adipose stem cells expressed during cell adhesion at 21 days on Low Oxygen Graphene using immunofluorescence.

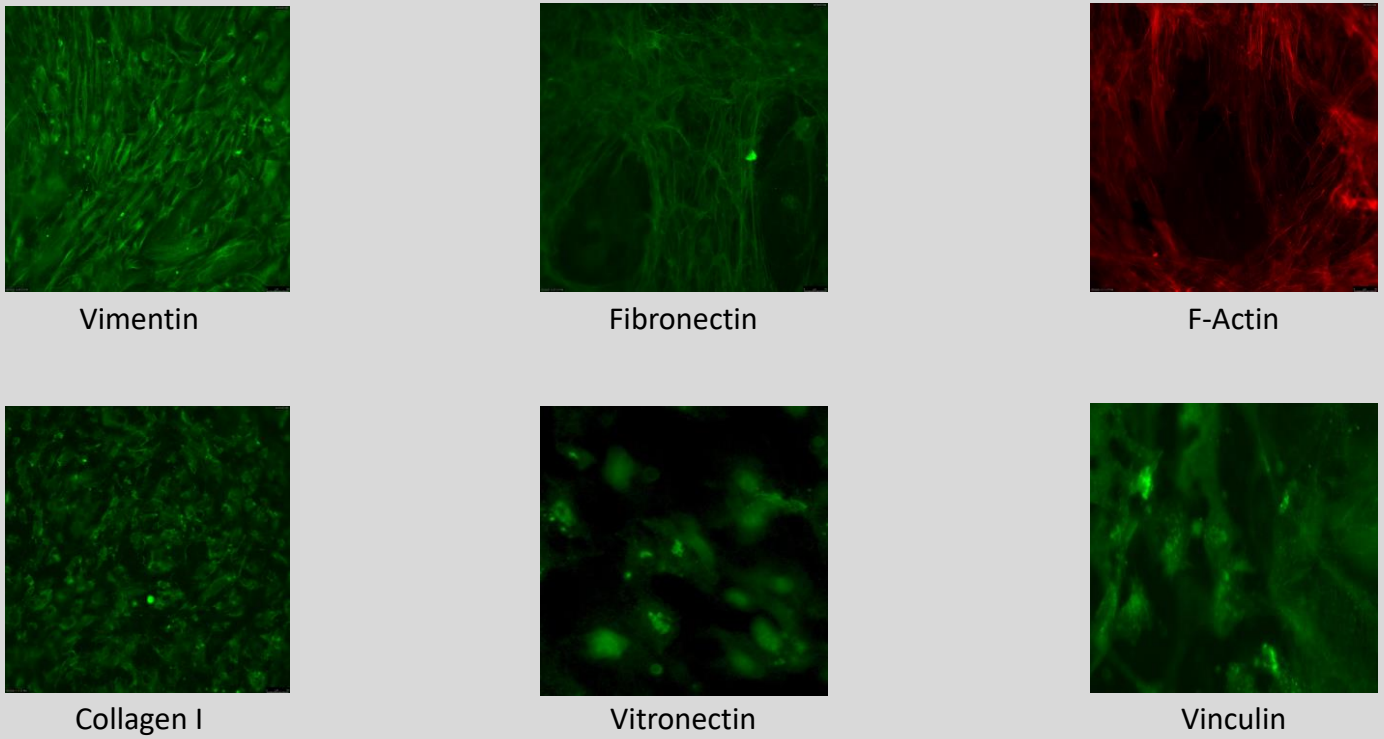

Figure 3.14. Representative image of expression of extracellular matrix proteins. Proteins of Patient 3 adipose stem cells expressed during cell adhesion at 24 hours on reduced Graphene Oxide using immunofluorescence.

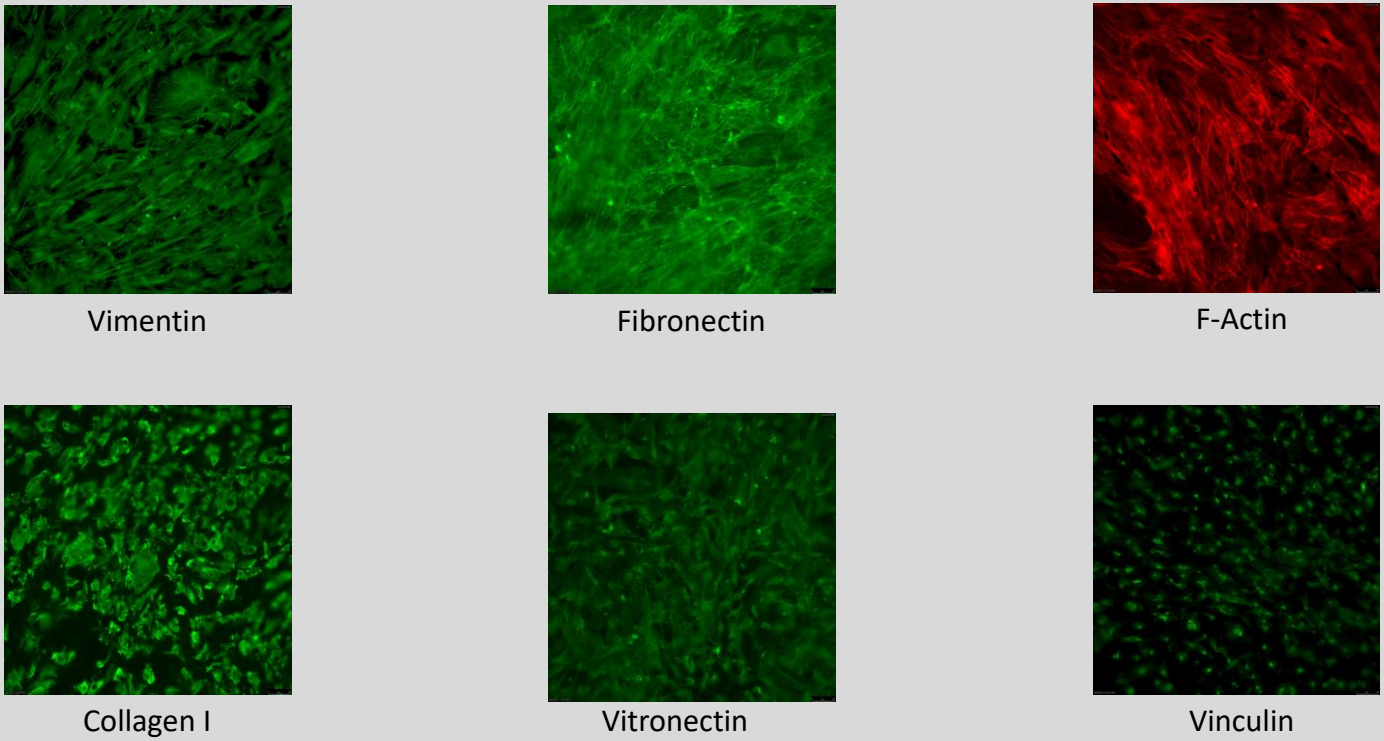

Figure 3.15. Representative image of expression of extracellular matrix proteins. Proteins of Patient 3 adipose stem cells expressed during cell adhesion at 21 days on reduced Graphene Oxide using immunofluorescence.

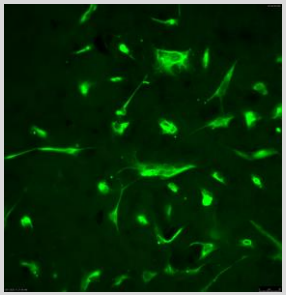

Vimentin

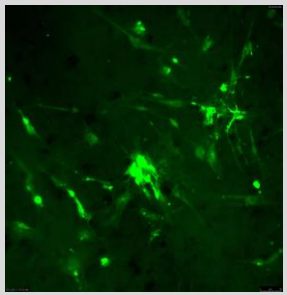

Fibronectin

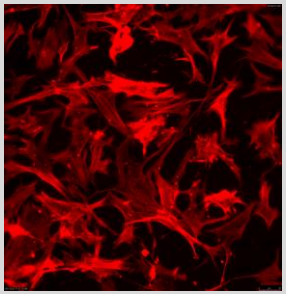

F-Actin

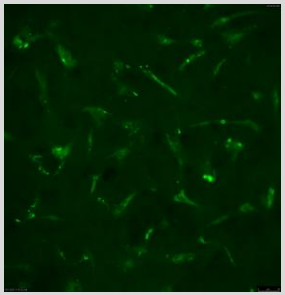

Collagen I

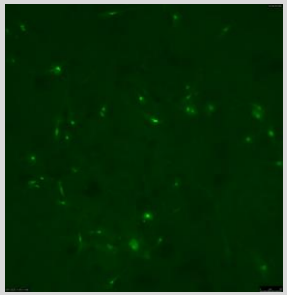

Vitronectin

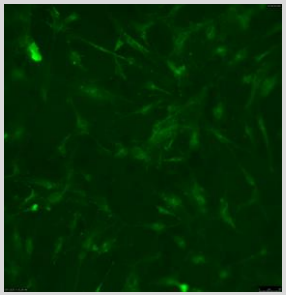

Vinculin

Figure 3.16. Representative image of expression of extracellular matrix proteins. Proteins of bone marrow stem cells expressed during cell adhesion at 24 hours on Low Oxygen Graphene using immunofluorescence.

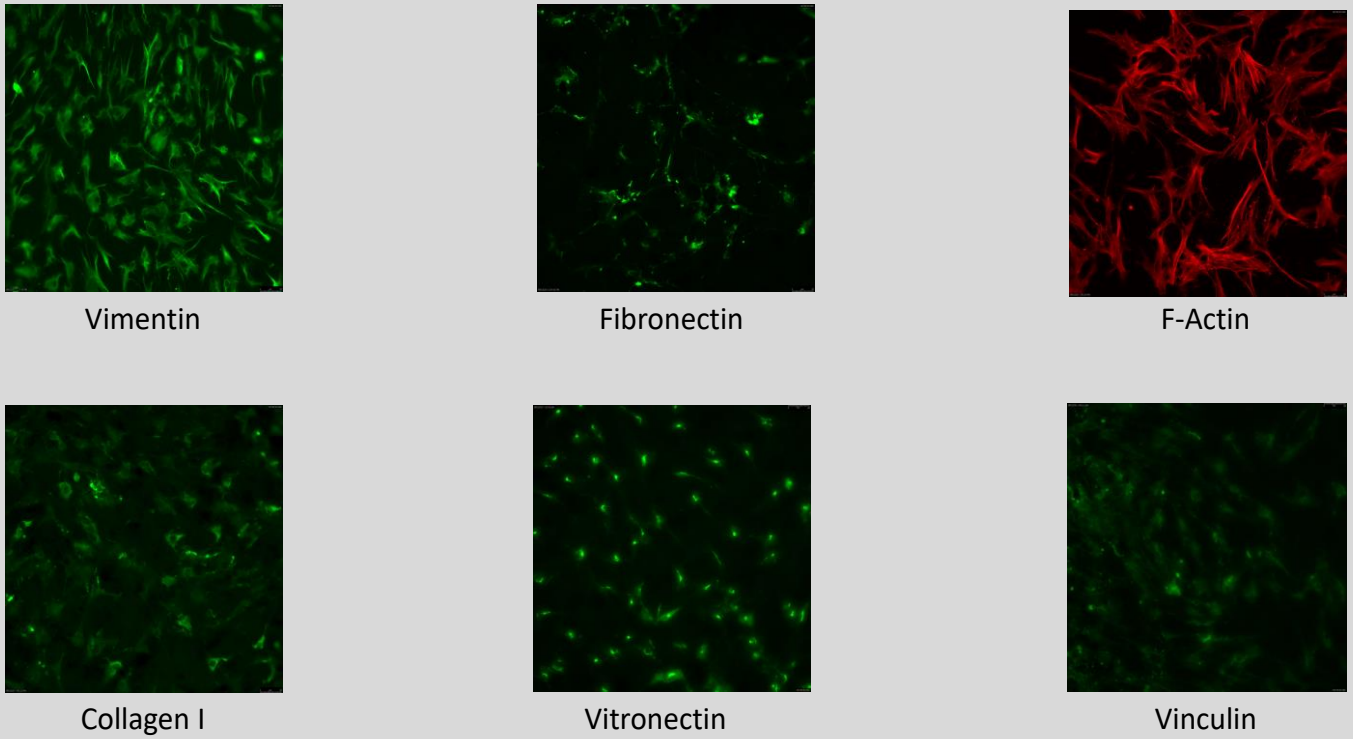

Figure 3.17. Representative image of expression of extracellular matrix proteins. Proteins of bone marrow stem cells expressed during cell adhesion at 21 days on Low Oxygen Graphene using immunofluorescence.

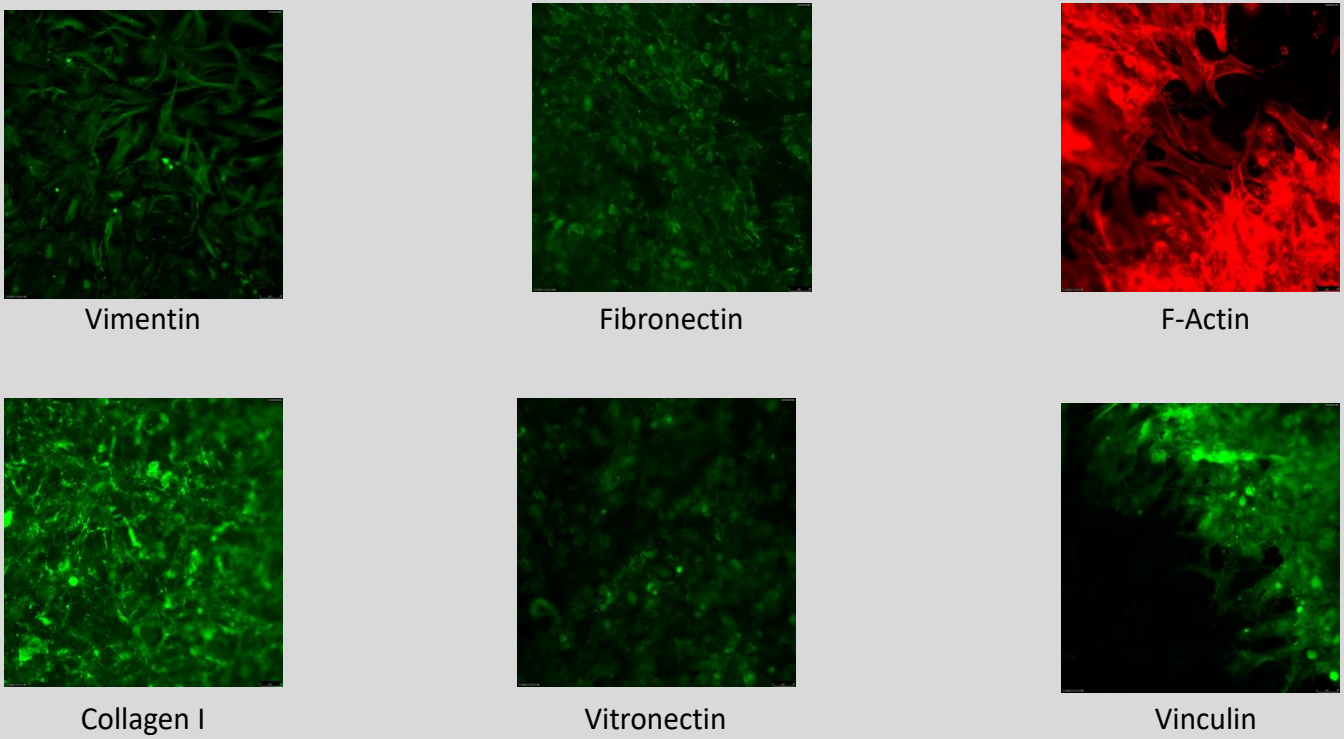

Figure 3.18. Representative image of expression of extracellular matrix proteins. Proteins of bone marrow stem cells expressed during cell adhesion at 24 hours on reduced Graphene Oxide using immunofluorescence.

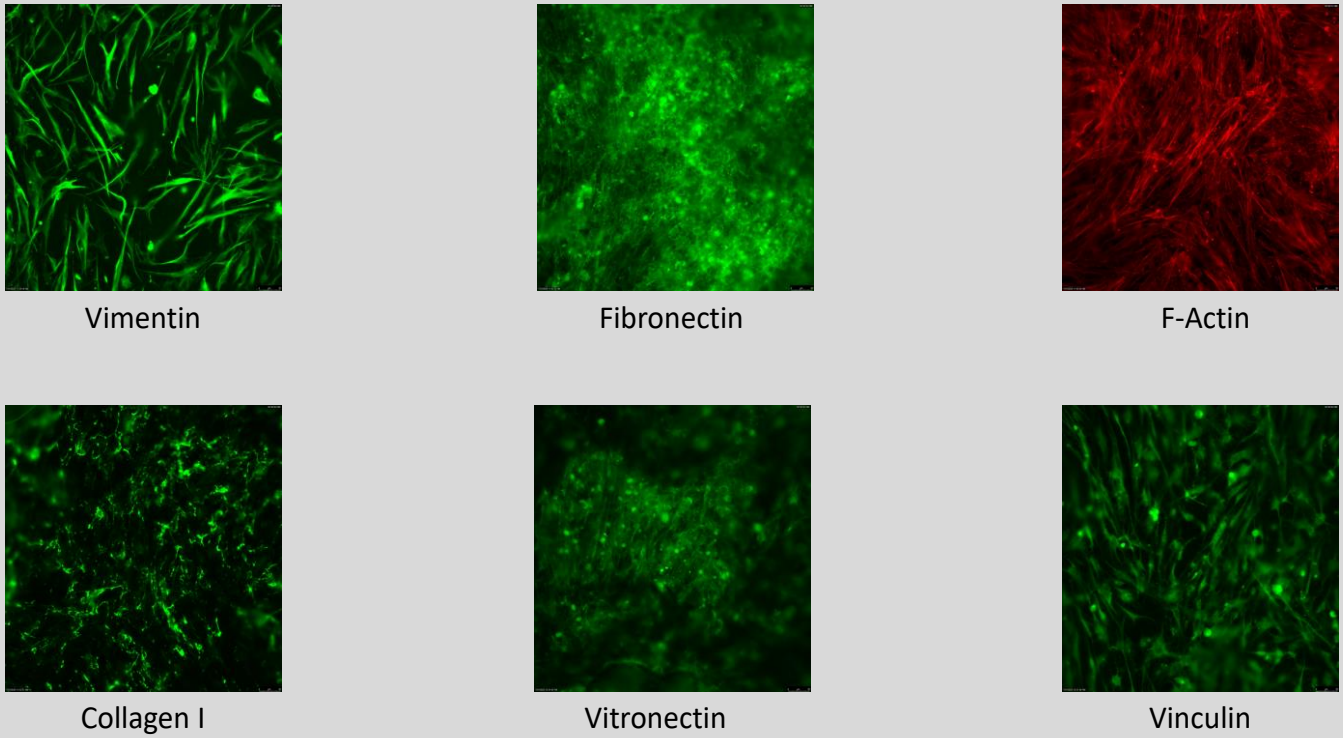

Figure 3.19. Representative image of expression of extracellular matrix proteins. Proteins of bone marrow stem cells expressed during cell adhesion at 21 days on reduced Graphene Oxide using immunofluorescence.

CHAPTER IV:
BIOFABRICATION OF NOVEL THERAPEUTICS FOR MUSCULOSKELETAL REPAIR

Versions of this chapter were originally presented as a Research Day Abstract as an oral presentation for the Comparative and Experimental Medicine Department: presented in-house only no commercial presentation:

Permission was obtained by Dr. Madhu Dhar, mentoring author of the chapter.

Abstract

This chapter covers the core, which is Biofabrication. The long-term goal is to develop a biocompatible scaffold containing cells and sufficient vascularization using 3D bioprinting and bioreactor mechanics to influence the biological processes. Tissue-engineering technologies have the potential to provide a more effective approach to bone regeneration that will speed healing, improve patients' chances of recovery from debilitating injuries and diseases, and return normal form and function. I hypothesize that a new nanoengineered construct composed of graphene-Poly Lactic-*co*-Glycolic Acid (PLGA) will create an environment suitable for mesenchymal stem cell proliferation and differentiation for osteogenesis and angiogenesis. I also hypothesize that in order to improve the outcomes in the use of graphene-PLGA materials and mesenchymal stem cells, it is important to mimic the signaling pathways that are triggered when cells adhere to the construct and also to monitor the changes associated with these processes for future scaffold development.

In this section, we describe the fabrication, physicochemical and biological properties of a nanoconstruct generated for musculoskeletal repair. Scaffolds were designed to induce human adipose tissue – derived mesenchymal stem cells (hADMSCs) to undergo osteogenesis and angiogenesis. Scaffolds were printed using a commercial pneumatic based Aether 1 3D printer. The printer was operated using a numerically controlled G-code. The G-code was designed to obtain a specific hatched lattice pattern conducive for bone cell and vascular network formation. The scaffold consisted of a blend of two molecular weight forms of PLGAs and a low oxygen functionalized derivative of graphene. Human ADMSCs were used to evaluate the cytocompatibility and morphology via fluorescent assays of the nanoconstruct. A multicomponent nanoengineered graphene-PLGA bone material could form the foundation for novel scaffold technology to promote rapid bone regeneration to advance bioengineering and promote human and animal health.

Introduction

Tissue engineering using stem cell regenerative strategies with the aim to remodel, replace or regenerate damaged tissues or organs with combining a biodegradable scaffold in a three-dimensional matrix to form the ideal bone graft is a significant challenge. For generations two-dimensional static cell work has dominated the study of cellular response but a shift to a more physiological three-dimensional format allowing for the study of biochemical markers and biomechanical stresses (Duval et al., 2016). Biofabrication has been presented as an application of 3D manufacturing strategies (Groll,2016). Biofabrication is defined as "the automated production of biologically functional products with structural organization from living cells, bioactive molecules, extracellular matrix, biomaterials, cell aggregates, through bioprinting or bioassembly and successive tissue transformation processes" (Moroni, 2017). In general, the biofabricated design provides a provisional 3D device to create a network with cells and control their performance in a multiplex process in tissue development and regeneration. No matter the tissue ECM type, a multitude of variables are essential when designing the complexity of a scaffold for physiological tissue replacement. The variables of importance in the design layout are architecture, mechanics, biocompatibility and the rate of biodegradability having the surface properties for cell adhesion, proliferation and differentiation for the biofabricated construct (**Figure 4.1**). Integration of the construct into the body's ECM allows cells to utilize unique mechanosensitive to promote pathological progression for regeneration (Yeung et al., 2005). The construct must also be able to stimulate biological pathways with the design of pores, topography, growth factors, biochemical ques in vitro and in vivo to intensify tissue viability, performance and morphogenesis (Dvir, 2011).

3D biofabricated constructs consisting of natural and synthetic polymers, with adult MSCs presents a novel and biomimetic approach in bone tissue engineering. Graphene has been found to be one of the most versatile biocompatible biomaterials that can interact with physiological biomolecules for biomedical applications (Shin et al., 2016). Currently, no studies have reported the osteogenic potential of adult MSCs proliferating on a 3D graphene-PLGA nanoengineered construct with dynamic support

in vivo or *in vitro*. Graphene nanomaterials as a scaffold has been shown to increase cell proliferation and a positive impact on viability of human adipose-derived stem cells (Wang et al., 2016). 3D bioprinting is the arrangement of biological and or synthetic materials and living cells in a discrete pattern that is optimal for biomimetic bone tissue engineering scaffolds that should be biocompatible, bioresorbable, and have the potential to be synthesized in an implantable form. Due to the lack of microvasculature the establishment of neovascularization is necessary if tissue engineered devices are to be progressive and provide a physical skeleton comparable to the innate extracellular matrix to enhance cell adherence, proliferation, and differentiation for bone regeneration.

A nanoconstruct was biofabricated for bone engineering using additive manufacturing with a commercial 3D bioprinter, Aether 1 (San Francisco, USA). A consistent and reproducible pattern was biofabricated with the pneumatic based bioprinter to print a PLGA-carbon based nanomaterial which consists in the designing of PLGA melting protocols to determine extrusion pressures and speed values. Various pressures were chosen based on blending viscosity and printer nozzles 0.2 mm, 0.3 mm and 0.4 mm diameters for thread runs. After an extrusion pressure was set, a grid platform, one for each speed and nozzle, were printed and evaluated. Every test was conducted multiple times with the results of the analysis suggested the printing parameters used to manufacture the 0°/45°/90° deposition pattern with a diameter of 5 mm. There were 122 in total, with heights from 0.5mm to 5mm for analysis subject to compression test, biological analysis, which consisted in cell seeding of human adipose MSCs and viability test, to implants for a rat segmental femur study.

Poly(lactic-*co*-glycolic) acid (PLGA) and Graphene

PLGA

As a linear copolymer PLGA has properties to be used for biofabrication in the areas of osteo and angiogenesis. PLGAs utilizations include drug delivery systems, biodegradable medical suture and, of course, biofabricated scaffolds for bone and vascular tissue regeneration. Due to PLGAs utilizations in having Food and Drug Administration (FDA) approval for clinical use, the ability to modify surface chemistry for biocompatibility, molecular weight and copolymer ratios to tailor biodegradation rate in

scaffold designs is what makes PLGA the choice for the study. It is highly biodegradable in physiological environments which is an imperative property for biomedical device applications. PLGA can be processed at diverse ratios within its constituent monomers, lactic acid (LA) and glycolic acid (GA) (**Figure 4.2**). Different ratios of LA to GA used in polymerization can be attained and identify the copolymer by the molar ratio of the monomers, 65:35 – 65% LA and 35% GA.

Dissolving PLGA can be performed by using a number of different solvents, such as, chlorinated solvents, chloroform, ethyl acetate, methanol and acetone which allows engineering the size, shape and be utilized in biomolecular transport (Makadia, 2011). Hydrolysis of the ester linkages is the process for degradation of PLGA. During the degradation process the byproducts lactic acid and glycolic acid are formed, but rates of degradation have several variables involved. First, molecular weight of the polymer giving ranges of several weeks to several months for polymer breakdown. Second, the ratio of acids to each other plays a large step in the breakdown with a higher content of lactic acid present making the polymer less hydrophilic, thereby absorbing less water and consequently degrade at a slower rate. Higher amounts of glycolic acid drives the degradation rate, the ratio 50:50 is an omission to the rule by which this copolymer exhibits a faster degradation rate. The degradation of PLGA has given fabrication and biofabrication a great deal of flexibility for many medical device applications.

Graphene

Graphene is a synthetic material of carbon atoms in a monolayer that is being researched in areas from thermodynamics, biosensing and now biomaterials for tissue engineering. Studies have shown that composite materials containing graphene and its derivatives can promote adhesion, proliferation, and osteogenic differentiation of MSCs in vitro (Caplan, 2005). Graphene is a 2D honeycomb high surface area lattice structure that is can be oxidized with or without further functionalization into derivatives for nanoengineering. Two- and three-dimensional nanocomposite materials containing various forms of graphene, especially oxidized graphene, have been incorporated into in vitro cell cultures to study their effect on cell proliferation and differentiation (Caplan, 2005). Commercially available derivatives of graphene include graphene oxide (GO)

and reduced graphene oxide (rGO). GO is a form of graphene that includes the functional oxygen also having functional groups being hydrophilic, such as carboxyl, epoxy and hydroxyl, which allows for a higher dispersibility in aqueous solutions and better hydrophilicity than pristine graphene (Dikin et al., 2007). The reduction of graphene oxide by chemical treatment yields reduced graphene oxide. rGO is formed and the oxidized functional groups are removed, to obtain a graphene material that contains only small amounts of residual oxygen and heteroatoms.

Adding to polymers, graphene and its descendants have shown to greatly improve mechanical properties (Sayyar et al., 2015). A modification of pristine graphene, which result in product similar but distinct from rGO in heteroatom content, was made by the University of Arkansas at Little Rock Center for Integrative Nanotechnology Sciences. This modification of pristine graphene produced a low oxygen graphene with an oxygen ratio of 6% to 10% that will be blended with PLGA and 3D printed for this study (Bourdo et al., 2017).

The combination of the polymer PLGA with a graphene oxide has been explored for the utilization of tissue engineering (Shin et al., 2015). Reports from several groups including ours have shown that nanocomposites containing graphene and its derivatives have varying physical and chemical properties, by virtue of which they can affect cell behavior. We and other groups have shown that graphene containing nanocomposites can promote adhesion, proliferation, and osteogenic differentiation of MSCs *in vitro* and *in vivo* (Dubey et al., 2015; Zhang et al.,2011; Elkhenany et al., 2017; Nayak et al., 2011), making graphene nanoparticles strong candidates for bone tissue engineering. Various sources of stem cells, such as ESCs, MSCs, and iPSCs, have been identified as potential osteoprogenitors for bone tissue and vascular engineering. Adult MSCs are favored because of their multipotency, immuno-modulatory properties, and ability to release trophic factors (VEGF). Bone marrow and adipose - derived MSCs have been benchmarked as the most applicable cell sources for bone tissue engineering due to their well-defined *in vitro* and *in vivo* osteogenic differentiation patterns (Al-Nbaheen et al., 2013; Barry, 2004; Caplan, 2007; Pittenger, 2008; Storti et al., 2019). Most importantly, the use of MSCs alleviates the need to use ES cells which is particularly important given the ethical and the political concerns associated with ES cell use. There

is a need to identify a cell source in the osteoprogenitors i.e., MSCs, which not only expresses endothelial cells that produce VEGF, but also demonstrates enhanced osteogenesis, to be efficient in both angiogenesis and osteogenesis.

Methods

All biochemicals, cell culture supplements, and disposable tissue culture supplies were purchased from Thermo Fisher Scientific unless otherwise stated. In all preparation steps, deionized (DI) water from a Millipore system unit with a resistance of 18M/cm was used. The molecular weights of PLGA were purchased from Sigma-Aldrich (St. Louis, MO). The oxidized form of graphene was obtained from our collaborators at the University of Arkansas, Little Rock. The reduced graphene oxide form of graphene was commercially obtained (Cheap Tubes Inc).

Construct biofabrication

To fabricate a viable layered orthopedic scaffold to support sufficient osteogenesis and vascularization. Three forms of commercially available PLGA (Sigma Aldrich):

1) 50:50 ratio and molecular weights of 30,000-60,000,
2) 65:35 ratio and molecular weight of 40,000-75,000 and
3) 75:25 ratio and molecular weight of 66,00-107,000 were used.

Functionalized form of graphene, oxidized to give graphene nanoparticles consisting of 6-10% oxygen was obtained from our collaborators (Dr. Shawn Bourdo's group) at the University of Arkansas at Little Rock, AR. This form of graphene is referred to as low oxygen graphene (LOG). The synthesis and physicochemical properties of LOG nanoparticles has been described in Chapter 3 and in published papers from our groups (Bourdo, 2017; Elkhenany et al., 2017). 1mg powder of LOG was obtained from UALR.

Another form of functionalized graphene consisting of approximately 12% oxygen was obtained from commercial sources from Cheap Tubes Inc (Grafton, VT, USA). This form of graphene is referred to as reduced graphene oxide (rGO). The physicochemical properties of rGO were provided by the manufacturer (www.cheaptubes.com). The

specific details of rGO have been described in Chapter 3. 4.0mgs of rGO powder was obtained.

A blend of two molecular weights of PLGA with LOG was used to 3D print the construct (**Figure 4.4-4.5**). The material blend was prepared by mixing 1 gram of each form of PLGA with 1 mL DMSO as a solvent in a 2:1 w/v ratio. 1 mg of LOG powder was added to the PLGA blend to give a final concentration of 0.05 wt%. The mixture was continuously rotated in a rotisserie oven for two hours at 65^{o}C. The mixture was hand mixed every 15 minutes to ensure a uniform and complete blending of PLGA and graphene. Two iterations with varying molecular weights of PLGA blended with 1.0 mg of LOG were generated. On the second day, the mixture was gas sterilized using hydrogen peroxide using a 28-minute protocol (Sterilis Solutions, MA). The blend was stored in the pneumatic syringe at -20^{o}C until use. Two iterations of the nanoconstructs consisting of 50:65 and 50:75 molecular weights of PLGA blended with LOG were finally fabricated.

The polymer/graphene blends were removed from the freezer and brought to room temperature before loading the syringe onto the printer. The scaffolds were printed on tissue culture polystyrene dish with the platform temperature maintained at 15 to 30 °C. The temperature required for extrusion depends strongly on the molecular weights and inner diameter of the nozzle. The extrusion was conducted with 4-6 bars pressure with an average of 0.5-1.0mm/s using a 0.2mm to 0.3mm inner diameter nozzle. The choice of the inner diameter of the printer nozzle provides a great balance between speed and precision. The printed scaffolds were kept at -20^{o}C to preserve the design. The printed scaffolds were removed from the freezer and used either *in vitro* or *in vivo*.

Each scaffold was subjectively evaluated while printing and at completion. If visual inspection found it unsatisfactory, the polymer blend was reheated and reprinted.

3D Bioprinter Setup

The PLGA/graphene nanoconstructs were printed using the 3D printer called Aether 1, made by a small start-up company, Aether in San Francisco, CA. It is in the Large Animal Regenerative Medicine Laboratory at the University of Tennessee,

College of Veterinary Medicine (**Figure 4.6**). Pneumatic extrusion-based printing was used. Unlike in FDM, where extrusion is a gear driven system, bioprinting nozzle in Aether 1 is pressurized, therefore pressure dictates extrusion flow. Aether is an 8 pneumatic syringe extruder with a vertical retraction system with one anodized aluminum heated syringe mount, double head FFF hot end filament extruder and solenoid microvalve droplet jetting extruders which all move along the x-y axes, while the anodized aluminum heated stage moves along the z axis. Printer chamber has UV blacklight LED lighting system, automatic syringe tip cleaning areas, and center attached camera. The printer comes with an external air compressor, which provides air flow on a range of 2 to 100psi. The syringe units allow for nozzles of different gauges for material selections. Heated syringe allows to print high heat polymers and the microvalve droplet jetting allows printing of different kinds of cells in single or double syringe loads.

The main features of Aether 1 are as follows: Extrusion System – Pneumatic based, Print Heads – 1 Heated 30cc Pneumatic Print Head as well as 7 Pneumatic Syringe Heads and 2 FFF Hot End Filament Extruders, Air Supply – External Compressor, UV Crosslinking Wave Lengths - 365 nm & 405 nm, X / Y Axis - 1.055 micron [0.001055mm], Z Axis - 0.43 nanometers [0.00000043mm], Operating Pressure-13.78kPa (0.13 Bars) - 689.47 kPa (6.89 Bars), Layer Resolution - 100 µm.

Biofabrication Design Parameters

CAD Software: The scaffold for biofabrication was designed using a CAD software, Autodesk Fusion 360. The goal was to fabricate a scaffold with a pattern consisting of alternating angles of 45^{o} and 90^{o}.

First, a 2D design was laid out to specify the contact angle of the scaffold. The aim was to replicate the nozzle path on the stage. A 5mm diameter circle was formed, and a layer-by-layer build was made to match the rat femur design. Vertical lines for each guideline were laid out in lengths from left to right format with 0.30mm apart making the first single scaffold layer. Once the single layer is completed, the two construct prototypes could be made as an assembly of the design. The first layer was secured on the grid and copied: this second layer was then relocated 0.3 mm along the

z-axis and rotated 45°. This operation was repeated until the desired geometries were achieved. The final pattern consisted of 15 layers for the 5mm high (**Figure 4.6**).

A critical point is to maintain construct porosity within the layers. The filament gap and layer orientation of 0°/90°, 0°/45°/90° must be considered when seeding sells for differentiation. Once the porosity values are set the strand diameter must be chosen which is evaluated by the combination of the bars of pressure and speed, along with your strand distance which may change as well, since its value includes the porosity gap value for the adjustments of the strain diameter

Slicer: Once the CAD which is represented as .stl file is complete, it is then loaded in the slicing software, Element. The scaffold design from the CAD is a series of bidirectional cross sections, which is then processed by the slicer software, creating a mathematical interpretation of the design. Element software provided with Aether1 bioprinter sets the slicing parameters, print dimensions, as well as the post processing script. The slicing software effectively translates the 3D scaffold into a control language known as a G-code file (**Figure 4.7 - 4.10**). Programming parameters such as print bed temperature, stand thickness, extruder temperature, flow rate speed and pneumatic pressure are the main parameters set manually for the bioprinting process.

Layer height design: Layer height thickness is a measure of the layer height of each consecutive addition in the process. The layer height is crucial to the design of the vertical resolution of the z-axis. A layer height was reviewed in two methods, 2.5mm or a full 5mm height, one for the plain PLGA double molar ratio iteration and one for the PLGA double molar ratio/LOG iteration based on the femur model. This is an important consideration in the design of the constructs because we intend to use it in a weight – bearing rat femoral defect model. Some stability issues could arise, if the strand diameter is thin (0.2mm) and the layer height is low. It could cause the structure to collapse.

Physicochemical and biological testing

Instron Compression Test

After multiple prints of each iteration, analyses were conducted. Mechanical analysis consisted in compression on 3D PLGA 50:50+65:35+LOG and PLGA 50:50+75:25+LOG with a 5 mm diameter, 5mm height and 0°/45°/90° deposition pattern, so to evaluate scaffolds mechanical properties. The test was conducted using an INSTRON 5965 (*Illinois Tool Works Inc, Norwood, MA*), compressed until 2.5mm/min deformation was reached (**Figure 4.11**).

Scanning Electron Microscopy (SEM)

SEM allows for imaging the morphology of the biofabricated construct so as to gather data on the physical characteristics of topography, spatial distribution of the thread spacing and porosity and analyze the variability in the materials composition. All of these factors are fundamental to evaluate the functional biocompatibility of a biomaterial. The constructs were prep in the lab using a SEM protocol. Samples were place in vials. Next, a fixative solution of glutaraldehyde was poured to cover samples at room temperature 2 hours. Samples were then washed 3 times with 0.1M of phosphate buffer for 10 minutes each. Osmium solution prepped at 2% was then poured over the samples for 2 hours at room temperature and kept in a dark location. Samples were then washed 3 times with 0.1M of phosphate buffer for 10 minutes each. Dehydration sequence was then performed by taking EtOH in increasing order of 30%/50%/70%/80%/90%/96%/100% - each percentage was for 15 minutes. Samples were then placed in desiccator overnight then take to the scope for imaging.

Calcein Assay

Calcein-am staining was used to appraise viability cell and proliferation on the PLGA-graphene construct. Calcein-am is a non-fluorescent compound that permeates the cellular membrane of living cells, where intracellular esterase is immediately hydrolyzed, a process that transforms the calcein-am to calcein identifying cell viability on the material. 50,000 cells were seeded per sample of PLGA+graphene for 48 hours. For evaluation, samples were incubated with 0.5 mL of staining solution, containing 10

μg/ml calcein-am reconstituted with dimethyl sulfoxide, for 5 minutes at 37°C, and the fluorescence was viewed on Lecia fluorescent microscope.

Biodegradation Assessment Study

Biodegradable polymers such as PLGA in a physiological environment can degrade gradually and then dissipate following implantation. This degradation is critical for tissue-engineering operations, on account of the polymer dissipating as functional tissue regenerates. Interactions of cell-matrix interactions with an assortment of biodegradable polymers have been studied (Gentile, 2014). The hydrolytic biodegradation of PLGA may contribute an additional level of regulation over cellular interactions: during degradation progress, the surface of the PLGA is constantly renewed by physiological enzymatic reactions, providing a dynamic substrate for cell attachment and growth. This focused on the degradation properties of the mixed molar iterations of the PLGA and carbon-based nanomaterial. The iterations will be compared in the effects of the ionic content of phosphate buffered saline (PBS) on the 3D printed degradation properties. Therefore, in this study the direct *in vitro* degradation of PBS solution with a designed continuous flow-spinner bioreactor, that can flow fluids through the porous scaffolds in a controlled environment. The construct was systematically inspected to reveal the variations in morphological changes and in terms of degradation rate analyzed weight loss of the 3D printed PLGA composite construct. Then, the different reactions can be compared to fully understand the reactions in vivo which may be closely resembled by the degradation in *in vivo*. Each scaffolds iteration will be placed into the continuous flow-spinner flask bioreactor at 37°C with 5% CO2 and spinner at 65rpm and peristaltic pump at 55mLs per min. Initial dry weight was taken and initial wet was taken at 48 hours in each solution. Samples weights will be collected each week for 8 weeks for analyses and the PBS solution will be replaced weekly. At predetermined time points, the construct pieces were removed from the PBS solution and quickly washed with DDI water to remove excess salts or solution accumulation on the surface. The scaffolds are air dried for one hour then weights were measured.

Results

In this study we chose a novel blend of two different molecular weights of PLGA each with two different iterations of carbon – based nanoparticles to form a nanoconstruct conducive for osteogenesis and angiogenesis of mesenchymal stem cells. PLGA is an FDA – approved, biodegradable polymer commonly used in biomedical research and 3D printing. The two molecular weights of PLGA were chosen because of their distinct degradation properties (Gentile, 2014), with a long - term goal of providing a structure to support new and damaged bone and vasculature.

The pattern design and topography of the biofabricated scaffolds has to meet the native tissue architecture to have a strong development and achievement for a positive cell behavior. The basement membrane of the ECM forms a multi complex mesh of pores, fibers, ridges and contact angles (Yang, 2011). Contact guidance of cells guided by topographical cues mimicking the ECM independent of biochemistry is the reasoning of using PLGA and carbon-based nanomaterials for the advancement of adhesion, migration and differentiation to promote changes in cytoskeletal organization and gene expression. The pattern designs were fabricated to attain 75-80% porosity, between 100 and 300 μm interconnectivity, with contact angles at 45 and 90° to support the osteogenic and angiogenic potential of mesenchymal stem cells.

The biofabricated blend and CAD design were chosen corresponding to support the bone's ECM architecture, which shows a polymer that is bioactive, biocompatible and controllable biodegradability, so to support bone behavior for all the regeneration development.

Identification of solvents on PLGA for Fabrication

There are reports to show various different solvents for PLGA polymers (Guo et al., 2017). We first started out using an emulsion based solvent combination. The organic solvent chloroform was used to dissolve the two molar ratios of PLGA with the blending of the carbon-based nanomaterial. Methanol was then added to the mix to induce a PLGA+nanomaterial precipitate. This mixture worked will but the needed temperatures to print a construct ranged from 165 – 182^{o}C with PSI of 85 to 100.

Printing with 0.2mm and 0.3 mm nozzles did produce a thread. The mixing of double molar ratios caused viscosity that was challenging to work with. The target thread size was 200 μm to 300 μm diameter, for which a full height of 5 mm.

We then moved to the study using DMSO. DMSO is a polar, aprotic solvent that is frequently utilized in biomedicine and cell culture research. This solvent can breakdown polar and nonpolar compounds, including all molar ratios of PLGA. DMSO plays a dual role allowing increased mobility at lower temperatures and as a polar aprotic solvent shield's ester bonds allowing for minimal degradation from hydrolysis reducing biodegradation while *in vitro* and *in vivo* (Dong, et al., 2006).

We were able to accomplish a visually homogenous mixture of the two scaffolds each with different molar ratios of PLGA with carbon-based nanomaterial and DMSO. In our hands, DMSO was found to be suitable and hence, was used as the solvent for the blending process. When constructs were placed in -20^{o}C the DMSO would also be used as a cryoprotectant.

Identification of Fabrication and Printing Conditions

General characterization consisted of the extrusion of material design with changes in CAD or written in the G-code to evaluate material threading diameter using different nozzle sizes, pneumatic pressure and extrusion speed values. Results from multiple test prints using 0.2 mm and 0.3 mm nozzles at PSI test ranging from 65 to 95, temperature ranges 45^{o}C to 90^{o}C and speeds 0.2 mm/s to 1.0 mm/s with heights of 1-5mm's. The addition of the carbon-based nanoparticles did not alter the viscosity or presented any print pattern issues.

The evaluation of the bioprinter's behavior when it came to changes in temperature variations and pneumatic pressures were applied to find the best pressure/speed combination that will provide a diameter thread for detailed design and porosity of the construct. After comparison of data between 0.2 mm and 0.3 mm nozzles for thread diameter to build the construct were compared and the 0.2 mm nozzle showed smooth clean threads with a consistent thickness. Extrusion speed of 0.6 mm/s was chosen for both material blends while the pneumatic pressure was set at 75 psi and temperatures maintained at 65°C. The highest printing quality for the Aether

1 was obtained at the settings listed - *Pressure 5-6 bar, Temperature 65^{o}C, Extrusion speed 0.6 mm/s and Nozzle 0.2mm.*

Each construct print time was 2 hours and 14 minutes. 88 iterations of each molar ratio were made at 0.5 mm high, and 36 iterations of each molar ratio were made at 5 mm high dimensions. These contracts were printed to be tested in multitude of levels from cellular culture studies, mechanical and degradation stress and *in vivo* study to follow.

Compression Test

Mechanical characterization consisted of a compression test done on the Instron unit. This test was carried out using an animator, until 50% deformation level was reached being 2.5 mm tall. Compression test showed that the Young's modulus of the PLGA/carbon-based nanoparticles/DMSO scaffolds for 50:50-65:35 was 224.657 MPa while that of 50:50-75:25 was 268.104 MPa. These values were similar for the nanoconstructs containing LOG and rGO (**Figure 4.12 – 4.13**). Results showed a PLGA/ DMSO with carbon-based nanomaterials can handle compression needed for bone tissue engineering.

Sterilization

All iterations of PLGA and graphene mixtures were sterilized using multiple methods.

1. Steam using a 30 min cycle.
2. Gas - hydrogen peroxide gas using a 28 min cycle,
3. -20 to -80 freezer for 4h hours
4. Ultraviolet light - 2-4 hours of exposure.

Visual evaluation was first performed for each method. Subsequently, each scaffold was tested for cytotoxicity using human mesenchymal stem cells for a seven-day period. All samples tested with calcein AM cell viability assay. Each method of sterilization showed they could support cell life on the material as well as proliferation. None of the samples showed any bacterial or fungal contamination. Freezer method was chosen for future storge and preparations of the blend. The blend was also stored in the metal syringe at -20^{o}C between prints with all iterations performing well. The

constructs printed at 0.5 mm high were sterilized in -20^{o}C freezer for several day and then one hour of UV radiation before seeding with adult human adipose mesenchymal stem cells. Viability of cells measured a calcein assay showing sales biocompatibility with the construct design. To further show biocompatibility cells were seated and track starting at 24 hours going to 21 days by images for proliferation.

In vitro Biodegradation

PLGA+graphene at 50:65 and 50:75 blend was maintained for 8 weeks in order to determine the degradation rate on the membrane. The samples were kept at 36.8^{o}C to 37.2^{o}C with a magnetic stir bar set at 65 rpm and a peristaltic pump set at 50mL/min. This unit ran 24 hours a day with material checks one time a week per protocol. Each week material fatigue could be seen by eye and a weight chart was kept. Week 7 each blend constructs microporous matrix began to show cracks that could been seen without magnification. Crystals were found scattered on the surface of the construct membrane. Weight loss are numbers used for the degradation index. Both constructs showed limited weight loss that could be explained by the residual DMSO which has been shown to reduce the degradation of PLGA by buffering of the ester bonds (Guo, et. al., 2018) (**Figure 4.14**). Furthermore, it is thought that crystal formation on the PBS may also play a role in the measurements which could skew the actual mass degradation. Future studies using simulated body fluids will need to be performed to have a stronger understand of PLGA biodegradation.

Scanning Electron Microscopy

The topography of the 3D biofabricated construct was assessed using SEM. As shown in figure 4.14 (**Figure 4.15 a-e**), the presence of thread structure, valleys, roughness and porosity are visible and replicated on the constructs. Figure 4 (f) was imaged to show cell attachment on surface with extensive filopodia on the construct. Both blends topography profile was within the limits for an optimal construct for future studies.

Cell Proliferation and Viability

The calcein Live/Dead fluorescent analysis was conducted to evaluate cytocompatibility and proliferation on the PLGA+LOG construct post 48-hour seeding. Seeding was completed throughout the construct. The evaluation and imaging of calcein-am on the PLGA+LOG construct was present confirming proliferation and cytocompatible on the construct, but fluorescence was weak (**Figure 4.16**). Leading to the next study of seeding the constructs with transduced MSCs.

Cell Proliferation and Attachment

At multiple time points the during the culture period, the distribution of the GFP and RFP transduced adipose MSCs were investigated on PLGA+LOG and PLGA +rGO contracts. The visualization of the cells was imaged using a fluorescence microscope showing PLGA+LOG using RFP cells and PLGA+rGO using GFP cells (**Figure 4.17 - 4.20**). The images show live cells on the construct at 24 hours and 7, 14, and 21 days of the culture. Close to 100% cell viability with cells present throughout the construct with no problems in proliferation morphology and reduction in color. This methodology is repeatable for cells and can definitely be utilized in future studies for tracking proliferation and possible differentiation in biofabricated constructs.

Conclusion

The advancement of additive manufacturing techniques, such as 3D Biofabrication / Bioprinting, helps in creating 3D biocompatible implants on which multiple cell types can be seeded. This progress in technology gives an encouraging substitute to autogenous bone grafting and growth in material science development.

In this chapter, the architecture of a micro and nano cylindrical 0°/45°/90° construct was biofabricated, via additive manufacturing technique, in precise 3D bioprinting, and in conclusion analyzed. Those 3D constructs were designed of compounded material, of 2 different molar ratios of PLGA matrix to mimic the ECM and reinforced a carbon-based nanoparticle, which to support differentiation of cells for osteogenesis in angiogenesis.

This study provided data to show that we were able to successfully fabricate PLGA/carbon nanoparticle nanoscaffolds, which exhibited adequate mechanical strength, biodegradation, and *in vitro* biocompatibility. These results warrant in vivo application in a long bone defect model to fully understand and evaluate the biocompatibility and osteogenic potential.

References

Alford, Andrea I., et al. "Extracellular Matrix Networks in Bone Remodeling." *The International Journal of Biochemistry & Cell Biology,* vol. 65, 2015, pp. 20-31.

Al-Nbaheen, M., et al., *Human stromal (mesenchymal) stem cells from bone marrow, adipose tissue and skin exhibit differences in molecular phenotype and differentiation potential.* Stem Cell Rev, 2013. **9**(1): p. 32-43.

Barry, F.P. and J.M. Murphy, *Mesenchymal stem cells: clinical applications and biological characterization.*Int J Biochem Cell Biol, 2004. **36**(4): p. 568-84.

Bourdo, S.E., et al., *Physicochemical characteristics of pristine and functionalized graphene.* J Appl Toxicol, 2017. **37**(11): p. 1288-1296.

Caplan, A.I., *Adult mesenchymal stem cells for tissue engineering versus regenerative medicine.* Journal of Cellular Physiology, 2007. **213**(2): p. 341-347.

Causa, F, Netti, PA, and Ambrosio, L. A multi-functional scaffold for tissue regeneration: the need to engineer a tissue analogue. Biomaterials, 28(34):5093–5099, 2007.

De Miguel, M.P., et al., *Immunosuppressive Properties of Mesenchymal Stem Cells: Advances and Applications.* Current Molecular Medicine, 2012. **12**(5): p. 574-591.

Dikin D.A., Stankovich S., Zimney E.J., Piner R.D., Dommett G.H.B., Evmenenko G., Nguyen S.T., Ruoff R.S., Preparation and characterization of graphene oxide paper, Nature, 448 (2007) 457–460. https://doi.org/10.1038/nature06016 PMID: 17653188

Dong W.Y., Korber M., V. Esguerra Lopez, Bodmeier, R., Stability of poly(D,L-lactide-co-glycolide) and leuprolide acetate in in-situ forming drug delivery systems, J. Control Release 115 (2) (2006) 158-167.

Dubey, N., et al., *Graphene: A Versatile Carbon-Based Material for Bone Tissue Engineering.*Stem Cells Int, 2015. **2015**: p. 804213.

Dvir T, Timko B P, Kohane D S and Langer R 2011 Nanotechnological strategies for engineering complex tissues. Nat. Nanotechnol. 6 13–22.

Elkhenany, H., et al., *Graphene supports in vitro proliferation and osteogenic differentiation f goat adult mesenchymal stem cells: potential for bone tissue engineering.* J Appl Toxicol, 2015. **35**(4): p. 367-74.

Elkhenany, H., et al., *Graphene nanoparticles as osteoinductive and osteoconductive platform for stem cell and bone regeneration.* Nanomedicine, 2017. **13**(7): p. 2117-2126.

Gloria, A, R De Santis, and L Ambrosio. Polymer-based composite scaffolds for tissue engineering. Journal of Applied Biomaterials & Biomechanics, 8(2), 2010.

Gloria, A, T Russo, U D'Amora, S Zeppetelli, T D'Alessandro, M Sandri, M Bañobre-López, Y Piñeiro-Redondo, M Uhlarz, Anna Tampieri, et al. Magnetic poly ("-caprolactone)/iron-doped hydroxyapatite nanocomposite substrates for advanced bone tissue engineering. Journal of The Royal Society Interface, 10(80):20120833, 2013.

Gloria, A, T Russo, R De Santis, and L Ambrosio. 3d fiber deposition technique to make multifunctional and tailor-made scaffolds for tissue engineering applications. Journal of Applied Biomaterials & Biomechanics, 7(3), 2009.

Gentile P, Chiono V, Carmagnola I, Hatton PV. An overview of poly(lactic-co-glycolic) acid (PLGA)-based biomaterials for bone tissue engineering. *Int J Mol Sci*. 2014;15(3):3640-3659. Published 2014 Feb 28. doi:10.3390/ijms15033640.

Groll, J, Boland, T, Blunk, T, Burdick, J A Cho, D, Dalton, PD, Derby, B, Forgacs, G, Li, Q, Vladimir, A M, , et al. Biofabrication: reappraising the definition of an evolving field. Biofabrication, 8(1):013001, 2016.

Guo, T., Casey G. Lim, Maeesha Noshin, Julia P. Ringel, John P. Fisher, 3D printing bioactive PLGA scaffolds using DMSO as a removable solvent, Bioprinting, Volume 10, 2018, e00038, ISSN 2405-8866.

Guo, T., Holzberg, T.R., Lim, C.G., Gao, F., Gargava, A., Trachtenberg, J.E., Mikos, A.G. Fisher, J.P., 3D printing PLGA: a quantitative examination of the effects of polymer composition and printing parameters on print resolution, Biofabrication 9 (2) (2017) 024101.

Hutmacher DW, Sittinger,M, and Risbud, MV. Scaffold-based tissue engineering: rationale for computer-aided design and solid free-form fabrication systems. TRENDS in Biotechnology, 22(7):354–362, 2004.

Im, G.I., *Bone marrow-derived stem/stromal cells and adipose tissue-derived stem/stromal cells: Their comparative efficacies and synergistic effects.* J Biomed Mater Res A, 2017. **105**(9): p. 2640-2648.

Mahmood, M., et al., *Cytotoxicity and biological effects of functional nanomaterials delivered to various cell lines.* Journal of Applied Toxicology, 2010. **30**(1): p. 74-83.

Majeed, W., et al., *The role of surface chemistry in the cytotoxicity profile of graphene.* J Appl Toxicol, 2017. **37**(4): p. 462-470.

Makadia, H.K.; Siegel, S.J. Poly lactic-*co*-glycolic acid (plga) as biodegradable controlled drug delivery carrier. *Polymers-Basel* **2011**, *3*, 1377–1397.

Moroni L, Boland T, Burdick JA, De Maria C, Derby B, Forgacs G, Groll J, Li Q, Malda J, Mironov VA, Mota C, Nakamura M, Shu W, Takeuchi S, Woodfield TBF, Xu T, Yoo JJ, Vozzi G. Biofabrication: A Guide to Technology and Terminology. Trends Biotechnol. 2018 Apr;36(4):384-402. doi: 10.1016/j.tibtech.2017.10.015. Epub 2017 Nov 11. PMID: 29137814.

Nayak, T.R., et al., *Graphene for controlled and accelerated osteogenic differentiation of human mesenchymal stem cells.* ACS Nano, 2011. **5**(6): p. 4670-8.

Pittenger, M.F., *Mesenchymal stem cells from adult bone marrow.* Methods Mol Biol, 2008. **449**: p. 27-44.
Sayyar, S., Murray, E., Thompson, B. C., Chung, J., Officer, D. L., Gambhir, S., Spinks, G. M. and Wallace, G. G., J. Mater. Chem. B, 2015, 3, 481–490.

Shin, Y.C., Lee, J.H., Jin, L., Kim, M.J., Kim, Y.J., Hyun, J.K., Jung, T. G., Hong, S. W. and Han, D. W., J. Nanobiotechnol., 2015, 13, 21.

Storti, G., et al., *Adipose-Derived Stem Cells in Bone Tissue Engineering: Useful Tools with New Applications.* Stem Cells Int, 2019. **2019**: p. 3673857.

Yang MT, Fu J, Wang YK, Desai RA, Chen CS. Assaying stem cell mechanobiology on microfabricated elastomeric substrates with geometrically modulated rigidity. Nat Protoc 2011; 6:187e213.

Yeung, T., Georges, P.C., Flanagan, L.A., Marg, B., Ortiz, M., Funaki, M., Zahir, N., W. Ming, Weaver, V., P.A. Janmey, Effects of substrate stiffness on cell morphology, cytoskeleton structure and adhesion. *Cell Motil. Cytoskeleton* 60, 24-34 (2005).

Vacanti, JP and Langer, R. Tissue engineering: the design and fabrication of living replace- ment devices for surgical reconstruction and transplantation. The lancet, 354: S32–S34, 1999

Ventre M, Causa F, Netti PA. 2012 Determinants of cell – material crosstalk at the interface: towards engineering of cell instructive materials. J. R. Soc. Interface 9, 2017 – 2032. (doi:10.1098/rsif.2012.0308

Wick, P., Louw-Gaume, A.E., Kucki, M., et al., *Classification framework for graphene-based materials.* Angew. Chem. Int. Ed., 2014. **53**: p. 7714-7718.

Zhang, B., et al., *Interactions of graphene with mammalian cells: Molecular mechanisms and biomedical insights.* Adv Drug Deliv Rev, 2016. **105**(Pt B): p. 145-162.

Zhang, Z.G., et al., *Advances in bone repair with nanobiomaterials: mini review.* Cytotechnology, 2011.**63**(5): p. 437-43.

Appendix

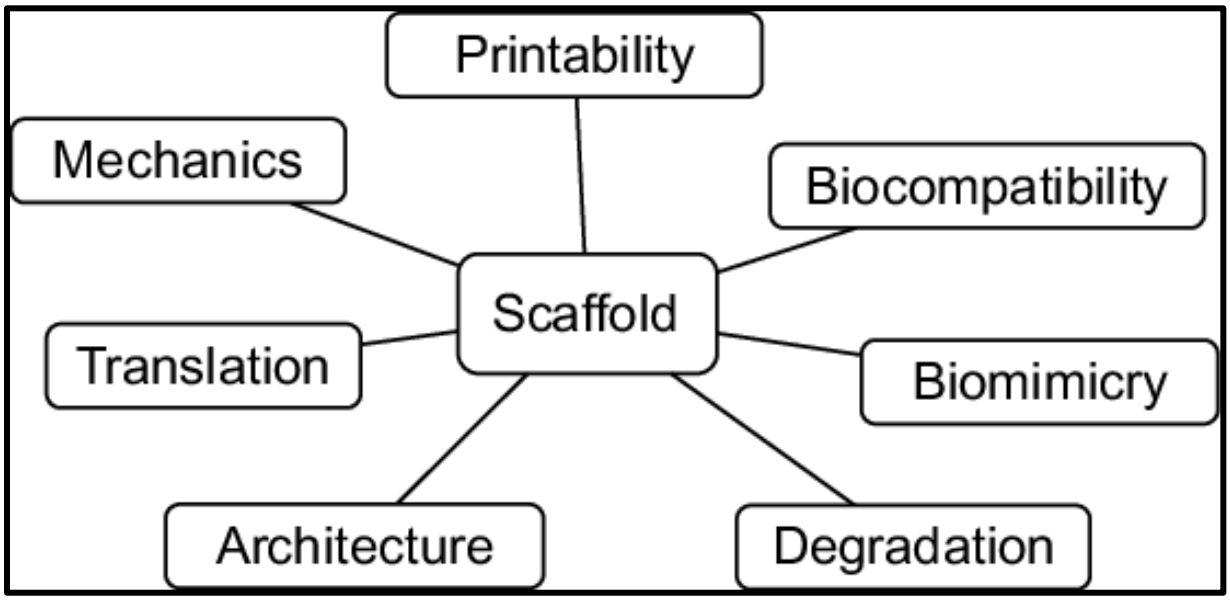

Figure 4.1. Design layout should provide a three-dimensional space and meet as many of the parameters as possible.

(a.) Sigma-Aldrich

P2191-5G	50:50	Mol wt. 30,000 – 60,000
P2066-5G	65:35	Mol wt. 40,000 – 75,000
P1941-5G	75:25	Mol wt. 56,000 – 107,000

(b.)

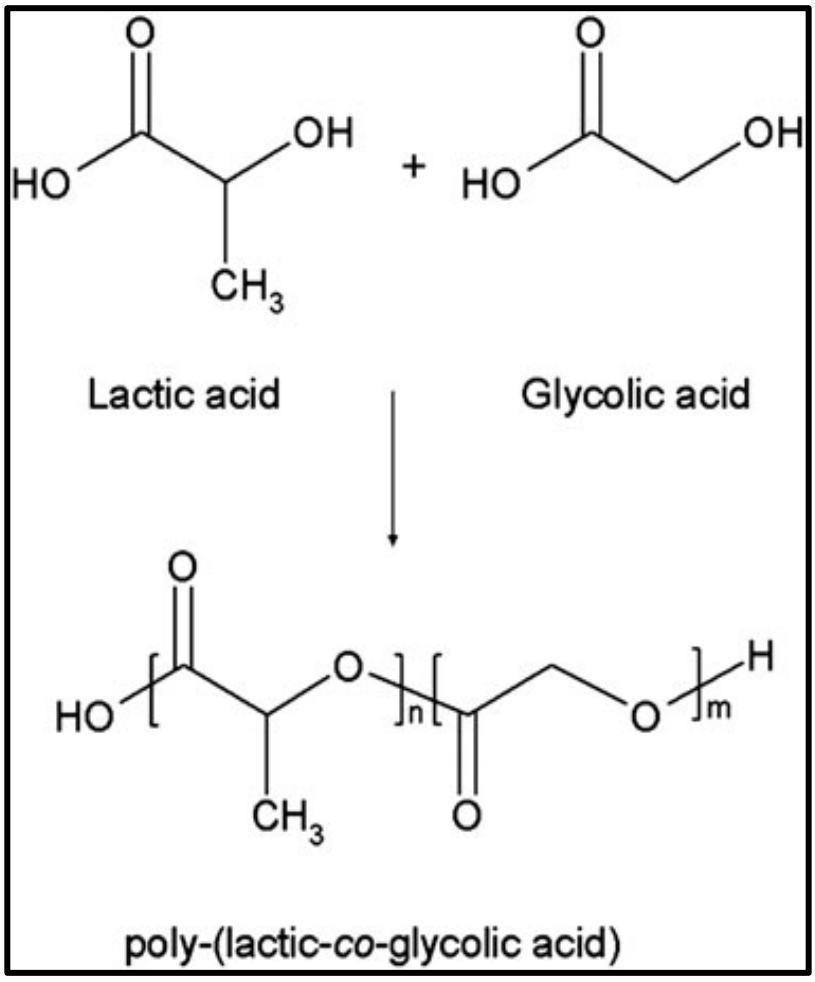

Figure 4.2 (a). Sigma-Aldrich codes and PLGA ratios used. (b) Chemical structure of poly (lactic-*co*-glycolic acid) and its monomers.

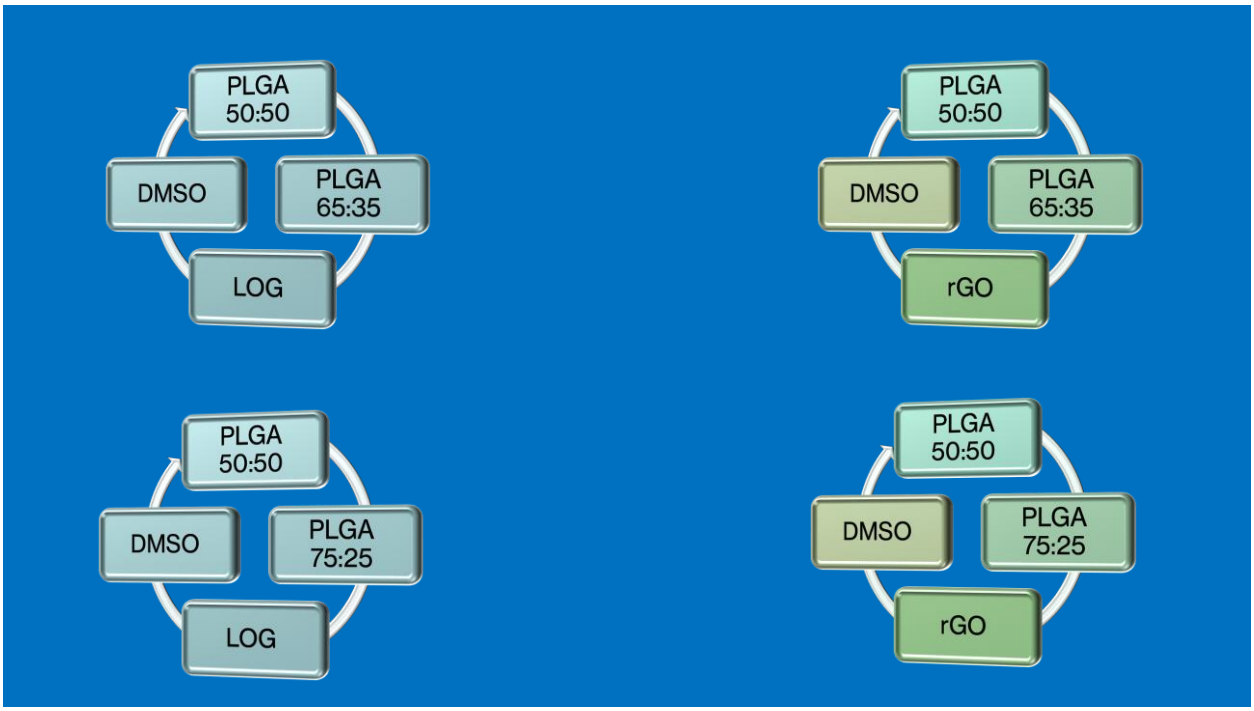

Figure 4.4. PLGA:Carbon-based nanoparticle Mix Layout

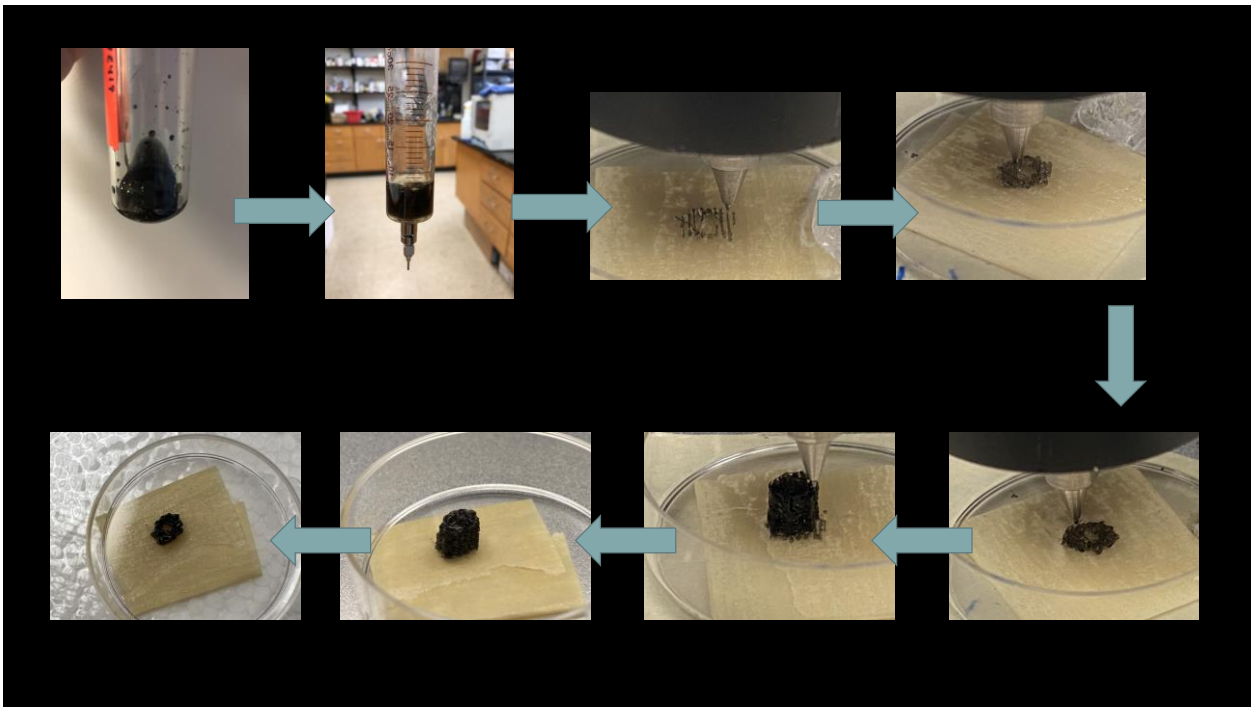

Figure 4.5. Layout of prints from blend mix of two molar ratios of PLGA+LOG showing a layer print until the programmed height is complete.

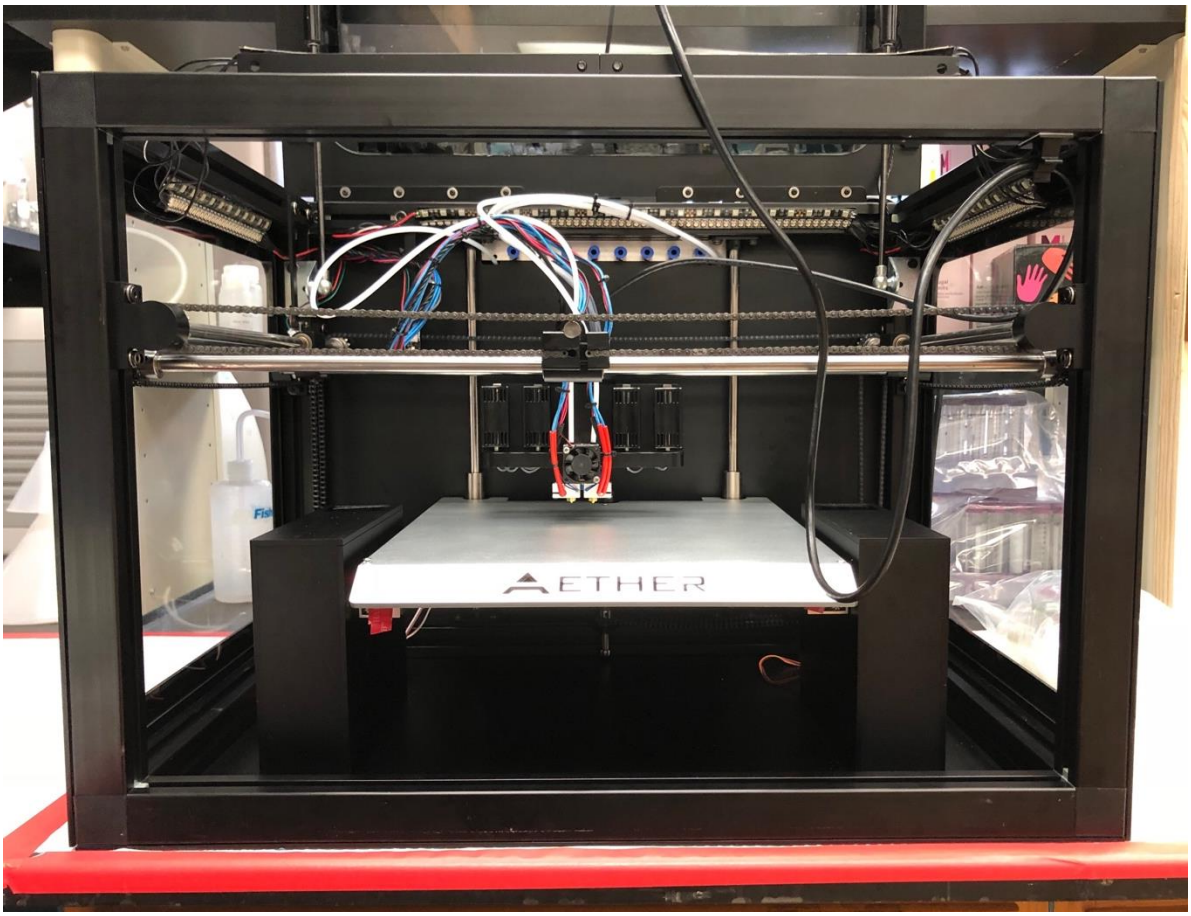

Figure 4.6. Aether 1 Bioprinter at the College of Veterinary Medicine, Large Animal Clinical Sciences, Regenerative Medicine Lab.

(a)

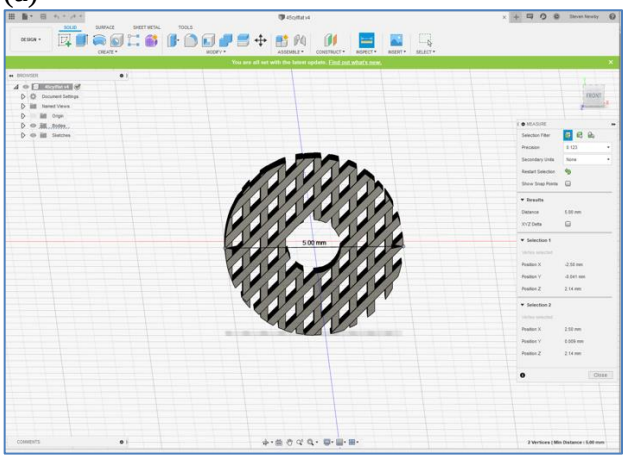

(b)

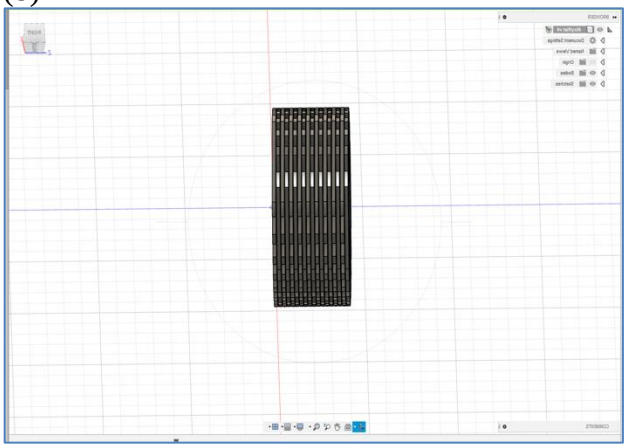

(c)

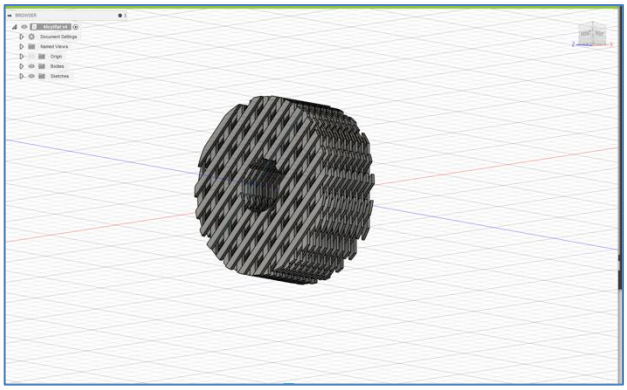

Figure 4.7. Biofabrication design – Autodesk 360 software views, (a) Front view, (b) Side view and (c) Oblique view.

G CODE
; Generated with MatterSlice 1.0
; filamentDiameter = 1.75
; extrusionWidth = 0.2
; firstLayerExtrusionWidth = 0.2
; layerThickness = 0.1
; firstLayerThickness = 0.1
; automatic settings before start_gcode
G21 ; set units to millimeters
M107 ; fan off
; settings from start_gcode
G28 ; home all axes
M86 D0
M87 D1
M76 D0
M72 D0
; automatic settings after start_gcode
G90 ; use absolute coordinates
G92 E0 ; reset the expected extruder position
M82 ; use absolute distance for extrusion
M78 B1 P99 D0
M109 T2 S60
T0 B1
M205 X10
; Layer count: 50
; Layer Change GCode
; LAYER:0
M205 X5
M87 B1 D1
M400
M107
G0 Z1.25
G0 F4800 X147.739 Y88.189 Z1.3
; TYPE:WALL-OUTER
G0 Z0.05
M400
M87 B1 D0
M78 B1 D1
M86 B1 D1
G1 F16.5 X147.719 Y88.236
G1 X147.719 Y91.763
G1 X147.739 Y91.81
M400
M86 B1 D0
G0 Z1.3
G0 F4800 X147.139 Y90.453
G0 Z0.05
M400
M86 B1 D1
G1 F16.5 X147.12 Y90.109
G1 X147.128 Y89.679
G1 X147.139 Y89.559
M400
M86 B1 D0
G0 F4800 X147.144 Y90.546
; TYPE:FILL
M400
M86 B1 D1
G1 F16.5 X147.12 Y90.109
G1 X147.128 Y89.679
G1 X147.139 Y89.559
M400
M86 B1 D0
G0 F4800 X147.144 Y90.546
; TYPE:FILL
M400
M86 B1 D1
G1 F16.5 X147.199 Y90.97
M400
M86 B1 D0
G0 Z1.3
G0 F4800 X148.339 Y92.374
; TYPE:WALL-OUTER
G0 Z0.05
M400
M86 B1 D1
G1 F16.5 X148.319 Y92.347
G1 X148.319 Y87.652
G1 X148.339 Y87.625
M400
M86 B1 D0
G0 Z1.3
G0 F4800 X148.939 Y87.303
G0 Z0.05
M400
M86 B1 D1
G1 F16.5 X148.919 Y87.318
G1 X148.919 Y92.681
G1 X148.939 Y92.696
M400
M86 B1 D0
G0 Z1.3
G0 F4800 X149.499 Y89.137
G0 Z0.05
M400
M86 B1 D1
G1 F16.5 X149.519 Y89.113
G1 X149.519 Y87.145
G1 X149.539 Y87.139
M400
M86 B1 D0
G0 Z1.3
G0 F4800 X150.099 Y87.104
G0 Z0.05
M400
M86 B1 D1
G1 F16.5 X150.119 Y87.105
G1 X150.119 Y89.009
G1 X150.139 Y89.013
M400
M86 B1 D0
G0 Z1.3
G0 F4800 X150.739 Y89.339
G0 Z0.05
M400
M86 B1 D1
G1 F16.5 X150.719 Y89.292
G1 X150.719 Y87.197
G1 X150.699 Y87.187
M400
M86 B1 D0
G0 Z1.3
G0 F4800 X152.499 Y88.541
G0 Z0.05
M400
M86 B1 D1
G1 F16.5 X152.519 Y88.604
G1 X152.519 Y91.395
G1 X152.499 Y91.458
M400
M86 B1 D0
G0 Z1.3
G0 F4800 X150.731 Y90.68
G0 Z0.05
M400
M86 B1 D1
G1 F16.5 X150.715 Y90.711
G1 X150.719 Y92.802
G1 X150.699 Y92.812
M400
M86 B1 D0
G0 Z1.3
G0 F4800 X150.752 Y90.594
; TYPE:FILL
G0 Z0.05
M400
M86 B1 D1
G1 F16.5 X150.778 Y90.544
G1 X150.83 Y90.436
M400
M86 B1 D0
G0 Z1.3
G0 F4800 X150.139 Y90.987
; TYPE:WALL-OUTER
G0 Z0.05
M400
M86 B1 D1
G1 F16.5 X150.119 Y90.995
G1 X150.119 Y92.894
G1 X150.099 Y92.896
M400
M86 B1 D0
G0 Z1.3
G0 F4800 X149.539 Y92.86
G0 Z0.05
M400
M86 B1 D1
G1 F16.5 X149.519 Y92.854
G1 X149.519 Y90.882
G1 X149.499 Y90.859
; Layer Change GCode
; LAYER:1

Figure 4.8. G-code that repeats for each layer. Above is 1layer of code.

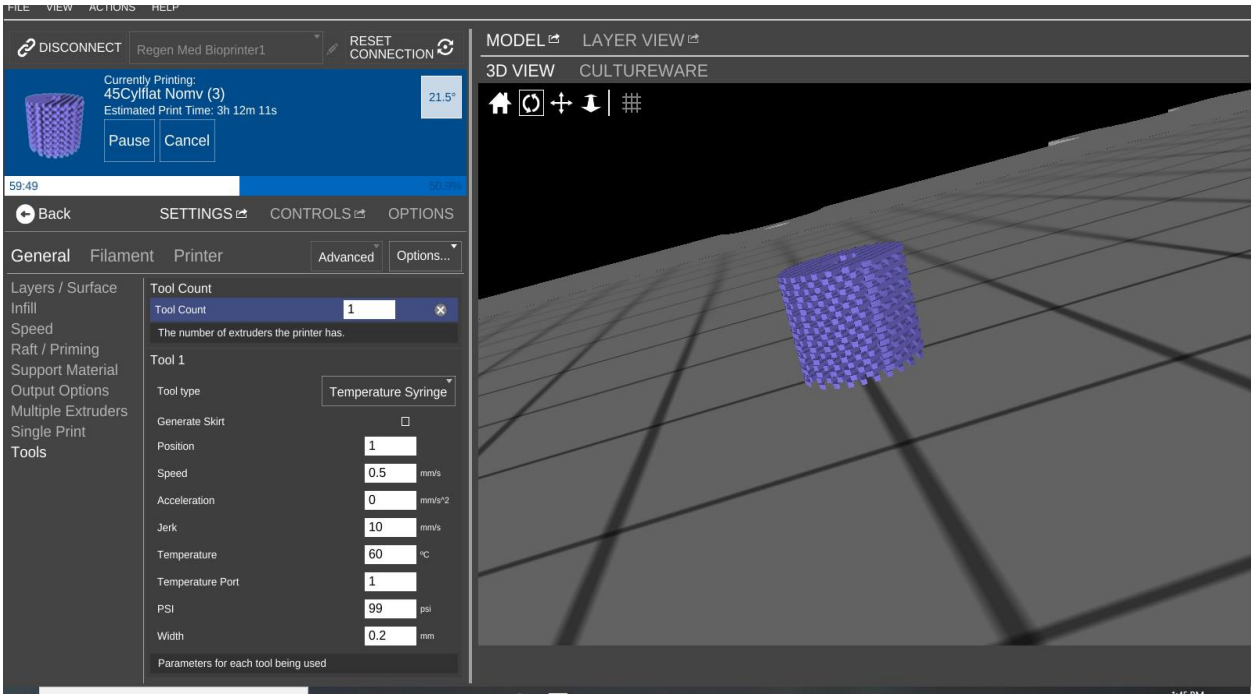

Figure 4.9. Element Slicer 3D view of 45Cylflat Nomv (3) Print time 3hours 12min 11sec.

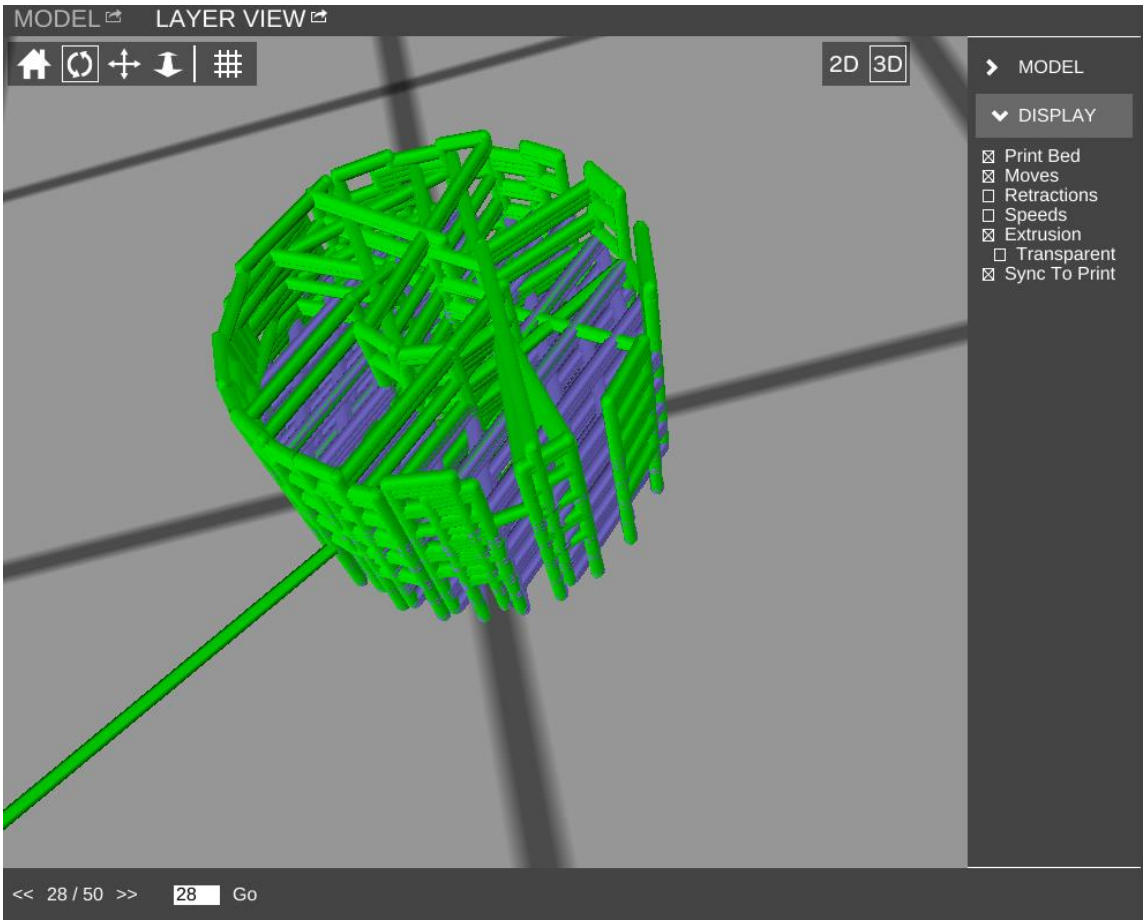

Figure 4.10. Display of Element model view showing Layer-Layer move of Nozzle while printing.

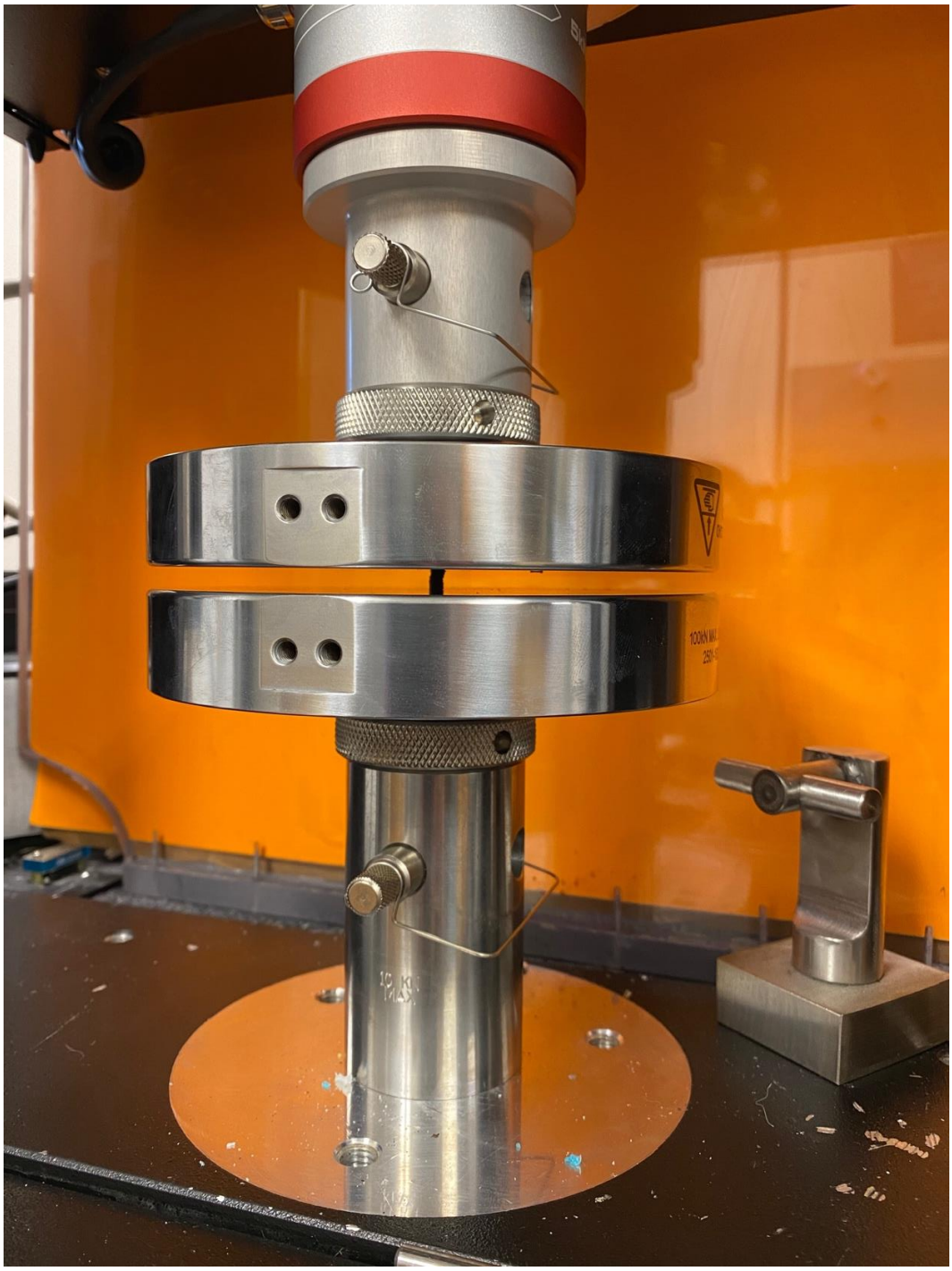

Figure 4.11. Instron compressive test on a 5mm PLGA+LOG construct.

50-65 LOG

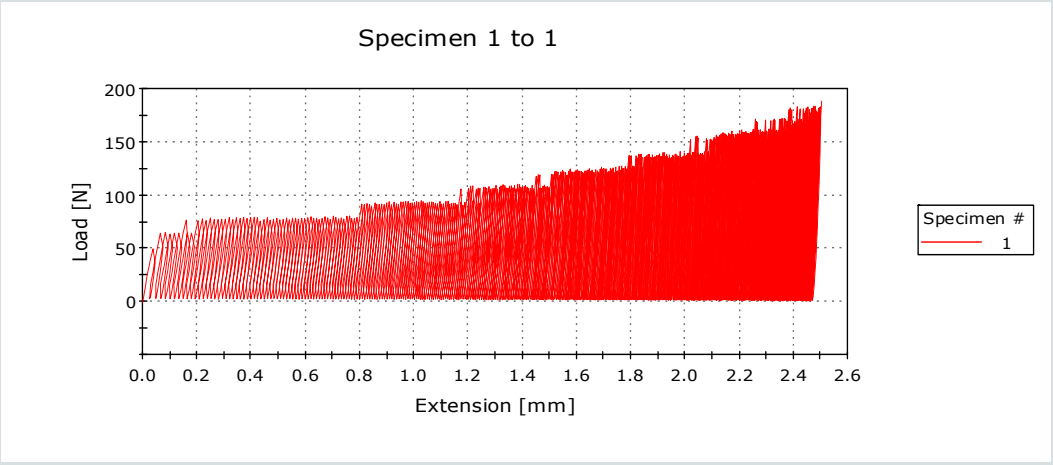

	System ID	Maximum Extension [mm]	Maximum Load [N]	Modulus (Automatic Young's) [MPa]
1	5965B13341	2.50026	188.19717	224.65766
Maximum		2.50026	188.19717	224.65766
Mean		2.50026	188.19717	224.65766
Minimum		2.50026	188.19717	224.65766

	Load at Yield (Zero slope) [N]	Extension at Yield (Zero slope) [mm]	Load at Total creep [N]	Extension at Total creep [mm]
1	-----	-----	188.20639	2.50026
Maximum	-----	-----	188.20639	2.50026
Mean	-----	-----	188.20639	2.50026
Minimum	-----	-----	188.20639	2.50026

	Load at Total relaxation [N]	Extension at Total relaxation [mm]
1	188.20639	2.50026
Maximum	188.20639	2.50026
Mean	188.20639	2.50026
Minimum	188.20639	2.50026

Page 1 of 1

Figure 4.12. Young's modulus of the PLGA/carbon-based nanomaterial/DMSO construct for 50:50-65:35 value 224.657 MPa.

50-75 LOG

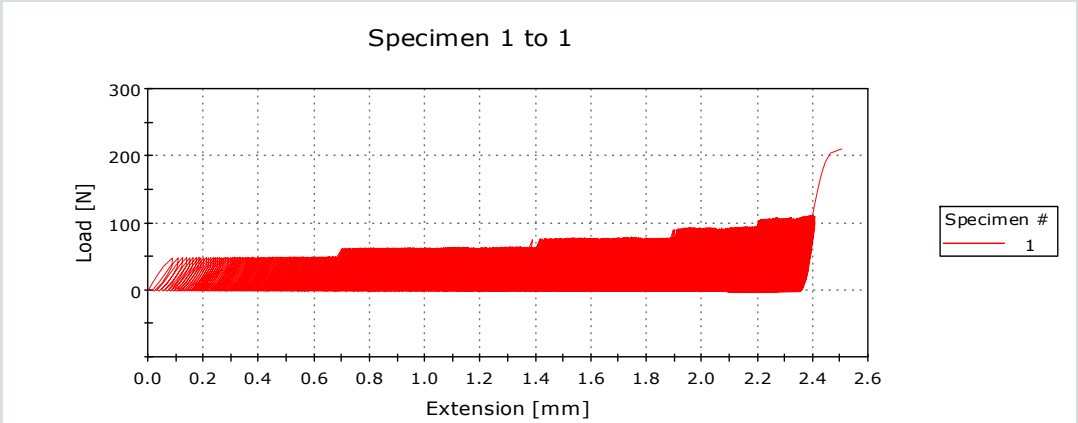

	System ID	Maximum Extension [mm]	Maximum Load [N]	Modulus (Automatic Young's) [MPa]
1	5965B13341	2.50087	210.64801	268.10427
Maximum		2.50087	210.64801	268.10427
Mean		2.50087	210.64801	268.10427
Minimum		2.50087	210.64801	268.10427

	Load at Yield (Zero slope) [N]	Extension at Yield (Zero slope) [mm]	Load at Total creep [N]	Extension at Total creep [mm]
1	-----	-----	210.70533	2.50087
Maximum	-----	-----	210.70533	2.50087
Mean	-----	-----	210.70533	2.50087
Minimum	-----	-----	210.70533	2.50087

	Load at Total relaxation [N]	Extension at Total relaxation [mm]
1	213.03381	0.25896
Maximum	213.03381	0.25896
Mean	213.03381	0.25896
Minimum	213.03381	0.25896

Page 1 of 1

Figure 4.13. Young's modulus of the PLGA/carbon-based nanomaterial/DMSO constructs for 50:50-75:25 higher value at 268.104 MPa.

(a)

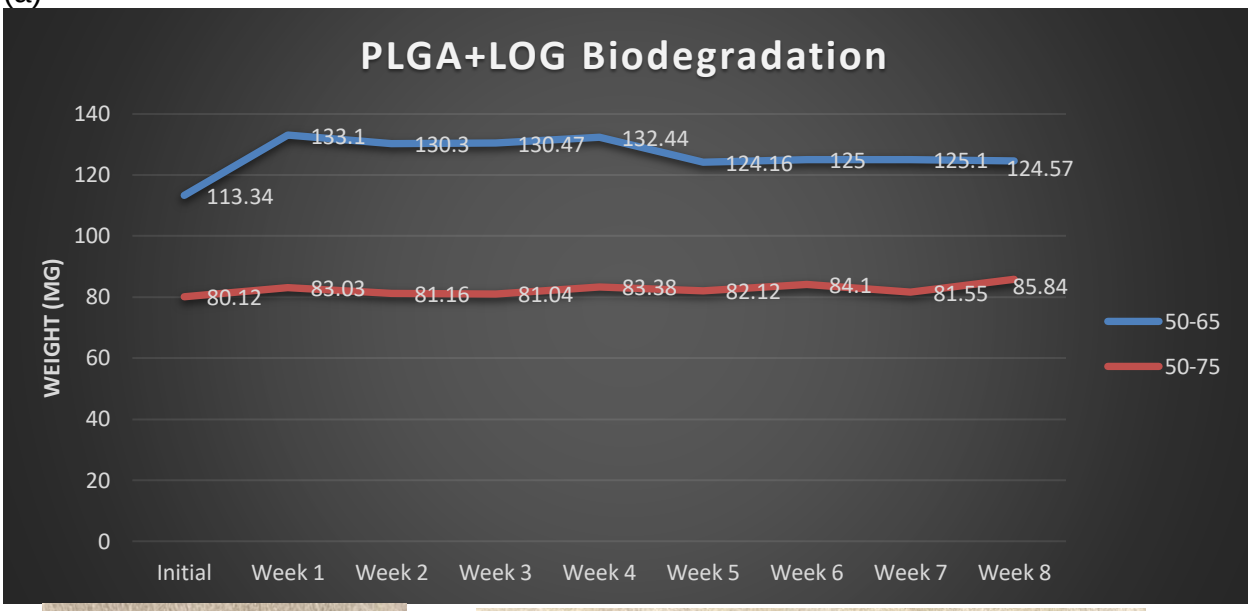

(b)

(c)

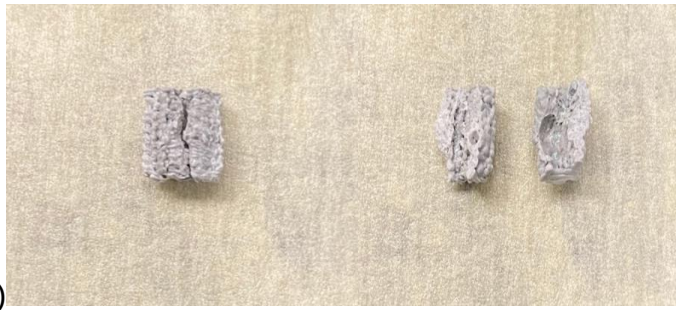

Figure 4.14 (a)Both constructs showed limited weight loss that could be explained by the crystal formation on the PLGA by the PBS. (b)PLGA+LOG at start. (c)at 8-week time point of degradation in dynamic bioreactor.

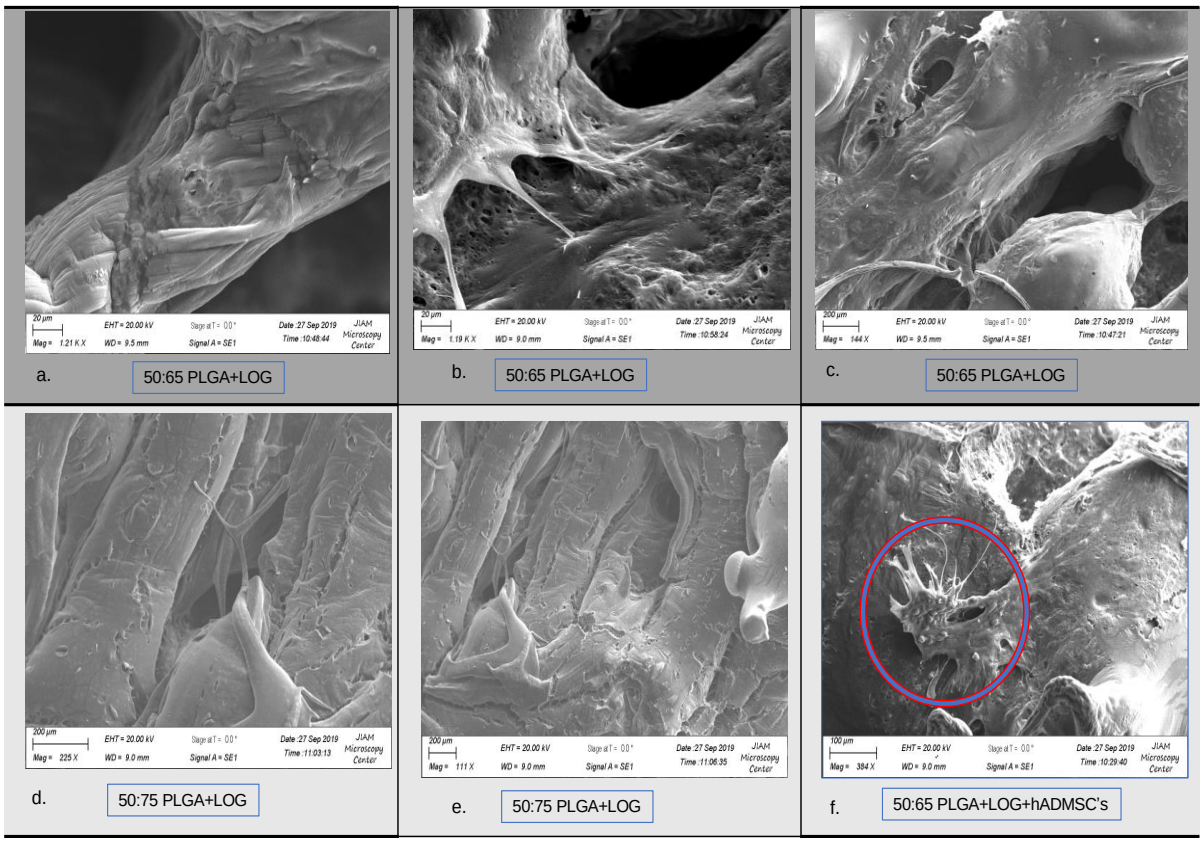

Figure 4.15. SEM images of microarchitecture of blended PLGA with LOG. (a - c) 50:65 PLGA+LOG. (d - e) 50:75 PLGA+LOG and (f) 50:65 PLGA+LOG+hADMSCs.

(a) 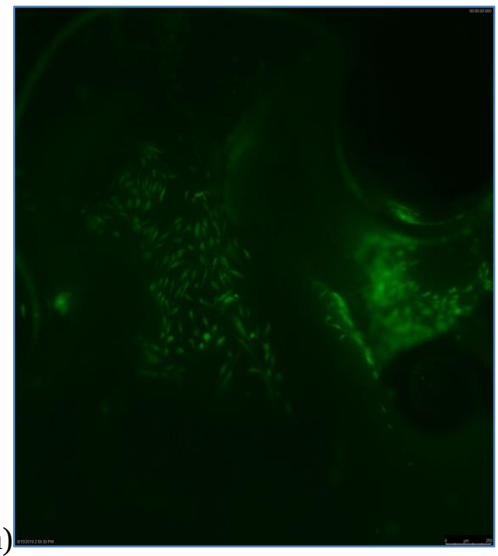 (b) 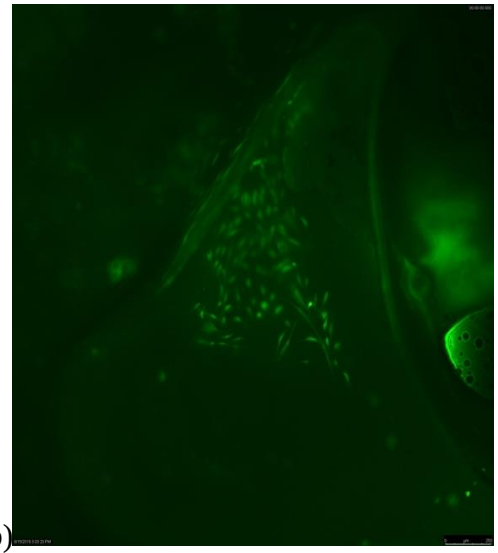

Figure 4.16. Cell viability and adhesion on PLGA+LOG construct using calcein-am analyzed 24 hours post seeding at 5x. (a) Top view with pore (b) Side view.

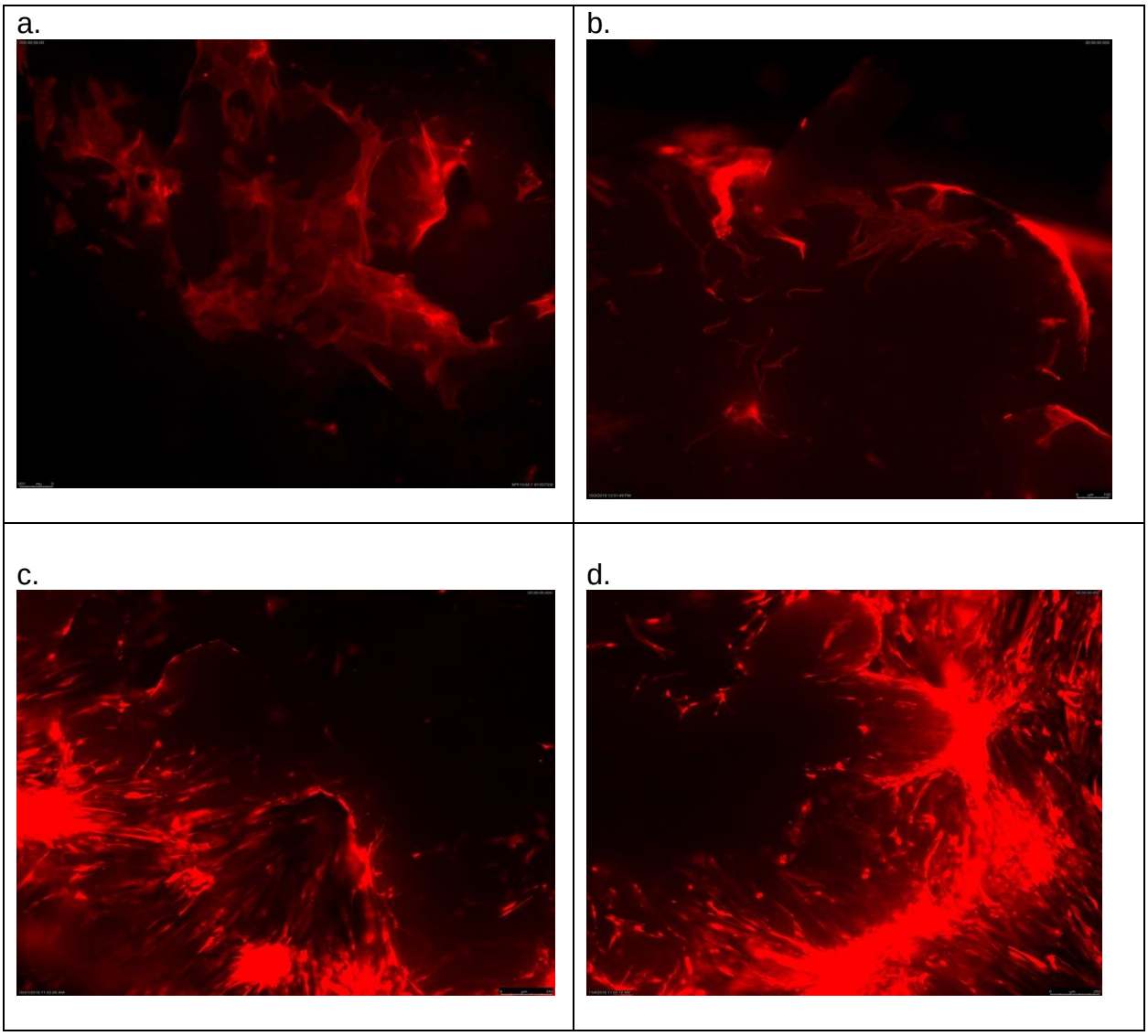

Figure 4.17. PLGA+LOG utilizing RFP cells to track proliferation at (a) 50:50/65:35 at 24 hours. (b) 50:50/65:35 at 7 days (c) 50:50/65:35 at 14 days and (d) 50:50/65:35 at 21 days.

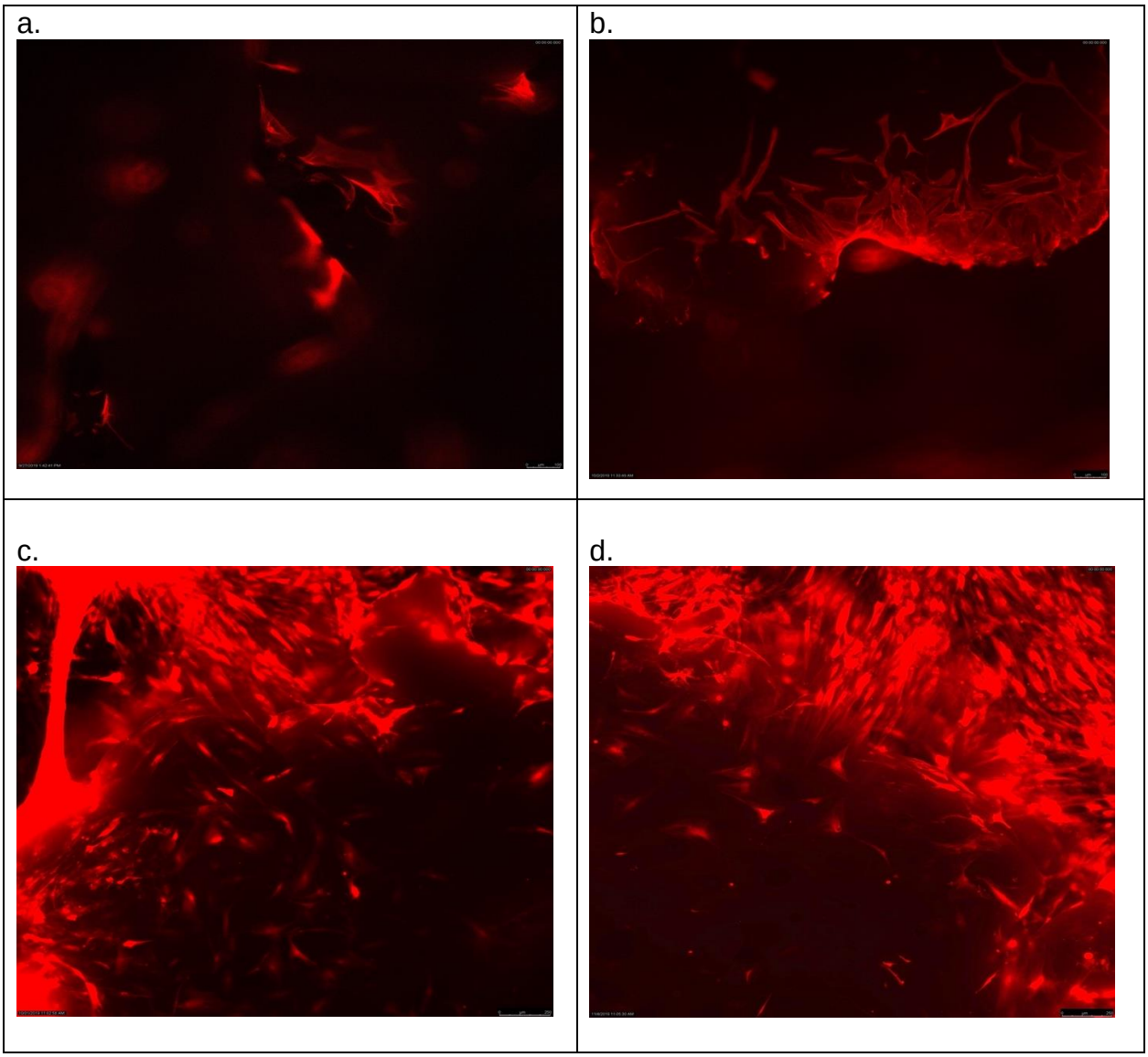

Figure 4.18. PLGA+LOG utilizing RFP cells to track proliferation at (a) 50:50/75:25 at 24 hours. (b) 50:50/75:25 at 7 days (c) 50:50/75:25 at 14 days and (d) 50:50/75:25 at 21 days.

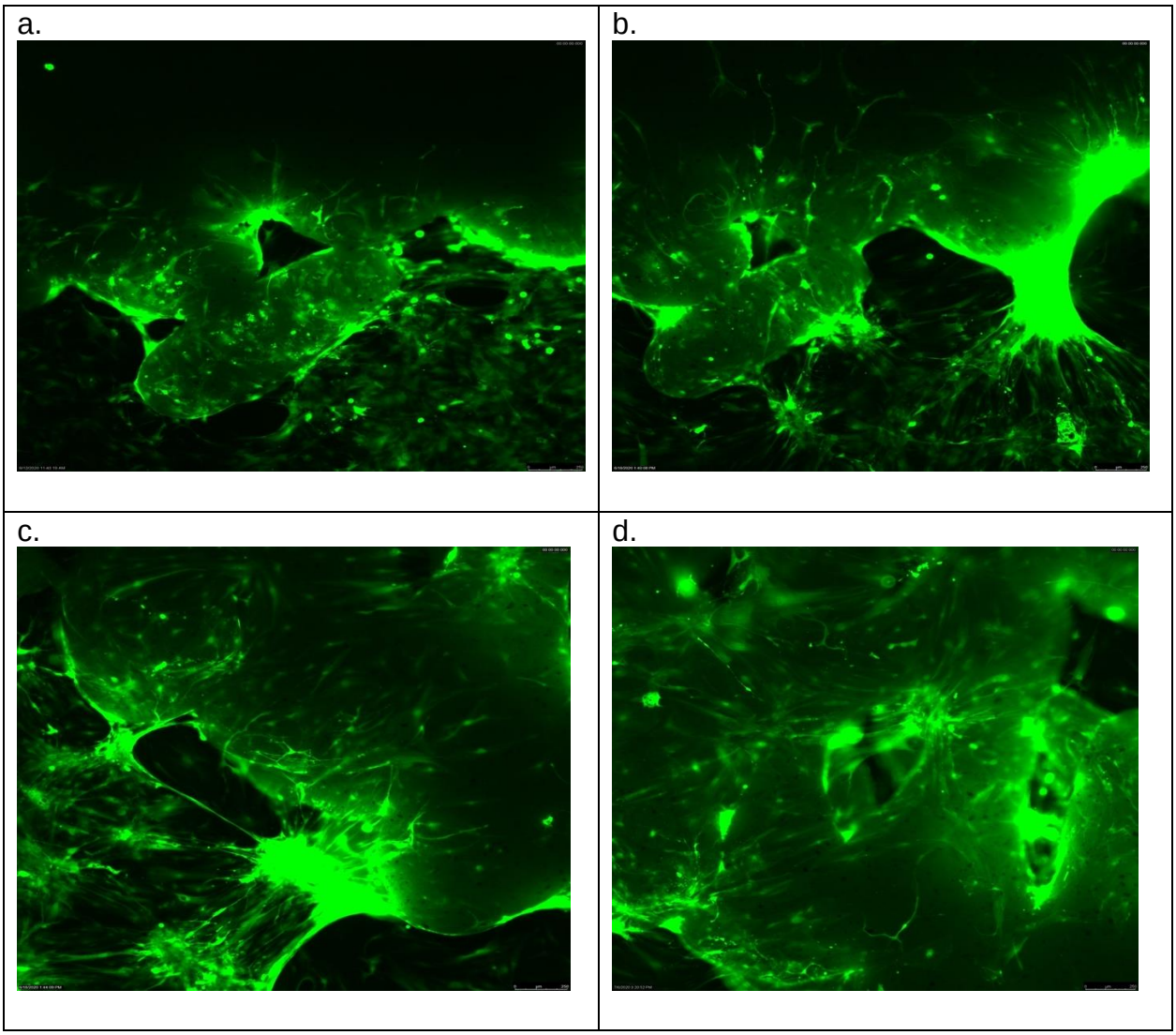

Figure 4.19. PLGA+rGO utilizing GFP cells to track proliferation at (a) 50:50/65:35 at 24 hours. (b) 50:50/65:35 at 7 days (c) 50:50/65:35 at 14 days and (d) 50:50/65:35 at 21 days.

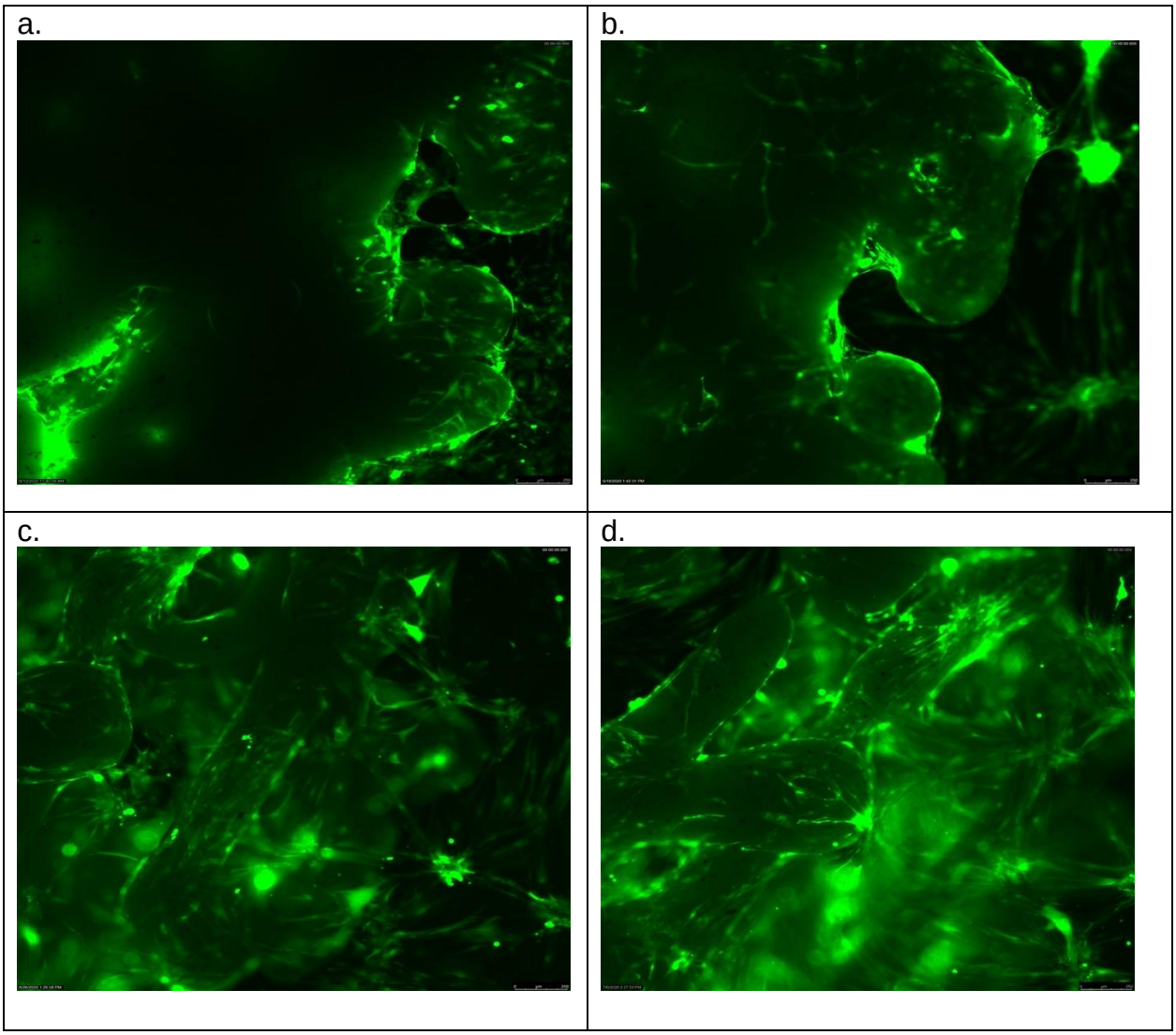

Figure 4.20. PLGA+rGO utilizing GFP cells to track proliferation at (a) 50:50/75:25 at 24 hours. (b) 50:50/75:25 at 7 days (c) 50:50/75:25 at 14 days and (d) 50:50/75:25 at 21 days.

CHAPTER V:
IN VIVO MODEL TO EVALUATE OSTEOINDUCTION, OSTEOCONDUCTION AND OSSEOINTERGRATION OF BIOFABRICATED NANOSCAFFOLDS

Abstract

Surgeon’s face some of the most challenging bone deficiencies. Reconstruction is limited to patient autografts or some biomedical device implant to facilitate bone regeneration. Bone tissue engineering focuses on therapeutic concepts to by using the applications of cellular biology, chemistry of material science and biomedical engineering by utilizing small animal model for translation. Therefore, this section of the study is to investigate multiple rat models using a novel 3D biofabricated PLGA and carbon-based nanoparticle construct in an intramuscular implant model and a reproducible 5mm critically sized mechanical load bearing segmental femur defect model. An analysis of the results including radiological, immunohistochemical staining and microcomputed tomography to give insight to future studies.

Introduction

The examination of the biological mechanism was described in 1959 with experiments in spinal fusion treatment by Hurley et al called the “Guided Bone Regeneration” (GBR) (Hurley et al., 1959). The understanding of GBR is the development of a mechanical barrier that is transplanted to the site to prolong cells migrating to the site such as fibroblast from surrounding tissue that will impede bone development. In hopes that favored cells such as osteogenic and pluripotent cells from the bony tissue or periosteum promote growth in the defect (Liu, 2014).

The regenerative process in the body for bone tissues experiences the same healing demeanor as other tissue wounds. First step following the initial damage to the tissue is hemostasis. Platelet activation along with vascular eruption are seen at the site. Immediately growth and clotting factors are supporting the coagulation cascade as the platelets pack the vasculature to form a stable clot of fibrin (Thiruvoth, 2015). The recruitment of cells stimulating multiple signaling cascades in response to the inflammation process such as polymorphonuclear (PMN) cells and later macrophages are import to debris removal (Wang, 2006). The continued stimulation of a great many factors in the immune process continues as the end result is proliferation of new supported tissue. The process of healing the bone matrix is complex hoping the end result of the biofabricated construct stimulates recruitment and differentiation of MSCs to the osteoblast lineage and the local osteoblast further stimulates the extracellular matrix for new bone formation. The 3D biofabricated nanoconstruct must try to meet the grafting gold standard for bone healing and repair. Will the construct stimulate differentiation of endogenous or transplanted cell lines to formation being osteoinductive? Is the construct osteoconductive by providing a 3D frame for uniformity and growth on the surface. Osseointegration is the balanced anchorage of a construct accomplished by direct bone-to-construct contact. The model of a critical sized segmental defect is the most important approach of taking a biocompatible biofabricated construct from bench to bedside for regenerative medicine.

Bone: Complex Structure

Highly dynamic, complex nanocomposite architecture and intricate cellular composition is the makeup of the structure bone. Bone physiology is an understanding that is crucial for tissue engineers to take a biofabricated construct from bench to surgical setting. The composition of this organ has components that are organic and inorganic leading to its complexity. Type I Collagen and water is the organic phase allowing viscoelasticity and rigidity, while hydroxyapatite matrix makes up the complex stiffness and structural reinforcement composing the inorganic component and non-collagenous proteins responding from cellular behavior forming a microenvironment (Webster, 2007). This complexity is based on a system structural architecture forming at diverse levels including cortical and cancellous bone at the macroarchitecture, osteons and Harversian system at micro, lamellae at sub-micro, minerals and fibrillar collagen at the nanoarchitecture and finishing at the sub-nano with collagen, minerals and non-collagenous proteins (McAllister, 2007). Trabecular bone containing increased porosity is at the distal and proximal ends surrounded by a layer of cortical bone to progress the transfer of the articular load (Webster, 2007). This transfer in the load stimulus in a healthy bone has been described in many studies using Wolff's law (Frost, 1994). Biofabrication must also understand the complex porosity within the bone structure. With a porosity range of 50-90% of its average 1mm spacing for trabecular bone and 3-12% for cortical bone makes a complex geometrical structure remodeling challenging (Barrère et al. 2008).

The structure further broken-down into layers at a microscopic range shows that mineralized collagen fibers stacked in layers in a parallel form called lamella are approximately 3-7 micrometers and staked in a +/- 45^{o} forming the trabecular struts. Replicating the lamella in bone engineering is very important as their formation contains the Haversian canal which contains the blood vessels and nerve for bone support and nutrition (Rho, 1998). The dynamic properties of bone are controlled by a very intertwined activity of cells: osteoblast – bone forming, osteoclast – bone consumer and osteocytes- bone remodeling mechanosensors, that reside in the intramedullary canal within the bone marrow (Marks, 2002). Bone is continuously remodeling tissue based on very demanding functional and structural mechanical loading requirements. Porosity

and mineralization make up the composition and the cortical and trabecular orientations and architecture describes the mechanical properties. From a biofabrication geometrical analysis of the bone matrix a material design needs to be a composite material that supports the lamellar matrix design, influences cell behavior, biodegrades the same as the remodeling activity and further stimulates the mechanical properties of bone.

Experimental model – Critical size defect

With the advances in biofabrication focusing on multiple forms of engineering to optimize organ growth two important needs that must be maintained and considered, first the biocompatible biomaterial and second the animal defect model, to calculate outcomes and effectiveness of the construct. When establishing model design, you must develop a standardized process in evaluating the needed tissue growth of study, which is osteogenesis for our team. The model must have a "critical size defect" (CSD) which was defined by JP Schmitz stating that the animal of the study must have the smallest diameter intraosseous damage in the appropriate bone that will not regenerate spontaneously during the lifetime of the model (Schmitz, 1986).

Femur segmental defect

To determine if the biofabricated construct complies with the qualifications of biocompatibility and mechanical strength, the construct must be accountable to testing *in vitro and in vivo*. A segmental long bone defect in order to be a critical size is configured by multiplying 2.0-2.5 by the diaphyseal diameter (Garcia-Gareta, 2015). From a researcher's perspective and communication with both human and animal orthopedic surgeons that long bone segmental trauma are the most demanding graft sites to repair to support load bearing issues. The implant to the graft site being natural or synthetic most undergo physiological stress soon after implant, in defiance of the surgeon's approach in which internal fixation support, but also experiences lack of vascular coverage to support bone regeneration and tissue repair. The content and structural design must intel mechanical properties to take load bearing stress as well as maintain all the levels of structure- nano, micro, and macro for cell support and growth.

The mechanical characteristics of the biofabricated construct must complement the bone graft surroundings not allowing for structural failure which is imperative to allow advancement of tissue repair. The engineered external construct must support sensory transduction to support mechanical signals to stimulate surrounding progenitor cells into differentiation of the desired new tissue (Tzioupis, 2007). With the 5mm critical size defect being reproduced successfully and by implanting our PLGA-LOG construct we are now investigating the potential for osteogenesis.

Osteoinductive Study of PLGA+LOG Biofabricated Construct

An osteoinduction study is an important process in the biofabrication of a possible bone construct. This process is defined in which osteogenesis occurs by the implantation of a biomaterial in the pocket of connective tissue with the result of new bone formation. Chai et al. 2012 states that osteoinduction has many factors that must be met by the biomaterial (Chai et al 2012). Properties should include surface topography including all levels architectural geometry, composition solubility effect of the biomaterial, inflammatory response that stimulates chemotaxis of osteoclast to the biomaterial, and the implantation site and healing time of the animal model (Li et al., 2011, Chai et al., 2012). The biofabricated biomaterial should activate bone formation heterotopically, implying the enlistment of immature cells and the stimulation of these cells to expand into precursors of mature bone cells to support the impute of the biomaterial's properties are osteoinductive and not stimulated by osteoconductive formation by the implantation (Davies, 2000). Analyses of osteoinduction helps to understand the mechanism of bone healing in the presence of the construct when used *in vivo*.

Methods

Construct Biofabrication – For Intramuscular and Femur Study

Intramuscular and femur constructs were biofabricated from double molar ratio PLGA+LOG using additive manufacturing with the Aether 1 bioprinter as previously described in chapter 4. Construct outer and height dimensions remained. On day of surgery acellular constructs were removed from -20^{o}C freezer and placed under UV irradiation for 1 hour before implant. Cellular constructs were removed from -20^{o}C freezer and placed under UV irradiation for 1 hour then seeded with $1x10^{6}$ hADMSCs and incubated overnight. Constructs were brought to operating room one at a time as needed for implant.

In-vivo Intramuscular Study

Surgical Procedure

All animal handling and surgical procedures were strictly conducted under the University of Tennessee Institutional Animal Care and Use Committee (IACUC).

Each group consisted of 6 Sprague-Dawley rats 8-12 weeks old and weighing between 225 and 240g a muscle implantation of a biofabricated construct to evaluate the osteoinductive capacity of a construct in bone healing. Evaluation of osteoinductive potential of a novel construct will provide valuable information on the mechanism by which the progenitor cells undergo differentiation. Each patient will be anesthetized with isoflurane at 1.5 to 2% with 2 L/min Oxygen by induction tank then placed on mask support for remaining time in the operating room. Before surgery, each rat will be given the analgesic buprenorphine (0.05 mg/kg) based on IACUC protocol. Next, removal of hair from the hindquarter, using small clippers. The skin area was then prepped for sterility with chlorhexidine and alcohol. While holding the skin taught, using a sterile blade, make a longitudinal incision of about 10-12 mm, and the entire femoral shaft will be exposed using blunt dissection. Using thumb forceps to hold the edge of the skin and slowly separating the skin from the muscle using Metzenbaum scissors. Using the blunt dissection, a 4-5 mm deep pocket was made in the biceps femoris. The acellular

or cellular construct was carefully inserted into the muscle pocket. Suturing the fascia overlying the muscle was done using 4-0 PDS resorbable suture. Closure of skin incision was completed with 4-0 suture. For the 3 days postoperative, the rats will be given buprenorphine injection every eight to twelve hours for pain management and antibiotic will be in the Gatorade water mix and changed every three days. Each group was assessed at a 14-day time point.

In-vivo Femur Study

Surgical Procedure

All animal handling and surgical procedures were strictly conducted under the University of Tennessee Institutional Animal Care and Use Committee (IACUC).

Each group consisted of 6 Sprague-Dawley rats 8-12 weeks old and weighing between 225 and 240g. A defect of critical size in the rat femur - measuring 5 mm of the hind limb of each rat was performed in a rotating format (**Figure 5.1**) will be used to evaluate the osteogenesis and angiogenesis of production by the scaffold. Each patient will be anesthetized with isoflurane at 1.5 to 2% with 2 L/min Oxygen by induction tank then placed on mask support for remaining time in the operating room. Once removed from the tank the patient was placed in a lateral position with procedure side up. Before surgery, each rat will be given the analgesic buprenorphine (0.05 mg/kg) based on IACUC protocol. Next, removal of hair from the hindquarter, using small clippers. The skin area was then prepped for sterility with chlorhexidine and alcohol. While holding the skin taught, using a sterile blade, make a longitudinal incision of about 12-15 mm, and the entire femoral shaft will be exposed using blunt dissection. The fascia will be cut separating the tensor fascia lata and biceps femoris muscles, and the vastus lateralis muscle will be freed from the greater trochanter to the lateral femoral condyle. 2 cuts (one proximal and the other distal) in the middle of the diaphysis will be made, and a 5mm bone segment will be cut and removed using a reciprocal saw. The defect will be held in place using a 1.1 mm K-wire, which will be placed in the intramedullary cavity between the proximal and the distal ends of the defect. The K-wire is a thin, semi-stiff wire used in orthopedic surgery to assist in holding structured bone in place, and the

small diameter allows for its use in the rat model as a form of intramedullary nailing. The K-wire will be inserted into the 3D PLGA: Carbon-based nanoparticle biofabricated construct and then held at the proximal and distal locations. Suture the fascia overlying the muscle using 3.0-5.0 PDS resorbable sutures and close the wound.
For the 7 days postoperative, the rats will be given buprenorphine injection every eight to twelve hours for pain management and antibiotic will be in the Gatorade water mix and changed every three days.
Constructs receiving cells were placed in 10mm petri dish, then seeded with one million hADMSCs then placed in the incubator at 37^{o}C 12-16 hours before surgery. This step will ensure that the cells impregnate the construct.

Groups were formed for the study.
Group 1 - PLGA 50:50/65:35+1.0mg Low Oxygen Graphene
Group 2 - PLGA 50:50/75:25+1.0mg Low Oxygen Graphene
Group 3 - PLGA 50:50/65:35+1.0mg Low Oxygen Graphene with human adipose-derived mesenchymal stem cells
Group 4 - PLGA 50:50/65:35+1.0mg Low Oxygen Graphene with human adipose-derived mesenchymal stem cells

Each group will be assessed at 60-day time point. Rats from each treatment group will be euthanized at specified time point and bone healing will be evaluated with conventional radiological analysis, microcomputed tomography, histomorphometrically using H&E and von Kossa staining for use in the histological visualization of calcium deposits.

Radiology analysis – Femur Study

A digital radiography system (Philips Easy Diagnost RF System; Cannon DR plates (CXDI-50G); EDR6 Clinical Diagnostic Radiography System) was used to assess bone healing. X-rays of the patients were taken 12 hours post-surgery to confirm correct K-wire and construct placement as well as to establish a base line for the study. A series of X-ray analysis in a lateral plane were conducted at 12 hours, 7 days, 30 days

and 60 days post-surgery to assess formation of newly formed mineralized bone tissue and changes within the segmental bridging.

Microcomputed Tomography Imaging – Femur Study

Micro-CT analysis is to provide data on the temporal progression of mineralization development during the regenerative process of the femur. Preparation for micro-CT imaging, all femurs were stored in 10% formalin for 48 hours, then placed in cotton wrap soaked in 70% ethanol and stored in a 50mL conical tube for shipping. Femur specimens were sent to Roseman University of Health, College of Dental Medicine. Specimens were then processed using a desktop Micro-CT system (SkyScan 1173, Bruketr Kontich, Belgium) to perform the evaluations. The unit is equipped with a sample tube and aluminum filter, femurs were scanned at an energy of 80 kVp and intensity of 100 μA, resulting in a pixel size 31.99 μm and 1120 rows x 1120 columns. Each femur was placed in a cylinder and attached to holder with the femur oriented perpendicular to the image plane.

3D data analysis of the full femur was evaluated. The region of interest (ROI) was completed manually by drawing polygonal regions. The analyzed ROI included the defect region and adjacent newly formed bone. Analyses included tissue area, bone area, percent bone area / tissue area (bone volume density), trabecular thickness (Tb. Th), trabecular separation (Tb. Sp), trabecular number (Tb. N) and total porosity (Po total). Threshold values range of 45-65, 65-85, 85-105 and 105-255 were selected for segmentation of the PLGA/carbon-based nanoparticle construct and newly formed bone. 3D models were generated in CTAn and formed in a. stl format for visual representation.

Histological and Immunohistochemistry Staining

Intramuscular tissue surrounding the implant and femoral tissue from the critical size defect were prepared for histological examination. Samples were sent to the appropriate labs for prep and cuts. Extra slides were requested for in-house immunostaining. Masson trichrome was to analyze surrounding connective tissue. ECM marker Fibronectin was used to analyze cell-matrix communication. CD34 and

von Willebrand Factor was used to analyze vessel density. CD44 analyzed MSC recruitment to the construct site.

Intramuscular Study

Samples were sent to the Ridge Microtome Services where samples were embedded in paraffin. Hematoxylin and eosin (H&E) and Masson's trichrome staining was performed on deparaffinized sections to evaluate histological features with extra slides cut for inhouse IHC to be performed for osteogenic and endothelial markers. For immunohistochemistry, Day 1 - paraffin sections were deparaffinized with xylene 2 times for 20 minutes each and rehydrated with serial concentrations of ethanol gradient starting with 100%, then 95% then 70% at 5 minutes each all at room temperature. Subsequently, sections were rinsed in distilled water for 5 minutes.

Antigen retrieval steps: First, place samples Target Retrieval Solution (DAKO, Carpinteria, CA) at 80-85^{o}C for 30 minutes; then, remove container with slides from water bath in DAKO solution allow to cool at room temperature for 20 minutes, then decant solution with PBS at room temperature for 5 minutes.

Primary antibody staining: Surround the samples on the slide with ImmEdge pen (Vector Laboratories, Burlingame, CA), next add 1% Triton X-100 in PBS solution into the circled area for 30 minutes at room temperature followed by PBS wash for 5 minutes. Incubate sample in Super Block (ScyTek Laboratories, Logan, UT) at room temperature for 30 minutes. Next add Primary Antibody Solution (Dilution in Super Block) at 200 μL volume (In-house List Below); In house sections were incubated with the primarty antibody in humidified chambers at 4°C overnight.

Ridge Microtome Services:

1- Hematoxylin and eosin
2- Masson’s trichrome

In-house Primary IHC:

1- Fibronectin (1:100, abcam ab23751)
2- Osteopontin (OPN) (1:100 abcam ab8448)
3- Cluster of differentiation 44 (CD44) (1:200 abcam ab157107)
4- Von Willebrand Factor (vWF) (1:200 LS-BIO LS-B9918)

5- Cluster of differentiation 31 (CD31) (1:200 LS-BIO LS-B12093)
6- Cluster of differentiation 34 (CD34) (1:100 abcam ab185732)
7- Sp7/Osterix (1:100 abcam ab22552)

Day 2 – Remove primary antibody solution with a 1% PBS-TWEEN 20 wash for 5 minutes. Next, add Peroxidase Blocking Solution at room temp for 10 minutes followed by wash with PBS-TWEEN 20. Next, add Goat anti-Rabbit IgG Biotinylated at 4 drops to each sample for 30 minutes room temp. Rinse with PBS-TWEEN 20 3 times carefully. Now add Streptavidin Peroxidase (Vector Laboratories) at 4 drops to each sample at room temp for 30 minutes. Rinse with 1x Tris Buffered Saline 3 times carefully. In separate beaker mix NovaRed Substrate Kit Peroxidase: 5mL of DI water,3 drops Reagent 1, 2 drops Reagent 2, 2 drops Reagent 3, 2 drops Hydrogen Peroxide – add 200 μL of mix to each sample for 15 minutes. Rinse with PBS-TWEEN 20 2 times.

Day 2 - Phase III – Rinse slides with tap water, then immerse in Hematoxylin stain (Vector Laboratories) at room temp for 5 minutes, rinse with tap water until clear water is coming off sample. Next Acid Rinse – Slides were then put into a glass holder and at a medium motion slides were moved up then down (dip) repeating 10 times (Motion may cause sample to lift off slide – watch carefully), then same motion in tap water 10 dips, move over to Bluing Solution for 5 dips, followed by tap water with 15 dips. Next, dehydrate slide in an ethanol gradient with 95% for 3 minutes then up to 100% for 3 minutes, last move slide to xylene 2 times at 5 min each then lay slides to side for mounting.

Mounting will be done with Limonene-mount (Electron Microscopy Sciences, Hatfield, PA) apply 2 drops then gently add 22x22x1mm coverslip – limiting bubbles to the sample viewing area or moving coverslip once applied. Lay flat to dry overnight.

Femur Study

Samples were randomly divided into two groups of 12. First twelve were sent to Ridge Microtome Services where samples were decalcified and the remaining twelve were sent to Ratliff Histology Consultants, LLC and prepped in calcified IHC cuts. Decalcified femurs were done with Hematoxylin and eosin (H&E) and Masson's

trichrome staining with 7 extra slides cut for inhouse IHC staining. Staining was performed with primary antibodies specific to osteogenic and endothelial markers. Same protocol followed from intramuscular study and ICH markers for decalcified femur samples.

Ridge Microtome Services:

1- Hematoxylin and eosin
2- Masson's trichrome

In-house Primary IHC:

1- Fibronectin (1:100, abcam ab23751)
2- Osteopontin (1:100 abcam ab8448)
3- Cluster of differentiation 44 (CD44) (1:200 abcam ab157107)
4- Von Willebrand Factor (1:200 LS-BIO LS-B9918)
5- Cluster of differentiation 31 (CD31) (1:200 LS-BIO LS-B12093)
6- Cluster of differentiation 34 (CD34) (1:100 abcam ab185732)
7- Sp7/Osterix (1:100 abcam ab22552)

Ratliff Histology Consultants, LLC - Calcified sample stains:

1- Von Kossa/MacNeal's stain
2- Masson-Goldner trichrome

Results

Surgical Postoperative – Intramuscular Study

All 6 rats underwent the surgical procedure well. All construct implants stayed within the muscle pouch and no discharge or swelling during the 14-day length of the study. All rats had a positive weight gain.

Surgical Postoperative – Femur Study

All 24 rats underwent the surgical procedure well. All construct implants having the hole 3D printed made allowed for a successful manipulation of the K-wire. Postoperative recovery was successful without any complications in all the rats. Postoperative management was without any negative issues. There was no postoperative medical

complications or infections throughout the sixty-day study. All rats in both studies remained in good health during the experimental duration, with no signs of stress or hair loss and positive gaining of weight in the sixty-day period following surgery.

Radiographic results – Femur study only

Rats underwent protocol sedation at 24 hours, 7 days, 30 days and 60 days for tracking of implant and changes in bone structure. Correct positioning in a lateral recumbent position of the limb containing the implant 24 hours post-surgery to check K wire position or any possible complications.

7 days post-surgery changes in bone formation both distal and proximal of the construct in both acellular and cellular constructs. All rats were mobile still showing no signs of complications or depression. Palpation of the limb was done showing complete mobility of the knee and hip regions.

One-month post-surgery a notice of some movement of the K-wire has taken place. Various changes in bone structure on both sides of the construct implant. Some outcropping or finger like projections showing signs of early stages of bone remodeling were beginning to show radio-opaque on the radiographs as well as changes in the medullary cavity. Palpation of the limb showed no signs of mobility issues or swelling of tissue or redness to the sight and each rat was weight bearing and gaining weight.

Two months post-surgery, formation of new bone was observed in several rats and in both acellular and cellular groups but a higher bridging on bone and less remodeling in the medullary cavity in groups containing the 50:65 PLGA+ LOG. (**Figures 5.2-5.9 shows representative comparisons for each iteration (a) Phantom (b) radiological view at 24 hours and 60-day end point (c) stl of each threshold of micro-CT**).

Micro-CT

The unbiased technique is measuring bone at multiple densities. Multi-level thresholding is to evaluate bone mass at multiple density levels to reduce the difference of cortical bone from trabecular bone. Femur analysis by micro-CT confirmed results in regard to the construct involvement and the amount of new bone formation. All 24

femur defects in both acellular and cellular groups showed some bony formation after 60 days. Femurs with PLGA 50:65 acellular and cellular showed the highest values of newly formed bone. 3D stl reconstructions confirmed percent bone area / tissue area (bone volume density) showing a difference in both acellular and cellular groups. The evaluating results for the complete threshold of 45 to 255 showed no significant change throughout the bone development of the construct (**Figure 5.10**). Next, I decided to evaluate possible bone development at each threshold by utilizing the percent bone area / tissue area and plotting against the intact phantom femur. The stl images represents as an increase in threshold levels indicating formation of less dense bone to calcified cartilage to new bone modeling (Freeman, 2009). These results showed that PLGA+LOG 50:65 had a higher performance than PLGA+LOG 50:75 (**Figure 5.11**)

Immunohistochemistry and Histology

Histological analyses were performed on all 6 Intramuscular and 24 femurs. Routine staining by Masson's Trichrome and Hematoxylin-Eosin for all sets.

Intramuscular Immunohistochemistry

Samples of PLGA-LOG were removed from the muscle pouch site. The study had an n=3 acellular and n=3 cellular using human adipose stem cell source. Observation of the H&E staining tissue-construct interface showed no signs of inflammatory response or bacterial infection. Samples in both sets showed positive markers showing the cell communication with the biofabricated construct matrix. Cellular samples of CD 34 and vWF identified increased vascular frequency around the implant. Marker CD 44 showed MSC recruitment potential by the construct. Osteogenic marker OPN suggested in the dark brown dense tissue around the construct indicated osteogenic response. These results indicate the PLGA+LOG construct contains all properties for an osteoinductive material. (**Figure 5.12 -5.13**)

Femur Immunohistochemistry

Confirming the visual of radiological and micro-CT analysis, IHC confirmed that formation of bone tissue in the defect area and construct for all four groups. von Kossa

stain was used to visualize new bone formation with, and counter stained with MacNeal's tetrachrome for unmineralized tissue. Calcified embedded sections showed amounts of von Kossa - mineralized tissue (black) within the defects and constructs (**Figures 5.14 – 5.17**). In the cellular group's greater amounts of mineralization and bridging were formed. In **figure 5.18** the statistical analysis of the von Kossa shows the 50:65 LOG had a higher performance in the acellular construct and the 50:75 LOG construct was supported by the hADMSCs during the *in vivo* study. Mesenchymal stem cells acquire the possibility of differentiating into osteoblast if environment ques are present or aid to the native osteoblast which is supported by Miro CT and histochemistry. The extracellular matrix protein fibronectin confirms cell to matrix communication and support by the construct in both acellular and cellular samples. Bone formation in both PLGA groups by endochondral ossification based on the amount cartilage templates formed and over period of development replaced by bone matrix (**Figures 5.19 – 5.22**) to confirm increased bone remodeling and bone formation, we performed immunostaining of OPN marker which expressed an enhanced response. Cellular marker CD44 confirmed MSC migration throughout the multilayer construct. Cell markers CD34 and vWF expression confirmed and angiogenic response by the construct.

Conclusion

Double molar ratio blend PLGA plus LOG are novel alloplastic biofabricated constructs that will support bone enhancement procedures. Within the limits of the study, osteogenesis was partially enhanced using the two different iterations in acellular and cellular when implanted into a critical sized rat femur defect. Although numerous innovations over the last decades, this bone construct offers an equally dynamic combination of osteoconductive three-dimensional structure, osteogenic cells and osteoinductive growth factors with encouraging mechanical properties and could support and stimulate vascularization. The micro-CT and histology results of the study showed the iterations supported increased bone volume and under surgical conditions mechanical properties needed for a biofabricated implant. Future growth on this study using the segmental femur defect over longer time points and various concentrations of graphene nanoparticles will hopefully allow for optimization to bone formations and stronger support to our PLGA-LOG biofabricated construct.

References

Barrère, F., et al., Advanced biomaterials for skeletal tissue regeneration: Instructive and smart functions. Materials Science and Engineering: R: Reports, 2008. 59(1–6): p. 38-71.

Chai YC, Carlier A, Bolander J, Roberts SJ, Geris L, Schrooten J, Van Oosterwyck H, Luyten FP. Current views on calcium phosphate osteogenicity and the translation into effective bone regeneration strategies. Acta Biomater. 2012 Nov;8(11):3876-87. doi: 10.1016/j.actbio.2012.07.002. Epub 2012 Jul 13. PMID: 22796326.

Davies JE, Hosseini MM (2000) Histodynamics of endosseous wound healing. In: Bone Engineering (Davies JE, ed), Em squared Inc., Toronto, Canada, pp 1-14.

Freeman, T.A., Patel, P., Parvizi, J., Antoci, V., Jr. and Shapiro, I.M. (2009), Micro-CT analysis with multiple thresholds allows detection of bone formation and resorption during ultrasound-treated fracture healing. J. Orthop. Res., 27: 673-679. https://doi.org/10.1002/jor.20771

Frost HM. Wolff's Law and bone's structural adaptations to mechanical usage: an overview for clinicians. The Angle Orthodontist. 1994;64(3):175–188.

García-Gareta E, Coathup MJ, Blunn GW. Osteoinduction of bone grafting materials for bone repair and regeneration. Bone. 2015; 81:112–121.

Hurley, L.A., et al., The role of soft tissues in osteogenesis. An experimental study of canine spine fusions. J Bone Joint Surg Am, 1959. 41-A: p. 1243-54.

Liu, J. and D.G. Kerns, Mechanisms of Guided Bone Regeneration: A Review. The Open Dentistry Journal, 2014. 8: p. 56-65.

Marks Jr SC, O.P., Structure and development of the skeleton. Principles of bone biology, ed. R.L. Bilezikian JP, Rodan GA. Vol. 2nd ed. 2002, San Diego: Academic Press.

McAllister BS, Haghighat K. Bone Augmentation Techniques. Journal of Periodontology. 2007;78(3):377–396.

Rho, J.-Y., L. Kuhn-Spearing, and P. Zioupos, Mechanical properties and the hierarchical structure of bone. Medical Engineering & Physics, 1998. 20(2): p. 92-102.

Schmitz JP, Hollinger JO. The critical size defect as an experimental model for craniomandibulofacial nonunions. Clinical Orthopaedics and Related Research. 1986;(205):299–308.

Tzioupis, C. and P.V. Giannoudis, Prevalence of long-bone non-unions. Injury, 2007. 38 Suppl 2: p. S3-9.

Thiruvoth FM, Mohapatra DP, Kumar D, Chittoria SRK, Nandhagopal V. Current concepts in the physiology of adult wound healing. Plastic and Anesthetic Research. 2015; 2:250-256.

Wang J. Neutrophils in tissue injury and repair. Cell and Tissue Research. 2018;371(3):531–539.

Webster, T.J. and E.S. Ahn, *Nanostructured biomaterials for tissue engineering bone.* Adv Biochem Eng Biotechnol, 2007. **103**: p. 275-308.

X. Li, H. Liu, X. Niu, Y. Fan, Q. Feng, F.Z. Cui, *et al.*
Osteogenic differentiation of human adipose-derived stem cells induced by osteoinductive calcium phosphate ceramics J Biomed Mater Res B Appl Biomater, 97 (2011), pp. 10-19

Appendix

Figure 5.1. Overview of Femur Surgical Construct Implant.

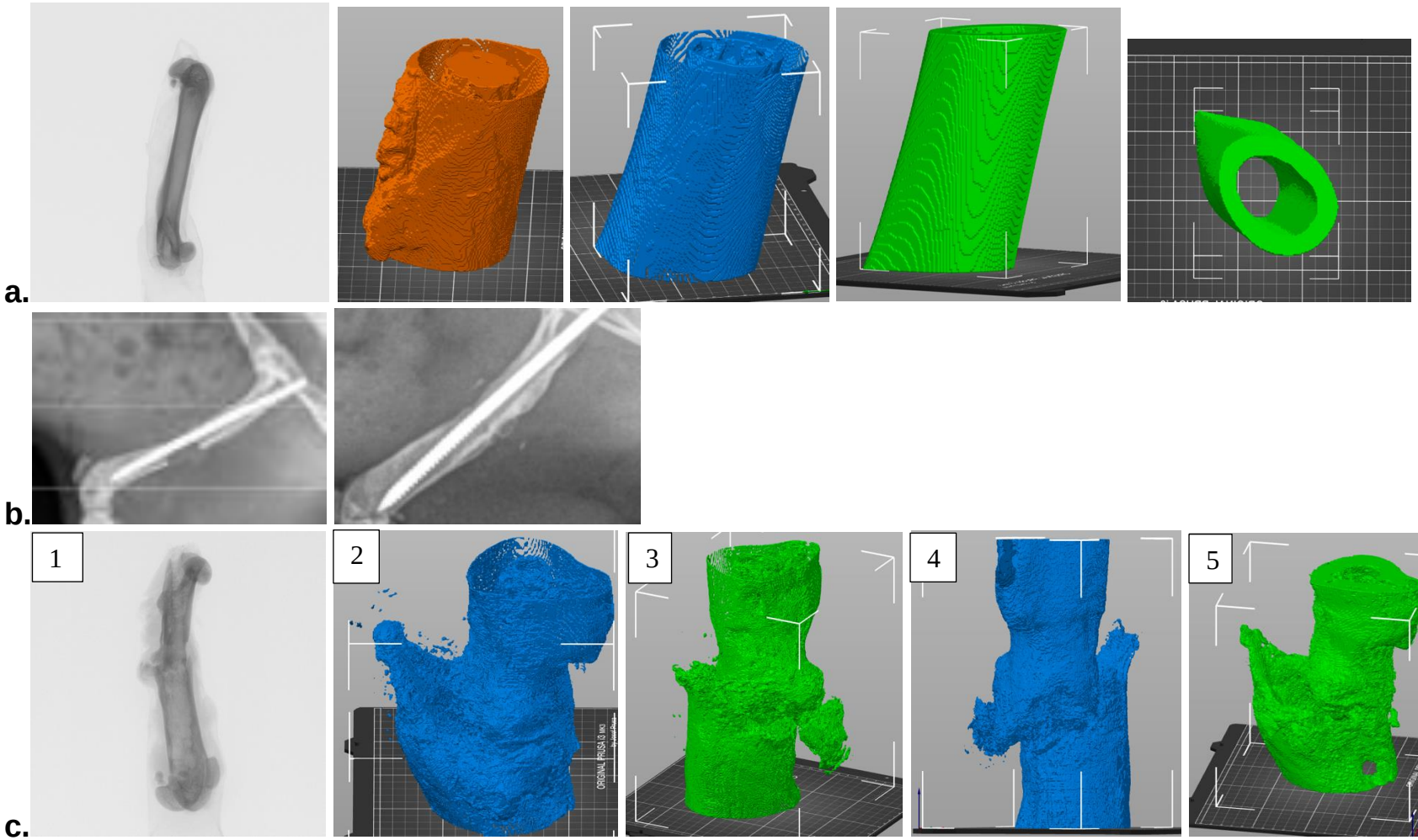

Figure 5.2. Overview of results Femur 1 50:65 PLGA-LOG Acellular – Decalcified. (a) shows phantom femur micro-CT scan with stl of ROI slices equal to all samples. (b) 24-hour X-ray of Rat 1 Femur 50:65 acellular and 60-day post X-ray. (c) (1) micro-CT femur 1 with stl views of bone growth around the PLGA-LOG construct – (c2) Threshold 45-65, (c3) Threshold 65-85, (c4) Threshold 85-105 and (c5) Threshold 105-255.

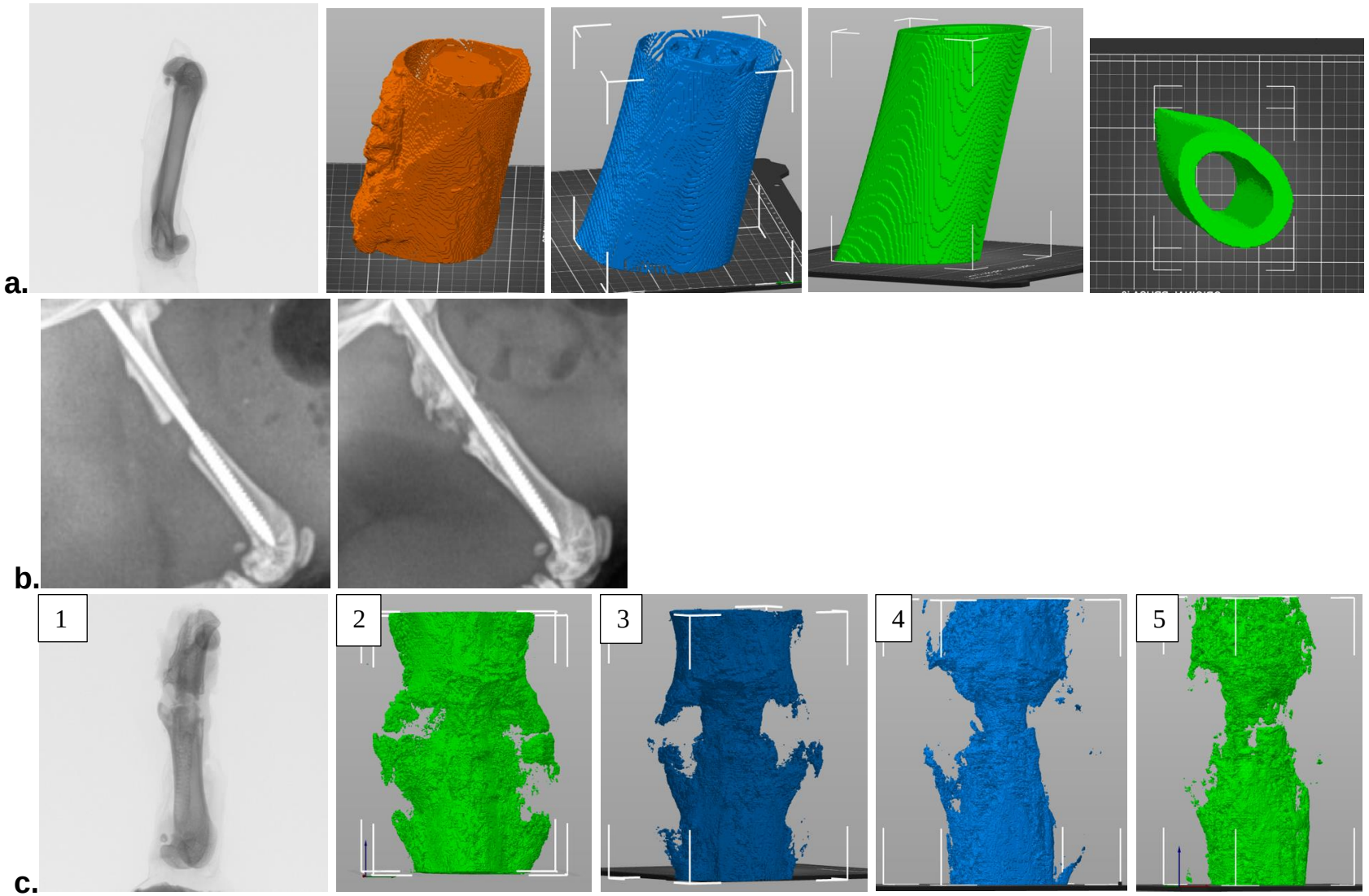

Figure 5.3. Overview of results Femur 4 50:65 PLGA-LOG Acellular – Calcified. (a) shows phantom femur micro-CT scan with stl of ROI slices equal to all samples. (b) 24-hour X-ray of Rat 4 Femur 50:65 acellular and 60-day post X-ray. (c) micro-CT femur 4 with stl views of bone growth around the PLGA-LOG construct – (c2) Threshold 45-65, (c3) Threshold 65-85, (c4) Threshold 85-105 and (c5) Threshold 105-255.

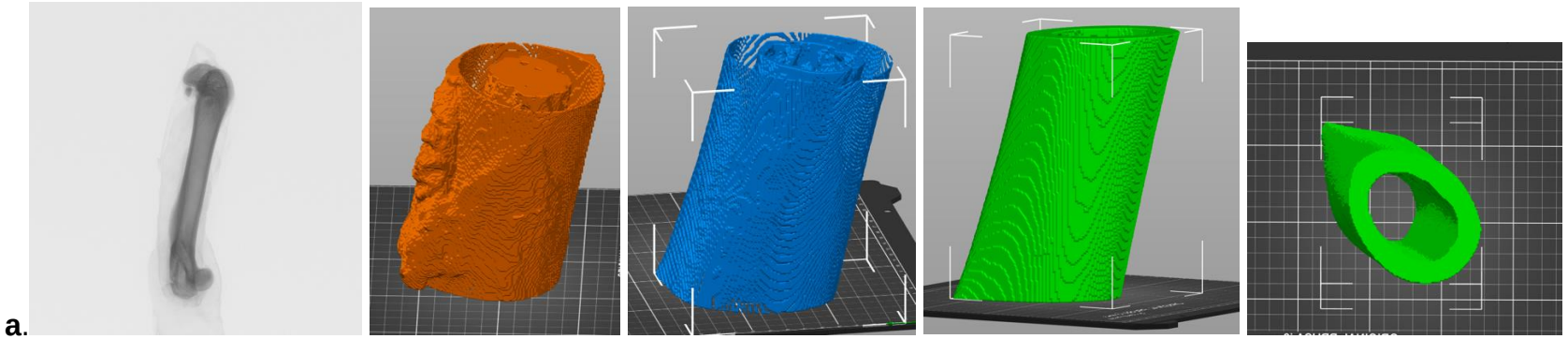

a.

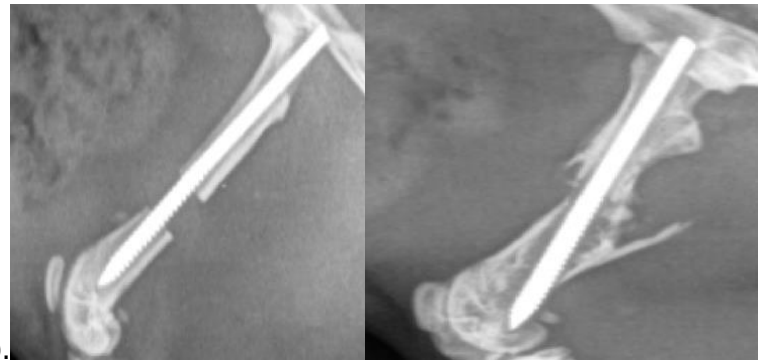

b.

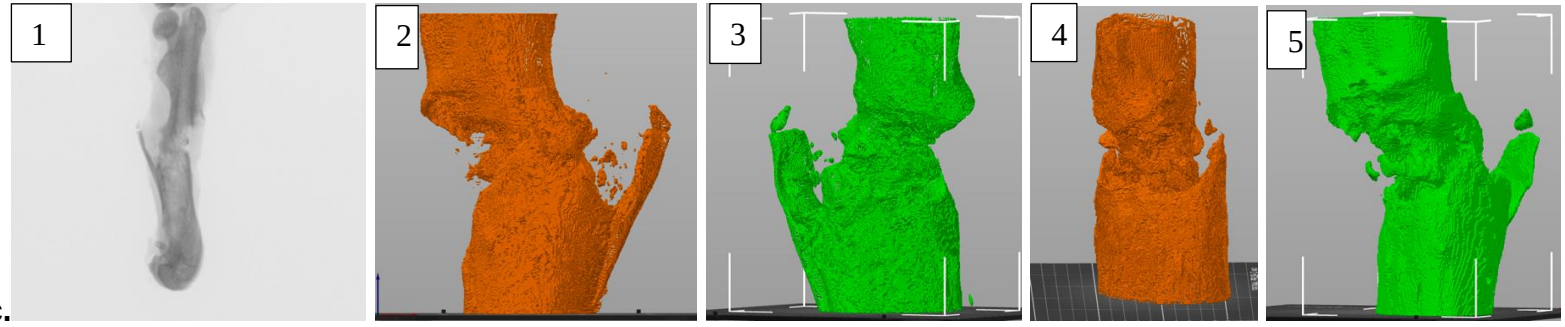

c.

Figure 5.4. Overview of results Femur 7 50:75 PLGA-LOG Acellular – Decalcified. (a) shows phantom femur micro-CT scan with stl of ROI slices equal to all samples. (b) 24-hour X-ray of Rat 7 Femur 50:75 acellular and 60-day post X-ray. (c) micro-CT femur 7 with stl views of bone growth around the PLGA-LOG construct – (c2) Threshold 45-65, (c3) Threshold 65-85, (c4) Threshold 85-105 and (c5) Threshold 105-255.

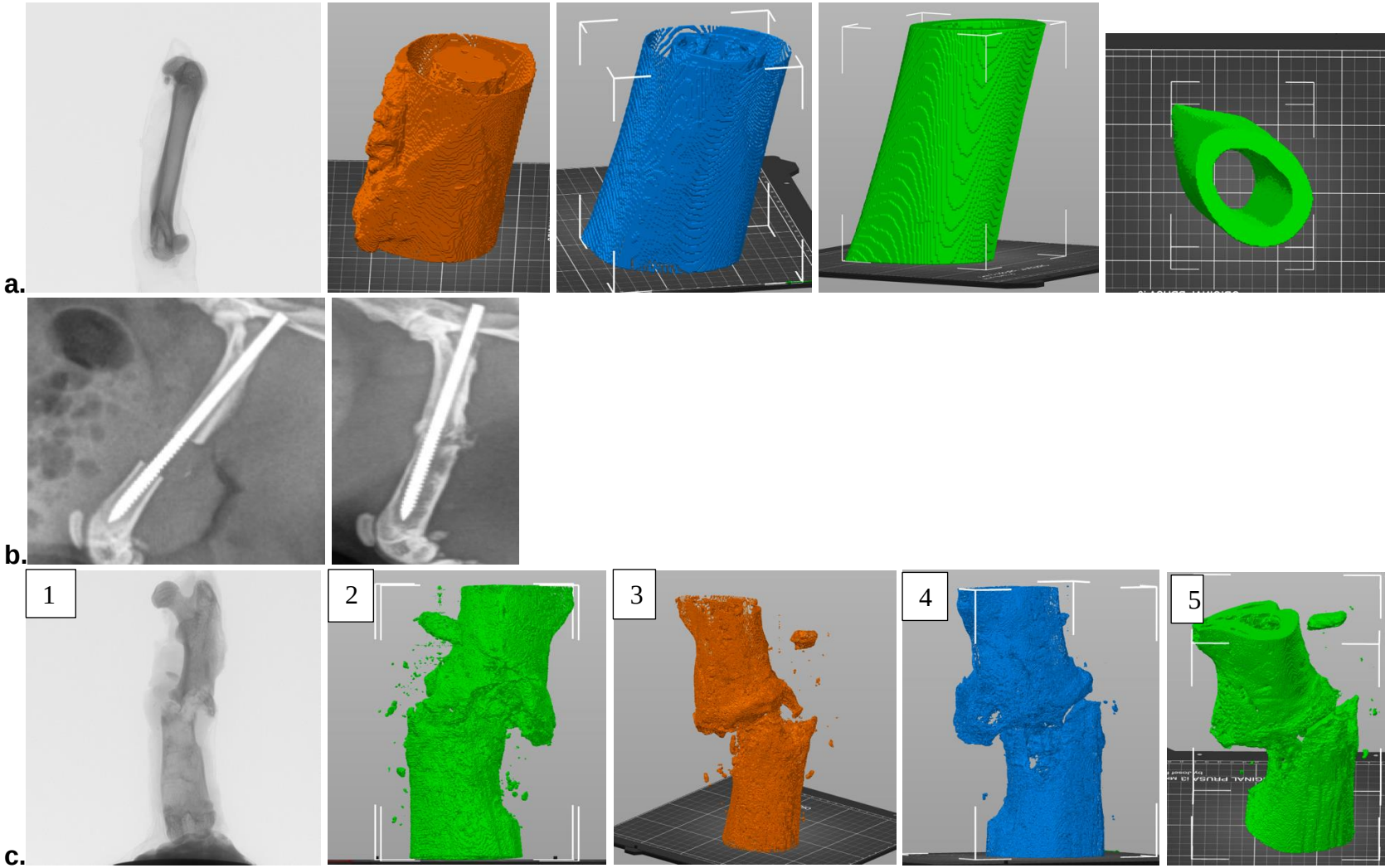

Figure 5.5. Overview of results Femur 11 50:75 PLGA-LOG Acellular – Calcified**.** (a) shows phantom femur micro-CT scan with stl of ROI slices equal to all samples. (b) 24-hour X-ray of Rat 11 Femur 50:75 acellular and 60-day post X-ray. (c) micro-CT femur 11 with stl views of bone growth around the PLGA-LOG construct – (c2) Threshold 45-65, (c3) Threshold 65-85, (c4) Threshold 85-105 and (c5) Threshold 105-255.

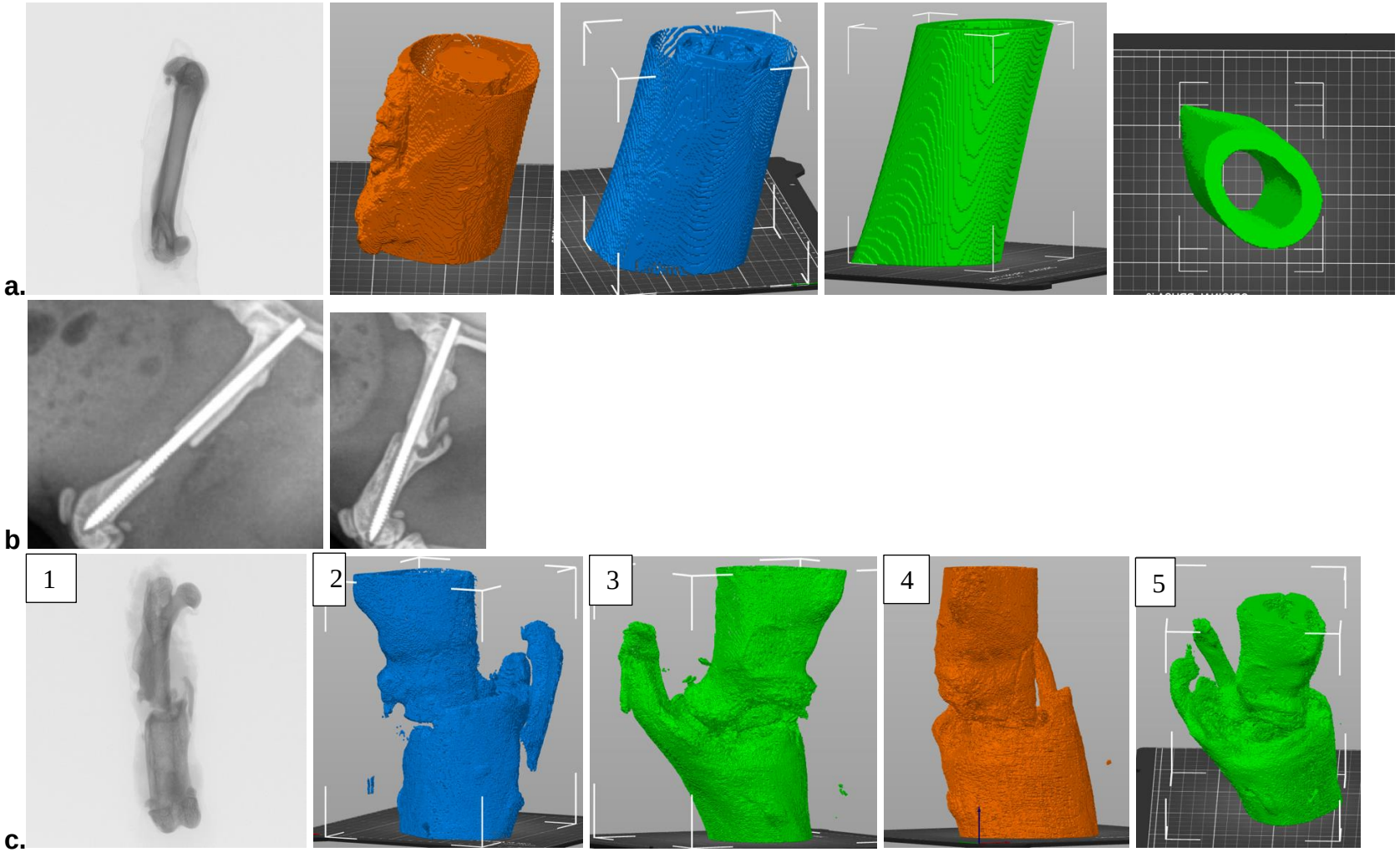

Figure 5.6. Overview of results Femur 15 50:65 PLGA-LOG Cellular – Decalcified**.** (a) shows phantom femur micro-CT scan with stl of ROI slices equal to all samples. (b) 24-hour X-ray of Rat 15 Femur 50:65 cellular and 60-day post X-ray. (c) micro-CT femur 15 with stl views of bone growth around the PLGA-LOG construct – (c2) Threshold 45-65, (c3) Threshold 65-85, (c4) Threshold 85-105 and (c5) Threshold 105-255.

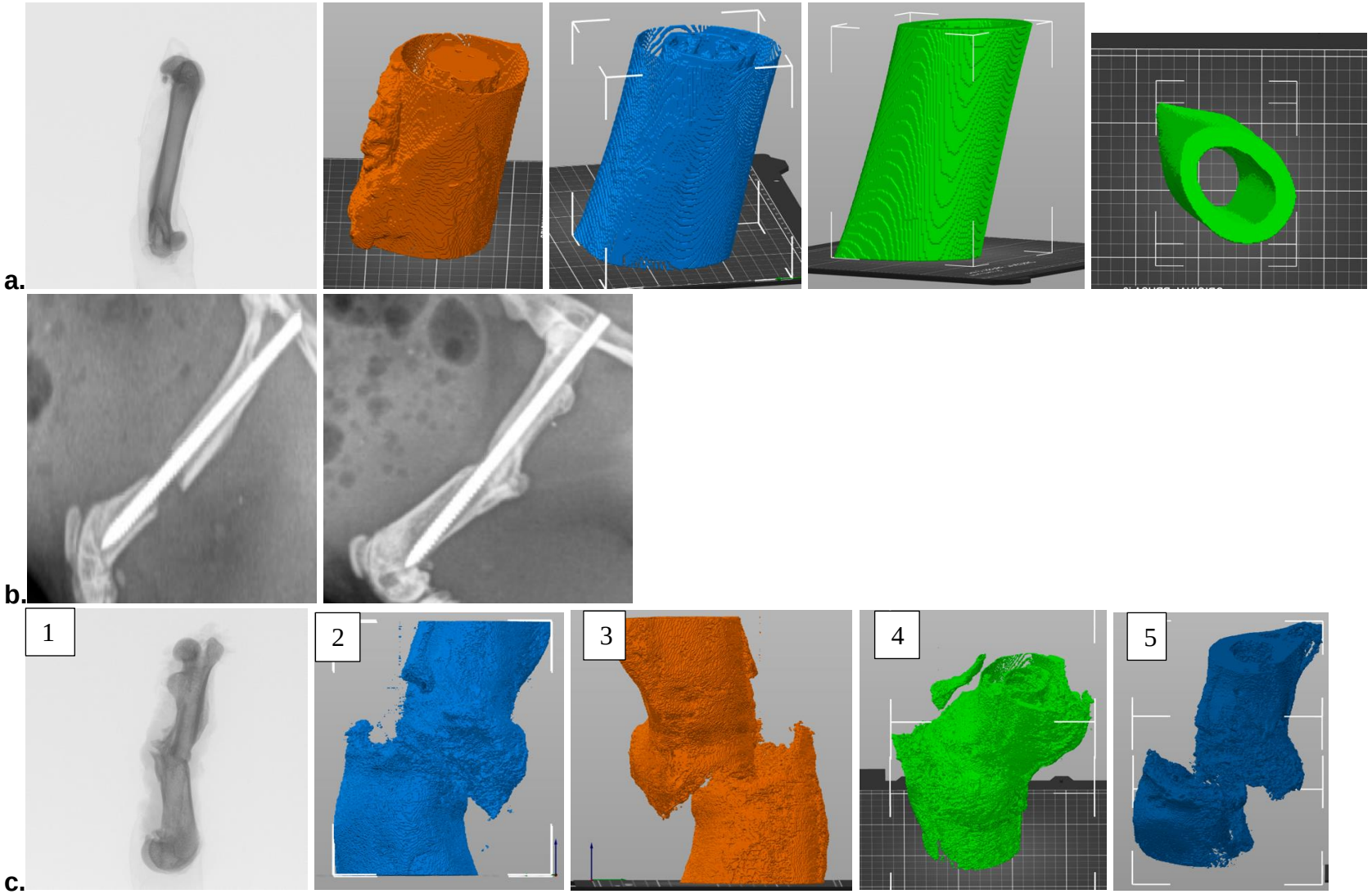

Figure 5.7. Overview of results Femur 19 50:65 PLGA-LOG Cellular – Calcified. (a) shows phantom femur micro-CT scan with stl of ROI slices equal to all samples. (b) 24-hour X-ray of Rat 19 Femur 50:65 cellular and 60-day post X-ray. (c) micro-CT femur 19 with stl views of bone growth around the PLGA-LOG construct – (c2) Threshold 45-65, (c3) Threshold 65-85, (c4) Threshold 85-105 and (c5) Threshold 105-255.

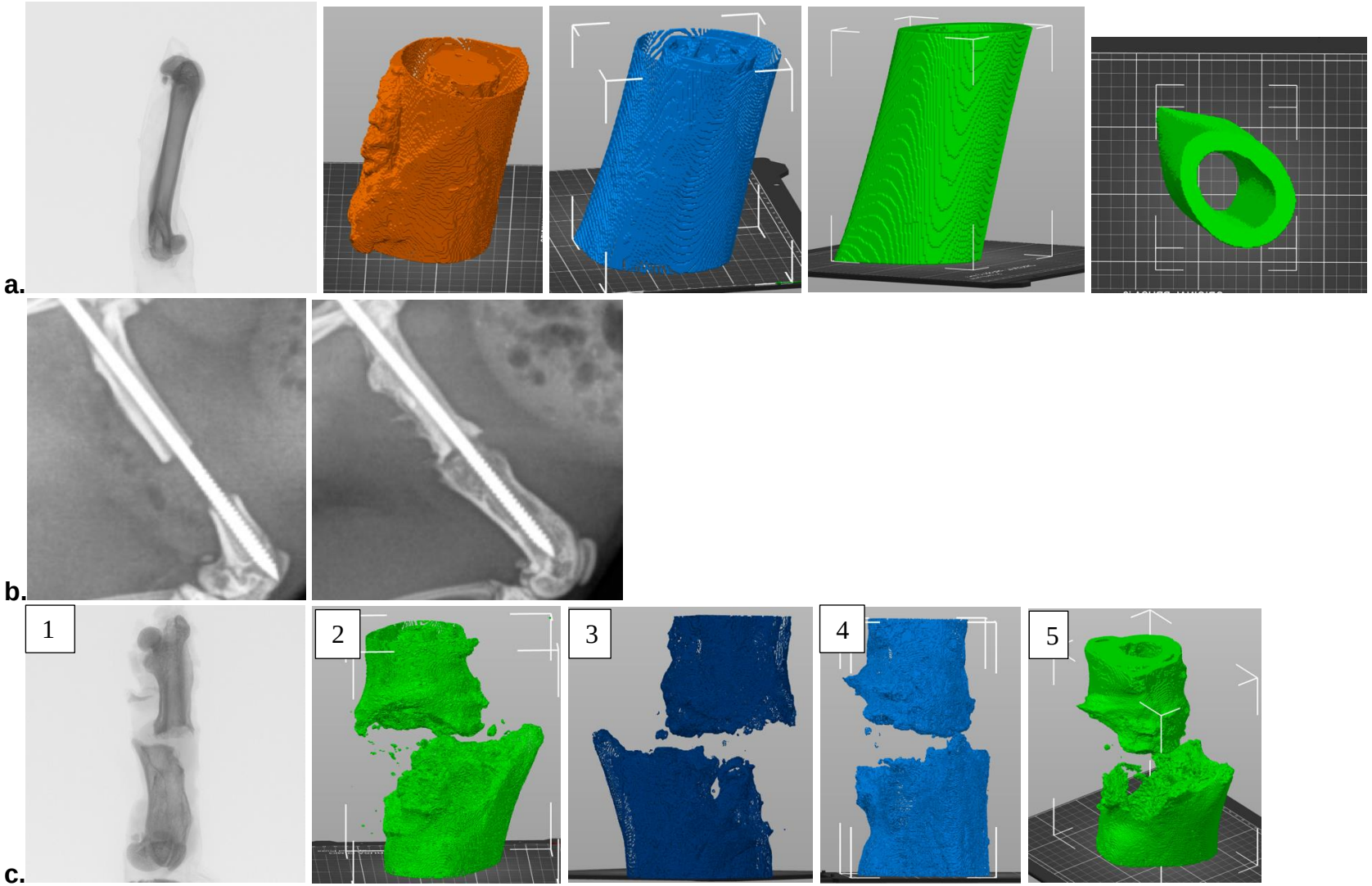

Figure 5.8. Overview of results Femur 20 50:75 PLGA-LOG Cellular – Calcified. (a) shows phantom femur micro-CT scan with stl of ROI slices equal to all samples. (b) 24-hour X-ray of Rat 20 Femur 50:75 cellular and 60-day post X-ray. (c) micro-CT femur 20 with stl views of bone growth around the PLGA-LOG construct – (c2) Threshold 45-65, (c3) Threshold 65-85, (c4) Threshold 85-105 and (c5) Threshold 105-255.

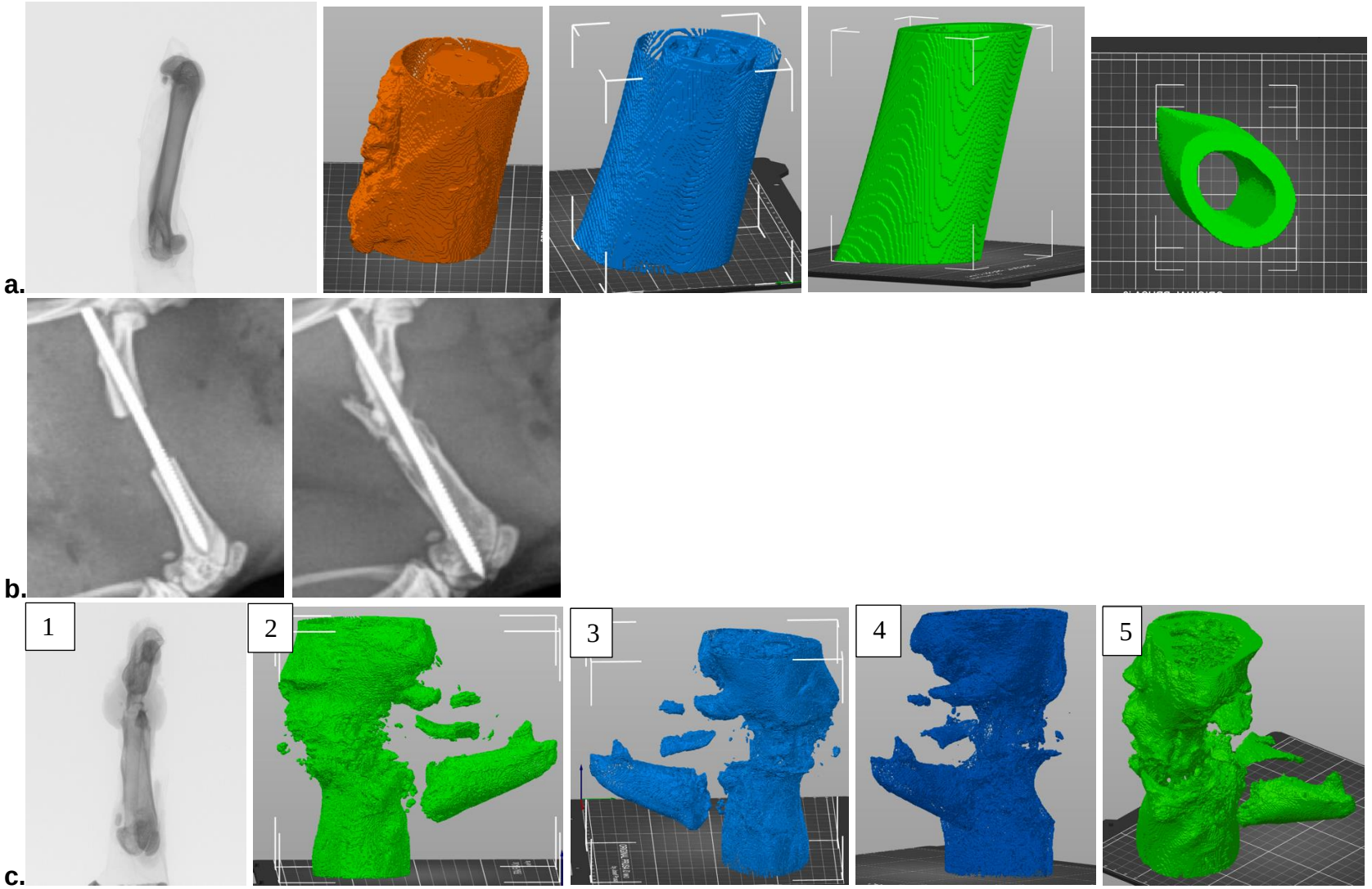

Figure 5.9. Overview of results Femur 22 50:75 PLGA-LOG cellular – Decalcified. (a) shows phantom femur micro-CT scan with stl of ROI slices equal to all samples. (b) 24-hour X-ray of Rat 22 Femur 50:75 cellular and 60-day post X-ray. (c) micro-CT femur 22 with stl views of bone growth around the PLGA-LOG construct – (c2) Threshold 45-65, (c3) Threshold 65-85, (c4) Threshold 85-105 and (c5) Threshold 105-255.

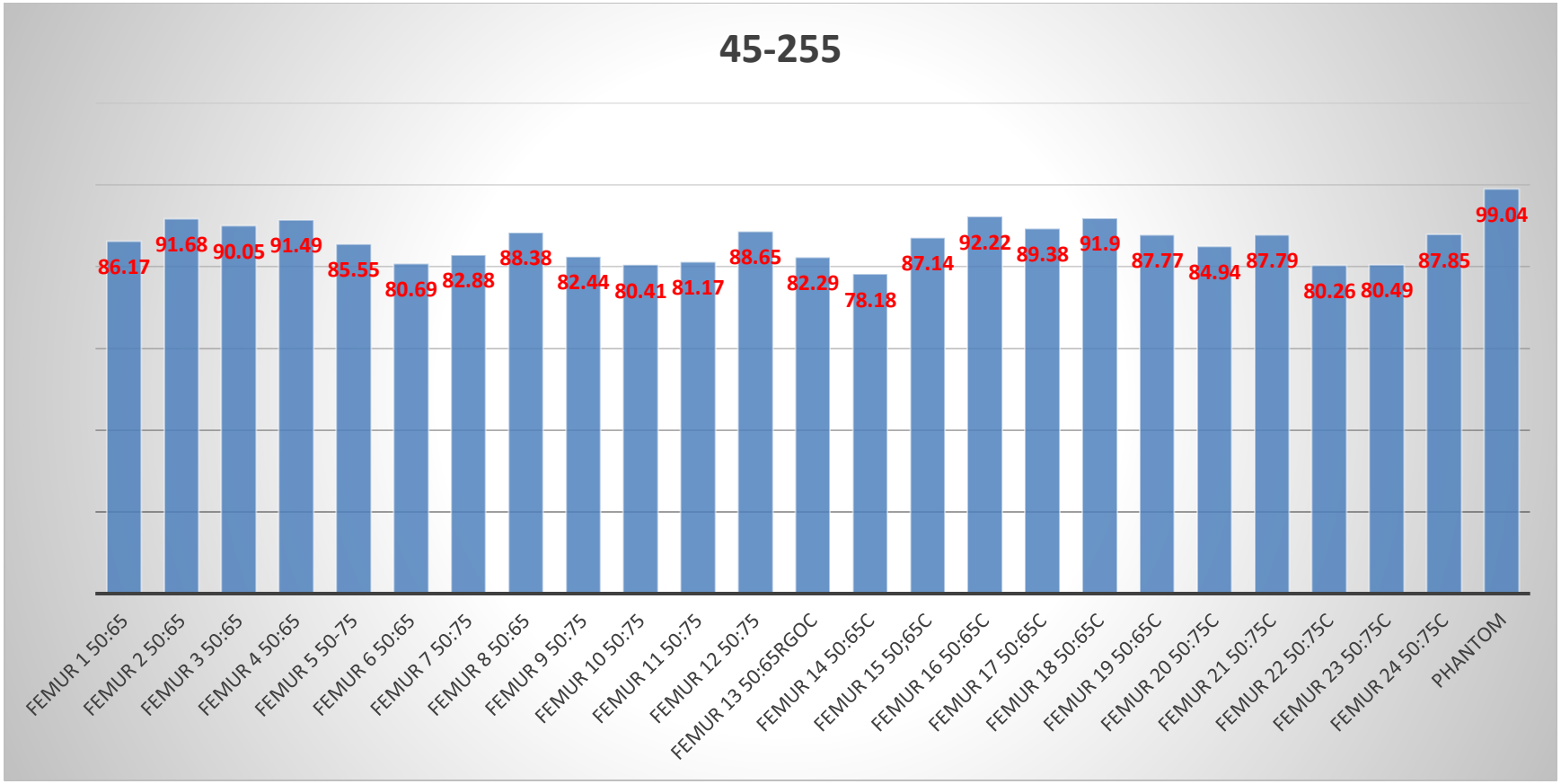

Figure 5.10. Results for the complete threshold of 45 to 255 showed no significant change throughout the bone development of the construct.

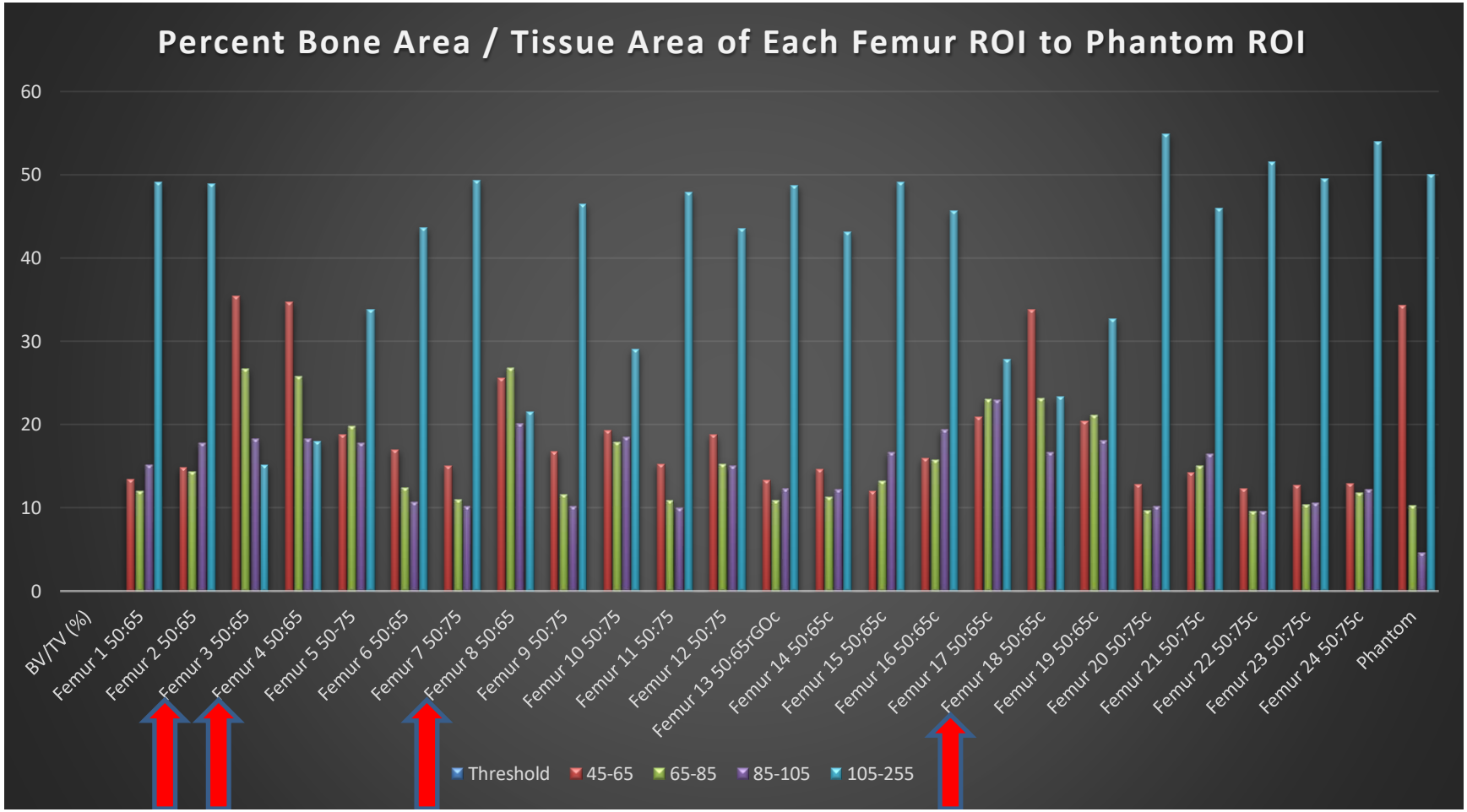

Figure 5.11. Results showing bone development at each threshold by utilizing the percent bone area / tissue area and plotting against the intact phantom femur.

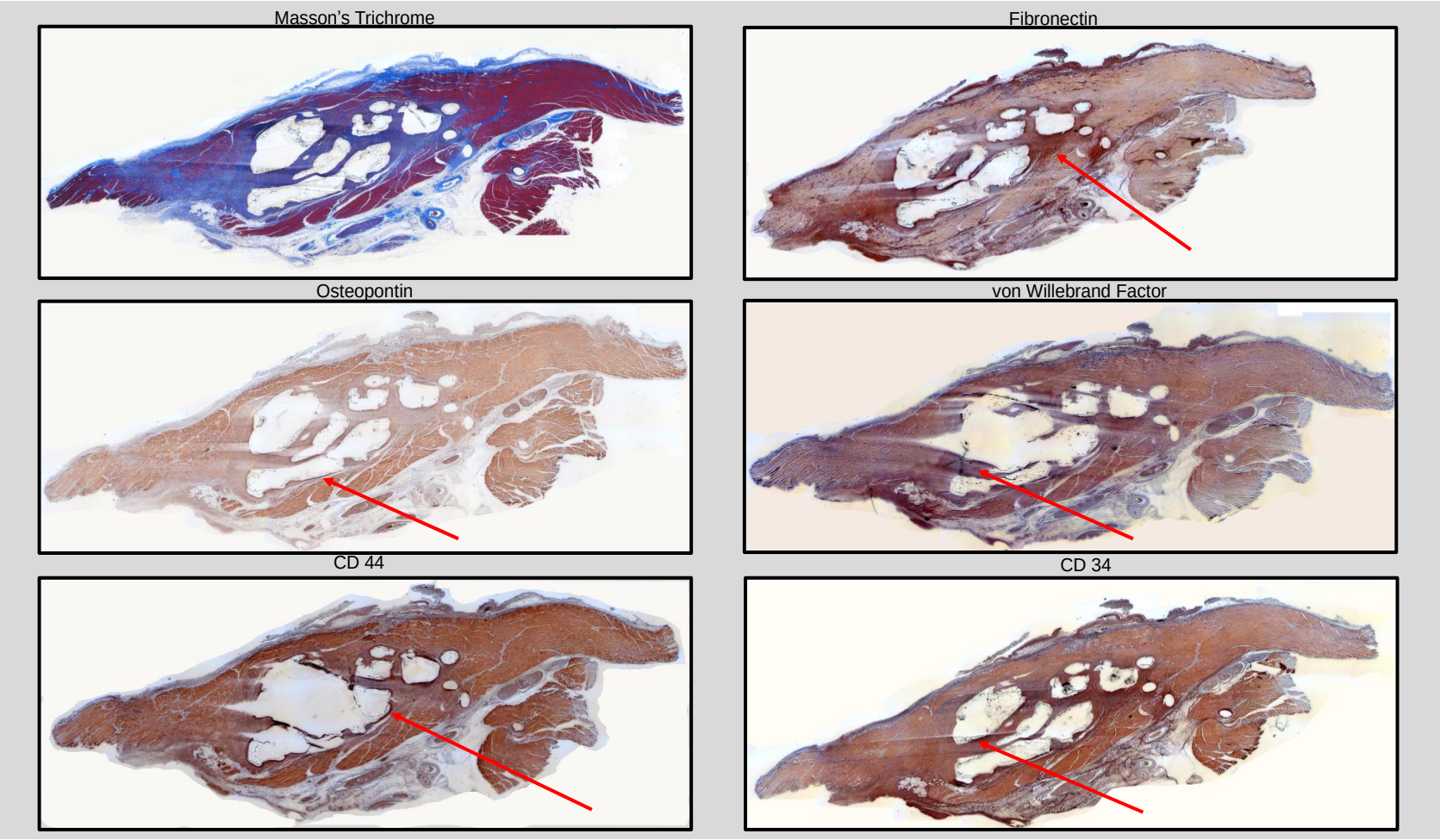

Figure 5.12. Representative image of the Intramuscular Osteoinductive Study Acellular Sample. Red arrows identify areas of antibody expression at the tissue-construct interface.

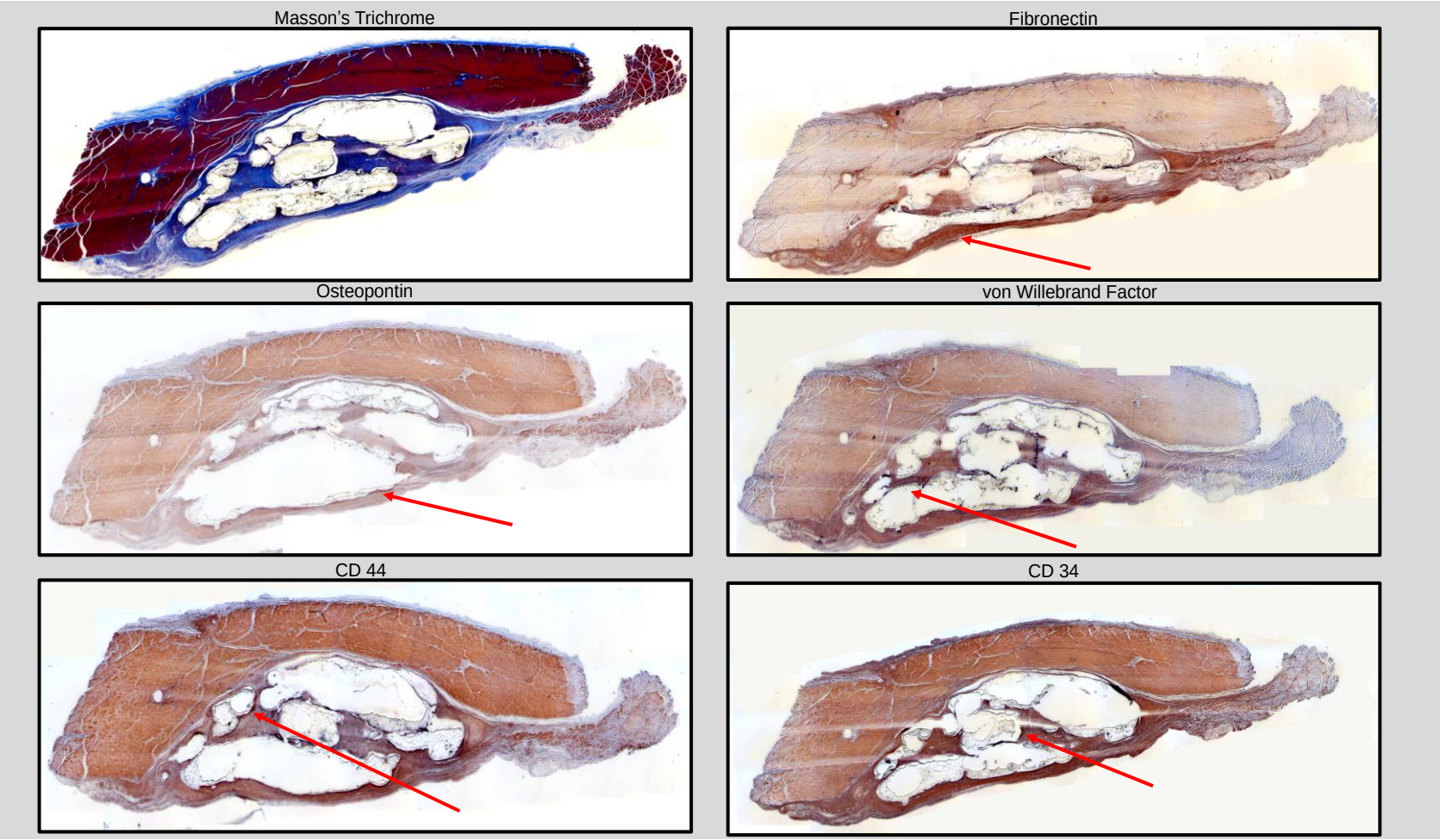

Figure 5.13. Representative image of the Intramuscular Osteoinductive Study Cellular Sample. Red arrows identify areas of antibody expression at the tissue-construct interface.

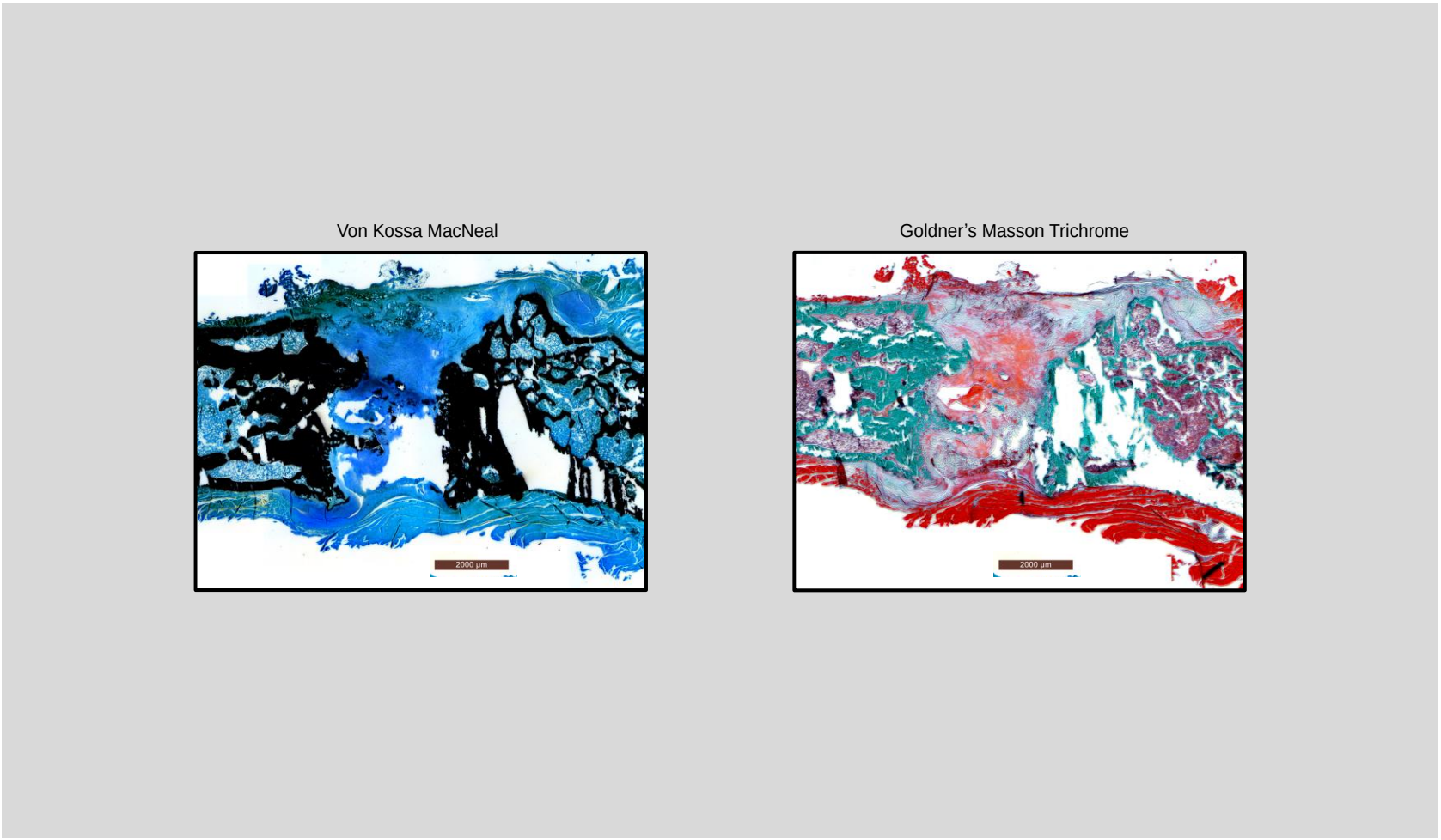

Figure 5.14. Representative image of Femur 4 Region of Interest 50:65 PLGA-LOG Acellular. Representation of Calcified cuts stained with von Kossa MacNeal- mineralized bone expressed with black color and Goldner's Masson Trichrome- collagen expressed with green color. Brown scale bar: 2000µm.

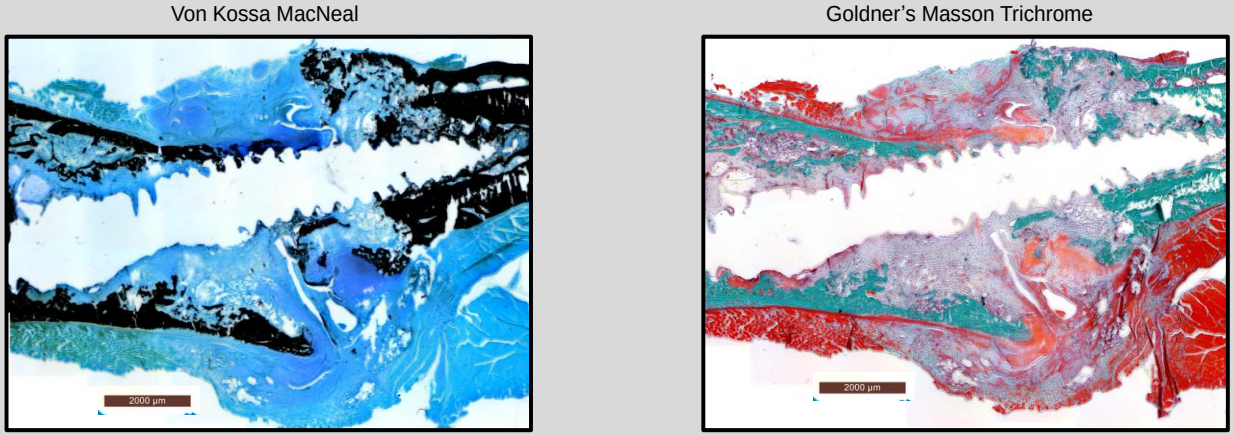

Figure 5.15. Representative image of Femur 11 Region of Interest 50:75 PLGA-LOG Acellular. Representation of Calcified cuts stained von Kossa MacNeal- mineralized bone expressed with black color and Goldner's Masson Trichrome- collagen expressed with green color. Brown scale bar: 2000µm.

Von Kossa MacNeal

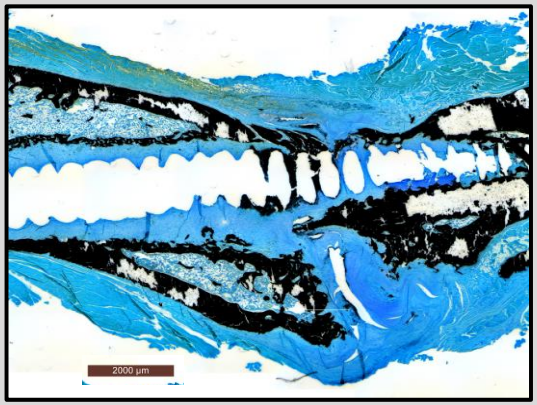

Goldner's Masson Trichrome

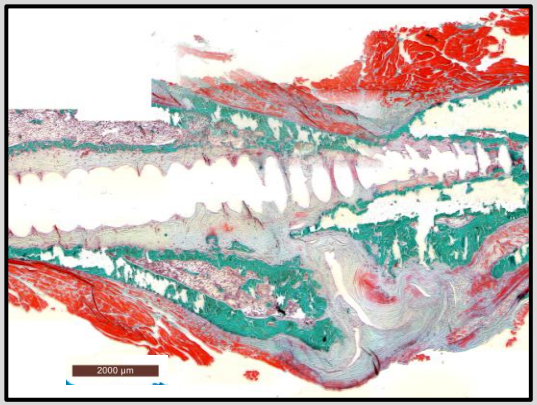

Figure 5.16. Representative Image of Femur 19 Region of Interest 50:65 PLGA-LOG Cellular. Representation of Calcified cuts stained von Kossa MacNeal- mineralized bone expressed with black color and Goldner's Masson Trichrome- collagen expressed with green color. Brown scale bar: 2000µm.

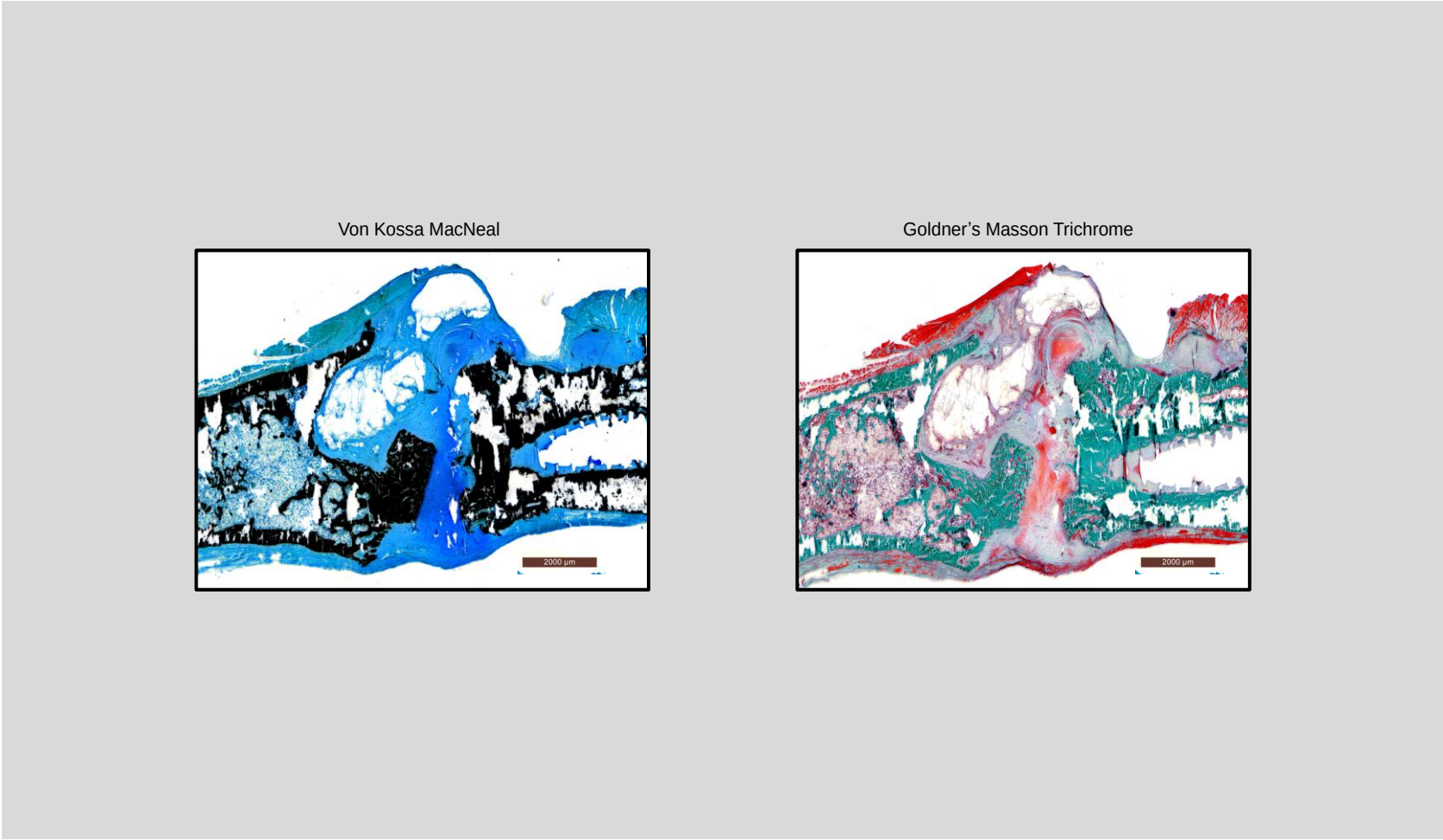

Figure 5.17. Representative Image of Femur 20 Region of Interest 50:75 PLGA-LOG Cellular. Representation of Calcified cuts stained von Kossa MacNeal- mineralized bone expressed with black color and Goldner's Masson Trichrome- collagen expressed with green color. Brown scale bar: 2000µm.

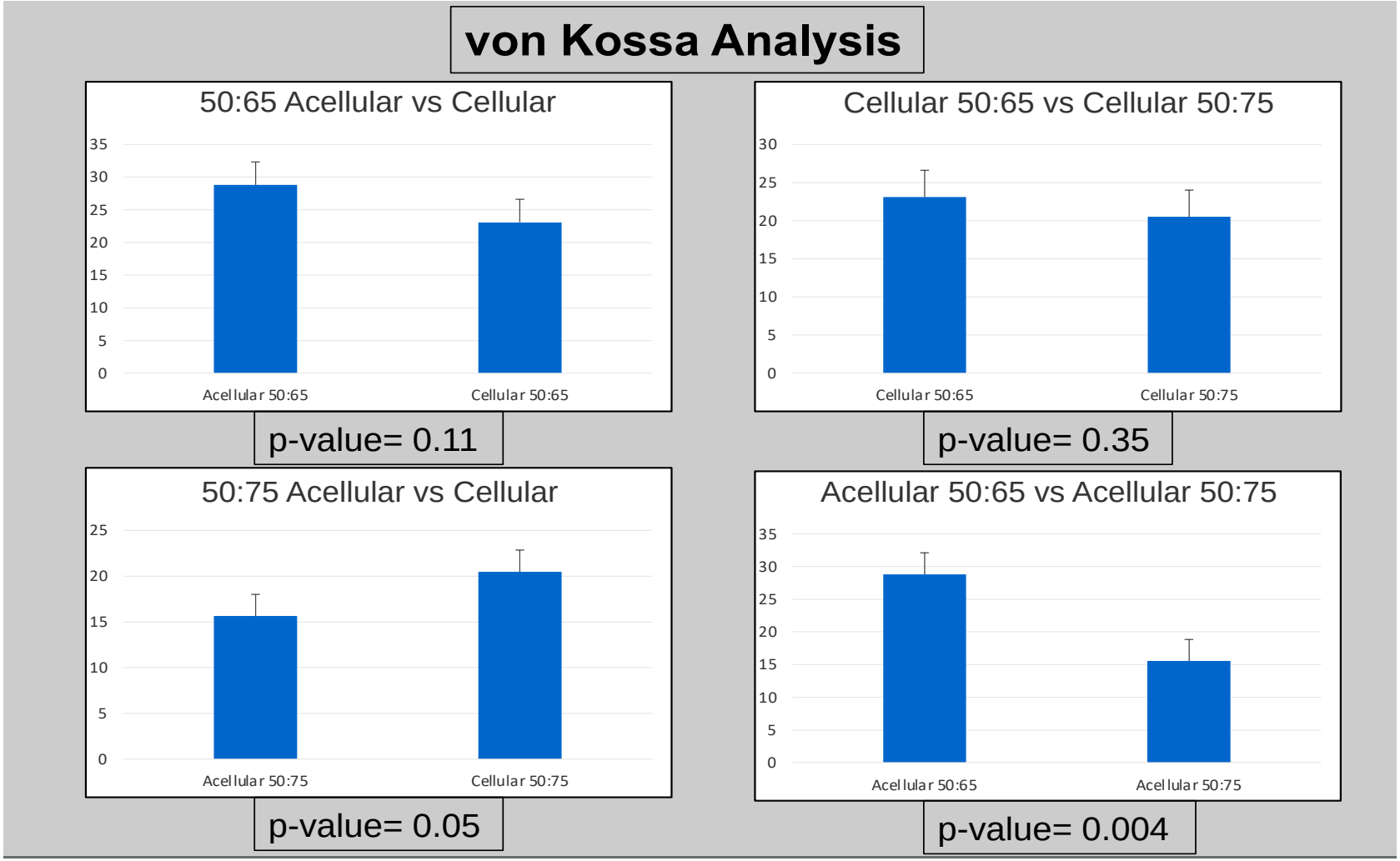

5.18. von Kossa analysis of acellular vs cellular constructs. Data shows that 50:75 LOG performs with cellular support and 50:65 LOG performs without cellular support *in vivo*.

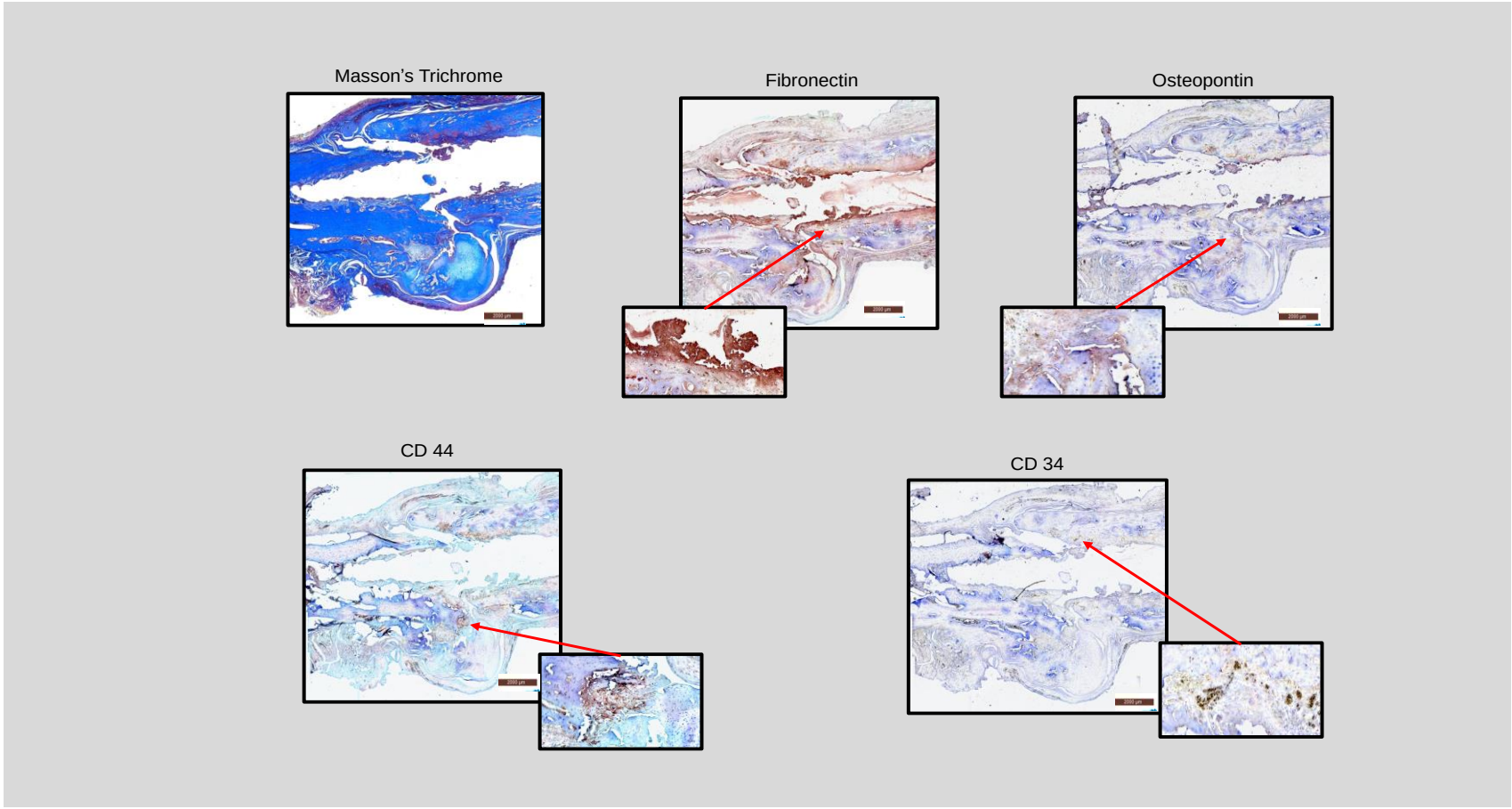

Figure 5.19. Representative Image of Femur 1 Region of Interest 50:65 PLGA-LOG Acellular. Representation of Decalcified cuts stained with Masson's Trichrome, Immunohistochemical staining for ECM protein - Fibronectin, Osteo marker - Osteopontin, Cell Markers CD44 and CD 34 with windows identifying expression of stain. Brown scale bar: 2000µm.

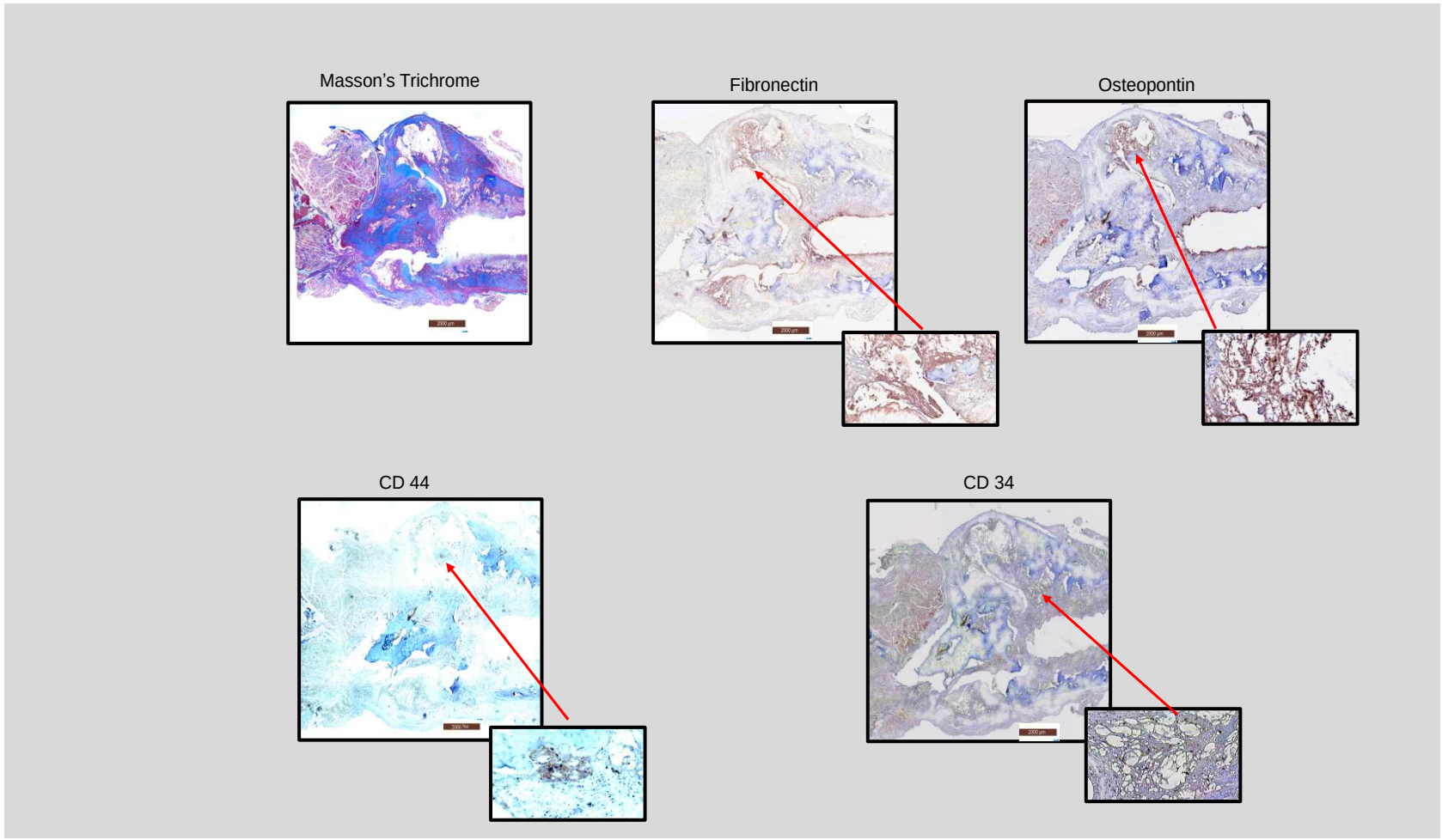

Figure 5.20. Representative Image of Femur 7 Region of Interest 50:75 PLGA-LOG Acellular. Representation of Decalcified cuts stained with Masson's Trichrome, Immunohistochemical staining for ECM protein - Fibronectin, Osteo marker -Osteopontin, Cell Markers CD44 and CD 34 with windows identifying expression of stain. Brown scale bar: 2000µm.

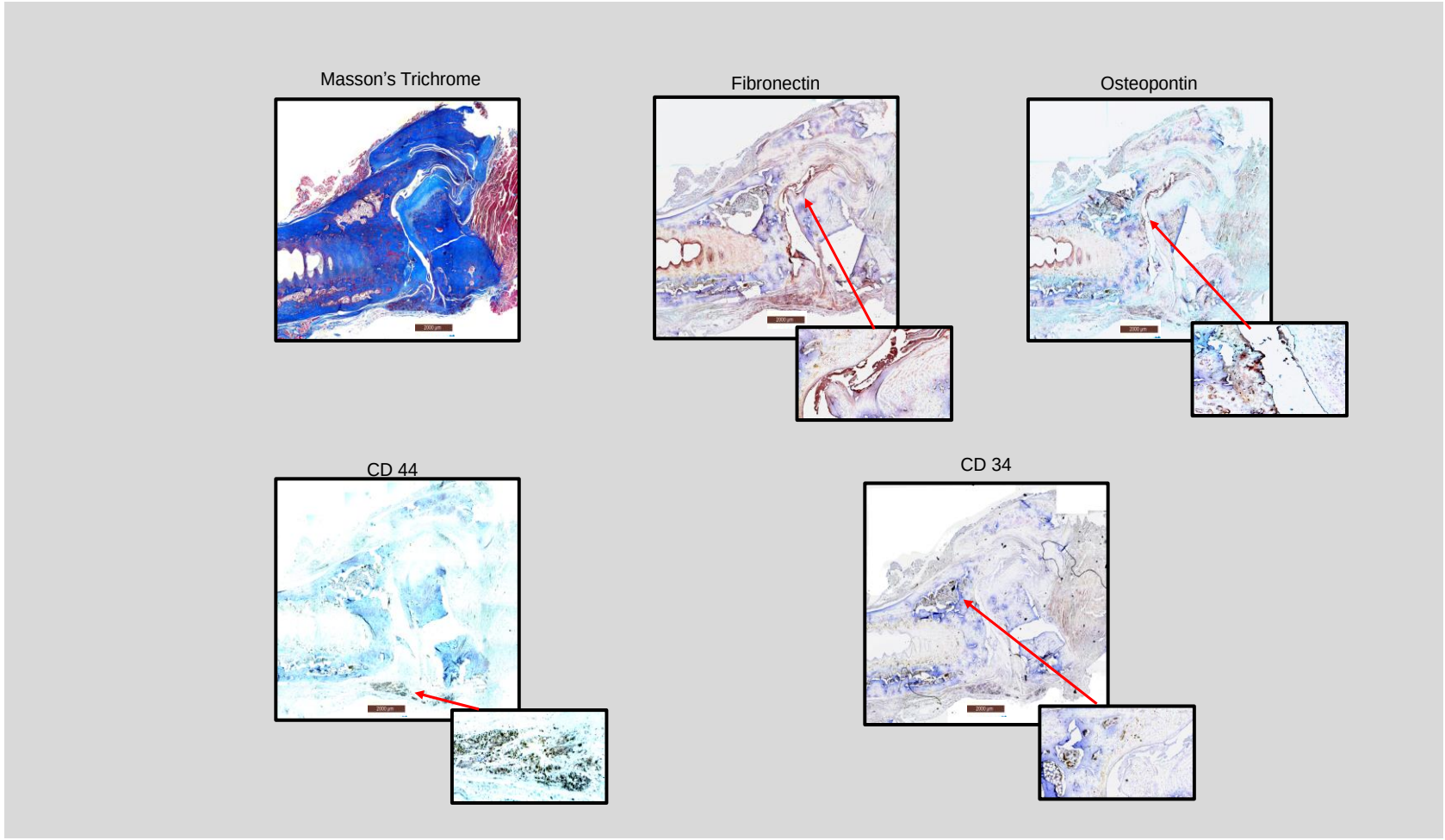

Figure 5.21. Representative Image of Femur 15 Region of Interest 50:65 PLGA-LOG Cellular. Representation of Decalcified cuts stained with Masson's Trichrome, Immunohistochemical staining for ECM protein - Fibronectin, Osteo marker - Osteopontin, Cell Markers CD44 and CD 34 with windows identifying expression of stain. Brown scale bar: 2000µm.

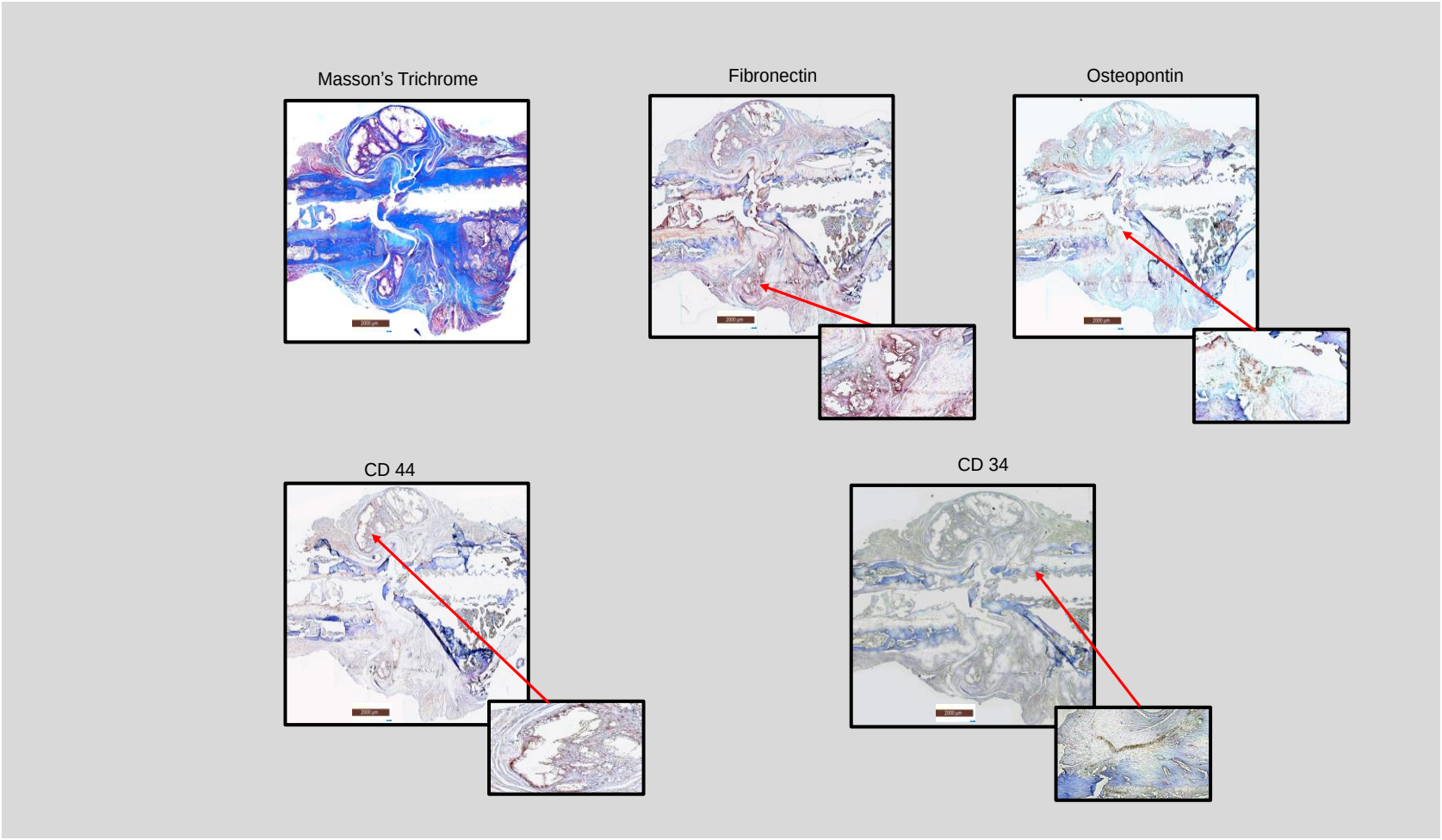

Figure 5.22. Representative Image of Femur 22 Region of Interest 50:75 PLGA-LOG Cellular. Representation of Decalcified cuts stained with Masson's Trichrome, Immunohistochemical staining for ECM protein - Fibronectin, Osteo marker -Osteopontin, Cell Markers CD44 and CD 34 with windows identifying expression of stain. Brown scale bar: 2000µm.

CHAPTER VI:
CONCLUSIONS AND FUTURE DIRECTION

CONCLUSIONS AND FUTURE DEVELOPMENTS

This thesis presents a characterization of the relationship of MSCs working with graphene nanoparticles, then forming a blended PLGA-graphene cylindrical construct using the additive manufacturing technique 3D bioprinting for biofabrication in bone tissue engineering. The material design for the 3D constructs utilizing a PLGA matrix, which provides cellular support for ECM production during the organic phase, reinforced with LOG nanoparticles, which supports the ECM transfer of cells in the mineral phase of the regenerative development.

The first part of the design was showing that undifferentiated MSCs would support a relationship and longevity on 2D films of LOG. The important component consisted of the blending and characterization of the PLGA-LOG for printing on the Aether1 bioprinter. The use of DMSO changed the approach at many levels using two molar ratios of PLGA and a nanoparticle. Characterization consisted in fiber width, using various conical nozzles and a continuous pressure and speed settings. Those results were used to establish a printing protocol to meet all parameters to find the best pressure and speed combination that could provide a fiber at 0.2mm diameter.

As the construct building blocks came together, samples were printed at 0.5mm high and 5mm in diameter and were sterilized in multiple methods to check material stability. Cell viability was measured with Calcein-AM and showed positive results which allowed to move to seeding constructs with transduced MSCs for biocompatibility, proliferation and migrations up to the 21-day time point. The results showed that the blend using DMSO did not have a negative effect on long term cell patterns. The final study was implanting the 5mm x 5mm construct into a 5mm critical sized segmental femur defect to show *in vivo* compatibility. This work opened the door to many questions and many directions for future work.

3D bioprinting has encountered accelerated progress over the last five years. Future developments of the research deal with material, construct and biological aspects.

Material development: Various combinations of single ratios and multimaterial printing outside this study and various concentrations of LOG and rGO need to be studied. This could increase mechanical and biological enhancement and optimize topological ques for cellular ECM enrichment.

Construct developments: Multimaterial extrusion allows for biofabricating complex architecture with rapid and smooth transition between divergent biomaterials. Porosity is very important to the whole process which depends on fiber distance and layer and angle orientation. If any variance in those parameters, porosity dimensions and geometrical output will vary as well allowing for analysis of various cell lines. Construct geometry can impact mechanical behavior.

Biological developments: Multiple methodologies can be used to proceed in biological investigations. Further studies on various stem cell lines and co-culturing would greatly support the construct's ability to be studied for an ECM matrix for multiple organs. Bioprinting 3D tissue models for simulation of a disease environment for clinical studies could be utilized. This will allow for open access to the 4D bioprinting of dynamic tissues with designs in programmable constructs for dynamic variations from biological triggers.

VITA

Steven D. Newby, born in March 1972, attended Clinton High School from August 1986 to May 1990 where I took AP classes in Chemistry and Biology. Worked at Clinch River Environmental Organization and Raptor Center studying snake habits and breeding ranges. 1991 went into the United States Air Force, after serving returned home. Began working in Veterinary Medicine working my way up from kennel assistant to technician and in 1998 with my wife purchased the hospital I started at, Clinton Animal Hospital. Over a 16-year period served as Chief of Anderson County Rescue Squad and Deputy Chief of Claxton Fire. In 2007 Built Norris Animal Hospital and started coaching my daughter's softball teams. Returned to College at the University of Tennessee Knoxville and majored in Biochemistry and Molecular Biology. In 2015 started applying to the Comparative and Experimental Medicine to pursue PhD under the mentorship of Dr. Madhu Dhar at UTK. Studies focused on stem cell-based regenerative medicine which later focused on the biofabrication design of a bone tissue construct.

During my time in graduate school, studied concepts in advance biochemistry and engineering focusing on biomaterial sciences. Apart from journal articles, I presented a collection of posters and oral presentations at symposia and conferences hosted by the CEM department at UTK. I had five publications, with one as shared first author and as a first author and one book chapter with Dr. Dhar. First author publication constitutes *Chapter II* in this work. I have written and submitted my dissertation for review, for a planned graduation in May of 2021.